Université de Sherbrooke
Faculté de génie
Département de génie civil et de génie du bâtiment

La Rochelle Université
Faculté des sciences et de la technologie
Département de génie civil

Development of Self-Consolidating Earth Concrete (SCEC) with Improved Multifunctional Performance for Green Construction

Développement d'un béton de terre autoplaçant (SCEC) avec des performances multifonctionnelles améliorées pour une construction verte

Thèse de doctorat
Spécialité : Génie civil

Mojtaba KOHANDELNIA

A dissertation submitted in partial fulfillment of the requirements for the degree of Doctor of Philosophy in Civil Engineering

(Thèse présentée au département de génie civil et de génie du bâtiment en vue de l'obtention du grade Docteur en philosophie en génie)

Jury:	Ammar Yahia	Director
	Rafik Belarbi	Co-director
	Richard Gagné	Reporter
	Stéphanie Bonnet	Evaluator
	Seif Khiati	Evaluator
	Claudiane Ouellet-Plamondon	Evaluator
	Marie Duquesne	Evaluator

Sherbrooke (Québec), Canada December 2022

To my mother, Parvin, who taught me how to love

and my father, Mohammad, who taught me how to fight

ABSTRACT

The earth construction has been used as a sustainable construction method since ancient time. Rammed earth (RE) walls are among the most common elements for earth construction. This technique is identified as a green construction by using locally available materials with low environmental impacts and superior thermal performance. Earthen constructions were neglected for a period; however, it is grasping great interest in the last years to fulfill the environmental constraints. Besides all the advantages of this construction material, the casting process can be very time and energy consuming due to the nature of dynamic compaction. This study aimed to evaluate the feasibility of achieving self-consolidating earth concrete (SCEC) with introduction of its potential challenges and investigating its rheo-thermomechanical performance. As the first challenge, the presence of fine particles in earth, especially clay, can hinder the flowability of SCEC. Promoting the setting time is the second challenge due to the low cement content. The last challenge comes from the diversity of earth with different behaviors which makes it difficult to propose a comprehensive guideline to design SCEC.

This study was conducted in four different and complementary phases. Phase 1 involved a comprehensive literature review with introduction of advantages and disadvantages of earthen constructions. In addition, potential solutions were introduced to achieve SCEC and address the inefficiency of earth materials. In the Phase 2, the main objective was to understand the efficiency of different chemical admixtures in presence of various ternary powder systems (i.e., clay, silt, and cement). The Taguchi method was used to evaluate the workability and compressive strength of self-consolidating earth paste (SCEP) mixtures and evaluate the significance of the influencing parameters, including clay type, cement content, water-to-powder ratio (W/P), cement-to-clay ratio (Ce/Cl), and admixture type. Several statistical models were introduced to predict the workability and compressive strength of SCEP mixtures. These models were also used to establish a new guideline to design SCEP considering the characterization parameters of earth (i.e., Atterberg limits).

A new concrete-equivalent mortar (CEM) approach was introduced in the Phase 3. Accordingly, the CEM and concrete mixtures were investigated to verify the feasibility of SCEC. The workability, compressive strength, and drying shrinkage of the investigated mixtures were assessed. Beside the evaluation of the influencing parameters on each response, this multiscale

investigation allowed to propose good relationships to predict CEM and SCEC performance from their corresponding paste and CEM mixtures, respectively. Rheology of paste, CEM, and SCEC mixtures was investigated in Phase 4. The importance of different mixture constituents and admixture types resulted in different rheological behaviors. Furthermore, new relationships between the rheological parameters and workability were recommended for paste, CEM and concrete.

In the last phase (Phase 5), the hygrothermal and microstructural characteristics of the selected SCEC mixtures were investigated. This novel material offers a new microstructural system, hence leading to a different hygrothermal performance compared to conventional earthen materials. The hygrothermal tests included sorption isotherm, water vapor and gas permeability, heat capacity, and thermal performance (i.e., conductivity, diffusivity, and effusivity). These results along with the pore size distributions resulted in meaningful correlations between cumulative pore volumes in different classes with permeability, drying shrinkage, and compressive strength of the investigated SCEC mixtures.

Keywords: Sustainable construction; Self-consolidating earth concrete (SCEC); Rheo-thermomechanical; Ternary powder system; Concrete-equivalent mortar (CEM).

RÉSUMÉ (en français)

La construction en terre est utilisée comme méthode de construction durable depuis les temps anciens. Les murs en terre battue (TB) sont parmi les éléments les plus courants de la construction en terre. Cette technique est considérée comme une construction verte en utilisant des matériaux disponibles localement avec un faible impact environnemental et une performance thermique supérieure. Les constructions en terre ont été négligées pendant un certain temps; cependant, elles suscitent un grand intérêt ces dernières années pour répondre aux contraintes environnementales. Malgré les avantages de ce matériau de construction, le processus de coulage est très consommateur de temps et d'énergie à cause de l'application de la compaction dynamique. Cette étude a pour but d'évaluer la faisabilité de formuler un béton de terre autoplaçant (BTAP) tout en étudiant ses performances rhéo-thermomécaniques et en identifiant les différents défis. Le premier défi est la présence de particules fines dans la terre, en particulier les particules argileuses, qui peuvent entraver la fluidité du BTAP. L'augmentation du temps de prise est le deuxième défi en raison de la faible teneur en ciment. Le dernier défi vient de la diversité des terres avec des comportements différents, ce qui rend difficile la proposition d'une ligne directrice complète pour la conception des BTAP.

Cette étude a été menée en quatre différentes phases complémentaires. La Phase 1 a consisté en une revue complète de la littérature, notamment les avantages et des inconvénients des constructions en terre. En outre, des solutions potentielles ont été introduites pour réaliser le BTAP afin de remédier à l'inefficacité des matériaux en terre. À la Phase 2, il s'agit essentiellement de comprendre l'efficacité de différents adjuvants chimiques en présence des systèmes ternaires (c'est-à-dire l'argile, le limon et le ciment). La méthode de Taguchi a été utilisée pour évaluer l'effet des paramètres de formulation et leur signification sur la maniabilité et la résistance à la compression des pâtes de terre autoplaçantes (PTAP). Le type d'argile, la teneur en ciment, le rapport eau/poudre (E/P), le rapport ciment/argile (Ci/Ar) et le type d'adjuvant sont étudiés. Des modèles statistiques ont été développés pour prédire la maniabilité et la résistance à la compression des mélanges de PTAP et une nouvelle approche a été proposée pour concevoir les PTAP en tenant compte des caractéristiques de la terre (c'est-à-dire les limites d'Atterberg).

Une nouvelle approche de mortier du béton équivalent (MBE) a été introduite à la Phase 3. En conséquence, le MBE et les formulations de béton ont été étudiés pour vérifier la faisabilité du

BTAP. La maniabilité, la résistance à la compression et le retrait de séchage des mélanges étudiés ont été évalués. En plus de l'évaluation des paramètres de formulation sur les propriétés étudiées, cette étude multiéchelle a permis de proposer des corrélations pour prédire la performance du MBE et du BTAP à partir de celle de leur pâte et de leur MBE correspondants. La rhéologie des pâtes, des MBE et des BTAP a également été étudiée à la Phase 4. Les résultats obtenus montrent que l'effet important des différents constituants du mélange et du type d'adjuvant a entraîné sur le comportement rhéologique des formulations étudiées. En outre, de nouvelles corrélations entre les paramètres rhéologiques et l'ouvrabilité des différentes formulations étudiées ont été recommandées.

À la dernière phase (Phase 5), les caractéristiques hygrothermiques et microstructurales des BTAP optimisés ont été étudiées. Ce nouveau matériau offre une microstructure conduisant à une performance hygrothermique différente de celle des matériaux en terre conventionnels. Les essais hygrothermiques comprenaient l'isotherme de sorption, la perméabilité à la vapeur d'eau et au gaz, la capacité thermique et la performance thermique (c'est-à-dire la conductivité, la diffusivité et l'effusivité). Ces résultats hygrothermiques et la distribution des tailles de pores ont permis d'établir des corrélations significatives entre les volumes de pores cumulés et la perméabilité, le retrait au séchage et la résistance à la compression des BTAP étudiés.

Mots-clés: Construction durable; Béton de terre autoplaçant (BTAP); Rhéo-thermomécanique; Système de poudre ternaire; mortier du béton équivalent (MBE).

ACKNOWLEDGEMENT

First, I would like to genuinely express my gratitude to my supervisor Prof. Ammar Yahia for granting me his confidence, continuous support, and patience through all those years. All his guidance, patience and encouragement are highly appreciated. I have always learned from him, especially having perseverance during good and not-so-good days. PhD journey for me was one of those good memories I will always remember, and I will be proud to be one of his scholars.

I would also like to thank my co-supervisor, Professor Rafik Belarbi, for his endless support in my whole PhD experience. I would like to thank him for having me in France and being always supportive. It was a pleasure to collaborate with him in my PhD from whom I learned a lot.

I would also wish to thank Dr. Masoud Hosseinpoor for his collaboration and endless support during this project. He always pushed me forward with enthusiasm which is much appreciated. Thanks to all the professors of Civil and Building Engineering Department at Université de Sherbrooke, research assistants, technicians, industrial partners of the Industrial Chair on BFRA, and all our Group members and colleagues. Similarly, I sincerely thank the technicians and staff at La Rochelle Université for their valuable help and support during my stay in France. The author is also thankful to the members of the dissertation committee for their valuable comments and advice.

Last but not least, special thanks to my parents, Parvin and Mohammad, and my sister, Parisa, for their continuous encouragement, care and love during this journey. Thanks for having confidence in me and raising me to be the person I am today.

Mojtaba Kohandelnia

December 2022

TABLE OF CONTENT

List of Figures

List of Tables

List of symbols

W/P	Water-to-powder ratio
Ce/Cl	Cement-to-clay ratio
V_P	Paste volume
S/A	Sand-to-total aggregate ratio
s	Suction
u_a	Pore air pressure
u_a	Pore water pressure
LL	Liquid limit
PL	Plastic limit
PI	Plasticity index
LS	Linear shrinkage
A_c	Clay activity
MBV	Moisture buffer value
RH	Relative humidity
SSA	Specific surface area
CEC	Cation-exchange capacity
MSF	Mini-slump flow
MCT	Marsh cone flow time
φ	Volumetric content
φ_{max}	Packing density
V_{CP}	Compacted paste volume
V_{CA}	Compacted aggregate volume
V_{EP}	Excess paste volume
e_{EP}	Excess paste thickness
A_{3D}/V	Surface area-to-volume ratio
MVF	Mini V-funnel
SF	Slump flow
VF	V-funnel
f′	Compressive strength

τ	Shear stress
τ_0	Yield stress
μ_p	Plastic viscosity
$\dot{\gamma}$	Shear rate
k	Consistency index
n	Pseudoplastic index
K_A	Specific permeability coefficient
μ	Dynamic viscosity of the gas
P_0	Entrance absolute pressure
P_1	Exit absolute pressure
Q	Volumetric flow
L	Sample thickness
A	Surface area of the sample section
V	Volume of the bubble flowmeter
t_{avg}	Average passing time
K_{int}	Intrinsic permeability
ε_p	Total porosity
M_{air}	Weight of saturated sample after removing from the water
M_{dry}	Dry sample weight
M_{water}	Hydrostatic weight of the sample saturated in water
λ	Thermal conductivity
ρ	Dry density
C_P	Specific heat capacity
D	Diffusivity
E	Effusivity

CHAPTER 1. INTRODUCTION

1.1 Synopsis

Since the construction all around the world is on a growing path, it is important to preserve the ecosystem, which is a responsibility of civil engineers. From the environmental point of view, the construction industry accounts for 30% of carbon dioxide emissions [1]. This high demand of construction should be addressed mostly by novel and more sustainable construction materials and techniques.

Concrete is the most used construction material around, due to its simplicity and versatility. Cement, which is an essential ingredient for concrete, production leads to the highest CO_2 emissions compared to other construction materials [2]. High demand of cement production and the effect on global warming and natural resource consumption are the main negative environmental impacts of cement-based concrete. Supplementary cementitious materials (SCMs) were investigated to improve the overall sustainability of construction and reduction of CO_2 emission [3]. On the other hand, earth construction was used from ancient years in different applications and is still being investigated in various studies [1]. Rammed earth (RE) was one of the most common and widespread earth construction methods. However, during the first half of the 20^{th} century, earth construction is significantly reduced because of the rapid emerging of new materials and construction techniques, including cement-based mortars and concrete [4].

Local availability of earth materials can significantly reduce the transportation costs. Moreover, other advantages of earthen constructions compared to cement-based concrete include lower environmental impact and embodied energy, better insulation properties, wider variety of textures and finishing techniques, and appropriate performance with or without stabilization [5,6]. They can therefore be incorporated as a partial replacement of cement in concrete mixture proportioning [3]. The use of earth materials aims to limit the consumption of new natural resources and promote the usage of recycled and available resources. Earth materials are environmental-friendly due to use of lower cement contents thanks to the incorporation of locally available materials. On the other hand, energy consumption of RE construction and compaction is negligible compared to required energy

for cement production [7]. However, earth construction materials are less durable compared to conventional materials. They are also more labor intensive, time consuming, and water sensitive, hence resulting in poor structural behavior. Moreover, they are only suitable for in-situ construction due to their special maintenance requirements and higher wall thicknesses [8]. The process of layer-by-layer RE construction is shown in Fig. 1.1 [9]. This casting method can be very time consuming and cause different moisture contents and compaction conditions for each layer, hence resulting in performance deficiencies.

Fig. 1.1. The process of layer-by-layer RE construction [9].

Regarding the energy aspects, the energy consumption in buildings can be classified in three main categories, as follow: (1) the energy embedded in the production and transportation of materials, (2) the energy required for building activities, and (3) the energy consumed to provide users with the necessary comfort conditions. The locally available natural materials can significantly save the energy and cost corresponding to production and transportation (1st category) [1]. Moreover, the natural materials do not need to install special equipment, thus reduce the labor force and building duration (2nd category) [7]. Furthermore, the third category depends on living comfort brought by high hygrothermal performance of earth materials which can minimize the air-conditioning energy, hence leading to appropriate living comfort (3rd category) [10].

In the case of thermal performance and indoor air quality, a comprehensive hygrothermal study is necessary to investigate the coupled heat and mass transfers in porous building materials, such as earth concrete. Moisture may play an important role on heat transfer. Excess moisture can negatively influence the building performance, in terms of durability, discomfort, allergies, and respiratory diseases [11]. It is worthy to mention that the thermal conductivity of liquid water is thirty times higher than air [12]. Therefore, the increase of thermal conductivity due to water content must be considered to evaluate the hygrothermal performance of the material. Materials

with the ability to control the humidity level can similarly act as heating, ventilation, and air-conditioning (HVAC) systems, resulting in thermal comfort and satisfying indoor air-quality.

1.2 Research objectives

Earthen construction was used since ancient times but was ignored for several years due to emerging technologies. However, these materials are grasping interest and new studies are recently being focused on different aspects of earthen constructions, including the seismic, thermal behavior, and mechanical performance. This study aims to develop self-consolidating earth concrete (SCEC) incorporating limited content of cement. SCEC can facilitate the casting process and reduce the time consuming and labor-intensive issues of earthen constructions. Moreover, in the case of conventional RE, the lower layers can be more compacted compared to the higher ones due to different compaction conditions in each layer. Moreover, there will be deficiencies and crack propagation in the interfaces between the layers, leading to failure of the RE elements. Developing a highly flowable earth concrete (i.e., SCEC) can resolve the disadvantages related to the layer-by-layer compaction method.

The proposed approach in this study consists of combining earth, cement, water, and dispersing agent to develop SCEC and explore potential benefit of using earthen materials in construction. Three important challenges must be taken into consideration to develop a durable SCEC mixture, including:

1) Deflocculation of materials to achieve a flowable concrete SCEC (the process of making a clay slurry) due to the presence of fine clay particles;

2) Adequate control of the setting time of SCEC to speed-up the formwork removal;

3) Develop a guideline to select the appropriate earth type among the existing diverse earth types depending on their extracted local which hinders achieving a conventional mixture proportioning.

In this study, the SCEC mixtures were first optimized by considering their corresponding paste mixtures in terms of workability properties and mechanical performance. This approach allowed to investigate a wide variety of ternary powder systems, including clay, silt, and cement. The study was then extended on concrete scale to optimize and control the effect of the key influencing parameters as identified in the phase carried out on the paste scale. Multiscale rheology investigation was then conducted to establish meaningful correlations between different mixture parameters and properties at different scales (paste, CEM and concrete). The hygrothermal properties of the optimized SECE mixtures were then evaluated with respect to their microstructures. The advantages of incorporating earthen materials in SCEC to achieve superior hygrothermal performance compared to conventional concrete is highlighted.

1.3 Scientific contribution and originality

The results of this experimental study represented a step towards the incorporation of earthen materials in concrete to achieve SCEC as a novel and sustainable construction method to reduce the cost and negative environmental impacts. These materials can be used as building envelopes with superior thermal performance and relative humidity regulator. The experimental approach conducted in this study can be used as a comprehensive guideline for designing SCEC with adapted performance. Different dispersing agents and earth types were used in this study to investigate the compatibility between fine constituents and the admixture types. This led to a comparative study on workability and compressive strength of the corresponding paste mixtures of SCEC to identify the optimum levels of the influencing factors. It is worthy to mention that Atterberg limits [13] are the key parameters to be assigned for the earth type. The investigation was extended on a new concrete-equivalent mortar (CEM) and concrete mixtures as well. This can save time and energy to predict the workability, compressive strength, and drying shrinkage of SCEC mixtures from those of the CEM and paste mixtures. Rheological parameters, including yield stress, plastic viscosity, and thixotropy, are evaluated at different multiscale. Finally, the hygrothermal and microstructural properties of the optimized SCEC mixtures were characterized. The obtained properties confirm the advantages of the incorporation of earthen materials in concrete (i.e., SCEC). This can lead to new building materials with satisfying hygrothermal performance and adequate mechanical performance.

1.4 Outline of the thesis

This thesis is organized into 8 chapters that can be summarized, as follows:

Chapter 1 presents an overview of the project contexts and research problems, followed by the objectives of the research activities carried out in this study. The major scientific contributions and originality of this study are presented in this chapter as well.

Chapter 2 provides a comprehensive literature review on the topic. The advantages and disadvantages of earthen materials are discussed. Introduction of SCEC is discussed with its potential challenges and the recent studies on each one.

Chapter 3 presents a summary of the methodologies employed in this study, including the testing methods. This chapter is an introduction of the following chapters in the study concerning the objectives mentioned in Chapter 1.

Chapter 4 provides a comprehensive study on self-consolidating earth paste (SCEP) mixtures. The workability and compressive strength of the SCEP mixtures with their novel ternary powder system (i.e., clay, silt, and cement) are investigated. The Taguchi method is applied to highlight the effect and significance of the key mixture parameters on the investigated properties. Finally, a new approach is proposed to design SCEP mixtures with targeted workability and compressive strength values.

Chapter 5 extends the study on mortar and SCEC scales. A new concrete-equivalent mortar based on the excess paste thickness theory is proposed to predict workability, compressive strength, and drying shrinkage of SCEC. This multiscale investigation facilitates the designing procedure of SCEC with adapted properties. Furthermore, the significance of each influencing parameters introduced in Chapter 4 is investigated to find meaningful relationships between the different investigated properties.

Chapter 6 deals with the rheology of paste, CEM, and SCEC mixtures. Initially, the contribution of each influencing parameter on yield stress and plastic viscosity values is investigated. Secondly,

prediction of rheological parameters from the workability values are evaluated, followed by establishing relationships between different scales.

Chapter 7 introduces the experiments carried out to investigate the hygrothermal and microstructural characterization of three optimized SCEC mixtures and a reference SCC mixture (with no clay and silt). This chapter evaluates the hygrothermal advantages of incorporating earthen materials in SCEC. Furthermore, pores distributions of the investigated mixtures are considered as a key factor to identify their correlations with water vapor and gas permeability, compressive strength, and drying shrinkage.

Chapter 8 provides a summary of the main findings obtained in the study. Furthermore, perspectives for future work are presented in this chapter.

It is important to mention that Chapters 4-7correspond to the four research papers published or submitted for possible publications. Chapter 4 includes a scientific article published in Construction and Building Materials journal. This article is entitled “A new approach for proportioning self-consolidating earth paste (SCEP) using the Taguchi method” which was published in 2022. The findings of this paper helped the optimization and control of designing SCEP through a comprehensive designing approach. Chapter 5 corresponds to the second scientific paper (Multiscale investigation of self-consolidating earthen materials using a novel concrete-equivalent mortar approach) submitted to Construction and Building Materials journal. This paper aimed on extending the findings of Chapter 4 at the new CEM approach and SCEC scales. This approach can be helpful for designing SCEC using the corresponding paste and CEM mixtures. Chapter 6 investigates the rheology of multiscale SCEC mixtures, and the findings were submitted for possible publication in the Powder Technology journal. The submitted paper is entitled “New insight on rheology of self-consolidating earth concrete (SCEC)”. This chapter offers an optimization procedure of the rheology of SCEC mixtures. Chapter 7 includes a comparative hygrothermal study entitled “Hygrothermal and microstructural characterization of self-consolidating earth concrete (SCEC)”, submitted to Journal of Building Engineering. This chapter highlights the hygrothermal performance of SCEC mixtures compared to other building envelopes to evaluate the effect of incorporating earthen materials in SCEC.

REFERENCES

[1] F. Pacheco-Torgal, S. Jalali, Earth construction: Lessons from the past for future eco-efficient construction, Constr. Build. Mater. 29 (2012) 512–519. https://doi.org/10.1016/j.conbuildmat.2011.10.054.

[2] International Energy Agency, The Reduction of Greenhouse Gas Emissions From The Cement Industry, Report PH3/7, Paris, France, 1999.

[3] A. Coelho, Preliminary study for self-sufficiency of construction materials in a Portuguese region - Évora, J. Clean. Prod. 112 (2016) 771–786. https://doi.org/10.1016/j.jclepro.2015.06.113.

[4] P.G. McHenry, Adobe and Rammed Earth Buildings: Design and Construction, University of Arizona Press, Arizona, 1989.

[5] R. Bahar, M. Benazzoug, S. Kenai, Performance of compacted cement-stabilised soil, Cem. Concr. Compos. 26 (2004) 811–820. https://doi.org/10.1016/j.cemconcomp.2004.01.003.

[6] M. Hall, Y. Djerbib, Rammed earth sample production: Context, recommendations and consistency, Constr. Build. Mater. 18 (2004) 281–286. https://doi.org/10.1016/j.conbuildmat.2003.11.001.

[7] B. V. Venkatarama Reddy, P. Prasanna Kumar, Embodied energy in cement stabilised rammed earth walls, Energy Build. 42 (2010) 380–385. https://doi.org/10.1016/j.enbuild.2009.10.005.

[8] M. Zami, A. Lee, Stabilised or un-stabilised earth construction for contemporary urban housing?, in: 5th Int. Conf. Responsive Manuf. 'Green Manuf., China, 2010: pp. 11–13.

[9] L. Miccoli, U. Müller, P. Fontana, Mechanical behaviour of earthen materials: A comparison between earth block masonry, rammed earth and cob, Constr. Build. Mater. 61 (2014) 327–339. https://doi.org/10.1016/j.conbuildmat.2014.03.009.

[10] Z. Rao, S. Wang, Z. Zhang, Energy saving latent heat storage and environmental friendly humidity-controlled materials for indoor climate, Renew. Sustain. Energy Rev. 16 (2012) 3136–3145.

[11] P. Wargocki, D. Wyon, Y. Baik, G. Clausen, P. Fanger, Perceived air quality, sick building syndrome (SBS) symptoms and productivity in an office with two different pollution loads, Indoor Air. 9 (1999) 165–179.

[12] L.F. Dutra, Development of an innovative material of high hygrothermal performance, Université Grenoble Alpes, 2005.

[13] ASTM D4318 − 17, Standard Test Methods for Liquid Limit, Plastic Limit, and Plasticity Index of Soils, ASTM Stand. (2017).

CHAPTER 2. Literature review "Assessment of earthen materials in self-consolidating earth concrete (SCEC): A critical review and perspective"

Authors and affiliations

Mojtaba Kohandelnia: Ph.D. candidate, Cement and Concrete Research Group, Department of Civil and Building Engineering, Université de Sherbrooke, Sherbrooke, Québec, Canada, J1K 2R1.

Masoud Hosseinpoor: Post-Doc, Cement and Concrete Research Group, Department of Civil and Building Engineering, Université de Sherbrooke, Sherbrooke, Québec, Canada, J1K 2R1.

Ammar Yahia: Professor, Cement and Concrete Research Group, Department of Civil and Building Engineering, Université de Sherbrooke, Sherbrooke, Québec, Canada, J1K 2R1.

Rafik Belarbi: Professor, LaSIE UMR CNRS 7356, La Rochelle Université, La Rochelle, France.

Article Status: Submitted
Journal: Journal of Building Engineering - Elsevier
Initial date of submission: November 20th, 2022
Titre française: Évaluation des matériaux terreux dans le béton de terre autoplaçant (BTAP): Une revue critique et une perspective.

Abstract

The earthen construction has been used worldwide since ancient time. Recently, this technique is gaining more interest by researchers despite the rapid emerging of new construction materials, for addressing the recent environmental constraints. This paper reviews the recent development, advantages, and perspectives of this method of construction. Environmental, energy, and thermal performance are the most important advantages of earth construction. However, the main disadvantages of earthen construction include weak mechanical and seismic performance, as well as it time-consuming and labor-intensive construction process. Given the advantages of incorporating earthen materials, self-consolidating earth concrete (SCEC) can be a new alternative for faster construction. Accordingly, it is necessary to find out efficient solutions to improve the workability of the earthen mixtures containing fine clay particles. Depending on their type and content, dispersion of fine clay particles is challenging due to the possible incompatibilities with chemical admixtures in presence or absence of cement. The other challenge includes the promotion of setting and strength development, as an important criterion for formwork removal due to no/low cement content. Finally, providing a comprehensive guideline for proportioning of earth concrete mixtures is debatable due to diversity of soil types containing different particle size distribution, type and content of clay. The key characterization parameters of soil are recommended to be employed as criteria to design earth concrete with desired workability.

Keywords: Cement; Clay; Earth construction; Self-consolidating earth concrete (SCEC); Sustainable construction.

2.1 Introduction

Cement concrete is the most used construction material after water, due to its simplicity and versatility. As one the largest manufactured product on earth, cement is responsible for 5% of the world CO_2 emissions [1]. High energy demand and its effect on global warming and consumption of natural resource are the main negative environmental impacts of cement and concrete production [2]. Given the application in hand, the development and use of more sustainable construction materials and techniques are essential to reduce their environmental impact. Consequently, supplementary cementitious materials (SCMs) were involved in this industry for years to improve

the overall sustainability of construction and reduce CO_2 emission [3]. This is essential to preserve the natural resources and ecosystem while addressing the increasing construction demand. Earth-based materials are environmental-friendly due to their availability, both locally and quantitatively [4]. These materials have been used in various applications since ancient time, depending on the required mechanical performance [2].

Earthen materials can be classified into wattle and daub, cob, masonry adobe bricks, and rammed earth (RE) [5]. Although these construction materials were of the most common and widespread earth construction methods, their use has been significantly reduced in the first half of the 20th century because of the rapid emerging of new materials and construction techniques, including cement-based mortars and concrete [6]. Local availability of earth materials can significantly reduce the transportation costs. Other advantages of earthen construction include lower environmental impact and embodied energy, satisfying thermal performance, wider variety of textures, and finishing techniques, as well as appropriate performance with or without stabilization [7,8]. The use of earthen materials aims to limit the consumption of new manufactured resources and promote the usage of recycled and available local resources. Stabilization process by means of cement or lime is performed to increase mechanical performance and durability of earthen materials. Taking cement-stabilized rammed earth (CSRE) as an example, the energy consumption for construction and compaction is negligible compared to the energy required for cement production [9]. However, there are disadvantages regarding earthen materials, such as being labor-intensive and time-consuming (especially in the case of RE), and water sensitive, hence resulting in poor structural behavior.

Enhancing the productivity of earthen materials is essential to promote its wide use and take advantage of the low environmental impacts and superior hygrothermal characteristics. This study aims to highlight the advantages and limitations of earthen constructions. Furthermore, the state of the art of the potential of incorporating earthen materials in concrete is discussed. Finally, the challenges to achieve self-consolidating earth concrete (SCEC), as a novel generation of earth concrete are introduced to investigate the possibility to broaden this construction method.

2.2 Earth construction

Recently, there is an increasing interest in using earthen construction with improved performance to take advantage of its environmental impacts, energy aspects, and thermal performance. Rammed

earth (RE), as one of the most common types of earth construction, is also used in different regions worldwide to provide more architectural diversities. As can be observed in Fig. 2.1, the number of published documents in the area of RE and earth construction considerably increased during the last decade [10,11]. It can highlight the importance of green construction where more studies are focused on extending the application of these materials and discovering new potentials.

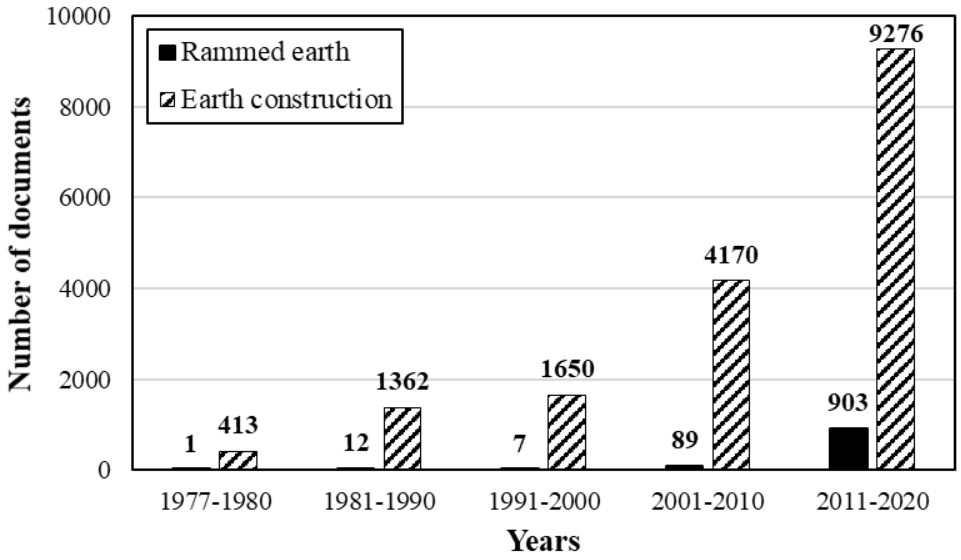

Fig. 2.1. Number of scientific publications since 1977 using keywords "rammed earth" and "earth construction" in Scopus, available by January 2020 [10,11].

A summary of the advantages and disadvantages of earthen materials (with a more focus on RE) discussed in this study are presented in Fig. 2.2. In next section, aiming to improve the workability of earth concrete mixtures, the potential application of the earthen materials is discussed. The workability-related challenges of the typical earth concrete mixtures are then addressed by introducing self-consolidating earth concrete (SCEC).

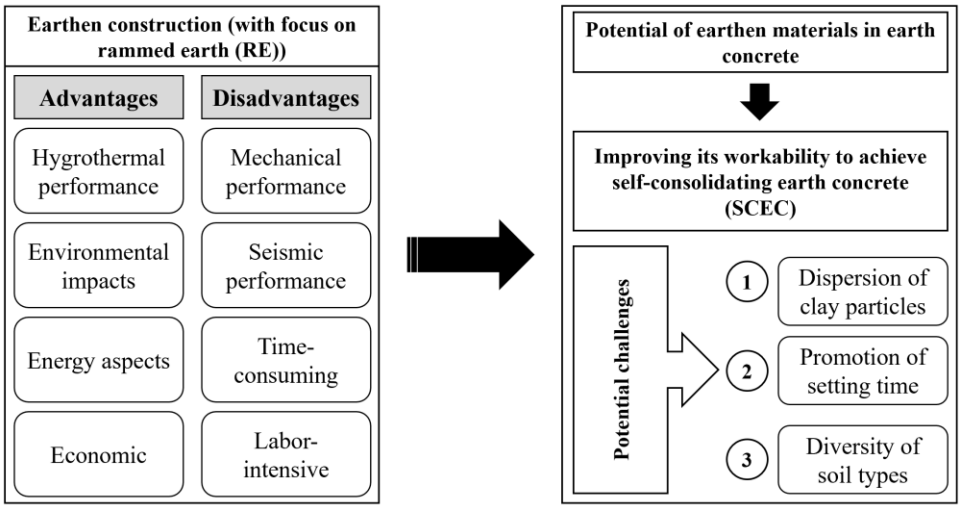

Fig. 2.2. The sequence of the review in this study: advantages and disadvantages of earthen construction, as well as introducing SCEC as an alternative solution.

2.2.1 Earth construction

Earth consists of clay, silt, sand, and gravel in an ascending order of size (depending on the classification scheme) from sub-μm to several mm [4]. It should be noted that particle-size distribution (PSD) of aggregate (sand and gravel) and fine powders (e.g., silt and clay) should be carefully selected using the sieve analysis, laser diffraction, and hydrometer analysis. Earthen materials, such as RE, were used unstabilized (URE), as damp earth [12], cement-stabilized (CSRE) [13], or stabilized with lime or other means [14]. The stabilization with lime is a traditional technique, more sustainable in comparison to those stabilized with cement [14]. Indeed, the strength of URE mostly originates from PSD and interlock of particles, type and content of clay as binder, and pore water suction. Gerard et al. [15] reported that water suction acts as an internal confining stress to URE, depending on the relative humidity and voids. The equilibrium between the pore air pressure u_a and pore water pressure u_w can lead to an additional stress, acting as an apparent cohesion ($s = u_a - u_w$) [16]. Cohesion increases with water suction, which is due to the development of additional capillary cohesion [17]. Also, the compaction procedure and drying period contribute to the strength development. Drying of the material also leads to higher strength as an unsaturated medium in which soil particles are surrounded by air and water [18]. However, in the case of CSRE, cement hydration process is the main source of strength development, which produces a solid matrix and binds the soil particles [19,20]. In lime-stabilized earth, the formation

of cementing agents, mainly the products of silica hydrates, are referred to the source of strength [21].

There is a wide variety of soils which can be used for earth construction. In general, high contents of sand and gravel in addition to silt and clay, as binders, are required [22]. In the case of RE, due to dynamic compaction, large particles are turned into smaller ones, thus a wide range of soils can be suitable [13]. Bahar et al. [7] reported that high percentage of large-size particles are suitable for RE. In some cases, recycled materials can also be used for earthen construction [23]. It should be noted that packing of particles should be highlighted to ensure higher density and strength. In the case of CSRE, the recommended cement content should be in the range of 4%–12%, and clay content (finer than 2 μm) between 5%–20% by mass of total solid particles [22]. Perera and Jayasinghe [24] recommended the content of fine constituents, including clay and silt, to be less than 30%, by mass, to achieve higher strength. Also, the authors reported a drastic decrease in strength in the case of fine content beyond 40%, by mass of the total solids. Regarding the earth composition, shrinkage is an important factor to be controlled. Sand particles were found to be effective to reduce the shrinkage-induced deformations [7]. On the other hand, the clay content is significantly important in terms of strength development and shrinkage. Bryan [25] recommended the use of low clay content to improve the compaction purposes, while limiting its content to reduce the shrinkage and ensure effective stabilization. Clay minerals available in earth significantly alter the swelling potential, from high potential in montmorillonite/bentonite to almost none in kaolinite [26]. This potential in earth compositions can dictate the shrinkage over time.

Due to diversity of earth composition in different regions, it is necessary to use other soil parameters to assess their suitability for earth construction. For RE application, high clay content leads to an unfavorably high plasticity of the soil. Based on the geotechnical aspects of soil, soil suitability for construction was reflected by its Atterberg limits [27]. These include the liquid limit (LL) and plasticity index (PI), which characterize the plasticity of soil. The LL and PI were recommended to be lower than 45% and 10%–30%, respectively [22]. Burroughs [28] reported that a soil with linear shrinkage (LS) and PI greater than 6% and 15%, respectively, has only low tendency to gain strength. Another parameter for determination of soil behavior is clay activity (A_c). This was defined as the ratio of PI-to-the percentage of clay particles finer than 2 μm and is dependent on the type of clay minerals. Different levels of clay activity are presented in Table 2.1.

It is worthy to mention that high A_c values are not favorable in earthen constructions [29], which can be related to the higher plasticity and, consequently, lower strength.

Table 2.1. Classification of different clay activity A_c values [30].

Clay type	A_c (PI / %clay)
Low activity	$A_c < 0.75$
Medium Activity	$0.75 < A_c < 1.25$
Active	$1.25 < A_c < 2.0$
High Activity	$A_c > 2.0$

One of the main defections of earth construction is sensitivity to water, leading to high plasticity resulted from clay fraction, hence not favorable for the strength development. At early ages, the curing process is highly important to minimize the shrinkage of cement stabilized soil. Jayasinghe and Kamaladasa [13] reported that shrinkage of cement-stabilized earth is significant in first four days, while it becomes slower in later ages. The quantity of fine constituents (i.e., clay and silt) should be also controlled to reduce shrinkage [31]. In the case of cement-stabilized earth, 28 days of curing at relative humidity of 95% and room temperature led to acceptable mature compressive strength values. However, the curing time can be extended between 7 to 60 weeks in the case of lime-stabilized earthen construction to reach maturity [32,33].

The most common applications of earth-based materials were found as building envelopes (one or two story). These sustainable materials can be also used as structural elements if the strength level is enhanced by stabilization yet keeping the low environmental impacts.

2.2.2 Drying process and reinforcement

As mentioned earlier, water sensitivity of earthen materials is considerable and drying can enhance their strength. Drying on sides of the walls was found to be faster, while it can take several years for the core of the walls. The speed of such hygroscopic transfer is mainly controlled by permeability. Drying of material can change the hygroscopic conditions and lead to further settlements. François et al. [34] reported that the plastic hinges, created in the wall, disappear when the wall is dry and, therefore, the wall behavior becomes more elastic. Hence, the age plays a positive role to enhance the stability of the earthen structure due to material drying. This can therefore contribute to enhance the durability of earth construction. Suction increases with age which leads to higher strength development. Furthermore, the interior side of the wall is less affected for water sensitivity compared to its exposed sides.

The use of reinforcement is not recommended for unstabilized earthen construction due to a lack of strong anchorage [35]. The service life of the reinforced elements depends on the initiation and propagation of corrosion. However, the high alkalinity of cement paste can protect the steel reinforcing bars from corrosion [36]. Meek et al. [37] reported that the pH of CSRE is able to provide appropriate environment for passivation of steel reinforcement. Similar to conventional concrete, the hydrated cement particles contribute to the alkalinity of the matrix. However, if the alkalinity decreases, the depassivation of steel is induced by carbonation or chlorides. The moisture content of earth constructions is thus responsible for the corrosion potential.

2.3 Advantages

Earthen materials can be great alternative for conventional cement concrete to reduce the environmental impacts of construction industry. This can contribute to reduce CO_2 emission of cement production, global warming, and natural resource consumption. The advantages of earthen materials are discussed in the following sections to assess their potential for other applications.

2.3.1 Hygrothermal performance

The deterioration of the materials and energy waste in building envelopes can be controlled by improving the hygrothermal behavior of the construction materials [38]. The improvement in the hygrothermal properties of the exterior envelopes can minimize the energy losses due to the heat flux. Thus, the indoor climate becomes highly efficient and provides more comfort for living conditions. Good thermal performance can also affect the energy consumption. The energy consumption is also minimized by good thermal performance of building envelopes [39].

2.3.1.1 Hygric performance

Moisture can play a significant role on energy efficiency due to its effect on the heat transfer of the building envelope. Protecting the wall from the moisture resources can decrease the thermal transmittance and provide less energy spent by the air-conditioning facilities. The buffering potential of earth materials assessed by moisture buffering value (MBV), defined as mass variation over moderate moistening cycles, has resulted in values higher than 1 which lies in good and excellent classification of moisture regulator [40]. As another critical hygric property, water vapor permeability is essential for characterization of moisture migration in building materials. Earth brick samples showed high permeability values, ranging from 1.45E-10 to 1.80E-10 $kg.s^{-1}.m^{-1}.Pa^{-1}$ [41]. Similarly, high permeability values were reported for RE [42] and light earth [43,44].

Another hygric parameter is the sorption isotherm of the building materials which determines the water content with respect to RH values. A hygroscopic material is capable of absorbing/desorbing moisture from/to surrounding atmosphere. This can lead to an attenuation of RH variations, hence improving living conditions. Hygroscopic materials can have a significant effect in regularizing the relative humidity and variations of the indoor air, the quality of air, and comfort of habitants [45]. Under high RH conditions, clay particles are capable to adsorb water vapor and release it when the humidity falls due to its hygroscopic properties. The highest sorption isotherm values correspond to the montmorillonite clays followed by illite and kaolinite [46]. This regulation performance of earth helps better indoor air quality compared to the industrial materials containing dangerous chemical materials, such as heavy metals. High humidity induces condensation and decay of materials, facilitated due to moisture accumulation, hence leading to fungal growth [42].

Regarding the moisture content as function of the RH, there is a hysteresis effect between the absorption and desorption isotherms, meaning that the desorption isotherm always gives a higher equilibrium moisture content than absorption for a given RH. The sorption capacity also changes with the age of the construction materials due to changes in their porosity. Temperature also has an influence on sorption isotherms, whereby higher temperature level results in a lower moisture content for a given RH. Different forms of moisture transport depend on the pore structure of the material and environmental conditions. Sorption capacity is linked to the porous structure of the material. A high porous structure, mainly composed of mesopores [47] and a wide specific area [48], similar as earth, may favor moisture buffer. This microstructural configuration leads to a material with low density and thermal conductivity.

In addition to the porous structure, other factors can also influence the buffering capacity, such as clay mineralogy. For example, kaolinite clay minerals show lower surface affinity and surface area than montmorillonite ones which exhibit higher surface area due to their active interlayer space [49]. Being exposed to different RH conditions, the moisture capacity of hygroscopic materials can change. However, the non-hygroscopic materials do not change their moisture content due to different environmental effects [38,50]. The ratio of hygroscopic water content-to-clay fraction for different clay minerals is defined as a constant, showing its lowest and highest values for kaolinite and montmorillonite, respectively [46].

Sources of moisture can be divided into exterior and interior sources. The exterior sources include precipitation, soil moisture, and groundwater. On the other hand, the interior sources can be the water vapor and leakage from the water network [51]. This is due to the building envelope which wastes more heating and cooling energy in the case of higher water contents in the walls and floors [38]. The moisture evolution is due to the high RH at the boundary conditions. Thermal conductivity is a function of temperature and water content and increases with temperature, water content, and density. Lower density materials thus induce a low thermal conductivity and provide better insulation.

2.3.1.2 Thermal performance

Thermal conductivity is a physical property of a material that characterizes its capacity to diffuse heat in the media without macroscopic displacement of matter. Thermal conductivity is affected by temperature, chemical compositions, porosity, humidity, and microstructure [52]. Since heat travels faster through water and moisture due to high conductivity of water than that of air (dry pores and voids in materials), thermal conductivity is a moisture dependent parameter.

Many studies were conducted on thermal characteristic of earth-based materials. Masonry walls with various insulating systems can provide high thermal mass which is concluded due to the fewer temperature fluctuations inside the residence, compared to other construction materials [53]. Lovec et al. [54] reported the low thermal conductivity of RE walls with high heat capacity and favorable thermal mass effect as the key element of thermal stability. According to the literature, the thermal conductivity of earthen constructions (RE or unfired earth) ranges from 650 to 1100 $mW.m^{-1}.K^{-1}$ [42,55–57]. It was also reported for a 60-cm thick cob wall to possess twice of the required thermal stability according to UK requirements for residence [58]. Straw and earth block masonry constructions were also chosen as an appropriate choice in UK based on their thermal performance [59–61]. Also, corn cobs showed adequate thermal properties [62]. Soebarto [63] reported comparable indoor temperatures for insulated and uninsulated RE in summer; however, the temperature in winter was 5°C lower in the latter. Giada et al. [40] reported that thermal conductivity of earthen materials increases with density, gaining the lowest values for light earth followed by adobe/cob/wattle and daub, and RE/compressed earth block with the highest values.

Thermal mass represents the ability of the material to keep its initial temperature when subjected to a temperature change and can reflect how long it takes for the material to reach a new

equilibrium. Thermal insulation and thermal mass increase with higher wall thickness. However, this is not the best solution since this can decrease the useable space and make the building vulnerable to seismic risks due to the higher mass. Materials with higher thermal mass values tend to transit heat slower. Soudani et al. [64] reported that temperature buffering and time lag (the difference of interior and exterior highest temperatures) increase with higher thermal mass values. Thermal diffusivity and effusivity properties are mainly used to quantify the thermal mass of a construction material as an indication of its ability to transmit temperature variations, and exchange energy with its surroundings and absorb heat, respectively. Finding a good combination of low diffusivity and high effusivity is an effective approach to improve the thermal performance of a material. It is worthy to mention that the earth materials, either dry, wet, or as solid brick, present both low diffusivity and high effusivity properties [64]. This can confirm the high thermal mass of earthen materials. Various studies reported that high thermal mass properties can avoid undesirable cold and hot temperatures during winter and summer seasons, respectively [65–67]. Interior temperature change is limited in different exterior conditions in the case of RE envelopes [64].

In a porous material, high RH can lead to the evolution of water in pores replacing the air. Due to significantly higher thermal conductivity of water compared to air, it is thus important to study the thermal conductivity as a function of RH. Water can act as a bridge linking grains and lead to higher heat conduction. Therefore, there is a positive correlation between the thermal effusivity and moisture in soils [68]. Heat capacity of water is also much higher than that of the air. More attention must be then paid to the water sources in the building construction materials, where higher heating and cooling energy are wasted from the walls and floors depending on their water contents. However, the formation of microcracks in the material can decrease its thermal conductivity [69].

2.3.2 Environmental impacts

Building and construction industry is responsible for over 30% of the extracted resources and 48% of the energy-related CO_2 emissions [70]. Re-consumption of construction materials can reduce a significant proportion of this waste. Earthen materials have shown an emerging possibility to integrate them into a circular cycle. Most conventional building systems, such as concrete, aluminum, steel, and glass are industrially-based materials with high embodied energy and disastrous environmental impacts [71]. However, Cabeza et al. [72] reported the best performance-based level of embodied energy and CO_2 emission for timber and earthen materials. Partially reduction of cement by low environmental impact materials can significantly reduce the negative

environmental impacts of the construction industry. The life cycle assessment (LCA) can be successfully used to analyze the environmental performance of the entire life cycle of a product or a process [73]. In fact, LCA allows a balance for the usage of material and energy and leads to evaluate the overall environmental impacts [74]. The lower environmental impacts of URE compared to stabilized RE proved the significant advantage of earth-based materials regarding ecosystem, human health, and resources [75]. Using local earth, as well as adding a low content of stabilizer (e.g. cement) can contribute to low values of embodied carbon (kg $CO_{2\text{-}eq}/m^2$) and energy (MJ_{eq}/m^2) indicators [76].

Sustainable management of resources needs a new cycle of production which is a circular model of production, use, and recycling to prevent waste production and new resource consumption [77–79]. Earth and vernacular construction were proved to be used as alternatives to current building technologies. These construction techniques were used for centuries due to their locally available sources, low requirements for transportation from extraction to the construction site, low embodied energy, easier manufacturing processes, and reduced negative environmental impacts [76,80].

2.3.3 Energy aspects

Among the energy consumptions reported in EU and USA, buildings consume 20%–40% of total energy, exceeding the other major sectors including industrial and transportation energy consumption [81]. This corresponds to both embodied and maintenance energies which depend on the location conditions of the building. Locally available earth materials can thus significantly decrease these energy consumptions.

As discussed earlier, the construction systems mostly include materials with high embodied energy. However, RE construction consumes about 1% of the energy needed for conventional concrete construction and transportation, hence resulting in lower CO_2 emission [82]. Embodied energy in CSRE consists of the energy consumed during transportation, mixing, compaction, and cement production processes. The reduction in cement content used for stabilization significantly contributes to reduce this aspect. Venkatarama Reddy and Prasanna Kumar [9] indicated that compaction energy rises with clay content and dry density. Furthermore, the energy reported for compaction process is negligible in comparison with cement energy content. Therefore, it is preferable to determine the parameters affecting the strength instead of increasing cement content which is accounted for very high embodied energy. Increasing dry density (reduction in porosity)

and curing period, as well as fly ash and lime content can contribute to achieve higher compressive strength [83].

Fernandes et al. [84] studied the environmental performance of earthen materials. The authors carried out LCA of RE based on specific life cycle inventory values [84]. The study revealed that for lime stabilized RE, even using small percentages of lime, there is a high contribution to the environmental impacts and embodied energy compared to earthen materials. Moreover, the authors presented the possibility to recycle these materials in a circular loop [84]. It should be mentioned that addition of stabilizers can hinder the circular consumption of earthen materials.

2.3.4 Economic advantages

Using earth as a locally available material can reduce the cost of construction and improve local economies by using available materials and labor force [77]. Earth construction can also contribute to saving energy and cost related to air-conditioning systems, given its appropriate hygrothermal performance. Earth construction in parallel with insulators in different thicknesses allows good thermal performance and reduces the cost of cooling and heating energy [38]. This can thus be concluded that earth accounts for saving significant cost and energy in pre-construction, construction, and post-construction periods.

2.4 Disadvantages

Despite the various advantages of earthen construction, several disadvantages can be pointed out for earthen constructions (especially RE). For instant, the low mechanical and seismic performance of earthen materials [85] can limit their application. Moreover, the construction of RE (stabilized or unstabilized) is time-consuming and requires a lot of labor forces.

2.4.1 Mechanical properties

Earthen materials exhibit high and low strength values in dry and saturated states, respectively. De-cohesion of the earth occurs when it contains high water content. The earth contains a high content of sand and coarse-sized silt fractions [86], which can increase the de-cohesion process. On the other hand, hygroscopic condition exhibits a direct effect on mechanical performance of soil [87]. The impact of the hygroscopic conditions on the mechanical behavior of earthen construction is significant. Various experimental studies reported that partial drying of earth materials significantly increases their strength and stiffness [20,88]. It should be noted that all soils are not

suitable to achieve satisfying strength where compressive strength of optimized URE ranges from 0.5 to 2.5 MPa [89,90]. Therefore, stabilization with cement or lime was considered to enhance the strength and reduce the tendency to swelling, shrinkage, and cracking [91,92]. It should be noted that cement is a good stabilizer when there is more content of sand and gravel, while soils with more silt and clay should be stabilized with hydrated and natural lime [91].

Dao et al. [93] reported that addition of cement to clayey soil in adobe resulted in formation of calcite, C–S–H, and ettringite which are resistant to water erosion by increasing the compressive strength. However, thermal conductivity decreased by addition of 2% and 4% of cement (by mass), while increased with more cement content. This can highlight the microstructural effect with addition of cement. Van Damme and Houben [4] reported that cement-stabilized bricks, RE, and clay concrete do not seem to be efficient since they require 9, 7, and 3 times of the cement content in high performance concrete to obtain 1 MPa compressive strength, respectively. Therefore, cement stabilization does not seem to be the most appropriate approach in earthen materials, except the applications which do not require high strength values. Achieving the optimum strength should be important by other means, such as packing of the granular skeleton. As reported by Jayasinghe et al. [23], different constituents ratios were used to achieve the optimum compressive strength values.

Strength characteristics of earth composites should also be considered due to their sensitivity to water. Using triaxial tests, Jaquin et al. [20] reported that a decrease in water content induces an increase in strength and stiffness. Therefore, wet strength is an important factor to be considered for earth-based materials. Heathcote [94] indicated that the ratio of wet-to-dry strength of earth-based materials is an index of durability. Accordingly, a ratio of 0.33 to 0.50 can be appropriate due to the rainfall.

The nature of compaction in RE leads to better performance compared to other earth-based materials. Miccoli et al. [86] investigated the behavior of stress-strain curves of earth block masonry, RE, and cob. As reported by the authors, RE showed the lowest ductility, but the highest stiffness and compressive strength compared to the other investigated materials [86]. Another problem in earthen construction is the difference of compressive strength and stiffness of rendering and substrate, which causes high tensions at their interface. Different thermal expansion may also lead to detachment of rendering [95,96]. Mateus et al. [95] concluded that in the case of RE

buildings, the compressive strength of the coatings is much higher than the substrate material, hence causing stresses at the interface. This can promote loss of adherence, cracking, and spalling of the coatings. As alternative, similar compositions as the existing coating can lead to better mechanical compatibility. Marais et al. [97] recommended that cement and polymer stabilized earth footings can be used as satisfactory foundations.

2.4.2 Seismic performance

Seismic performance of earth-based structural elements is significantly low, as frequently observed in some earthquakes around the world [98–100]. The mass of the wall supports dictates their seismic performance, induced by the vertical dead and live loads. On the other hand, this can lead to significantly high inertial stresses [101]. Morris and Walker [102] investigated the post-seismic performance of RE walls whereby only minor cracks were observed. This confirmed that RE buildings can outperform the predicted performance under seismic conditions. Bui et al. [103] indicated that two-story RE buildings can have satisfying in-plane earthquake behavior up to ground motions of 0.23 g, while one-story RE buildings can support motions until 0.32 g without any significant damages. The RE walls also showed more resistance to seismic loading than adobe masonry walls by 40% higher values [86]. Indeed, the RE walls act as a homogeneous material, in contrary to adobe masonry ones.

Ciancio et al. [14] reported that when the clay content of the earth is too low or the grain-size proportions are not optimal, lime can be added to the system to increase the strength and cohesiveness. The layered structure of RE influences the crack mechanism, but the mechanical behavior of RE does not seem to be distinctively anisotropic [104]. Silva et al. [105] reported that the seismic behavior of traditional RE case studies in Portugal benefits from many features. This can be due to the construction of buildings with no more than a single story (low rise buildings), with no complex plan, and having very thick walls. It seems that there are limited studies on more complex RE construction, especially in high seismic risk regions where more accurate design is required and various factors affecting the seismic response of the system must be considered.

The seismic behavior of RE buildings is still unknown and needs more investigations. The RE does not seem favorable under earthquake due to their low compression behavior, very low tensile strength, and high inertial forces (due to their high thickness). However, based on several post-seismic studies, RE walls showed acceptable behaviors [89,90,102,106]. A low height-to-thickness

ratio can improve the out-of-plane performance of RE walls and guarantee that adequate seismic performance can be achieved by appropriate designs of such buildings.

2.4.3 Time-consuming and labor-intensive

The layer-by-layer compaction method in RE construction is very time consuming and labor intensive. This can be favorable in regions where work force is not expensive. However, this construction technique can be challenging in developed countries due to high cost of labor force. Moreover, crack propagation can be induced between successive layers. Considering these drawbacks, a highly flowable vertical earth concrete element with adequate thermal and environmental advantages can be a promising solution to replace traditional RE.

2.5 SCEC: new generation of earth concrete

Development of new construction techniques with earth-based materials, yet keeping their advantages, should be further investigated to benefit from these natural resources. Self-consolidating earth concrete (SCEC) can be considered as one of these new generation materials to produce construction elements by merging the knowledge on both SCC and earthen materials. Few studies have addressed this new technique in the last few years [107–109]. SCEC brings the feasibility to cast the material into the formworks rather than the layer-by-layer compaction by means of mechanical consolidation, increasing the quality of the final product, reducing costs and construction time, and contributing to competitive advantages of earth. This technology can be employed on several earth construction methods, such as RE and adobe. Earth consists of fine clay and silt particles which forms the ternary binder system of SCEC, in addition to cement as the stabilizer of the whole system [107,110].

It is well known that SCC needs more considerations compared to the conventional concrete to gain its benefits in terms of elimination of external and internal vibration, higher flowability, passing ability, and pumpability. Aïsson et al. [111] reported that rheology, stability, and compressive strength of SCC is significantly affected by packing density and quantity of fine particles. Moreover, plastic viscosity and yield stress of mortar matrix, which is the suspending phase, increased with fine content, hence leading to higher interparticle friction. This results also in better stability resistance [112,113], but higher flowability loss. As summarized in Table 2.2, earthen materials provide satisfying hygrothermal performance with low environmental impacts. However, their incorporation in SCEC is debatable due to the high impact of cement and chemical

admixtures and their new microstructures. Moreover, SCEC mixtures should be further investigated to identify the main influencing parameters on their shrinkage, rheology, and mechanical performance. Three main challenges to achieve SCEC are introduced and further discussed in the following sections.

Table 2.2. Comparison between the performance of earthen materials and SCEC.

Characteristics	Earthen materials (RE and adobe)	SCEC
Hygrothermal performance	Various studies confirm their satisfying performance [54,58,62]	Requires more research (due to the microstructural change)
Environmental impacts	Using locally natural materials with low impacts and embodied energy [76,80]	Requires more research (stabilizers and admixtures can significantly affect)
Mechanical performance	Dependent on the packing and stabilization [4,23]	Dependent on various parameters which needs to be considered
Time-consuming and labor-intensive	Yes	No
Layer-by-layer deficiencies	Yes	No
Complex architectural limitations	Yes	No
Shrinkage control	Controlled mostly by clay fraction (due to their sensitivity to water) [25,31]	Requires more research
Rheology	Not critical	Requires more research
Dispersion of clay particles	Not critical	Challenge I – nucleation of fine particles and physico-chemical interaction between clay and chemical admixtures
Formwork removal	Drying with passing time [20,88]	Challenge II – promotion of setting time
Mix proportioning	PSD and plasticity [22,28]	Challenge III – representative soil parameters

2.5.1 Challenge I – Dispersion of clay particles

As discussed earlier, clay consists in very fine particles with significantly higher specific surface area (SSA) compared to cements used in conventional SCC. Due to the presence of different clay types and contents in earth-based materials, achieving an earth concrete with self-consolidating properties (i.e., SCEC) is challenging. High SSA, water absorption, nucleation promotion, and the flocculation of fine particles can hinder reaching to desired flowability of SCC [114]. Indeed, deflocculation of clay particles required to allow higher flowability and achieve SCEC is tricky with their questionable compatibility with chemical admixtures in terms of colloidal interactions and adhesion depending on mineralogy and content of clay. Most of the recent studies on earthen construction is focused on their environmental impacts, architectural aspects, hygrothermal,

mechanical, and durability performance, while their physico-chemical interaction with admixtures is limited to few studies and still not well-known [115].

Fig. 2.3 presents different clay minerals available in earth acting as binder with high swelling capacity which should be controlled to avoid any hazardous failure. Among the common types of clay minerals, including kaolinite, montmorillonite, and illite, kaolinite has a 1:1 layer structure, one with aluminate groups and another one with silicate groups linked by hydrogen bonding. These bonding forces result in non-swelling properties of kaolinite [116]. However, kaolinite can easily disperse and migrate. Contrarily, structure of montmorillonite is 2:1 leading to a high degree of swelling. On the other hand, illite (with 2:1 structure) consists in a crystal structure balanced by potassium bonding between the layers. This type of bonding can result in lower and higher swelling capacity compared to montmorillonite and kaolinite, respectively [117]. Cation-exchange capacity (CEC) is the other factor referred to the quantity of cations retained on the surface of particles, available to be exchanged with other cations at a given pH. CEC and SSA of different clay minerals are summarized in Table 2.3. It can be concluded that content and type of clay, reflected by their CEC and SSA, can control the performance of earth concrete based on their synergy with the dispersing agents.

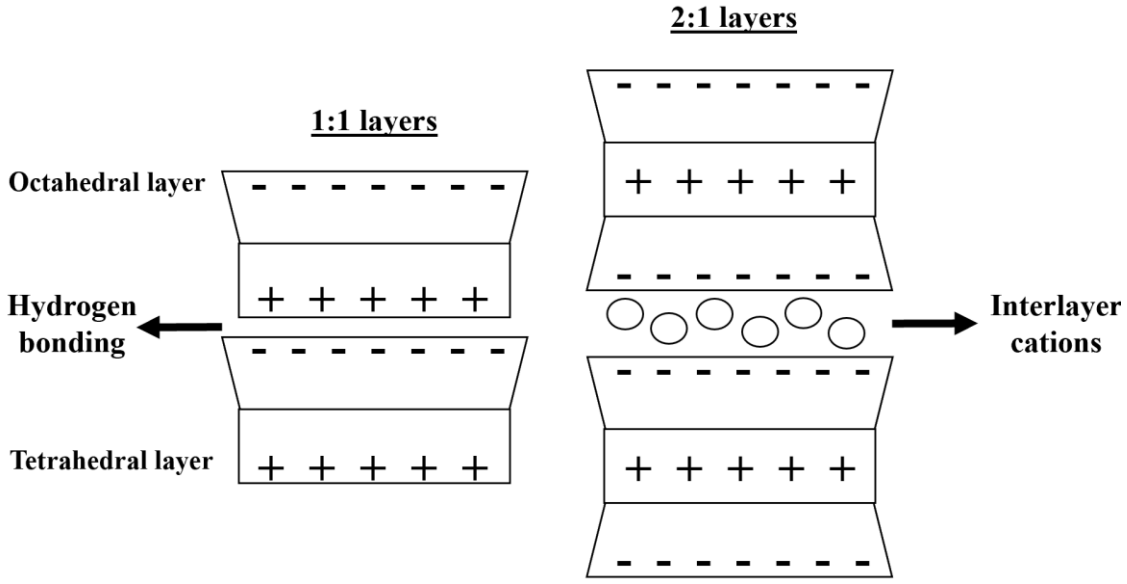

Fig. 2.3. The schematic structures of different types of clay minerals.

Table 2.3. Cation-exchange capacity and specific surface area of clay minerals [26]

Mineral	Cation exchange capacity at pH 7 (milliequivalents per 100 grams)	Specific surface area (m^2/g)
Kaolinite	3–15	5–40
Halloysite (hydrated)	40–50	1,100*
Illite	10–40	10–100
Chlorite	10–40	10–55
Vermiculite	100–150	760*
Smectite	80–120	40–800
Palygorskite-sepiolite	3–20	40–180
Allophane	30–135	2,200
Imogolite	20–30	1,540

*Depending on the fraction of internal specific surface area.

Accordingly, compatibility of different chemical admixtures with physical and chemical compositions of clay in earth is still ambiguous to achieve SCEC. Ouellet-Plamondon et al. [107] introduced a self-compacting clay-based concrete (SCCC). The authors reported that polycarboxylate ether-based superplasticizers (PCE), as high-range water-reducer (HRWR) agent, has significant effect on decreasing yield stress of the mixtures containing low amount of cement, hence improving its deformability. In addition to PCE which is efficient to disperse the ternary binder system of SCEC, among different commonly used deflocculants, sodium hexametaphosphate $(NaPO_3)_6$ exhibited a significant dispersion effect on natural clay materials. The dispersants used in cement and ceramic industries can change the surface interaction of clay particles. Their compositions cause the adsorption of phosphate anions, which consequently increase the overall negative surface charge and alkalinity of earth cations (replacing them with Na^+ cations) [118–121]. Sodium silicate (Na_2SiO_3) was also widely used to disperse raw clay and kaolin. It was also shown to be efficient as a deflocculant leading to increase the thickness of the layers, accompanying with an increase in the pH of the solution [122–124].

Landrou et al. [109] studied flowable earth without incorporation of cement. The authors used sodium hexametaphosphate (NaHMP) and sodium silicate (NaSil) as dispersant deflocculating the clay particles by creating interparticle repulsive forces [109]. The dispersants showed a positive effect to enhance the flowability of earth material. However, PCE did not contribute in decreasing yield stress without presence of cement which can be due to adsorption of PCE chains between the aluminosilicate layers, hence eliminating their dispersibility [125,126]. Zeta potential confirmed the repulsive interaction between clay particles with dispersing agents. This confirms that PCE causes only minor changes due to their dispersing capability through the steric hindrance, while

the other dispersant induces dispersing through the electrostatic repulsion [127]. By knowing the efficiency of dispersing agents on clay particles, and PCE on cement particles, more investigations are necessary to understand the behavior of ternary binder system of SCEC. The comparison of different dispersants and HRWR agents in terms of their efficiency and synergy to affect workability and rheology of SCEC needs to be further investigated. Furthermore, LCA can be applied to assess the impacts of used chemical admixtures with significant environmental impacts.

2.5.2 Challenge II – Promotion of setting time

Due to the low amount of cement, a packed aggregate skeleton can lead to higher compressive strength of the mixture. Early and late compressive strength developments of SCEC are key factors influencing the demolding timeline and ensuring durability, respectively. Several studies were carried out to use other materials along with earth (e.g., coagulants) to accelerate the formwork removal. Landrou et al. [109] investigated the efficiency of calcium products (calcium hydroxide ($Ca(OH)_2$), calcium carbonate ($CaCO_3$), and calcium chloride ($CaCl_2$)) on earth materials, dispersed with clay dispersants. Different Ca^{2+} release rates can precipitate in C–S–H formation in presence of dispersing agents by an anti-plasticity effect. According to Landrou et al. [109], the addition of calcium products (especially $Ca(OH)_2$) in mixtures dispersed with NaHMP and NaSil increased the storage modulus of the earthen suspensions with time. The SEM images revealed that the combination of NaSil and $Ca(OH)_2$ resulted in large plates of calcium hydroxide crystals and typical needles of C–S–H after 3 and 180 min, respectively. Another solution for fast demolding is using the gelling agents, such as Alginate [128–130]. Alginate is referred to alginic salts as seaweed biopolymers. The chains of alginate form a connection by intercalating divalent cations [131], hence increasing the mechanical performance and resistance of the earth depending on their interaction with clay particles.

SCCC proposed by Ouellet-Plamondon et al. [107] was proportioned using a calcium sulfoaluminate cement (CSA) which exhibited early setting time. This was related to the CSA potential to promote high early-age strength [132]. These mixtures were cast without applying any external mechanical consolidation, and then demolded within 24 hours. The mixture containing 5% CSA achieved compressive strength of 1 MPa after 6 hours of age, which is adequate for formwork removal. It can emphasize the significance of water reduction on strength development by means of using HRWR admixtures. It should be noted that using cement or other coagulants cannot be in favor of low environmental impact of earth-based materials. Therefore, the

comparison of the efficiency of available approaches to promote setting time should be further investigated considering their environmental impacts.

2.5.3 Challenge III – Representative soil parameters due to diversity of soil types

Earth is a mix of particles with different shapes, sizes, and mineralogical natures [4]. The difference of mineralogical composition from one extraction site to another can result in variable performance for earthen materials. Therefore, predicting the behavior of a specific earth is very difficult due to the complexity of the materials and numerous variables to be considered [133]. Compatibility of the admixture with clay is tricky due to mineralogy and high SSA of clay particles. Different clay minerals possess SSA of 50 to 1000 times higher than cement particles. Therefore, designing SCEC mixtures should take into account the clay contribution in the soil behavior. Based on the diversity of soils on earth, it is important to select soils with proper properties and clay content and type. It is also important to select aggregate skeleton with optimum PSD. In addition, soil characteristics can be used as key designing parameters to achieve the targeted flow performance of SCEC.

PSD, clay activity, and Atterberg limits are the key representative soil parameters to be used in designing earth concrete. Atterberg limits, including liquid and plasticity limits, can define soil behavior in presence of water, which is critical in case of the performance of earth concrete. It is reported that plasticity index (PI) can be used as a basic soil characteristic because of its correlations with other soil properties [134]. Soil type, degree of plasticity, and degree of cohesiveness can be deduced from PI. Plasticity of soil is highly dependent on its clay type and content, as well as silt constituent. Skempton [135] reported that PI of a soil increases with the percentage of clay fraction. Moreover, Laskar and Pal [136] found that PI decreases for higher sand content, which can be due to decrease of the interparticle attraction forces. The authors also reported that there are correlations between Atterberg limits and strength parameters [136]. Voight [137] reported that residual shear strength of soil is dependent on its mineral composition. Atterberg limits can be used for classification of different soil types. These properties can however be altered by different mineralogical factors. Since these powders are acting as binder in SCEC, in addition to cement, plasticity of soil seems to be a proper representative soil parameter to be considered to achieve SCEC in presence of various chemical admixtures.

The influencing parameters on performance of SCEC, as well as recommended considerations for designing SCEC are summarized in

Table **2.4**. The first influencing factor is clay type and content which can result in different soil characterization parameters to be assessed. As reported by Ciancio et al. [12], LL < 45% and PI < 30% is recommended as a performance requirement for earth buildings, including RE. Higher Atterberg limits seems to be problematic for workability means. The second parameter includes the type and content of cement used to promote setting time and control the durability. Cement contents higher than 200 kg/m^3 can result in high environmental impacts which hinders the sustainability of this method. The third parameter is admixture type which allows dispersion of ternary binder system of SCEC with different synergies. Paste volume is the next key parameter which should be considered since it affects rheological behavior, workability, shrinkage, and mechanical performance of SCEC. Assuming the presence of considerable fine content (i.e., clay and silt) in earth, next to cement and water in paste results in a higher paste volume than conventional SCC. By the recommended ranges for earthen construction in literature [12], paste volume exceeds 45%. Optimization of rheological properties of the paste matrix in SCEC, consisting in water and ternary binder system of earth concrete, is also of high importance to achieve SCEC with satisfying workability. Water-to-binder ratio (W/B) also affects the rheology, by controlling the solid fraction, synergy of the admixtures, and strength of SCEC. Using a compatible dispersing agent with W/B ratios of less than 0.5 can ensure the required workability of a stable SCEC [107,109]. The packing condition of granular skeleton should be also taken into account as one of the main influencing factors. An optimum packing density of aggregate can result in lower required paste volume and, consequently, lower binder content to achieve the targeted workability [138,139]. Furthermore, lower interparticle voids in a packed aggregate skeleton decreases the water demand and, therefore, contribute in achieving higher compressive strength [140,141]. Sand plays a significant role in the constituents of earth and the recommended sand-to-total aggregate ratio between 0.5 to 0.9 can guarantee the higher sand fraction in earth. By taking into account these influencing parameters on workability, mechanical properties, and durability of SCEC, a practical guideline can be suggested based on compatibility of admixtures with ternary binder system of SCEC considering the soil characteristics.

Table 2.4. Influencing parameters and recommended considerations to design SCEC.

Influencing parameters	Contribution	Recommended considerations
1. Clay type/content	To evaluate different soil representative parameters	Desirability based on defining higher Atterberg limits and specific surface area (LL < 45% and PI < 30%)
2. Cement type/content	To promote setting time and controlling durability	Low enough to maintain the low environmental impact (< 200 kg/m^3)
3. Chemical admixture type/dosage	Comparative study to evaluate compatibility of dispersing agents with ternary binder system	Considering the synergy on workability, workability loss and rheological behavior
4. Paste volume (V_P)	To assess the effect on rheology, workability, shrinkage, and mechanical performance	Higher than typical SCC due to the presence of ternary binder system (> 45%)
5. Water-to-binder ratio (W/B)	To investigate the effect of water and solid fraction	Low enough to gain higher strength (< 0.5)
6. Packing of the granular skeleton	To minimize the paste volume and binder content	In the range of available earth types (0.5 < sand/total aggregate < 0.9)

2.6 Concluding remarks and perspectives

Green construction can be achieved by reducing the consumption of new industrial materials and increasing the use of recycled and locally available materials to proportion low-environmental and added-values materials, such as earth-based materials. The extensive overview undertaken in this study highlighted the recent developments and applications of earthen construction. This study revealed that earth construction is an environment-friendly material with various advantages in terms of thermal performance, energy efficiency, economical, and environmental aspects. Besides all the mentioned advantages of earth construction, disadvantages of this construction method were comprehensively addressed and discussed. Some of these limitations can be resolved by using new added-value materials and innovative construction technics, including self-consolidating earth concrete (SCEC) and exploring clay technology to ensure a better control of clay-admixtures compatibility. Soil types can be selected based on their PSD and Atterberg limits to achieve targeted workability and mechanical properties of SCEC. According to this review, further studies are required to broaden the application of this construction method with enhanced performance and durability, as follow:

- The high time and labor-intensive consumption are important factors hindering the wide use of earthen materials. By incorporating earthen materials in earth concrete, it is necessary to improve the workability, facilitate casting, and speed-up the construction process to promote the use of earthen materials as green, eco-friendly, and sustainable construction material.

- The content and type of clay play important roles in earth, since it can act as a binder in concrete. Different clay mineral types result in different hygric performance, swelling potential, and hindrance to achieve desired flowability due to their high specific surface area. Therefore, these should be controlled and exploited to develop flowable material.

- Cement content should be controlled for both setting purposes and minimizing the negative environment impacts. Therefore, cement content less than 200 kg/m^3 was recommended to be accompanied with optimization of other parameters, such as W/B and packing density of granular skeleton, to achieve desired compressive strength. It should be noted that W/B ratio should be limited to an upper level for strength purposes, and lower level to minimize the demand of dispersing agents due to their very high negative environmental impacts.

- The compatibility of chemical admixture with clay particles can dictate the feasibility of designing SCEC, while the optimization of other influencing parameters, including cement content/type, paste volume, W/B, and packing of granular skeleton, can expand the applications of this construction method to structural elements.

- Designing SCEC should be addressed based on different soil types due to existing diversity of earth. Soil parameters (especially Atterberg limits) which are affected by clay fraction showed great potential to represent a criterion for feasibility to achieve SCEC and control its workability. Since higher Atterberg limits result in higher demand of dispersing agents and lower strength values, LL and PI values lower than 50% and 25%, respectively, were recommended for SCEC application.

- SCEC, as a new generation of earthen concrete exhibits new microstructure and environmental impacts which need to be assessed. New microstructures can lead to different hygrothermal and mechanical performance rather than conventional SCC mixtures and other earthen constructions. High thermal mass of earthen materials can lead to superior hygrothermal performance of SCEC compared to typical SCC mixtures. Higher porosity and lower density of SCEC mixtures can guarantee lower thermal conductivity rather than conventional SCC mixtures.

2.7 Declaration of competing interest

The authors declare that they have no known competing financial interests or personal relationships that could have appeared to influence the work reported in this paper.

2.8 Acknowledgement

The authors wish to thank the financial support of the National Science and Engineering Research Council of Canada (NSERC) and the eight industrial partners participating in the NSERC Industrial Chair (IRC) on Development of Flowable Concrete with Adapted Rheology and Their Application in Concrete Infrastructures, held by Professor Ammar Yahia at the Université de Sherbrooke.

REFERENCES

[1] E.M. Gartner, D.E. MacPhee, A physico-chemical basis for novel cementitious binders, Cem. Concr. Res. 41 (2011) 736–749. https://doi.org/10.1016/J.CEMCONRES.2011.03.006.

[2] F. Pacheco-Torgal, S. Jalali, Earth construction: Lessons from the past for future eco-efficient construction, Constr. Build. Mater. 29 (2012) 512–519. https://doi.org/10.1016/j.conbuildmat.2011.10.054.

[3] A. Coelho, Preliminary study for self-sufficiency of construction materials in a Portuguese region - Évora, J. Clean. Prod. 112 (2016) 771–786. https://doi.org/10.1016/j.jclepro.2015.06.113.

[4] H. Van Damme, H. Houben, Earth concrete. Stabilization revisited, Cem. Concr. Res. 114 (2018) 90–102. https://doi.org/10.1016/J.CEMCONRES.2017.02.035.

[5] H. Guillaud, H. Houben, Earth Construction: A Comprehensive Guide, Intermediate Technology Publications, 1994.

[6] P.G. McHenry, Adobe and Rammed Earth Buildings: Design and Construction, University of Arizona Press, Arizona, 1989.

[7] R. Bahar, M. Benazzoug, S. Kenai, Performance of compacted cement-stabilised soil, Cem. Concr.

Compos. 26 (2004) 811–820. https://doi.org/10.1016/j.cemconcomp.2004.01.003.

[8] M. Hall, Y. Djerbib, Rammed earth sample production: Context, recommendations and consistency, Constr. Build. Mater. 18 (2004) 281–286. https://doi.org/10.1016/j.conbuildmat.2003.11.001.

[9] B. V. Venkatarama Reddy, P. Prasanna Kumar, Embodied energy in cement stabilised rammed earth walls, Energy Build. 42 (2010) 380–385. https://doi.org/10.1016/j.enbuild.2009.10.005.

[10] Scopus, No Title, (2020). https://www.scopus.com/term/analyzer.uri?sid=29f66bb7f639d24dbfe7e671c5b9506f&origin=resultslist&src=s&s=TITLE-ABS-KEY%28%22earth+construction%22%29&sort=plf-f&sdt=b&sot=b&sl=35&count=455&analyzeResults=Analyze+results&txGid=5123743fe19e63ec48f6f6749ba9a9 (accessed January 13, 2020).

[11] Scopus, No Title, (2020). https://www.scopus.com/term/analyzer.uri?sid=8023ce0aef93413dec6bd86d8bfa091e&origin=resultslist&src=s&s=TITLE-ABS-KEY%28rammed+earth%29&sort=plf-f&sdt=b&sot=b&sl=27&count=915&analyzeResults=Analyze+results&txGid=0ede15170a2facdf0275ed9ae33bdfc4 (accessed January 13, 2020).

[12] D. Ciancio, P. Jaquin, P. Walker, Advances on the assessment of soil suitability for rammed earth, Constr. Build. Mater. 42 (2013) 40–47. https://doi.org/10.1016/j.conbuildmat.2012.12.049.

[13] C. Jayasinghe, N. Kamaladasa, Compressive strength characteristics of cement stabilized rammed earth walls, Constr. Build. Mater. 21 (2007) 1971–1976. https://doi.org/10.1016/j.conbuildmat.2006.05.049.

[14] D. Ciancio, C.T.S. Beckett, J.A.H. Carraro, Optimum lime content identification for lime-stabilised rammed earth, Constr. Build. Mater. 53 (2014) 59–65. https://doi.org/10.1016/j.conbuildmat.2013.11.077.

[15] P. Gerard, M. Mahdad, A.R. Mccormack, B. François, A unified failure criterion for unstabilized rammed earth materials upon varying relative humidity conditions, Constr. Build. Mater. 95 (2015) 437–447. https://doi.org/10.1016/j.conbuildmat.2015.07.100.

[16] H. Nowamooz, C. Chazallon, Finite element modelling of a rammed earth wall, Constr. Build. Mater. 25 (2011) 2112–2121. https://doi.org/10.1016/j.conbuildmat.2010.11.021.

[17] P. Chauhan, A. El Hajjar, N. Prime, O. Plé, Unsaturated behavior of rammed earth : Experimentation towards numerical modelling, Constr. Build. Mater. 227 (2019) 116646. https://doi.org/10.1016/j.conbuildmat.2019.08.027.

[18] P. Delage, Experimental unsaturated soil mechanics. In: Proc 3rd Int Conf on unsaturated soils, in: Proc 3rd Int Conf Unsaturated Soils, Brazil, 2002: pp. 973–96.

[19] C.T.S. Beckett, C.E. Augarde, The effect of climate on the unconfined compressive strength of rammed earth, (2011).

[20] P.A. Jaquin, C. Augarde, D. Gallipoli, D.G. Toll, The strength of unstabilised rammed earth materials, Geotechnique. 59 (2009) 487–90.

[21] M.R. Thompson, Factors influencing the plasticity and strength of lime-soil mixtures, Tech. Rep. Bulletin 492, Engineering Experiment Station. University of Illinios, 1967.

[22] P. Walker, R. Keable, J. Martin, V. Maniatidis, Rammed earth: design and construction guidelines,

IHS BRE, 2005.

[23] C. Jayasinghe, W.M.C.D.J. Fonseka, Y.M. Abeygunawardhene, Load bearing properties of composite masonry constructed with recycled building demolition waste and cement stabilized rammed earth, Constr. Build. Mater. 102 (2016) 471–477. https://doi.org/10.1016/j.conbuildmat.2015.10.136.

[24] A. Perera, C. Jayasinghe, Strength Characteristics and Structural Design Methods for Compressed Earth Block Walls, Mason. Int. 16 (2003) 34–38.

[25] A.J. Bryan, Criteria for the Suitability of Soil for Cement Stabilization, 23 (1988) 309–319.

[26] N. Kumari, C. Mohan, Basics of Clay Minerals and Their Characteristic Properties, in: Clay Clay Miner., 2021.

[27] ASTM D4318 − 17, Standard Test Methods for Liquid Limit, Plastic Limit, and Plasticity Index of Soils, ASTM Stand. (2017).

[28] S. Burroughs, Soil property criteria for rammed earth stabilization, J. Mater. Civ. Eng. 20 (2008) 264–273. https://doi.org/10.1061/(ASCE)0899-1561(2008)20:3(264).

[29] F. Pacheco-Torgal, S. Jalali, Eco-efficient Construction and Building Materials, Springer Science & Business Media, 2011.

[30] P. Doat, A. Hays, H. Houben, S. Matuk, F. Vitoux, Construire en terre, Editions Alternative et Parallèles, France, 1979.

[31] R. Bahar, M. Benazzoung, S. Kenai, Performance of compacted cement stabilized soil, Cem. Concr. Compos. 26 (2004) 811–820.

[32] N. Consoli, P. Prietto, J. Carraro, K. Heineck, Behavior of Compacted Soil-Fly Ash-Carbide Lime Mixtures, J. Geotech. Geoenvironmental Eng. 127 (2001) 774–782.

[33] J. Croft, The problem in predicting the suitability of soils for cementitious stabilization, Eng. Geol. 2 (1968) 397–424.

[34] B. François, L. Palazon, P. Gerard, Structural behaviour of unstabilized rammed earth constructions submitted to hygroscopic conditions, Constr. Build. Mater. 155 (2017) 164–175. https://doi.org/10.1016/j.conbuildmat.2017.08.012.

[35] P.J. Walker, S. Dobson, Pullout Tests on Deformed and Plain Rebars in Cement-Stabilized Rammed Earth, J. Mater. Civ. Eng. 13 (2001) 291–297.

[36] K. Tuutti, Corrosion of steel in concrete, (1982).

[37] A.H. Meek, C.T.S. Beckett, M. Carsana, D. Ciancio, Corrosion protection of steel embedded in cement-stabilised rammed earth, Constr. Build. Mater. 187 (2018) 942–953. https://doi.org/10.1016/j.conbuildmat.2018.07.210.

[38] R.Y.M. Allam, The heat and moisture effect on the structures, La Rochelle University, 2018.

[39] O. Kaynakli, A review of the economical and optimum thermal insulation thickness for building applications, Renew. Sustain. Energy Rev. 16 (2012) 415–425.

[40] G. Giada, R. Caponetto, F. Nocera, Hygrothermal Properties of Raw Earth Materials: A Literature Review, Sustainability. 11 (2019). https://doi.org/doi:10.3390/su11195342.

[41] R. Allam, N. Issaadi, R. Belarbi, M. El-Meligy, A. Altahrany, Hygrothermal behavior for a clay

brick wall, Heat Mass Transf. 54 (2018) 1579–1591. https://doi.org/10.1007/s00231-017-2271-5.

[42] M. Hall, D. Allinson, Analysis of the hygrothermal functional properties of stabilised rammed earth materials, Build. Environ. 44 (2009) 1935–1942. https://doi.org/10.1016/J.BUILDENV.2009.01.007.

[43] F. Volhard, Light Earth Building: A Handbook for Building with Wood and Earth, Birkhauser, Basel, Switzerland, 2016.

[44] M. Labat, C. Magniont, N. Oudhof, J.E. Aubert, From the experimental characterization of the hygrothermal properties of straw-clay mixtures to the numerical assessment of their buffering potential, Build. Environ. 97 (2016) 69–81. https://doi.org/10.1016/J.BUILDENV.2015.12.004.

[45] M. Salonvaara, T. Ojanen, A. Holm, H.M. Künzel, A.N. Karagiozis, Moisture buffering effects on indoor air quality-experimental and simulation results, in: Proc. Build. IX, Clearwater, Florida, 2004.

[46] M.N. Wuddivira, D.A. Robinson, I. Lebron, L. Bréchet, M. Atwell, S. De Caires, M. Oatham, S.B. Jones, H. Abdu, A.K. Verma, M. Tuller, Estimation of soil clay content from hygroscopic water content measurements, Soil Sci. Soc. Am. J. 76 (2012) 1529–1535.

[47] M. Raimondo, M. Dondi, F. Mazzanti, P. Stefanizzi, P. Bondi, Equilibrium moisture content of clay bricks: The influence of the porous structure, Build. Environ. 42 (2007) 926–932.

[48] D.-H. Vu, K.-S. Wang, B.H. Bac, B.X. Nam, Humidity control materials prepared from diatomite and volcanic ash, Constr. Build. Mater. 38 (2013) 1066–1072.

[49] F. McGregor, A. Heath, A. Shea, M. Lawrence, The moisture buffering capacity of unfired clay masonry, Build. Environ. 82 (2014) 599–607.

[50] H. Hens, Building Physics-Heat, Air and Moisture, 2nd ed., Wilhelm Ernst & Sohn, 2007.

[51] J. Straube, E. Burnett, Review of modeling methods for building enclosure design, University of Waterloo, 1999.

[52] H. Zhang, Heat-insulating Materials and Sound-absorbing Materials, Build. Mater. Civ. Eng. (2011) 304–423. https://doi.org/10.1533/9781845699567.304.

[53] A. Tavil, Thermal behavior of masonry walls in Istanbul, Constr. Build. Mater. 18 (2004) 111–118. https://doi.org/10.1016/J.CONBUILDMAT.2003.08.014.

[54] V.B. LOVEC, M.Đ. JOVANOVIC–POPOVIC, B.D. ZIVKOVIC, The thermal behavior of rammed earth wall in traditional house in Vojvodina: Thermal mass as a key element for thermal comfort, Therm. Sci. (2018).

[55] M.L. Indekeu, M. Woloszyn, A.-C. Grillet, L. Soudani, A. Fabbri, Towards hygrothermal characterization of rammed earth with small-scale dynamic methods, Energy Procedia. 132 (2017) 297–302.

[56] D. Allinson, M. Hall, Hygrothermal analysis of a stabilised rammed earth test building in the UK, Energy Build. 42 (2010) 845–852. https://doi.org/10.1016/J.ENBUILD.2009.12.005.

[57] D. Medjelekh, L. Ulmet, F. Dubois, Characterization of hygrothermal transfers in the unfired earth, Energy Procedia. 139 (2017) 487–492. https://doi.org/10.1016/J.EGYPRO.2017.11.242.

[58] S. Goodhew, R. Griffiths, Sustainable earth walls to meet the building regulations, Energy Build. 37 (2005) 451–459. https://doi.org/10.1016/J.ENBUILD.2004.08.005.

[59] C. MacDougall, Natural Building Materials in Mainstream Construction: Lessons from the UK, J. Green Build. 3 (2008) 3–14.

[60] N. Desborough, S. Samant, Is straw a viable building material for housing in the United Kingdom? Sustainability 2009;2:., Sustainability. 2 (2009) 368–374.

[61] C. Williams, S. Goodhew, R. Griffiths, L. Watson, The feasibility of earth block masonry for building sustainable walling in the United Kingdom, J. Build. Apprais. 6 (2010) 99–108.

[62] J. Pinto, A. Paiva, H. Varum, A. Costa, D. Cruz, S. Pereira, L. Fernandes, P. Tavares, J. Agarwal, Corn's cob as a potential ecological thermal insulation material, Energy Build. 43 (2011) 1985–1990. https://doi.org/10.1016/J.ENBUILD.2011.04.004.

[63] V. Soebarto, ANALYSIS OF INDOOR PERFORMANCE OF HOUSES USING RAMMED EARTH WALLS, in: Elev. Int. IBPSA Conf., Glasgow, Scotland, n.d.

[64] L. Soudani, M. Woloszyn, A. Fabbri, J. Morel, A. Grillet, Energy evaluation of rammed earth walls using long term in-situ measurements, Sol. Energy. 141 (2017) 70–80. https://doi.org/10.1016/j.solener.2016.11.002.

[65] N. Aste, A. Angelotti, M. Buzzetti, The influence of the external walls thermal inertia on the energy performance of well insulated buildings, Energy Build. 41 (2009) 1181–1187. https://doi.org/10.1016/j.enbuild.2009.06.005.

[66] J.L. Fernandez, M.A. Porta-Gandara, N. Chargoy, Rapid on-site evaluation of thermal comfort through heatcapacity in buildings, Energy Build. 37 (2005) 1205–1211.

[67] P. Taylor, M.B. Luther, Evaluating rammed earth walls : a case study, Sol. Energy. 76 (2004) 79–84. https://doi.org/10.1016/j.solener.2003.08.026.

[68] M.A. Oladunjoye, O.A. Sanuade, Thermal Diffusivity, Thermal Effusivity and Specific Heat of Soils in Olorunsogo Powerplant, Southwestern Nigeria, Int. J. Res. Rev. Appl. Sci. 13 (2012) 502–521.

[69] D. Jougnot, A. Revil, Thermal conductivity of unsaturated clay-rocks, Hydrol. Earth Syst. Sci. 14 (2010) 91–98.

[70] M.K. Dixit, Life cycle recurrent embodied energy calculation of buildings: A review, J. Clean. Prod. 209 (2019) 731–754. https://doi.org/10.1016/J.JCLEPRO.2018.10.230.

[71] I.Z. Bribián, A.V. Capilla, A.A. Usón, Life cycle assessment of building materials: Comparative analysis of energy and environmental impacts and evaluation of the eco-efficiency improvement potential, Build. Environ. 46 (2011) 1133–1140. https://doi.org/10.1016/j.buildenv.2010.12.002.

[72] L.F. Cabeza, C. Barreneche, L. Miró, J.M. Morera, E. Bartolí, A. Inés Fernández, Low carbon and low embodied energy materials in buildings: A review, Renew. Sustain. Energy Rev. 23 (2013) 536–542. https://doi.org/10.1016/j.rser.2013.03.017.

[73] D. Xiao, H. Wang, J. Zhu, S. Peng, Sequent and accumulative life cycle assessment of materials and products, Mater. Des. 22 (2001) 147–149.

[74] G. Finnveden, M.Z. Hauschild, T. Ekvall, J. Guinée, R. Heijungs, S. Hellweg, S. Suh, Recent developments in life cycle assessment, J. Environ. Manage. 91 (2009) 1–21.

[75] S. Serrano, C. Barreneche, L. Rincón, D. Boer, L.F. Cabeza, Optimization of three new compositions of stabilized rammed earth incorporating PCM : Thermal properties characterization and LCA, Constr. Build. Mater. 47 (2013) 872–878.

https://doi.org/10.1016/j.conbuildmat.2013.05.018.

[76] A. Arrigoni, C. Beckett, D. Ciancio, G. Dotelli, Life cycle analysis of environmental impact vs. durability of stabilised rammed earth, Constr. Build. Mater. 142 (2017) 128–136. https://doi.org/10.1016/j.conbuildmat.2017.03.066.

[77] J.C. Morel, A. Mesbah, M. Oggero, P. Walker, Building houses with local materials : means to drastically reduce the environmental impact of construction, 36 (2001) 1119–1126.

[78] P.S. Ramesh, Energy Procedia Appraisal of Vernacular Building Materials and Alternative Technoligies for Roofing and Terracing Options of Embodied Energy in Buildings, Energy Procedia. 14 (2012) 1843–1848. https://doi.org/10.1016/j.egypro.2011.12.1177.

[79] G. Wadel, J. Avellaneda, A. Cuchí, Sustainability in industrialised architecture: closing the materials cycle, Inf. La Construcción. 62 (2010) 37–51.

[80] J. Fernandes, R. Mateus, L. Bragança, The potential of vernacular materials to the sustainable building design, in: Vernac. Herit. Earthen Archit. Contrib. Sustain. Dev., CRC Press, Vila Nova da Cerveira, Portugal, 2013: pp. 623–629. https://doi.org/10.1201/b15685.

[81] L. Pérez-Lombard, J. Ortiz, C. Pout, A review on buildings energy consumption information, Energy Build. 40 (2008) 394–398. https://doi.org/10.1016/j.enbuild.2007.03.007.

[82] D. Gallipoli, A.W. Bruno, C. Perlot, N. Salmon, Raw earth construction : is there a role for unsaturated soil mechanics ?, in: Unsaturated Soils Res. Appl., 2014: pp. 55–62. https://doi.org/10.1201/b17034.

[83] C.G. da Rocha, N.C. Consoli, A.D.R. Johann, Greening stabilized rammed earth : devising more sustainable dosages based on strength controlling equations, J. Clean. Prod. 66 (2014) 19–26. https://doi.org/10.1016/j.jclepro.2013.11.041.

[84] J. Fernandes, M. Peixoto, R. Mateus, H. Gerv, Life cycle analysis of environmental impacts of earthen materials in the Portuguese context : Rammed earth and compressed earth blocks, J. Clean. Prod. 241 (2019). https://doi.org/10.1016/j.jclepro.2019.118286.

[85] M. Zami, A. Lee, Stabilised or un-stabilised earth construction for contemporary urban housing?, in: 5th Int. Conf. Responsive Manuf. 'Green Manuf., China, 2010: pp. 11–13.

[86] L. Miccoli, U. Müller, P. Fontana, Mechanical behaviour of earthen materials: A comparison between earth block masonry, rammed earth and cob, Constr. Build. Mater. 61 (2014) 327–339. https://doi.org/10.1016/j.conbuildmat.2014.03.009.

[87] D. Toll, A framework for unsaturated soil behavior, Géotechnique. 40 (1990) 31–44.

[88] F. Champiré, A. Fabbri, J. Morel, H. Wong, F. Mcgregor, Impact of relative humidity on the mechanical behavior of compacted earth as a building material, Constr. Build. Mater. 110 (2016) 70–78. https://doi.org/10.1016/j.conbuildmat.2016.01.027.

[89] V. Maniatidis, P. Walker, Structural Capacity of Rammed Earth in Compression, J. Mater. Civ. Eng. 20 (2008) 230–238.

[90] Q.-B. Bui, J.-C. Morel, S. Hans, N. Meunier, Compression behaviour of non-industrial materials in civil engineering by three scale experiments : the case of rammed earth, Mater. Struct. (2009) 1101–1116. https://doi.org/10.1617/s11527-008-9446-y.

[91] G. Minke, Building With Earth: Design and Technology of a Sustainable Architecture, Birkhäuser Basel, Switzerland, 2006.

[92] M.I. Gomes, T.D. Gonçalves, P. Faria, Hydric Behavior of Earth Materials and the Effects of Their Stabilization with Cement or Lime: Study on Repair Mortars for Historical Rammed Earth Structures, J. Mater. Civ. Eng. 7 (2016).

[93] K. Dao, M. Ouedraogo, Y. Millogo, J.E. Aubert, M. Gomina, Thermal, hydric and mechanical behaviours of adobes stabilized with cement, Constr. Build. Mater. 158 (2018) 84–96. https://doi.org/10.1016/J.CONBUILDMAT.2017.10.001.

[94] K.A. Heathcote, Durability of earthwall buildings, Constr. Build. Mater. 9 (1995) 185–189. https://doi.org/10.1016/0950-0618(95)00035-E.

[95] L. Mateus, J. de Brito, M.R. Veiga, In situ characterization of external ancient renderings of rammed earth constructions in the Algarve and of potential replacement commercial pre-mixed renderings, in: LEHM 2016 – Int. Conf. Build. with Earth, Weimar, Germany, 2016.

[96] L. Schueremans, Ö. Cizer, E. Janssens, G. Serré, K. Van Balen, Characterization of repair mortars for the assessment of their compatibility in restoration projects: Research and practice, Constr. Build. Mater. 25 (2011) 4338–4350. https://doi.org/10.1016/j.conbuildmat.2011.01.008.

[97] P. Marais, J. Littlewood, G. Karani, The use of polymer stabilised earth foundations for rammed earth construction, Energy Procedia. 83 (2015) 464–473. https://doi.org/10.1016/j.egypro.2015.12.166.

[98] D. D'Ayala, G. Benzoni, Historic and Traditional Structures during the 2010 Chile Earthquake: Observations, Codes, and Conservation Strategies, Earthq. Spectra. 28 (2012) 425–451.

[99] M. Idália, M. Lopes, J. De Brito, Seismic resistance of earth construction in Portugal, Eng. Struct. 33 (2011) 932–941. https://doi.org/10.1016/j.engstruct.2010.12.014.

[100] K. Sharma, L. Deng, C.C. Noguez, Field investigation on the performance of building structures during the April 25 , 2015 , Gorkha earthquake in Nepal, Eng. Struct. 121 (2016) 61–74. https://doi.org/10.1016/j.engstruct.2016.04.043.

[101] Q.B. Bui, T.-T. Bui, A. Limam, Assessing the seismic performance of rammed earth walls by using discrete elements, Cogent Eng. 3 (2016).

[102] H. Morris, R. Walker, Observation of the performance of earth buildings following the February 2011 Christchurch earthquake, Bull. New Zeal. Soc. Earthq. Eng. 44 (2011) 358–367.

[103] Q. Bui, A. Limam, T. Bui, Dynamic discrete element modelling for seismic assessment of rammed earth walls, Eng. Struct. 175 (2018) 690–699. https://doi.org/10.1016/j.engstruct.2018.08.084.

[104] P.A. Jaquin, Analysis of historic rammed earth construction, Durham theses, Durham University, 2008. http://etheses.dur.ac.uk/2169/.

[105] R.A. Silva, N. Mendes, D. V Oliveira, A. Romanazzi, O. Domínguez-martínez, T. Miranda, Evaluating the seismic behaviour of rammed earth buildings from Portugal : From simple tools to advanced approaches, Eng. Struct. 157 (2018) 144–156. https://doi.org/10.1016/j.engstruct.2017.12.021.

[106] D. Ciancio, C. Augarde, Capacity of unreinforced rammed earth walls subject to lateral wind force : Elastic analysis versus ultimate strength analysis Capacity of unreinforced rammed earth walls subject to lateral wind force : elastic analysis versus ultimate strength analysis, Mater. Struct. 46 (2013) 1569–1585. https://doi.org/10.1617/s11527-012-9998-8.

[107] C.M. Ouellet-Plamondon, G. Habert, Self-Compacted Clay based Concrete (SCCC): Proof-of-

concept, J. Clean. Prod. 117 (2016) 160–168. https://doi.org/10.1016/j.jclepro.2015.12.048.

[108] C. Ma, L. Chen, B. Chen, Experimental Study of Effect of Fly Ash on Self-Compacting Rammed Earth Construction Stabilized with Cement-Based Composites, J. Mater. Civ. Eng. 28 (2016). https://doi.org/https://doi.org/10.1061/(ASCE)MT.1943-5533.0001518.

[109] G. Landrou, C. Brumaud, F. Winnefeld, R.J. Flatt, G. Habert, Lime as an anti-plasticizer for self-compacting clay concrete, Materials (Basel). 9 (2016). https://doi.org/10.3390/ma9050330.

[110] D. Gélard, Identification and Characterization of Internal Cohesion of Earth Material in its Natural Condition (in French), in: INPG Grenoble, France, 2005.

[111] B.M. Aïssoun, S.-D. Hwang, K.H. Khayat, Influence of aggregate characteristics on workability of superworkable concrete, Mater. Struct. 49 (2016) 597–609.

[112] J.J. Chen, B.H. Li, P.L. Ng, A.K.H. Kwan, Adding granite polishing waste as sand replacement to improve packing density, rheology, strength and impermeability of mortar, Powder Technol. 364 (2020) 404–415.

[113] S.K. Ling, A.K.H. Kwan, Adding ground sand to decrease paste volume, increase cohesiveness and improve passing ability of SCC, Constr. Build. Mater. 84 (2015) 46–53.

[114] Y. Qian, G. De Schutter, Enhancing thixotropy of fresh cement pastes with nanoclay in presence of polycarboxylate ether superplasticizer (PCE), Cem. Concr. Res. 111 (2018) 15–22. https://doi.org/10.1016/J.CEMCONRES.2018.06.013.

[115] First International RILEM conference on Earthen Construction, (2022). https://conf-earth.sciencesconf.org/.

[116] K.C. Lombardi, Structural and morphological characterization of the PP-0559 kaolinite from the Brazilian Amazon region, J. Braz. Chem. Soc. 13 (2002).

[117] N. Mungan, Discussion of an overview of formation damage, J. Pet. Technol. 41 (1989) 1224.

[118] K.O. Adebowale, I.E. Unuabonah, B.I. Olu-Owolabi, Adsorption of some heavy metal ions on sulfate- and phosphate-modified kaolin, Appl. Clay Sci. 29 (2005) 145–148. https://doi.org/10.1016/j.clay.2004.10.003.

[119] F. Andreola, E. Castellini, T. Manfredini, M. Romagnoli, The role of sodium hexametaphosphate in the dissolution process of kaolinite and kaolin, J. Eur. Ceram. Soc. 24 (2004) 2113–2124. https://doi.org/10.1016/S0955-2219(03)00366-2.

[120] F. Andreola, E. Castellini, J.M.F. Ferreira, S. Olhero, M. Romagnoli, Effect of sodium hexametaphosphate and ageing on the rheological behaviour of kaolin dispersions, Appl. Clay Sci. 31 (2006) 56–64. https://doi.org/10.1016/j.clay.2005.08.004.

[121] F. Andreola, E. Castellini, G. Lusvardi, L. Menabue, M. Romagnoli, Release of ions from kaolinite dispersed in deflocculant solutions, Appl. Clay Sci. 36 (2007) 271–278. https://doi.org/10.1016/j.clay.2006.10.002.

[122] J.L. Amorós, V. Beltrán, V. Sanz, J.C. Jarque, Electrokinetic and rheological properties of highly concentrated kaolin dispersions: Influence of particle volume fraction and dispersant concentration, Appl. Clay Sci. 49 (2010) 33–43. https://doi.org/10.1016/j.clay.2010.03.020.

[123] H.M.M. Diz, B. Rand, The mechanism of deflocculation of kaolinite by polyanions, Br. Ceram. Trans. 89 (1990) 77–82.

[124] D. Penner, G. Lagaly, Influence of anions on the rheological properties of clay mineral dispersions D., Appl. Clay Sci. 19 (2001) 131–142.

[125] L. Lei, J. Plank, A study on the impact of different clay minerals on the dispersing force of conventional and modified vinyl ether based polycarboxylate superplasticizers, Cem. Concr. Res. 60 (2014) 1–10.

[126] S. Ng, J. Plank, Interaction mechanisms between Na montmorillonite clay and MPEG-based polycarboxylate superplasticizers, Cem. Concr. Res. 378 (2012) 222–231.

[127] D. Marchon, S. Mantellato, A.B. Eberhardt, R.J. Flatt, Adsorption of chemical admixtures, Sci. Technol. Concr. Admixtures. (2016) 219–256.

[128] C. Galán-Marín, C. Rivera-Gómez, J. Petric, Clay-based composite stabilized with natural polymer and fibre, Constr. Build. Mater. 24 (2010) 1462–1468. https://doi.org/10.1016/J.CONBUILDMAT.2010.01.008.

[129] M. Achenza, L. Fenu, On Earth Stabilization with Natural Polymers for Earth Masonry Construction, Mater. Struct. 39 (2006) 21–27.

[130] C.A. Dove, F.F. Bradley, S. V. Patwardhan, Seaweed biopolymers as additives for unfired clay bricks, Mater. Struct. 49 (2016) 4463–4482.

[131] T. Funami, Y. Fang, S. Noda, S. Ishihara, M. Nakauma, K.I. Draget, K. Nishinari, G.O. Phillips, Rheological properties of sodium alginate in an aqueous system during gelation in relation to supermolecular structures and Ca2+ binding, Food Hydrocoll. 23 (2009) 1746–1755. https://doi.org/10.1016/J.FOODHYD.2009.02.014.

[132] F. Winnefeld, B. Lothenbach, Hydration of calcium sulfoaluminate cements — Experimental findings and thermodynamic modelling, Cem. Concr. Res. 40 (2010) 1239–1247. https://doi.org/10.1016/J.CEMCONRES.2009.08.014.

[133] S. Guiheneuf, Formulation et renforts de blocs en matériau terre pour une utilisation structurelle, INSA de Rennes, 2020. https://tel.archives-ouvertes.fr/tel-03194559.

[134] P.P. Raj, Soil Mechanics and Foundation Engineering, Dorling Kindersley, (India) Pvt. Ltd., New Delhi, 2012.

[135] A.W. Skempton, The Colloidal activity of clays, in: 3rd Int. Conf. Soil Mech. Found. Eng., London, 1953: pp. 47–61.

[136] A. Laskar, S.K. Pal, Geotechnical characteristics of two different soils and their mixture and relationships between parameters, Electron. J. Geotech. Eng. 17 (2012) 2821–2832.

[137] B. Voight, Correlation between Atterberg plasticity limits and residual shear strength of natural soils, Géotechnique. 23 (1973) 265–267.

[138] X. Wang, K. Wang, P. Taylor, G. Morcous, Assessing particle packing based self-consolidating concrete mix design method, Constr. Build. Mater. 70 (2014) 439–452.

[139] W. Zuo, J. Liu, Q. Tian, W. Xu, W. She, P. Feng, C. Miao, Optimum design of low-binder Self-Compacting Concrete based on particle packing theories, Constr. Build. Mater. 163 (2018) 938–948.

[140] S.A.A.M. Fennis, J.C. Walraven, J.A. den Uijl, Defined-performance design of ecological concrete, Mater. Struct. 46 (2013) 639–650.

[141] L.G. Li, J.J. Chen, A.K.H. Kwan, Roles of packing density and water film thickness in strength and durability of limestone fines concrete, Mag. Concr. Res. 69 (2017) 595–605.

CHAPTER 3. METHODOLOGY

3.1 Introduction

Since the thesis follows an article-based structure, each chapter consists of the employed methodology. In this chapter, the sequence of the methodology, depending on the objectives of this study, as well as the logic behind the selection of the experimental program are presented.

3.2 Experimental Program

This study was conducted in 4 phases:

1. **Phase 1** is focused on self-consolidating earth paste (SCEP) mixtures with various influencing parameters to find the significance of each factor on workability and compressive strength responses.
2. **Phase 2** involves the testing methods related to a new concrete-equivalent mortar (CEM) and concrete scales to facilitate the designing procedure by saving time and cost. Contribution of the key factors are highlighted to design a required SCEC mixture depending on the required application.
3. **Phase 3** investigates the multiscale rheological properties of the SCEC mixtures to broaden the knowledge of the effect of different earth compositions and admixture types on yield stress, plastic viscosity, and thixotropy.
4. **Phase 4** summarizes the hygrothermal properties of the investigated mixtures. This phase was conducted in La Rochelle Université to validate the hygrothermal performance of this novel construction material (i.e., SCEC) with other conventional building envelopes and concrete.

Fig. 3.1 presents the organization of the employed experimental program undertaken in this study. The taken steps toward achieving the objectives of each phase are followed in this chapter.

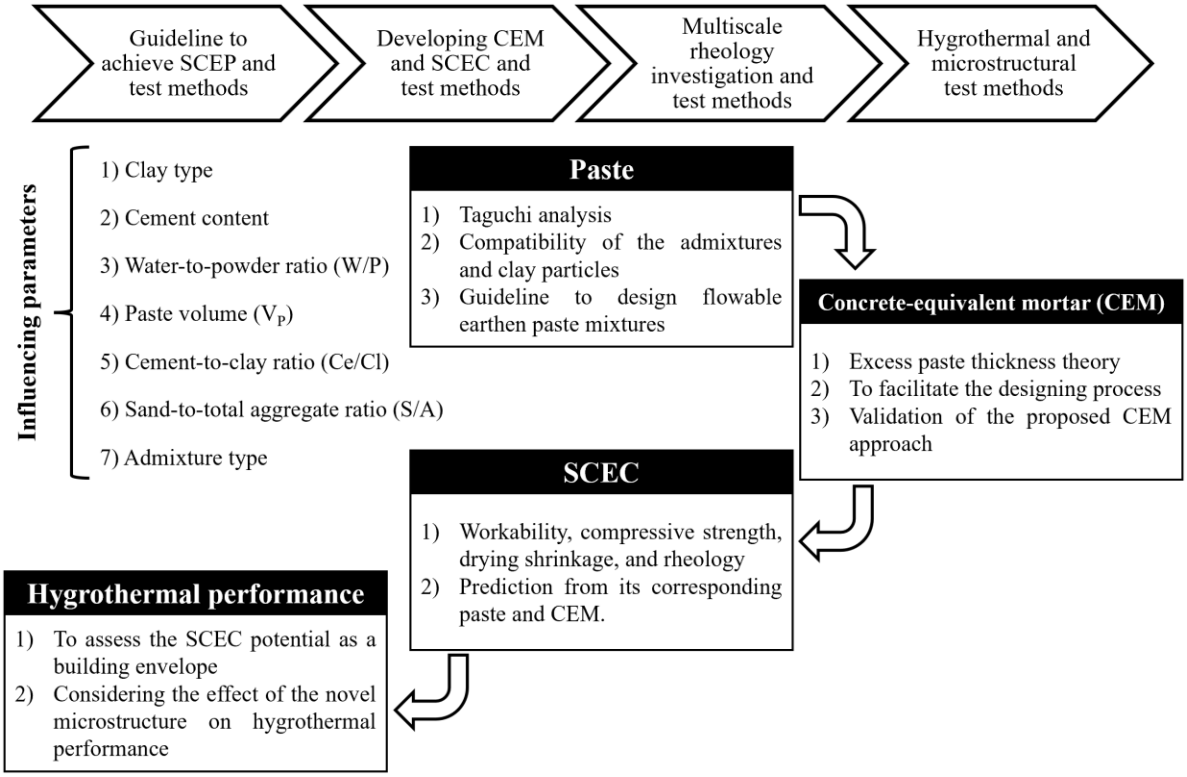

Fig. 3.1. The organization of the experimental program carried out in this study.

3.2.1 Phase 1: A new approach for proportioning self-consolidating earth paste (SCEP) using the Taguchi method

3.2.1.1 Taguchi method

Parametric optimization can be very time and energy consuming due to the high number of variables that affect the responses of SCEC. Taguchi design of experiment (TDOE) is a well-known method to optimize the number of experiments and determine the most influencing parameters on targeted responses. TDOE is based on fractional factorial experiments using the orthogonal arrays [1,2]. TDOE is useful to optimize the influencing parameters to achieve targeted responses with minimizing the experimental cost. The main investigated parameters in this study include clay type, cement content, volume of paste (V_P), water-to-powder ratio (W/P) (by mass), volumetric cement-to-clay ratio (Ce/Cl), volumetric sand-to-total aggregate ratio (S/A) of corresponding SCEC mixtures, and admixture type. The experimental results are converted into signal-to-noise (S/N) ratios reflecting the deviation of the actual experimental results from the

targeted ones. The investigated factors and their corresponding levels used for TDOE are summarized in Table 3.1.

Table 3.1. Investigated parameters and their corresponding levels.

Factors	Levels				
	1	2	3	4	5
Clay type	Type I	Type II	-	-	-
Cement content (kg/m^3)	60	90	120	150	180
Volume of paste (V_P) (%)	45	48	51	54	57
Water to powder ratio (W/P)	0.30	0.35	0.40	0.45	0.50
Cement to clay ratio (Ce/Cl)	0.50	0.75	1.00	1.25	1.50
Sand-to-total aggregate ratio (S/A)	0.5	0.6	0.7	0.8	0.9
Admixture	NaHMP	NaSil	PCE	PNS	NE-PC

As can be observed in Table 3.1, two different types of soil (i.e., two-level factor) were investigated to highlight the efficiency of clay mineralogy and broaden the evaluation on more diverse earth types. On the other hand, the other investigated factors were evaluated at five different levels. Cement contents corresponding to 60, 90, 120, 150, and 180 kg/m^3 were investigated, according to those recommended in literature for cement-stabilized earthen materials [3,4]. Moreover, volume of paste (V_P) of 45%, 48%, 51%, 54%, and 57% were evaluated. It is worthy to mention that the paste volume consists in air, water, and powders, including clay, silt, and cement. The investigated paste mixtures were proportioned with five W/P ratios of 0.30, 0.35, 0.40, 0.45, and 0.50. Furthermore, the volumetric cement-to-clay ratio (Ce/Cl) was selected as a main factor to control the clay content and evaluate the packing in the binder constituents. Accordingly, five different Ce/Cl of 0.50, 0.75, 1.00, 1.25, and 1.50 were selected. Five S/A of 0.5, 0.6, 0.7, 0.8, and 0.9 were also evaluated. These levels were selected to cover a wide range of characteristics of the investigated parameters. The effect of different types of admixtures, including sodium hexametaphosphate (NaHMP) and sodium silicate (NaSil) were used as dispersant in the suspensions containing clay. Their presence aims to increasing the overall negative surface charge and alkalinity of earth cations, accompanying with a rise in pH of the solution [5–13]. On the other hand, polycarboxylate ether (PCE), sodium polynaphtalene (PNS), and non-esterified polycarboxylate (NE-PC) were also investigated. The efficiency of these admixtures was investigated in cement pastes, while their performance in dispersion of ternary powder systems of SCEP is still questionable. The effect of two- and five-levels factors on the modelled properties are evaluated using a L50 orthogonal Taguchi array, which requires 50 fractional factorial

experiments. The fifty investigated mixtures are summarized in Table 3.3. The modelled responses include the flowability and compressive strength development.

Finally, calculation of signal-to-noise (S/N) ratio represents the loss function which represents the deviation of the actual experimental results and the targeted ones. The analysis of S/N ratio is based on three performance characteristics corresponding to Smaller-the-better, Larger-the-better, and Nominal-the-better defined in Eqs. (3.1)-(3.3), respectively [14], as follow:

Larger-the better $$S/N = -10 \times \log_{10}\left(\frac{1}{n}\sum_{i=1}^{n}\frac{1}{Y_i^2}\right) \quad (3.1)$$

Smaller-the better $$S/N = -10 \times \log_{10}\left(\frac{1}{n}\sum_{i=1}^{n}Y_i^2\right) \quad (3.2)$$

Nominal-the better $$S/N = -10 \times \log_{10}\left[\frac{1}{n}\sum_{i=1}^{n}(Y_i - Y_0)^2\right] \quad (3.3)$$

where S/N is the performance statistics, n is the number of repetitions for each level of a factor, Y_i is the response value of the i^{th} experiment, and Y_0 is the nominal value desired. The values of S/N ratio are used as a measure of robustness to identify the control factors reducing variability in a process by minimizing the effect of noise factors [14]. In this study, the larger-the better S/N characteristics (Eq. 3.1) was employed for compressive strength development at different ages. On the other hand, the smaller-the-better S/N characteristics (Eq. 3.2) was used to investigate the admixture demand, marsh cone flow, and mini-slump spread loss.

3.2.1.2 Materials and test methods

The investigated SCEP mixtures were proportioned using a general use Portland cement (GU) complying with the ASTM C150 specifications. The GU cement has a specific gravity of 3.15 and specific surface area of 0.3 m^2/g. The clay type I consists of kaolinite with specific surface area and specific gravity of 15 m^2/g and 2.73, respectively. The clay type II was composed of 50% kaolinite and 50% attapulgite. The specific surface area and specific gravity of attapulgite are 155 m^2/g and 2.75, respectively. The silt powder used is composed of quartz grains of 2 to 75 µm and specific gravity of 2.69. The chemical compositions of the binders are summarized in Table 3.2. On the other hand, NaHMP with purity of 96% was used as solution in water with a solid content of 37.1%. Moreover, NaSil solution composed of water, 10.6% Na_2O, and 26.5% SiO_2 was used

as inorganic deflocculant. PCE, PNS, and NE-PC with solid contents of 40%, 39.25%, and 36.44%, respectively, were used as high-range water-reducer (HRWR) admixtures.

Table 3.2. Chemical composition of the binders used in this study.

Chemical composition (% wt.)	Binder type			
	GU cement	Kaolinite	Attapulgite	Quartz silt
CaO	62.50	0.10	2.92	0.01
SiO_2	19.30	46.10	66.20	99.02
Al_2O_3	4.80	38.10	11.71	0.64
Fe_2O_3	3.00	0.50	4.02	0.22
MgO	2.70	0.10	9.70	0.01
SO_3	4.10	0.04	-	-
Others	1.40	1.56	1.47	0.10
LOI*	2.20	13.50	3.98	-

LOI*: Loss of ignition

The paste mixtures were mixed in batches of 1.5 L using a planetary Hobart mixer according to the ASTM C305 specifications [15]. Mini-slump flow (MSF) [16] and Marsh cone flow time (MCT) [17] were used to assess flowability of the investigated SCEP mixtures. The investigated mixtures were designed to achieve the targeted MSF of 280 ± 20 mm and ensure a highly flowable and stable mixture. Furthermore, MSF loss after 15 and 30 min of age was also determined to evaluate the efficiency of admixtures to maintain the initial workability. MCT corresponds to the required time to pass 500 mL of paste throughout a nozzle measuring 8-mm diameter. The test consists in pouring 1000 mL of sample in the cone to determine the flow time of 500 mL passing the nozzle. Higher flow time reflects lower fluidity of the mixture. In addition to flow properties, for each mixture, different 50 × 50 × 50 mm^3 cubes were sampled to determine the compressive strength at 1, 7, and 28 days of age in accordance with the ASTM C109 specifications [18].

3.2.1.3 Mixture proportioning of the investigated SCEP mixtures

The proportioning of the investigated mixtures summarized in Table 3.4 are established based on the levels of control factors in the L50 orthogonal array given in Table 3.1.

Table 3.3. Absolute values of the 7 modelled factors according to L50 orthogonal array

Experiment No.	Investigated factors							Experiment No.	Investigated factors						
	Clay type	Cement content (kg/m^3)	V_P (%)	W/P	Ce/Cl	S/A	Admixture		Clay type	Cement content (kg/m^3)	V_P (%)	W/P	Ce/Cl	S/A	Admixture
1			45	0.30	0.5	0.5	NaHMP	26		60	45	0.30	1.25	0.9	PNS
2			48	0.35	0.75	0.6	NaSil	27			48	0.35	1.5	0.5	NE-PC
3		60	51	0.40	1	0.7	PCE	28			51	0.40	0.5	0.6	NaHMP
4			54	0.45	1.25	0.8	PNS	29			54	0.45	0.75	0.7	NaSil
5			57	0.50	1.5	0.9	NE-PC	30			57	0.50	1	0.8	PCE
6			45	0.35	1	0.8	NE-PC	31		90	45	0.35	0.5	0.7	PCE
7			48	0.40	1.25	0.9	NaHMP	32			48	0.40	0.75	0.8	PNS
8		90	51	0.45	1.5	0.5	NaSil	33			51	0.45	1	0.9	NE-PC
9			54	0.50	0.5	0.6	PCE	34			54	0.50	1.25	0.5	NaHMP
10			57	0.30	0.75	0.7	PNS	35			57	0.30	1.5	0.6	NaSil
11			45	0.40	1.5	0.6	PNS	36		120	45	0.40	1	0.5	NaSil
12			48	0.45	0.5	0.7	NE-PC	37			48	0.45	1.25	0.6	PCE
13	I	120	51	0.50	0.75	0.8	NaHMP	38	II		51	0.50	1.5	0.7	PNS
14			54	0.30	1	0.9	NaSil	39			54	0.30	0.5	0.8	NE-PC
15			57	0.35	1.25	0.5	PCE	40			57	0.35	0.75	0.9	NaHMP
16			45	0.45	0.75	0.9	PCE	41		150	45	0.45	1.5	0.8	NaHMP
17			48	0.50	1	0.5	PNS	42			48	0.50	0.5	0.9	NaSil
18		150	51	0.30	1.25	0.6	NE-PC	43			51	0.30	0.75	0.5	PCE
19			54	0.35	1.5	0.7	NaHMP	44			54	0.35	1	0.6	PNS
20			57	0.40	0.5	0.8	NaSil	45			57	0.40	1.25	0.7	NE-PC
21			45	0.50	1.25	0.7	NaSil	46		180	45	0.5	0.75	0.6	NE-PC
22			48	0.30	1.5	0.8	PCE	47			48	0.3	1	0.7	NaHMP
23		180	51	0.35	0.5	0.9	PNS	48			51	0.35	1.25	0.8	NaSil
24			54	0.40	0.75	0.5	NE-PC	49			54	0.4	1.5	0.9	PCE
25			57	0.45	1	0.6	NaHMP	50			57	0.45	0.5	0.5	PNS

Table 3.4. Proportioning of the investigated SCEP mixtures based on L50 orthogonal array.

Mix No.	Cement (kg/m^3)	Water (kg/m^3)	Clay Type I (kg/m^3)	Silt (kg/m^3)	W/P	Mix No.	Cement (kg/m^3)	Water (kg/m^3)	Clay Type II (kg/m^3)	Silt (kg/m^3)	W/P
P1	133.3	450.4	231.1	1136.9	0.30	P26	133.3	450.1	92.4	1274.4	0.30
P2	125.0	488.6	144.4	1126.6	0.35	P27	125.0	488.4	72.2	1198.3	0.35
P3	117.6	521.9	102.0	1085.1	0.40	P28	117.6	522.2	203.9	983.9	0.40
P4	111.1	551.1	77.0	1036.6	0.45	P29	111.1	551.3	128.4	985.6	0.45
P5	105.3	577.0	60.8	988.0	0.50	P30	105.3	577.1	91.2	957.8	0.50
P6	200.0	490.7	173.3	1028.5	0.35	P31	200.0	491.1	346.7	856.5	0.35
P7	187.5	523.9	130.0	992.4	0.40	P32	187.5	524.2	216.7	906.3	0.40
P8	176.5	553.2	102.0	950.8	0.45	P33	176.5	553.3	152.9	900.2	0.45
P9	166.7	579.7	288.9	703.7	0.50	P34	166.7	579.1	115.6	876.0	0.50
P10	157.9	450.9	182.5	1162.5	0.30	P35	157.9	450.6	91.2	1253.0	0.30
P11	266.7	526.2	154.1	894.9	0.40	P36	266.7	526.5	231.1	818.4	0.40
P12	250.0	556.3	433.3	553.0	0.45	P37	250.0	555.6	173.3	811.3	0.45
P13	235.3	581.7	271.9	656.3	0.50	P38	235.3	581.3	135.9	791.4	0.50
P14	222.2	452.5	192.6	1093.4	0.30	P39	222.2	452.9	385.2	902.3	0.30
P15	210.5	490.9	146.0	1046.0	0.35	P40	210.5	491.1	243.3	949.4	0.35
P16	333.3	558.7	385.2	523.0	0.45	P41	333.3	558.1	192.6	714.3	0.45
P17	312.5	584.1	270.8	584.9	0.50	P42	312.5	585.0	541.7	315.8	0.50
P18	294.1	454.2	203.9	1016.0	0.30	P43	294.1	454.6	339.9	881.2	0.30
P19	277.8	492.7	160.5	969.4	0.35	P44	277.8	492.9	240.7	889.7	0.35
P20	263.2	527.0	456.1	598.2	0.40	P45	263.2	526.2	182.5	869.9	0.40
P21	400.0	586.9	277.3	496.4	0.50	P46	400.0	587.5	462.2	312.7	0.50
P22	375.0	456.2	216.7	929.1	0.30	P47	375.0	456.5	325.0	821.6	0.30
P23	352.9	495.8	611.8	452.0	0.35	P48	352.9	494.9	244.7	816.3	0.35
P24	333.3	528.8	385.2	603.4	0.40	P49	333.3	528.2	192.6	794.6	0.40
P25	315.8	557.8	273.7	650.1	0.45	P50	315.8	558.6	547.4	378.3	0.45

3.2.2 Phase 2: Multiscale investigation of self-consolidating earthen materials using a novel concrete-equivalent mortar approach

3.2.2.1 Concrete-equivalent mortar (CEM)

Flow properties of concrete can be modelled using the concrete-equivalent mortar (CEM) method. In this approach, the coarse aggregate fraction is replaced by sand of equal surface area, aiming to keep a constant total surface area of aggregate covered with cement paste [19]. The CEM method was successfully used to investigate the effect of binder-admixture interaction, packing density of the binder composition, robustness of the fresh properties, and rheological behavior of the suspending phase on the fresh and hardened properties of SCC [20]. Schwartzentruber and Catherine [19] employed the CEM approach to optimize the dosage of HRWR admixtures to achieve the targeted workability. Strong correlations were reported between the fresh properties of CEM and concrete mixtures. Assaad et al. [21] investigated the relationships between the fresh and hardened properties of concrete and their corresponding CEM mixtures. Erdem [22] reported satisfactory relationship between the rheological

properties of SCC and their corresponding CEM. However, considering equal surface area can neglect the variation of packing density of the granular skeleton. On the other hand, Kabagire et al. [23] introduced the excess paste theory to improve the agreements between the fresh properties of SCC and their corresponding CEM mixtures. Indeed, in addition to the portion of cement paste required to fill the interparticle voids of aggregate, the excess paste volume (excess paste EP) covers the aggregate surface area. More recently, Lee et. al [24] employed the EP theory to propose a correlation between yield stress of concrete and its corresponding CEM. The authors [24] successfully predicted the yield stress of concrete by establishing a relationship between the PCE dosage and the EP thickness in CEM. Therefore, EP thickness seems to be a key factor which is dependent on packing density of granular skeleton.

In this study, the workability, dying shrinkage, and mechanical performance of various SCEC mixtures were evaluated using their corresponding CEM. As mentioned earlier, the conventional CEM method was established to simulate the workability and mechanical performance of its corresponding concrete by keeping the total surface area of aggregate constant [21,23]. However, the variation of packing density of the granular skeleton was neglected. This can therefore induce change in the thickness of EP, which can impact on the correlation between the workability of concrete and its corresponding CEM. A schematic of a unit volume of concrete consisting in compacted aggregate and excess paste volume is shown in Fig. 3.2. Lower aggregate content than its maximum packing ($\varphi < \varphi_{max}$) may require low paste volume, namely compacted paste volume (V_{CP}), to fill the existing interparticle voids between the compacted aggregate (V_{CA}) and achieve the highest packing density (φ_{max}). The remaining paste volume, which is referred to the EP volume ($V_{EP} = 1- \frac{\varphi}{\varphi_{max}}$), can contribute to reducing the internal frictions between the aggregate, thus enhancing the flowability of the mixture. The excess paste volume is a function of the volumetric content-to-maximum packing density of aggregate ratio, namely the relative solid packing fraction $\left(\frac{\varphi}{\varphi_{max}}\right)$ [25].

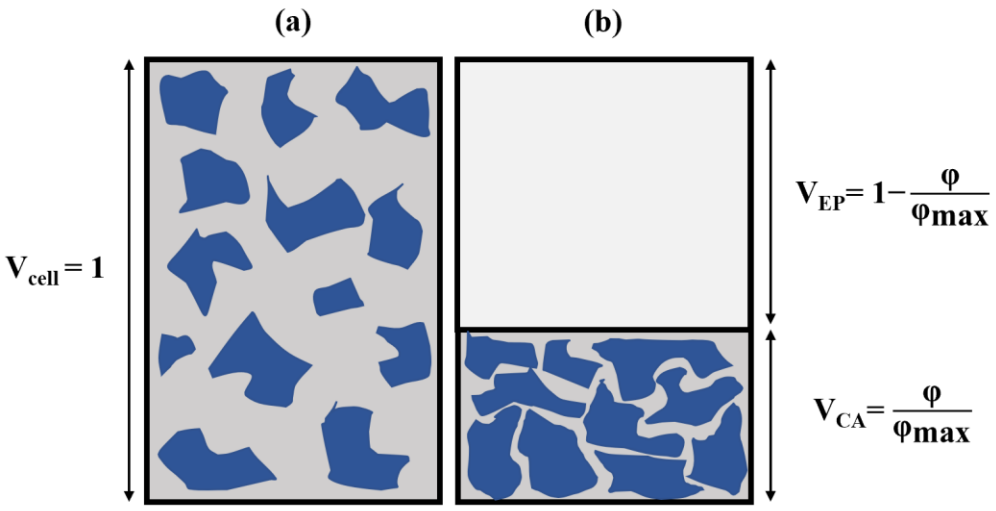

Fig. 3.2. (a) Schematic of a unit volume of concrete (V_{cell} = 1) as a suspension of aggregate in paste and (b) excess paste volume (V_{EP}) and compacted aggregate (V_{CA}).

The average EP thickness (e_{EP}) can then be estimated by the ratio of the V_{EP}-to-the total surface area of aggregate ($e_{EP} = V_{EP} / A_{Aggregate}$). In order to achieve comparable workability of concrete and its corresponding CEM, the coarse aggregate was replaced by sand while targeting an equal e_{EP}, as follows:

$$e_{EP} = \frac{1 - \frac{\varphi_{sand+gravel}}{\varphi_{max:sand+gravel}}}{A_{sand+gravel}} = \frac{1 - \frac{\varphi_{eq:sand}}{\varphi_{max:sand}}}{A_{eq:sand}} \quad (3.4)$$

where $\varphi_{sand+gravel}$, $\varphi_{eq:sand}$, $\varphi_{max:sand+gravel}$, $\varphi_{max:sand}$, $A_{sand+gravel}$, and $A_{eq:sand}$ are the volumetric contents, packing density, and surface area of sand and gravel in SCEC mixture, as well as sand in corresponding CEM mixtures, respectively. It is worthy to mention that in order to obtain 3D surface area-to-volume ratio (A_{3D}/V) of the aggregate particles coarser and finer than 1.25 mm, the Max3D laser scanner (Fig. 3.3a) and X-ray micro-CT scanner (Fig. 3.3b) were employed, respectively [26–28]. Different subclasses of particles of the sand and coarse aggregate, corresponding to different standard sieves, were scanned. The A_{3D}/V values of the investigated sand and coarse aggregate were then calculated using the volumetric-weighted arithmetic mean of A_{3D}/V values of their corresponding subclasses, given their particle-size distributions (PSD) (Table 3.5).

Fig. 3.3. (a) MAXscan 3D laser scanner and (b) X-ray micro-CT scanner.

3.2.2.2 Materials and test methods

A natural river sand (0-5 mm) and crushed limestone coarse aggregate (5-10 mm) were used. The PSD, A_{3D}/V, density, and water absorption of the aggregate are summarized in Table 3.5.

Table 3.5. Cumulative passing, 3D-surface area-to-volume ratio, density, and water absorption of sand and coarse aggregate.

Sieve size range (mm)	Sand, Nominal: 0-5 mm (%)	Coarse Aggregate, Nominal: 5-10 mm (%)
20-28	-	-
14-20	-	-
10-14	-	18.3
5-10	4.45	71.2
2.5-5	10.41	5.4
1.25-2.5	14.32	5.1
0.630-1.25	19.03	-
0.315-0.630	27.45	-
0.160-0.315	18.44	-
0.080-0.160	5.78	-
0-0.080	0.12	-
A_{3D}/V (m^2/m^3)	21583.4	859.8
Density (kg/m^3)	2670	2720
Water absorption (%)	1.09	0.42

In this study, five different volumetric S/A of 0.5, 0.6, 0.7, 0.8, and 0.9 were selected to evaluate the effect of packing density on concrete performance. The packing densities of the investigated sand ($\varphi_{max:sand}$) and granular ($\varphi_{max:sand+gravel}$) skeletons were then determined using the intensive compaction tester (ICT) device [29], [30]. It consists in applying 50 gyratory cycles at an angle of 40 mrad and a normal pressure of 20 kPa. These testing parameters were recommended to prevent crushing of aggregate [26] (Table 3.6).

Table 3.6. Packing density of the investigated sand ($\varphi_{max:sand}$) and gravel skeletons ($\varphi_{max:sand+gravel}$).

S/A	0	0.5	0.6	0.7	0.8	0.9
$\varphi_{max:\ sand\ +\ gravel}$	$\varphi_{max:\ sand}$ = 0.605	0.788	0.797	0.786	0.770	0.753

The binder used to proportion the investigated SCEC mixtures is similar to that used to carry out the research activities of Phase 1 detailed earlier. Similar influencing factors were considered, as summarized in Table 3.7.

Table 3.7. Modelled factors and their corresponding levels.

Levels	Factors						
	Clay type	Cement content (kg/m^3)	V_P (%)	W/P	Ce/Cl	S/A	Admixture type
1	Type I	60	45	0.30	0.50	0.5	NaHMP
2	Type II	90	48	0.35	0.75	0.6	NaSil
3	-	120	51	0.40	1.00	0.7	PCE
4	-	150	54	0.45	1.25	0.8	PNS
5	-	180	57	0.50	1.50	0.9	NE-PC

On the other hand, the CEM mixtures were made in batches of 6 L according to the ASTM C305 specifications [15] for mortar. The MSF [16] and mini V-Funnel (MVF) [31] tests were carried out at 0, 30, and 60 min immediately after mixing to evaluate the flowability and workability loss of the investigated mortar mixtures. In the case of MVF, the funnel was filled, and the bottom outlet was then opened to allow the mortar to flow out. The required time to empty the cone was recorded as the MVF time. In the case of mortar mixtures, the compressive strength was evaluated at different ages of 1, 7, and 28 days of age according to the ASTM C109 specifications [18]. Drying shrinkage of the CEM mixtures was measured according to the ASTM C596 specifications [32]. Moreover, the Atterberg limits [33], including the liquid (LL) and plastic limits (PL), in each soil (clay, silt, and sand < 425 μm) were determined. It is important to mention that the LL is defined as the moisture content above which the soil behaves as a liquid, and PL is the moisture content beyond which the soil behaves plastic. The plasticity index (PI) was also calculated as the difference between LL and PL values (PI = LL - PL).

All the SCEC mixtures were prepared in batches of 60 L using a rotating drum mixer. The mixing sequence consisted in homogenizing the aggregate (sand + coarse aggregate) for 90 s, then 1/3 of the mixing water was introduced and mixed for 60 s. The powder (silt, clay, and cement) was then added and mixed for 30 s. The second 1/3 of the mixing water and HRWR or dispersant admixture were added and mixed for an additional 60 s. The remaining 1/3 of water was then added and the mixing was resumed for another 90 s. After 120 s of rest, the mixing was presumed for an additional 180 s. Immediately after mixing, the slump flow (SF) [31] and V-Funnel [34] tests were carried out to evaluate the flowability of the investigated

SCEC mixtures. Moreover, the compressive strength of the investigated concrete mixtures was determined at 1, 7, and 28 days of age using cylindrical specimens of 100-mm diameter and 200-mm height conforming the ASTM C39 standard [35]. Drying shrinkage of the investigated SCEC and their corresponding CEM mixtures were also evaluated at 7, 14, 21, 28, and 90 days of age according to the ASTM C157 specifications [36].

3.2.2.3 Paste, CEM, and concrete mixture proportions

It should be mentioned that each phase is complementary to the previous previous one. Therefore, after conducting the first phase, the admixture demand to achieve the targeted MSF and $f'_{c\text{-}1d}$ of the 50 investigated SCEP mixtures (Phase 1) are summarized in Table 3.8 [37]. A minimum $f'_{c\text{-}1d}$ of 1 MPa was selected to ensure the feasibility of demolding after 24 hours of casting [38]. As can be observed in Fig. 3.4, the 50 paste mixtures were evaluated based on their MSF and $f'_{c\text{-}1d}$ to ensure good compatibility between admixture and ternary binder system and adequate strength for formwork removal. The paste mixtures satisfying these criteria were then selected for further workability, compressive strength, and drying shrinkage investigation on their CEM scale. CEM mixtures with optimum admixture dosage, 1-day compressive strength, and 28-day drying shrinkage were selected for investigation in concrete scale. Finally, key parameters were selected to predict CEM and concrete performance based on paste and CEM mixtures, respectively.

The mixtures with $f'_{c\text{-}1d}$ greater than 1 MPa were chosen to carry out the mortar tests. Although P14, P20, P21, P35, P36, P47, and P48 mixtures satisfied the required compressive strength values, but they were not chosen due to their significantly high admixture demand. In total, eighteen CEM mixtures were therefore selected for further investigation. The mixture proportioning of the investigated CEM mixtures and their corresponding excess paste thicknesses (e_{EP}) are summarized in Table 3.9.

According to the $f'_{c\text{-}1d}$ results of the investigated CEMs presented in Table 3.9, three concrete mixtures C16, C22, and C37 proportioned with PCE type were selected (Table 3.10). The selection criteria were based on their corresponding CEM mixtures achieving the targeted MSF of 280 ± 20 mm and the $f'_{c\text{-}1d}$ values higher than 1 MPa. Moreover, a cement-based reference mixture C_{ref} (i.e., without any clay) and its corresponding CEM (M_{ref}) and paste (P_{ref}) mixtures were proportioned with PCE, W/P of 0.40, V_P of 0.45, and S/A of 0.5, as presented in Table 3.10.

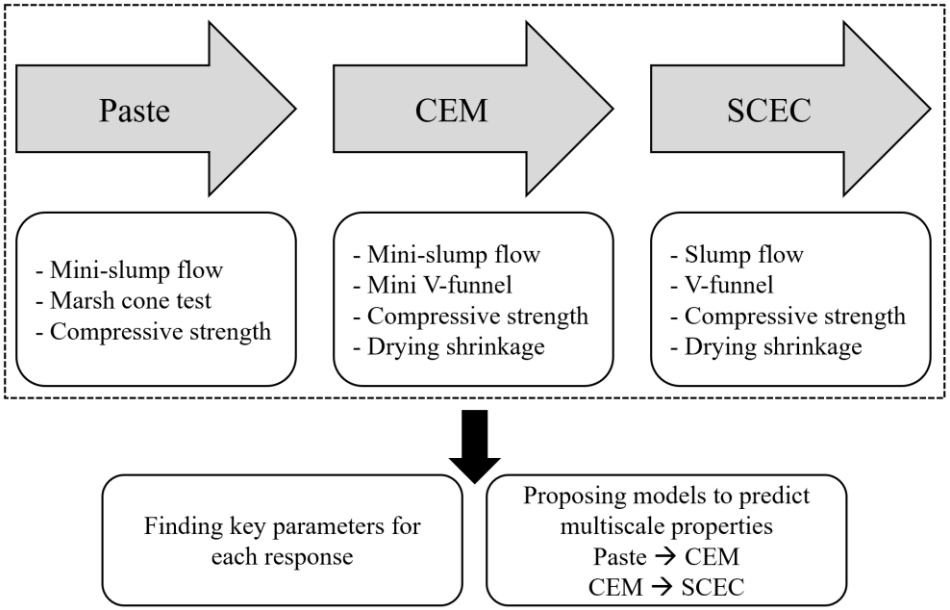

Fig. 3.4. Schematic sequence of the study carried out on paste, CEM, and concrete mixtures.

Table 3.8. Proportioning, admixture demand, and $f'_{c\text{-}1d}$ of the investigated SCEP mixtures [37].

Mix No.	Cement (kg/m^3)	Water (kg/m^3)	Clay type I (kg/m^3)	Silt (kg/m^3)	W/P	Admixture demand (% binder)	$f'_{c\text{-}1d}$ (MPa)	Mix No.	Cement (kg/m^3)	Water (kg/m^3)	Clay type II (kg/m^3)	Silt (kg/m^3)	W/P	Admixture demand (% binder)	$f'_{c\text{-}1d}$ (MPa)
P1	133.3	450.4	231.1	1136.9	0.30	0.510	0.75 (0.01)	P26	133.3	450.1	92.4	1274.4	0.30	0.400	1.04 (0.02)
P2	125.0	488.6	144.4	1126.6	0.35	2.700	0.67 (0.01)	P27	125.0	488.4	72.2	1198.3	0.35	0.240	0.50 (0.03)
P3	117.6	521.9	102.0	1085.1	0.40	0.065	0.32 (0.01)	P28	117.6	522.2	203.9	983.9	0.40	2.100	0.42 (0.04)
P4	111.1	551.1	77.0	1036.6	0.45	0.050	0.37 (0.01)	P29	111.1	551.3	128.4	985.6	0.45	6.500	0.46 (0.02)
P5	105.3	577.0	60.8	988.0	0.50	0.000	0.31 (0.02)	P30	105.3	577.1	91.2	957.8	0.50	0.090	0.29 (0.04)
P6	200.0	490.7	173.3	1028.5	0.35	0.071	1.17 (0.01)	P31	200.0	491.1	346.7	856.5	0.35	1.400	0.59 (0.02)
P7	187.5	523.9	130.0	992.4	0.40	0.350	0.41 (0.02)	P32	187.5	524.2	216.7	906.3	0.40	0.750	1.09 (0.04)
P8	176.5	553.2	102.0	950.8	0.45	0.600	0.48 (0.01)	P33	176.5	553.3	152.9	900.2	0.45	0.280	0.53 (0.03)
P9	166.7	579.7	288.9	703.7	0.50	0.110	0.51 (0.01)	P34	166.7	579.1	115.6	876.0	0.50	0.700	0.54 (0.07)
P10	157.9	450.9	182.5	1162.5	0.30	0.170	1.56 (0.04)	P35	157.9	450.6	91.2	1253.0	0.30	7.500	1.07 (0.04)
P11	266.7	526.2	154.1	894.9	0.40	0.120	3.11 (0.04)	P36	266.7	526.5	231.1	818.4	0.40	12.000	1.30 (0.04)
P12	250.0	556.3	433.3	553.0	0.45	0.081	1.46 (0.02)	P37	250.0	555.6	173.3	811.3	0.45	0.390	1.86 (0.09)
P13	235.3	581.7	271.9	656.3	0.50	0.490	0.40 (0.01)	P38	235.3	581.3	135.9	791.4	0.50	0.100	0.54 (0.04)
P14	222.2	452.5	192.6	1093.4	0.30	4.000	2.11 (0.01)	P39	222.2	452.9	385.2	902.3	0.30	NA*	-
P15	210.5	490.9	146.0	1046.0	0.35	0.075	2.60 (0.12)	P40	210.5	491.1	243.3	949.4	0.35	2.600	0.63 (0.04)
P16	333.3	558.7	385.2	523.0	0.45	0.175	2.94 (0.24)	P41	333.3	558.1	192.6	714.3	0.45	1.800	0.36 (0.03)
P17	312.5	584.1	270.8	584.9	0.50	0.100	1.91 (0.01)	P42	312.5	585.0	541.7	315.8	0.50	NA*	-
P18	294.1	454.2	203.9	1016.0	0.30	0.068	5.69 (0.09)	P43	294.1	454.6	339.9	881.2	0.30	2.400	0.85 (0.06)
P19	277.8	492.7	160.5	969.4	0.35	0.520	0.80 (0.04)	P44	277.8	492.9	240.7	889.7	0.35	1.050	2.19 (0.05)
P20	263.2	527.0	456.1	598.2	0.40	4.800	1.75 (0.03)	P45	263.2	526.2	182.5	869.9	0.40	0.420	1.33 (0.04)
P21	400.0	586.9	277.3	496.4	0.50	3.600	1.71 (0.07)	P46	400.0	587.5	462.2	312.7	0.50	6.400	0.34 (0.02)
P22	375.0	456.2	216.7	929.1	0.30	0.130	6.92 (0.21)	P47	375.0	456.5	325.0	821.6	0.30	4.900	3.13 (0.06)
P23	352.9	495.8	611.8	452.0	0.35	0.430	5.20 (0.09)	P48	352.9	494.9	244.7	816.3	0.35	15.000	2.14 (0.09)
P24	333.3	528.8	385.2	603.4	0.40	0.079	2.86 (0.04)	P49	333.3	528.2	192.6	794.6	0.40	0.380	2.04 (0.04)
P25	315.8	557.8	273.7	650.1	0.45	0.550	3.24 (0.02)	P50	315.8	558.6	547.4	378.3	0.45	8.300	0.43 (0.04)

* NA: Targeted MSF value not achieved; (): standard deviation

Table 3.9. Proportioning and e_{EP} of the investigated CEM mixtures.

Mix No.	Cement (kg/m^3)	Water (kg/m^3)	Clay type I (kg/m^3)	Clay type II (kg/m^3)	Silt (kg/m^3)	W/P	Sand (kg/m^3)	e_{EP} (µm)	$f'_{c\text{-}1d}$ (MPa)
M6	100.0	245.3	86.7	-	514.2	0.35	1197.2	40.2	-
M10	101.6	290.1	117.4	-	748.0	0.30	815.6	88.4	1.3 (0.04)
M11	149.3	294.6	86.2	-	500.9	0.40	1038.0	56.0	2.3 (0.08)
M12	139.6	310.7	242.0	-	308.8	0.45	1041.6	55.6	1.3 (0.04)
M15	147.0	342.8	101.9	-	730.4	0.35	669.6	121.4	1.7 (0.05)
M16	157.7	264.3	182.2	-	247.4	0.45	1268.7	34.4	2.8 (0.10)
M17	192.8	360.4	167.1	-	360.9	0.50	885.6	76.5	1.6 (0.04)
M18	181.5	280.4	125.9	-	627.2	0.30	885.1	76.5	4.6 (0.10)
M22	198.7	241.7	114.8	-	492.2	0.30	1117.7	47.6	5.6 (0.12)
M23	188.1	264.3	326.1	-	240.9	0.35	1109.1	48.4	3.6 (0.08)
M24	224.1	355.5	259.0	-	405.7	0.40	738.4	104.2	2.3 (0.14)
M25	212.0	374.5	183.7	-	436.4	0.45	741.4	103.5	0.5 (0.02)
M26	63.1	212.9	-	43.7	602.9	0.30	1268.7	34.4	-
M32	99.3	277.7	-	114.8	480.2	0.40	1117.7	47.6	-
M37	147.2	327.2	-	102.1	477.8	0.45	960.3	65.6	1.5 (0.02)
M44	179.1	317.8	-	155.2	573.6	0.35	812.1	89.1	-
M45	169.3	338.6	-	117.4	559.7	0.40	815.6	88.4	0.5 (0.02)
M49	187.6	297.3	-	108.4	447.2	0.40	1030.1	56.9	2.5 (0.04)

(): standard deviation

Table 3.10. Mixture proportions of the investigated SCEC mixtures, as well as reference CEM and paste ones.

Mix No.	Cement (kg/m^3)	Water (kg/m^3)	Clay type I (kg/m^3)	Clay type II (kg/m^3)	Silt (kg/m^3)	W/P	Sand (kg/m^3)	Gravel (kg/m^3)	e_{EP} (µm)
C16	150.0	251.4	173.3	-	235.3	0.45	1197.0	136.0	34.4
C22	180.0	219.0	104.0	-	445.9	0.30	1000.2	255.7	47.6
C37	120.0	266.7	-	83.2	389.4	0.45	750.1	511.4	65.6
C_{ref}	627.2	250.9	-	-	0	0.40	665.0	680.0	65.1
M_{ref}	818.7	327.5	-	-	0	0.40	964.5	0	65.1
P_{ref}	1393.8	557.5	-	-	0	0.40	0	0	-

3.2.3 Phase 3: New insight on rheology of self-consolidating earth concrete (SCEC)

3.2.3.1 Materials and testing methods

Similar materials used in Phases 1-2 were used to conduct the experiments of Phase 3. The PSDs of the aggregate are presented in Fig. 3.5.

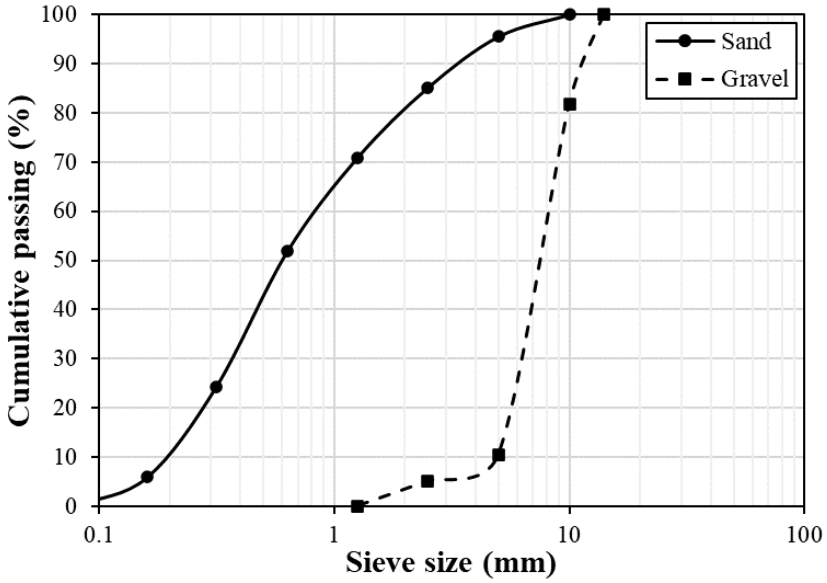

Fig. 3.5. Particle-size distributions of the sand and gravel.

Rheometric tests were conducted on the investigated paste mixtures using the Anton Paar MCR 302 rheometer with parallel-plates geometry, as shown in Fig. 3.6. It should be noted that coaxial geometry could not be employed due to the presence of silt particles up to 75 µm. The viscoplastic properties of the paste mixtures were measured using a shearing protocol that consists in applying a pre-shearing of 150 s^{-1} for 120 s, followed by stepwise descending regime to a shear rate of 1 s^{-1} during 105 s, as shown in Fig. 3.7a.

Moreover, a hysteresis-loop shearing protocol was applied to evaluate the thixotropy of the paste mixtures, as shown in Fig. 3.7b. This consists in applying a pre-shearing of 50 s^{-1} for 30 s, followed by a 30-s resting period (0 s^{-1}). After the resting period, the shear rate values increased step-wise from 0.1 s^{-1} to 150 s^{-1} during 90 s, followed by a step-wise shear-rate reduction to its initial value 0.1 s^{-1} for another 90-s period [39–41]. The enclosed area between the increasing (Up) and decreasing (Down) shear stress-shear rate curves was then calculated and used to assess the breakdown and thixotropy of the investigated paste mixtures [42]. On the other hand, the ConTec 5 and 6 rheometers were used to evaluate the rheological properties of the investigated concrete

mixtures and their corresponding CEMs, respectively. The Bingham and Herschel-Bulkley models were applied to estimate the rheological parameters of the investigated mixtures, as follow:

$$\text{Bingham model: } \tau = \tau_0 + \mu_p \times \dot{\gamma} \tag{3.5}$$

$$\text{Herschel-Bulkley model: } \tau = \tau_0 + k \times \dot{\gamma}^n \tag{3.6}$$

where τ, τ_0, μ_p, $\dot{\gamma}$, k, and n are shear stress, yield stress, plastic viscosity, shear rate, consistency, and pseudoplastic indices, respectively. It must be also noted that the viscoplastic and thixotropic measurements were carried out at 0, 30, and 60 min after mixing.

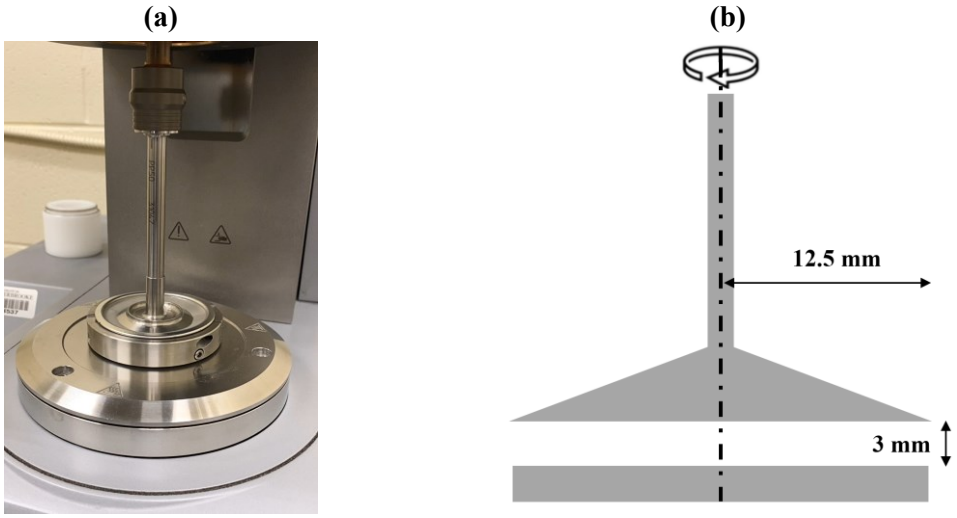

Fig. 3.6. (a) AntonPaar rheometer with parallel-plate geometry and (b) schematics of the parallel-plates system geometry.

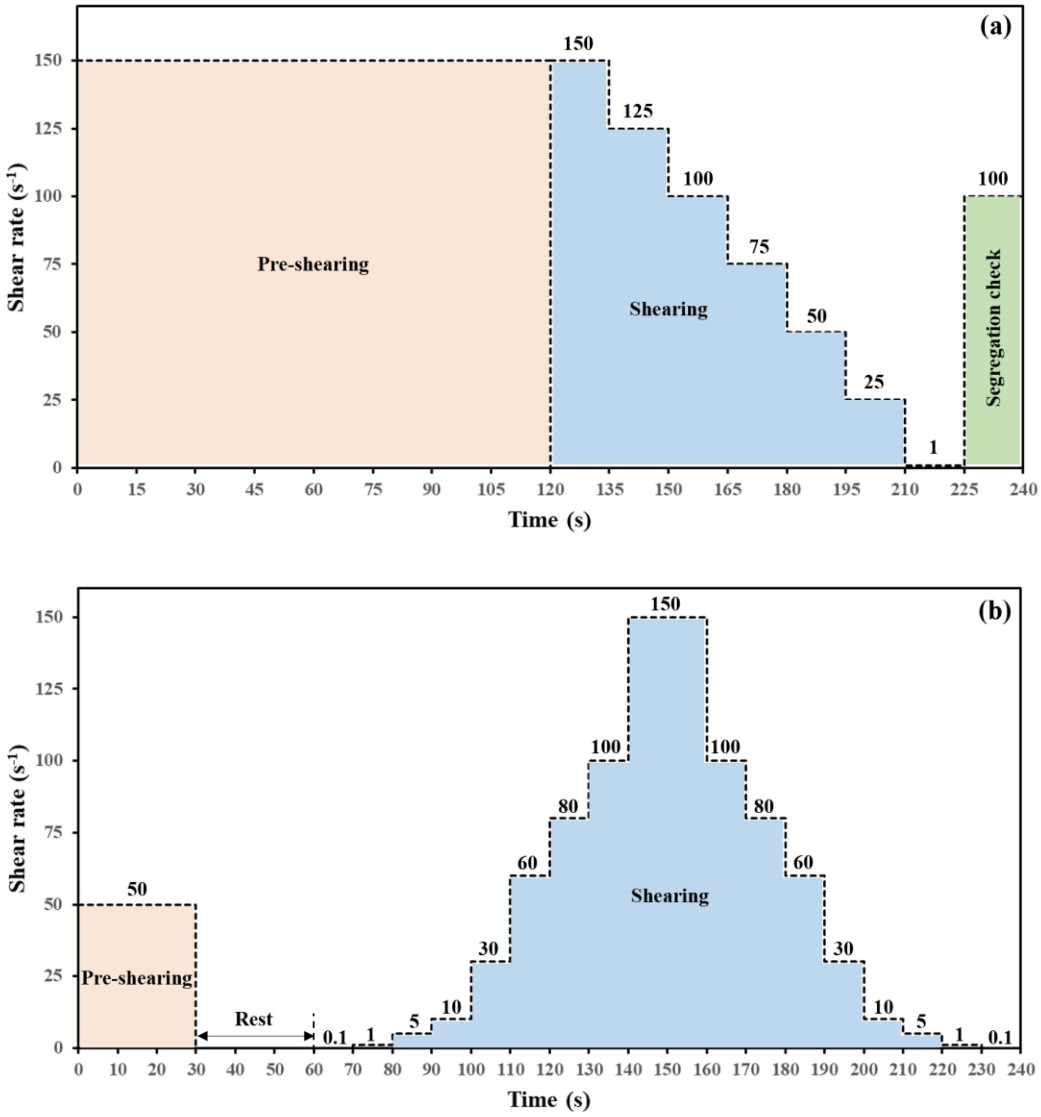

Fig. 3.7. Shear protocol employed to assess (a) viscoplastic properties and (b) thixotropy of the investigated paste mixtures.

3.2.3.2 Mixtures proportioning

First, eighteen paste mixtures were selected out of the 50 investigated mixtures [37] to proportion the CEM mixtures, based on their 1-day compressive strength (> 1 MPa) and admixture demand to achieve a targeted MSF of 280 ± 20 mm. Similarly, the MSF values of the 18 selected CEM mixtures were assessed to secure the targeted MSF of 280 ± 20 mm. Finally, according to the CEM results, three SCEC mixtures were selected. It is worthy to mention that only the SCEC mixtures proportioned with PCE were chosen to avoid complexity of admixture-type effect on the rheological results. Moreover, a reference concrete mixture (C_{ref}) and its corresponding CEM (M_{ref}) were also investigated. These mixtures were proportioned with PCE and without any clay content.

The mixture proportioning of the investigated paste (P), CEM (M), and SCEC (C) mixtures are summarized in Table 3.11.

Table 3.11. Investigated parameters and their corresponding levels to proportion the investigated SCEC mixtures [37].

	Mix No.	Admixture type	Cement (kg/m^3)	Water (kg/m^3)	Clay (kg/m^3)		Silt (kg/m^3)	W/P	V_P (%)	Sand (kg/m^3)	Gravel (kg/m^3)	S/A	e_{EP} (μm)
					Type I	Type II							
Paste	P6	NE-PC	200.0	490.7	173.3	-	1028.5	0.35	-	-	-	-	-
	P10	PNS	157.9	450.9	182.5	-	1162.5	0.30	-	-	-	-	-
	P11	PNS	266.7	526.2	154.1	-	894.9	0.40	-	-	-	-	-
	P12	NE-PC	250.0	556.3	433.3	-	553.0	0.45	-	-	-	-	-
	P15	PCE	210.5	490.9	146.0	-	1046.0	0.35	-	-	-	-	-
	P16	PCE	333.3	558.7	385.2	-	523.0	0.45	-	-	-	-	-
	P17	PNS	312.5	584.1	270.8	-	584.9	0.50	-	-	-	-	-
	P18	NE-PC	294.1	454.2	203.9	-	1016.0	0.30	-	-	-	-	-
	P22	PCE	375.0	456.2	216.7	-	929.1	0.30	-	-	-	-	-
	P23	PNS	352.9	495.8	611.8	-	452.0	0.35	-	-	-	-	-
	P24	NE-PC	333.3	528.8	385.2	-	603.4	0.40	-	-	-	-	-
	P25	NaHMP	315.8	557.8	273.7	-	650.1	0.45	-	-	-	-	-
	P26	PNS	133.3	450.1	-	92.4	1274.4	0.30	-	-	-	-	-
	P32	PNS	187.5	524.2	-	216.7	906.3	0.40	-	-	-	-	-
	P37	PCE	250.0	555.6	-	173.3	811.3	0.45	-	-	-	-	-
	P44	PNS	277.8	492.9	-	240.7	889.7	0.35	-	-	-	-	-
	P45	NE-PC	263.2	526.2	-	182.5	869.9	0.40	-	-	-	-	-
	P49	PCE	333.3	528.2	-	192.6	794.6	0.40	-	-	-	-	-
CEM	M6	NE-PC	100.0	245.3	86.7	-	514.2	0.35	45	1197.2	-	1	40.2
	M10	PNS	101.6	290.1	117.4	-	748.0	0.30	57	815.6	-	1	88.4
	M11	PNS	149.3	294.6	86.2	-	500.9	0.40	45	1038.0	-	1	56.0
	M12	NE-PC	139.6	310.7	242.0	-	308.8	0.45	48	1041.6	-	1	55.6
	M15	PCE	147.0	342.8	101.9	-	730.4	0.35	57	669.6	-	1	121.4
	M16	PCE	157.7	264.3	182.2	-	247.4	0.45	45	1268.7	-	1	34.4
	M17	PNS	192.8	360.4	167.1	-	360.9	0.50	48	885.6	-	1	76.5
	M18	NE-PC	181.5	280.4	125.9	-	627.2	0.30	51	885.1	-	1	76.5
	M22	PCE	198.7	241.7	114.8	-	492.2	0.30	48	1117.7	-	1	47.6
	M23	PNS	188.1	264.3	326.1	-	240.9	0.35	51	1109.1	-	1	48.4
	M24	NE-PC	224.1	355.5	259.0	-	405.7	0.40	54	738.4	-	1	104.2
	M25	NaHMP	212.0	374.5	183.7	-	436.4	0.45	57	741.4	-	1	103.5
	M26	PNS	63.1	212.9	-	43.7	602.9	0.30	45	1268.7	-	1	34.4
	M32	PNS	99.3	277.7	-	114.8	480.2	0.40	48	1117.7	-	1	47.6
	M37	PCE	147.2	327.2	-	102.1	477.8	0.45	48	960.3	-	1	65.6
	M44	PNS	179.1	317.8	-	155.2	573.6	0.35	54	812.1	-	1	89.1
	M45	NE-PC	169.3	338.6	-	117.4	559.7	0.40	57	815.6	-	1	88.4
	M49	PCE	187.6	297.3	-	108.4	447.2	0.40	54	1030.1	-	1	56.9
	M_{ref}	PCE	818.7	327.5	-	-	-	0.40	45	964.5	-	1	65.1
SCEC	C16	PCE	150.0	251.4	173.3	-	235.3	0.45	45	1197.0	136.0	0.9	34.4
	C22	PCE	180.0	219.0	104.0	-	445.9	0.30	48	1000.2	255.7	0.8	47.6
	C37	PCE	120.0	266.7	-	83.2	389.4	0.45	48	750.1	511.4	0.6	65.6
	C_{ref}	PCE	627.2	250.9	-	-	-	0.40	45	665.0	680.0	0.5	65.1

3.2.4 Phase 4: Hygrothermal and microstructural characterization of self-consolidating earth concrete (SCEC)

3.2.4.1 Materials and mixtures proportioning

The proportioning of the investigated concrete mixtures carried out to investigate the hygrothermal properties are summarized in Table 3.12. The three SCEC mixtures were carefully selected (based on 1-day compressive strength [35] of more than 1 MPa and achieving the slump flow [31] of 700 mm with no visual segregation). The SECE mixtures were proportioned with various clay types/contents and Atterberg limits [33], as presented in Table 3.13. Due to plasticity of earth-based materials containing clay, Atterberg limits of the corresponding earths (i.e., clay, silt, and sand < 425 μm) were evaluated in terms of liquid limit (LL), plastic limit (PL) and plasticity index (PI). It should be noted that Atterberg limits are presented only for SCEC mixtures since there is no clay and silt in the reference mixture. 28-day drying shrinkage [36] values of the investigated mixtures are also presented in Table 3.13, concluded from Phase Two.

Table 3.12. Proportioning of the investigated mixtures.

Mix No.	Cement (kg/m^3)	Water (kg/m^3)	Clay Type I (kg/m^3)	Clay Type II (kg/m^3)	Silt (kg/m^3)	W/P	Sand (kg/m^3)	Gravel (kg/m^3)
C_{ref}	627.2	250.9	-	-	0	0.40	665.0	680.0
C120-II	120.0	266.7	-	83.2	389.4	0.45	750.1	511.4
C150-I	150.0	251.4	173.3	-	235.3	0.45	1197.0	136.0
C180-I	180.0	219.0	104.0	-	445.9	0.30	1000.2	255.7

Table 3.13. Atterberg limits of the three investigated earth mixtures.

Mix No.	Atterberg limits			Compressive strength (MPa)		28-day drying shrinkage (%)
	LL (%)	PL (%)	PI (%)	1-day	28-day	
C_{ref}	-	-	-	22.7	52.4	0.037
C120-II	32.8	21.8	11.0	1.2	3.3	0.104
C150-I	18.9	14.9	4.0	1.9	6.2	0.093
C180-I	18.9	15.8	3.1	3.3	12.0	0.078

3.2.4.2 Test methods

Concrete mixtures were prepared using a rotating drum mixer. Hygrothermal and microstructural characterization of the samples were investigated after 28 days of curing at 23°C and 100% relative humidity, as follow:

3.2.4.2.1 Sorption isotherm

The sorption isotherm test, carried out in isothermal conditions, characterizes the relationship between water content and relative humidity of the surrounding environment in various moisture conditions ranging from 0 to 95%. The following procedure was treated for the measurements: The samples were oven dried at 40°C for 24 h followed by being degassed under air vacuum to ensure drying procedure. The samples were then weighed to calculate the dry mass and analyzed with SPS ProUmid device using manometric method, as presented in Fig. 3.8 [43]. The cubic samples, measuring 15 mm × 15 mm × 15 mm dimensions, were treated in adsorption-desorption isotherms. The changes in volume of water vapor adsorbed or desorbed were measured for each sample at a fixed temperature. The calculations were based on the adsorbed water by procurement of vapor pressure and perfect gas formula [44]. The volumetric method was treated for water vapor sorption isotherms. In order to achieve more precise measurements, Belsorp aqua-3® device is equipped with three analysis ports to allow high output measurements. This method can attenuate possible inaccuracies used in the gravimetric methods by overcoming the sensitivity of the weighing devices.

Fig. 3.8. Scheme of the Belsorp Aqua-3® device.

3.2.4.2.2 Water vapor permeability

As one of the critical hygric properties, water vapor permeability test is essential for characterization of building materials by providing information regarding migration of moisture in the samples. This migration is referred to vapor diffusion. The measurements were performed at 23°C using the cup method according to EN ISO 12572 standard [45]. The samples include cylinders of 78-mm diameter and 20-mm height. The test procedure aimed to apply a pressure gradient between two sides of the sample. The gradient for dry cup consisted of 3% relative humidity inside the cup, and 50% outside. By using a Gravitest® device as a climatic chamber, each cup was automatically weighed with a high precision of 0.00001 g.

3.2.4.2.3 Gas permeability

Gas permeability of the mixtures was measured by means of Cembureau permeameter, as presented in Fig. 3.9, on cylindrical samples measuring 11-mm diameter and 50-mm thickness [46]. The samples were preconditioned at 45°C temperature under vacuum until mass stabilization. These samples were then surrounded by a resin to ensure a unidirectional flow during the test.

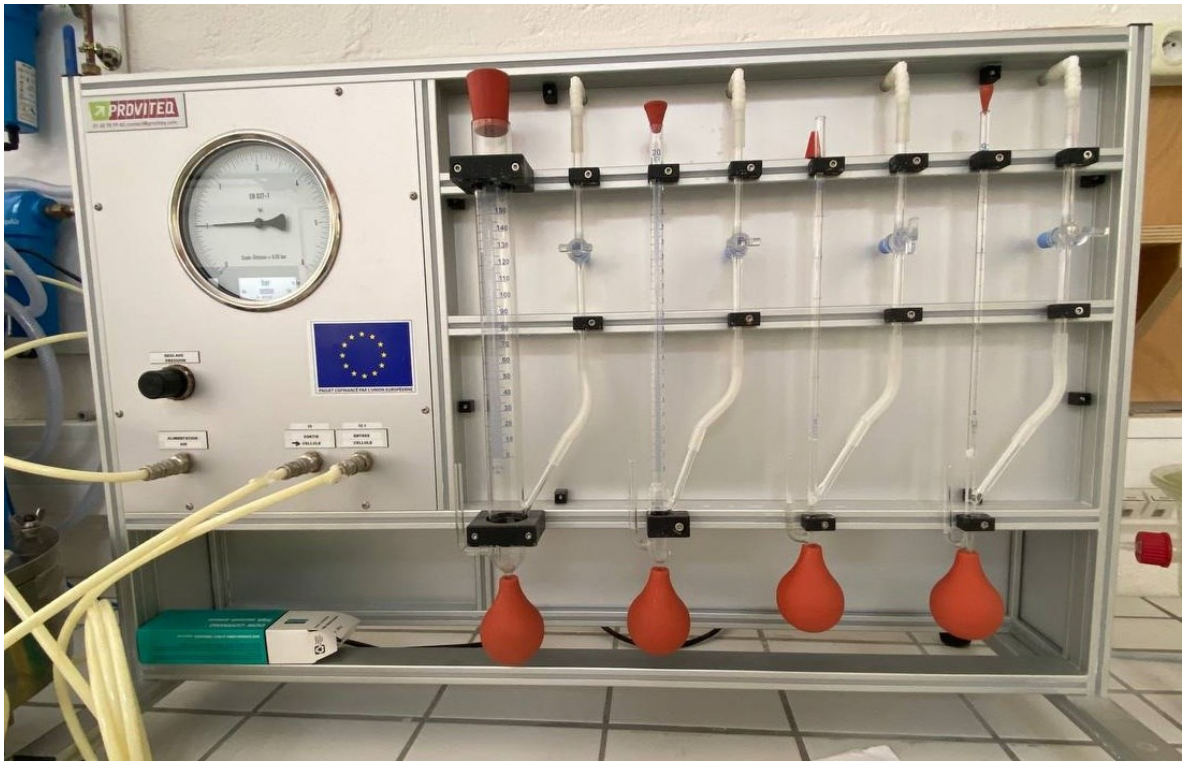

Fig. 3.9. Scheme of the Cembureau permeameter.

Specific permeability coefficient K_A was calculated using the modified Darcy's equation, as follows:

$$K_A=\frac{2\mu P_0 QL}{A(P_0^2-P_1^2)} \quad \text{where } Q=\frac{V}{t_{avg}} \tag{3.7}$$

where μ (Pa.s), P_0 (Pa), P_1 (Pa), Q (m^3/s), L (m), A (m^2), V (m^3), and t_{avg} (s) are the dynamic viscosity of the gas, entrance and exit absolute pressure values, volumetric flow, sample thickness, surface area of the sample section, volume of the bubble flowmeter, and average passing time, respectively. It should be noted that the measured permeability coefficient is apparent permeability. Each test was performed under three different high pressures of 150, 200, and 250 kPa to assess the intrinsic permeability (K_{int}). Using Klinkenberg method [47], K_{int} was calculated as the interception of the K_A curve with respect to $1/P_m$ (where $P_m=\frac{P_0+P_1}{2}$) as:

$$K_A=K_{int}\left(\frac{\beta}{P_m}+1\right) \tag{3.8}$$

where β (Pa) is the Klinkenberg coefficient which varies with the intrinsic permeability [48].

3.2.4.2.4 Heat capacity

Calvet® calorimeter was used to measure the specific heat capacity, as presented in Fig. 3.10. The samples included cylinders of 7 mm in diameter and 5 cm in height. The reference cell and tested sample, in sealed cylinders, were enclosed in the calorimeter block to perform the test. In this device, samples were surrounded by 3D Calvet sensors so that all the emitted heat can be measured. A cryostat was also connected to regulate the internal temperature of the calorimeter. The test was performed in a temperature range of -10 to 40°C with a heating rate of 0.1°C/min. It is worth mentioning that since the heat loss of the 3D sensors is less than 10%, rather than those of the 2D sensors (50% to 70%), the 3D Calvet sensors are more accurate than the 2D ones.

Fig. 3.10. Scheme of the Calvet calorimeter.

3.2.4.2.5 Thermal conductivity

This inherent thermal property was measured in stationary conditions using the standard method of guarded hot plate conforming with EN 12664 [49] and EN 12667 [50]. The samples measured 15 × 15 cm^2 with a height of approximately 5 cm. The tests were carried out using the λ-Meter® EP500e device, as shown in Fig. 3.11. This set-up enables the heat transfer through a surface plate limited between two parallel cold and hot isotherm planes to impose a fixed temperature gradient. It is worth mentioning that transversal heat dissipation should be prevented since the longitudinal heat flow through the sample thickness should be considered. Putting guard rings surrounding the side of the samples can be favorable for this purpose. Thermal conductivity was thus calculated through the electrical power provided by the device.

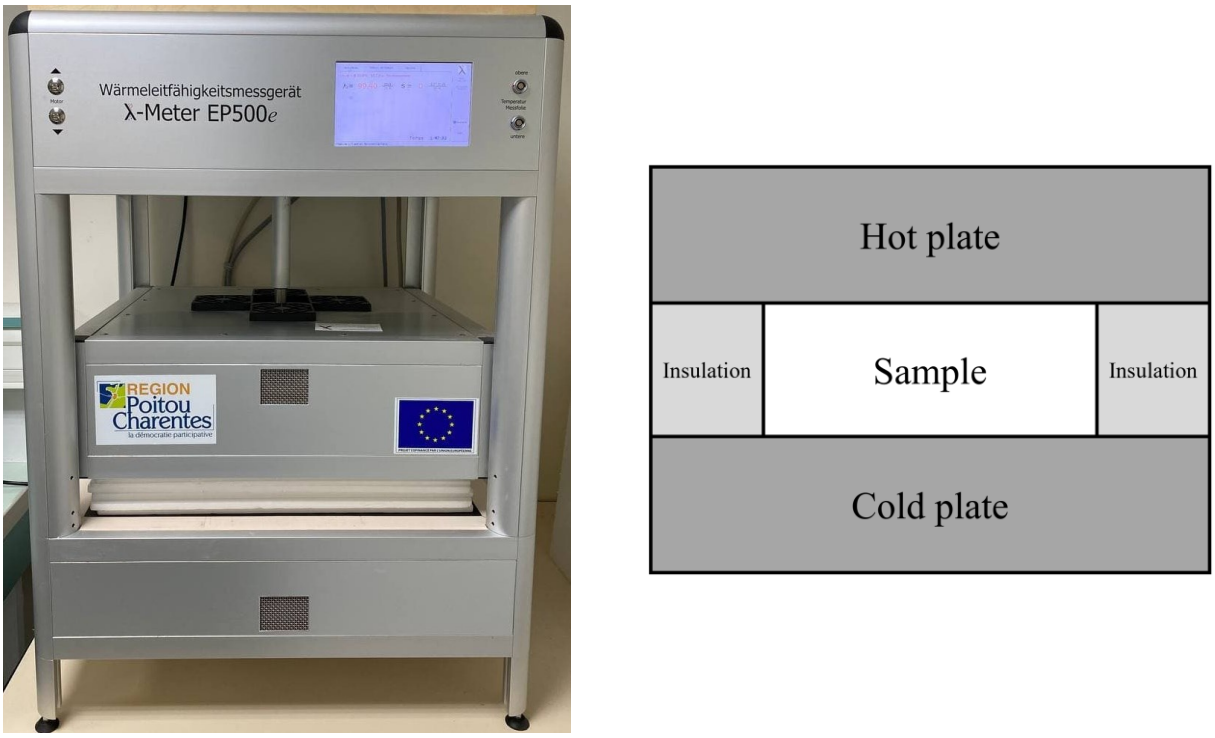

Fig. 3.11. Scheme of the Lambda-meter EP500e.

3.2.4.2.6 Thermogravimetric analysis (TGA)

The samples were vacuumed dried at 45°C to remove the water bound in the samples. Consequently, TGA procedure was performed on 100 mg of sample heated at a 10°C/min rate up to 1000°C.

3.2.4.2.7 Water porosity measurements

Three cubic samples of 5 × 5 × 5 cm^3 were used to determine the porosity of the concrete mixtures according to AFPC-AFREM [51]. Initially, the samples were water-saturated in order to obtain the saturated mass. The porosity was then calculated, as follows:

$$\varepsilon_p = \frac{M_{air} - M_{dry}}{M_{air} - M_{water}} \times 100\ (\%) \tag{3.9}$$

where M_{air}, M_{dry}, and M_{water} are the weight of saturated sample after removing from the water, dry sample weight (dried at 80 °C until mass stabilization), and hydrostatic weight of the sample saturated in water, respectively. Furthermore, surface pores and smoothness of the mixtures were also analyzed using a Keyence® VHX-7000 digital microscope.

3.2.4.2.8 Porosity measurements (3Flex)

The porous properties of the investigated mixtures, including surface area, pore volume, and pore size distribution, were measured using a 3Flex–high resolution surface characterization analyzer apparatus from Micromeritics®. Relative pressure (P/P_0) can be as low as 1.3×10^{-9} up to 1.0. The device allows advanced dosing method N_2 adsorption which can be measured by defining both pressure and volume increments. Hysteresis loop is associated with capillary condensation taking place in the mesopores which limits uptake at high relative pressure. It should be noted that prior to N_2 adsorption/desorption measurements, the samples (100–200 mg) were degassed in vacuum condition. The mass of each sample was measured with high precision microbalance with a resolution of ±1 μg. This testing reflects useful information for multilevel porosity, including the micropores (< 2 nm), mesopores (2–50 nm), and macropores (> 50 nm).

3.2.4.2.9 Mercury intrusion porosimetry (MIP)

The pore size distribution was determined using mercury intrusion. The samples were initially dried at a temperature of 45°C before the test until mass stabilization. Micromeritics Porosimeter (Autopore III 9420) with pressure range up to 400 MPa was used which can ensure the mercury to penetrate the pores ranging between 0.003 to 360 μm diameter, according to Laplace's law.

3.2.4.2.10 Microstructure observations

Surface microstructure observation was carried out using the CMOS-based digital microscope VHX 7000 (Keyence) with a magnification of ×6000 in the optical wavelength range. Magnifications of E20×20, E20×80, E100×150 and E500×500 were used to capture the observations. Furthermore, the morphological characteristics of the mixtures were analyzed using a scanning electron microscope (SEM) equipped with an Oxford Energy Dispersive Spectroscopy (EDS).

REFERENCES

[1] R.K. Roy, A Primer on the Taguchi Method, Competitive Manufacturing Series, 1990.

[2] G.S. Peace, Taguchi Method, Corporate and Professional Publishing Group, 1993.

[3] P. Walker, R. Keable, J. Martin, V. Maniatidis, Rammed earth: design and construction guidelines, IHS BRE, 2005.

[4] P. Walker, The Australian earth building handbook, Sydney : Standards Australia International,

2002.

[5] F. Andreola, E. Castellini, J.M.F. Ferreira, S. Olhero, M. Romagnoli, Effect of sodium hexametaphosphate and ageing on the rheological behaviour of kaolin dispersions, Appl. Clay Sci. 31 (2006) 56–64. https://doi.org/10.1016/j.clay.2005.08.004.

[6] F. Andreola, E. Castellini, T. Manfredini, M. Romagnoli, The role of sodium hexametaphosphate in the dissolution process of kaolinite and kaolin, J. Eur. Ceram. Soc. 24 (2004) 2113–2124. https://doi.org/10.1016/S0955-2219(03)00366-2.

[7] K.O. Adebowale, I.E. Unuabonah, B.I. Olu-Owolabi, Adsorption of some heavy metal ions on sulfate- and phosphate-modified kaolin, Appl. Clay Sci. 29 (2005) 145–148. https://doi.org/10.1016/j.clay.2004.10.003.

[8] F. Andreola, E. Castellini, G. Lusvardi, L. Menabue, M. Romagnoli, Release of ions from kaolinite dispersed in deflocculant solutions, Appl. Clay Sci. 36 (2007) 271–278. https://doi.org/10.1016/j.clay.2006.10.002.

[9] E. Castellini, C. Berthold, D. Malferrari, F. Bernini, Sodium hexametaphosphate interaction with 2:1 clay minerals illite and montmorillonite, Appl. Clay Sci. 83–84 (2013) 162–170. https://doi.org/10.1016/j.clay.2013.08.031.

[10] H.M.M. Diz, B. Rand, The mechanism of deflocculation of kaolinite by polyanions, Br. Ceram. Trans. 89 (1990) 77–82.

[11] J.L. Amorós, V. Beltrán, V. Sanz, J.C. Jarque, Electrokinetic and rheological properties of highly concentrated kaolin dispersions: Influence of particle volume fraction and dispersant concentration, Appl. Clay Sci. 49 (2010) 33–43. https://doi.org/10.1016/j.clay.2010.03.020.

[12] F. Andreola, M. Romagnoli, E. Castellini, G. Lusvardi, L. Menabue, Role of the surface treatment in the deflocculation of kaolinite, J. Am. Ceram. Soc. 89 (2006) 1107–1109. https://doi.org/10.1111/j.1551-2916.2005.00814.x.

[13] D. Penner, G. Lagaly, Influence of anions on the rheological properties of clay mineral dispersions D., Appl. Clay Sci. 19 (2001) 131–142.

[14] M.S. Phadke, Quality Engineering using Robust Design, Prentice Hall, New Jersey, 1989.

[15] ASTM C305-20, Standard Practice for Mechanical Mixing of Hydraulic Cement Pastes and Mortars of Plastic Consistency, ASTM Int. (2020) 1–3. https://doi.org/10.1520/C0305-20.2.

[16] N. Roussel, C. Stefani, R. Leroy, From mini-cone test to Abrams cone test: Measurement of cement-based materials yield stress using slump tests, Cem. Concr. Res. 35 (2005) 817–822. https://doi.org/10.1016/j.cemconres.2004.07.032.

[17] BS EN 445, Grout for prestressing tendons. Test methods, 2007.

[18] ASTM C109-20, Standard test method for compressive strength of hydraulic cement mortars (using 2-in. or [50-mm] cube specimens), ASTM Int. (2020). https://doi.org/10.1520/C0109_C0109M-20B.

[19] A. Schwartzentruber, C. Catherine, Method of Concrete Equivalent Mortar—A Novel Tool to Help in Formulation of Concrete with Admixtures, Mater. Struct. 33 (2000) 475–482.

[20] K.H. Khayat, S.-D. Hwang, Effect of High-Range Water- Reducing Admixture Type on Performance of Self-Consolidating Concrete, in: Eighth CANMET/ACI Int. Conf. Superplast. Other Chem. Admixtures Concr., American Concrete Institute, Farmington Hills, MI, 2006: pp. 185–200.

[21] J.J. Assaad, J. Harb, E. Chakar, Relationships between Key ASTM Test Methods Determined on Concrete and Concrete-Equivalent-Mortar Mixtures, J. ASTM Int. 6 (2008).

[22] T.K. Erdem, K.H. Khayat, A. Yahia, Correlating Rheology of Self-Consolidating Concrete to Corresponding Concrete-Equivalent Mortar, ACI Mater. J. (2009).

[23] D. Kabagire, P. Diederich, A. Yahia, New insight into the equivalent concrete mortar approach for self-consolidating concrete, J. Sustain. Cem. Mater. 4 (2015) 215–224. https://doi.org/10.1080/21650373.2015.1018983.

[24] J.H. Lee, J.H. Kim, J.Y. Yoon, Prediction of the yield stress of concrete considering the thickness of excess paste layer, Constr. Build. Mater. 173 (2018) 411–418. https://doi.org/10.1016/j.conbuildmat.2018.03.124.

[25] M. Hosseinpoor, B.I. Ouro Koura, A. Yahia, E.H. Kadri, Diphasic investigation of the visco-elastoplastic characteristics of highly flowable fine mortars, Constr. Build. Mater. 270 (2021) 121425. https://doi.org/10.1016/J.CONBUILDMAT.2020.121425.

[26] M. Hosseinpoor, B.-I.O. Koura, A. Yahia, Rheo-morphological investigation of Reynolds dilatancy and its effect on pumpability of self-consolidating concrete, Cem. Concr. Compos. 117 (2021).

[27] M. Hosseinpoor, B.I. Ouro Koura, A. Yahia, Rheo-morphological investigation of static and

dynamic stability of self-consolidating concrete: A biphasic approach, Cem. Concr. Compos. 121 (2021) 104072. https://doi.org/10.1016/j.cemconcomp.2021.104072.

[28] M. Hosseinpoor, B.I.O. Koura, A. Yahia, New diphasic insight into the restricted flowability and granular blocking of self-consolidating concrete: Effect of morphological characteristics of coarse aggregate on passing ability of SCC, Constr. Build. Mater. 308 (2021) 125001. https://doi.org/10.1016/J.CONBUILDMAT.2021.125001.

[29] Nordtest, Concrete, fresh: Compactibility with ic-tester (intensive compaction tester) (NT BUILD 427), 1994.

[30] B.M. Aïssoun, Study of the Influence of Aggregate Characteristics on the Rheology of Fluid Concrete with Adapted Rheology (in French), Université de Sherbrooke, 2011.

[31] EFNARC, Specification and Guidelines for Self-Compacting Concrete, (2002).

[32] ASTM C596-18, Standard Test Method for Drying Shrinkage of Mortar Containing Hydraulic Cement, ASTM Int. (2018). https://doi.org/10.1520/C0596-18.

[33] ASTM D4318 − 17, Standard Test Methods for Liquid Limit, Plastic Limit, and Plasticity Index of Soils, ASTM Stand. (2017).

[34] H. Okamura, M. Ouchi, Self-Compacting Concrete, J. Adv. Concr. Technol. 1 (2003) 5–15.

[35] ASTM C39, Standard Test Method for Compressive Strength of Cylindrical Concrete Specimens, ASTM Stand. (2021).

[36] ASTM C157, Standard Test Method for Length Change of Hardened Hydraulic-Cement Mortar and Concrete, ASTM Stand. (2017).

[37] M. Kohandelnia, M. Hosseinpoor, A. Yahia, R. Belarbi, A new approach for proportioning self-consolidating earth paste (SCEP) using the Taguchi method, Constr. Build. Mater. 347 (2022) 128579. https://doi.org/10.1016/J.CONBUILDMAT.2022.128579.

[38] C.M. Ouellet-Plamondon, G. Habert, Self-Compacted Clay based Concrete (SCCC): Proof-of-concept, J. Clean. Prod. 117 (2016) 160–168. https://doi.org/10.1016/j.jclepro.2015.12.048.

[39] Y.A. Abebe, L. Lohaus, Rheological characterization of the structural breakdown process to analyze the stability of flowable mortars under vibration, Constr. Build. Mater. 131 (2017) 517–525. https://doi.org/10.1016/J.CONBUILDMAT.2016.11.102.

[40] R.S. Ahari, T.K. Erdem, K. Ramyar, Thixotropy and structural breakdown properties of self

consolidating concrete containing various supplementary cementitious materials, Cem. Concr. Compos. 59 (2015) 26–37. https://doi.org/10.1016/J.CEMCONCOMP.2015.03.009.

[41] H.A. Barnes, Thixotropy—a review, J. Nonnewton. Fluid Mech. 70 (1997) 1–33. https://doi.org/10.1016/S0377-0257(97)00004-9.

[42] J.J. Assaad, K.H. Khayat, H.A. Mesbah, Assessment of Thixotropy of Flowable and Self-Consolidating Concrete, Aci Mater. J. 100 (2003) 99–107.

[43] N. Issaadi, A. Nouviaire, R. Belarbi, A. Aït-Mokhtar, Moisture characterization of cementitious material properties: assessment of water vapor sorption isotherm and permeability variation with ages, Constr. Build. Mater. 83 (2015) 237–247. https://doi.org/10.1016/j.conbuildmat.2015.03.030.

[44] M. Maaroufi, F. Bennai, R. Belarbi, K. Abahri, Experimental and numerical highlighting of water vapor sorption hysteresis in the coupled heat and moisture transfers, J. Build. Eng. 40 (2021) 102321. https://doi.org/10.1016/J.JOBE.2021.102321.

[45] European Standard ISO 12572, Determination of water vapor transmission properties (ISO/DIS 12572:1997), PrEN ISO 12572. (1997).

[46] N.X. P18-463, Norme XP P18-463 - Essai pour béton durci - Essai de perméabilité à l'air, 1999.

[47] L.J. Klinkenberg, The Permeability Of Porous Media To Liquids And Gases, Drill. Prod. Pract. (1941) 200–213.

[48] D.R. Gardner, A.D. Jefferson, R.J. Lark, An experimental, numerical and analytical investigation of gas flow characteristics in concrete, Cem. Concr. Res. 38 (2008) 360–367. https://doi.org/10.1016/J.CEMCONRES.2007.10.001.

[49] BS EN 12664, Thermal performance of building materials and products. Determination of thermal resistance by means of guarded hot plate and heat flow meter methods. Dry and moist products of medium and low thermal resistance, (2001).

[50] BS EN 12667, Thermal performance of building materials and products. Determination of thermal resistance by means of guarded hot plate and heat flow meter methods. Products of high and medium thermal resistance, (2001).

[51] AFPC-AFREM. Durabilité des Bétons-Mode Opératoire Recommandé: Détermination de la Masse Volumique Apparente et de la Porosité Accessible à L'eau, in: Proc. Compte Rendu Des Journées Tech. AFPC-AFREM, Toulouse, France, 1997: pp. 11–12.

CHAPTER 4. A new approach for proportioning self-consolidating earth paste (SCEP) using the Taguchi method

Authors and affiliations

Mojtaba Kohandelnia: Ph.D. candidate, Cement and Concrete Research Group, Department of Civil and Building Engineering, Université de Sherbrooke, Sherbrooke, Québec, Canada, J1K 2R1.

Masoud Hosseinpoor: Post-Doc, Cement and Concrete Research Group, Department of Civil and Building Engineering, Université de Sherbrooke, Sherbrooke, Québec, Canada, J1K 2R1.

Ammar Yahia: Professor, Cement and Concrete Research Group, Department of Civil and Building Engineering, Université de Sherbrooke, Sherbrooke, Québec, Canada, J1K 2R1.

Rafik Belarbi, Professor, LaSIE UMR CNRS 7356, La Rochelle Université, La Rochelle, France.

Article Status: Published
Journal: Construction and Building Materials – Elsevier
Reference: M. Kohandelnia, M. Hosseinpoor, A. Yahia, and R. Belarbi, "A new approach for proportioning self-consolidating earth paste (SCEP) using the Taguchi method," Constr. Build. Mater., vol. 347, p. 128579, Sep. 2022, doi: 10.1016/J.CONBUILDMAT.2022.128579.
Titre française: Une nouvelle approche pour le dosage de la pâte de terre autoplaçante (PTAP) à l'aide de la méthode Taguchi

Abstract

Rammed earth (RE) construction is an ancient sustainable construction method, which offers various economic and environmental advantages such as the availability of local materials. However, RE construction is a very time-consuming and labor-intensive process due to the consolidation required to achieve the targeted performance. The use of self-consolidating earth concrete (SCEC) can facilitate casting and speed the construction process. However, developing SCEC is challenging due to the presence of clay in earth, which can significantly hinder flowability. Optimizing the paste matrix of SCEC, namely self-consolidating earth paste (SCEP), is essential for achieving targeted workability performance of SCEC. In this study, the Taguchi method was employed to evaluate the effect of various mixture parameters, including clay and admixture type, cement content, and water-to-powder (W/P) and cement-to-clay (Ce/Cl) ratios to proportion SCEP mixtures. These parameters form different binder compositions with various Atterberg limits and water contents to investigate the compatibility and efficiency of different admixture types on the workability and compressive strength of their corresponding SCEP mixtures. Adequate clay dispersion was achieved using sodium hexametaphosphate (NaHMP) whereas polycarboxylate ether (PCE) was only efficient on cement particles. Sodium silicate (NaSil) did not contribute to dispersion of single-powder systems, while sodium polynaphtalene (PNS) and non-esterified polycarboxylate (NE-PC) showed compatibility with both clay and cement particles. Signal-to-noise ratio (S/N) analyses revealed that lower cement content and higher W/P and Ce/Cl resulted in lower admixture demand for targeted workability and marsh cone test (MCT) values. Regarding 1-day compressive strength, to facilitate the demolding process, PNS, PCE and NaSil showed the highest efficiency. As concluded from the analysis of variance (ANOVA), clay and admixture type had the highest contribution on workability, while cement content and W/P were significant on compressive strength. Several theoretical models were also established to predict the workability of SCEP mixtures from Atterberg limits of the corresponding soil. Finally, a new SCEP proportioning approach was proposed based on the established models and compressive strength contours to be used for different earth types.

Keywords: Self-consolidating earth paste; Clay; Ternary-binder system; Taguchi analysis; Atterberg limits.

4.1 Introduction

Building and construction industry accounts for over 30% of the extracted resources and 48% of energy-related CO_2 emissions [1]. As one of the most used materials in construction, cement is responsible for 5% of global CO_2 emissions [2]. One of the main approaches to reduce its carbon footprint is the use of sustainable construction materials as an alternative for cement clinkers [3]. Supplementary cementitious materials (SCMs) can decrease the demand of cement production and, consequently, reduce its negative environmental impacts. Earth construction, such as wattle and daub, cob, masonry adobe bricks, and rammed earth (RE) can contribute to getting the construction industry on track to reach global climate targets. RE, as one of the common earthen constructions, was neglected for a long time due to the evolution of cement-based materials [4]. Because of the low environmental impacts of earth-based materials, RE construction has recently gained interest in different applications. RE makes it possible to achieve a wider variety of textures compared to other conventional construction materials with better energy efficiency, and superior thermal performance, and indoor air quality [5,6]. Earth-based materials are also available resources which can contribute to decreasing the consumption of natural resources and industrial materials. Therefore, earthen materials can be used as SCM in concrete mixtures [7]. Despite the above-mentioned advantages of RE, the compaction process is time and energy consuming. Moreover, layer-by-layer casting can lead to moisture and compaction variation along the wall, which causes material performance deficiencies.

Self-consolidating earth concrete (SCEC) can eliminate the mechanical compaction and speed up the casting process. Earth is a composition of clay, silt, sand, and gravel in the order of their size from sub-µm to several mm [8]. Clay and silt are generally used as binder in earth concrete [9]. In stabilized earth concrete, cement, clay, and silt act as a ternary-binder system. On the other hand, earth consists of a wide variety of soils, which can be used as earth-based materials with variable clay fractions [10]. Clay minerals consist of fine particles with high specific surface area (SSA), depending on their minerals [11], hence leading to challenges in achieving proper deflocculation and high flowability of SCEC. Desired flowability can be hindered due to the high specific surface area, water absorption, nucleation promotion, and flocculation of fine particles [12]. A high concentration of fine particles increases the viscosity and yield stress of SCC and, consequently, stability due to higher interparticle friction. This can, however, lower its flowability. A flowable

paste can be only achieved when a compatible admixture-clay particle system is used. Oullet-Plamondon and Habert [9] reported the efficiency of polycarboxylate ether (PCE) as a high-range water reducer (HRWR) agent to enhance the flowability of self-compacting clay-based concrete in the presence of cement. However, in the absence of cement, PCE does not contribute to dispersing clay particles and decreasing the yield stress of earth-based materials [13]. Sodium hexametaphosphate and sodium silicate, used as deflocculants, exhibited significant dispersion effect on natural clay materials by increasing their overall negative surface charge and alkalinity [14–22]. There have been several attempts in the literature to evaluate the compatibility of chemical admixtures in SCEC mixtures. However, there is no comprehensive study to investigate the efficiency of clay dispersants and HRWR admixtures in the presence of different compositions of ternary binder systems, mineral types, and water contents. Their efficiency to achieve the desired flowability, in the presence of clay particles, remains ambiguous.

Due to the low cement content, the second challenge is the setting promotion to assess the feasibility of formwork removal. Similarly to self-consolidating concrete (SCC), rheology, stability, and compressive strength can be enhanced by using proper packing density and optimum content of fine particles [23–26]. Coagulants have been used to promote setting. Landrou et al. [13] investigated the efficiency of calcium products on earthen materials, dispersed with clay dispersants. The authors reported that different Ca2+ release rates precipitated in C–S–H formation in the presence of dispersing agents by an anti-plasticity effect. Gelling agents, such as alginic salts, have also been recommended for fast demolding [27–29]. Alginate chains form a connection by intercalating divalent cations [30]. Furthermore, Ouellet-Plamondon et al. [9] recommended using a calcium sulfoaluminate cement (CSA) to promote early setting time. This was related to the CSA potential to promote high early-age strength [31]. However, further studies are required to identify the appropriate cement and water content ranges for different types of earth.

In the case of earth concrete, it is common to use locally available earth. The existence of different soil types makes it difficult to establish a general mixture proportioning method (the third challenge of designing SCEC). Earth is a mixture of particles with different shapes, sizes and mineralogical natures [8]. The mineralogical composition in earthen materials varies from one extraction site to another. Therefore, predicting the behavior of earth is challenging due to the diversity of the materials and numerous variables that need to be considered [32]. Identifying the

key characteristics of soils affecting the properties of earth concrete is essential to facilitate the material selection and design procedure. In the case of soils, Atterberg limits are key parameters to characterize and predict their behavior given their constituents [33–36]. Atterberg limits [37], including the liquid (LL) and plastic limits (PL), are defined as the moisture contents beyond which the soil behaves as a liquid and plastically, respectively. The plasticity index (PI) is defined as the difference between LL and PL. These properties are important to define the behavior of soils in the presence of water, which is critical in the case of SCEC. Clay plays a significant role on the plasticity behavior of soils. In addition to its water content, the clay type and content have a dominant effect on Atterberg limits of a soil [33]. These soil characteristics can be used as key parameters to predict the workability of SCEC mixtures, proportioned with different admixture types. Practical guidelines can then be proposed for recommended soil characteristics to achieve targeted workability properties.

Using the conventional design of experiment methods, the number of experiments exponentially increases with a higher number of variables to be studied. This can lead to the consumption of a greater quantity of materials, longer time, and higher cost to perform such experimental sets. The Taguchi method has been commonly used as an alternative to optimize the number of experiments to evaluate the impact of a large number of variables [38,39]. In addition to the number and cost of the experiments, the influencing factors can be optimized to achieve the targeted values of the specific response using the Taguchi method [40].

In this study, the Taguchi design of experiment (TDOE) was employed to investigate the efficiency of various influencing factors, including cement content, clay type, water-to-powder ratio, cement-to-clay ratio, and admixture type, on the workability and compressive strength of self-consolidating earth pastes (SCEP) that can be used to proportion SCEC mixtures with targeted properties. Incorporating different types of admixtures with fifty different soil types with a wide range of Atterberg limits can broaden the application of SCEC on different rurally available earth types. Signal-to-noise ratio (S/N) and ANOVA analyses were also implemented to evaluate the contribution of each factor on modelled responses. The type of admixtures, as well as their specific synergy with different soil compositions and ternary binder systems of SCEP were considered as some of the main influencing parameters. The admixtures used in this study are the common HRWR admixtures for cement-based SCC and dispersants used as deflocculants for clay particles.

Synergy of these admixtures in the presence of ternary binder systems of SCEP was evaluated. Workability of the investigated SCEP mixtures was correlated to binder and soil characterization parameters. The results of this study can be useful to establish guidelines to facilitate proportioning SCEP mixtures based on key characteristics of powders and admixture types.

4.2 Experimental program

4.2.1 Taguchi method

This paper aims to study the effect of various factors on the workability, workability loss, and compressive strength of SCEP mixtures. Given the high number of variables that affect the workability and strength of SCEC, parametric optimization is time and energy consuming. The number of experiments will be numerous in a full factorial design, which is practically impossible to carry out. The Taguchi design of experiment (TDOE) has been widely used for experimental design of concrete materials studies [41,42]. TDOE is a well-known method to optimize the number of experiments and identify the most influencing parameters on modelled properties. TDOE is mainly based on fractional factorial experiments using orthogonal arrays [43,44]. Using the TDOE approach, the individual effects and interactions of a given number of factors can be studied with a significantly lower number of experiments. Using the TDOE, Gencel et al. [45] studied the effect of fly ash and foam contents, fiber ratio, and length on compressive strength and durability of hemp fiber reinforced foam concrete with fly ash. In another study, Dave and Bhogayata [46] used the TDOE approach to optimize the workability and strength criterion of geopolymer concrete with the introduction of four 3-level governing factors. In addition to minimizing the experimental cost, TDOE is useful for optimizing mixture parameters and achieving targeted properties.

The main parameters investigated in this study include the clay type, cement content, volume of paste V_P, water-to-powder ratio W/P (by mass), volumetric cement-to-clay ratio (Ce/Cl), volumetric sand-to-total aggregate ratio (S/A) of corresponding SCEC mixtures, and admixture type. The experimental results are converted into signal-to-noise (S/N) ratios reflecting the deviation of the actual experimental results from the targeted ones. The investigated factors and their corresponding levels used for TDOE are summarized in Table 4.1.

Table 4.1. Investigated factors and their corresponding levels.

Factors	Levels				
	1	2	3	4	5
Clay type	Type I	Type II	-	-	-
Cement content (kg/m^3)	60	90	120	150	180
Paste volume (V_P) (%)	45	48	51	54	57
Water to powder ratio (W/P)	0.30	0.35	0.40	0.45	0.50
Cement to clay ratio (Ce/Cl)	0.50	0.75	1.00	1.25	1.50
Sand-to-total aggregate ratio (S/A)	0.5	0.6	0.7	0.8	0.9
Admixture	NaHMP	NaSil	PCE	PNS	NE-PC

As can be observed in Table 4.1, two different types of soil (i.e., two-level factor) were investigated to highlight the efficiency of clay mineralogy and ensure the coverage of a wide range of Atterberg limits for modelled soils. On the other hand, the other investigated factors were evaluated at five different levels. Cement contents, as the key parameter of setting promotion, corresponding to 60, 90, 120, 150, and 180 kg/m^3 were investigated. These ranges are based on those recommended in the literature for cement-stabilized earth concrete [10,47]. Moreover, paste volumes (V_P) of 45%, 48%, 51%, 54%, and 57% were evaluated. It is worthy to mention that the paste consists in air, water, and powders, including clay, silt, and cement. The paste mixtures investigated were proportioned with five W/P ratios of 0.30, 0.35, 0.40, 0.45, and 0.50. Furthermore, the volumetric cement-to-clay ratio (Ce/Cl) was selected as a main factor to control the clay content and evaluate the packing and fineness of powder constituents. Accordingly, five different Ce/Cl ratios of 0.50, 0.75, 1.00, 1.25, and 1.50 were selected. Sand-to-total aggregate ratios (S/A) of 0.5, 0.6, 0.7, 0.8, and 0.9 were also evaluated. These levels were selected to cover a wide range of characteristics of the parameters investigated Finally, the chemical admixture types were considered in five levels to investigate their synergy on the ternary binder system (i.e., clay, silt, and cement). The first two admixtures were sodium hexametaphosphate $(NaPO_3)_6$ (noted as NaHMP in this paper) and sodium silicate Na_2SiO_3 (referred as NaSil), used as dispersing agents in the suspensions containing clay. They are used to increase the overall negative surface charge and alkalinity of earth cations, hence increasing pH of the solution [14–22]. Polycarboxylate ether (PCE), sodium polynaphtalene (PNS), and non-esterified polycarboxylate (NE-PC) admixtures were also investigated. The efficiency of these admixtures was investigated in cement pastes, although their performance in dispersion of ternary powder systems of SCEP is still ambiguous, as well as how they compare with clay dispersing agents. The effects of two- and five-levels factors on the modelled properties were evaluated using a L50 orthogonal Taguchi array, which required 50

fractional factorial experiments. The 50 mixtures investigated are summarized in Table 4.3. The modelled responses include the flowability and compressive strength development.

The performance characteristics can be evaluated by identifying the most significant factors and their levels. The optimization criteria consist of calculating the signal-to-noise ratio (S/N), which represents the loss function reflecting the deviation of the actual experimental results and the targeted ones. The analysis of the S/N ratio is based on three performance characteristics corresponding to larger-the better, smaller-the better, and nominal-the better defined in Eqs. (4.1)-(4.3), respectively [40], as follow:

Larger-the better $$S/N = -10 \times \log_{10}\left(\frac{1}{n}\sum_{i=1}^{n}\frac{1}{Y_i^2}\right) \quad (4.1)$$

Smaller-the better $$S/N = -10 \times \log_{10}\left(\frac{1}{n}\sum_{i=1}^{n}Y_i^2\right) \quad (4.2)$$

Nominal-the better $$S/N = -10 \times \log_{10}\left[\frac{1}{n}\sum_{i=1}^{n}(Y_i - Y_0)^2\right] \quad (4.3)$$

where S/N is the performance statistics, n is the number of repetitions for each level of a factor, Y_i is the response value of the i^{th} experiment, and Y_0 is the nominal value desired. The values of the S/N ratio are used as a measure of robustness to identify the control factors reducing variability in a process by minimizing the effect of noise factors [40]. In this study, the larger-the better S/N equation (Eq. (4.1)) was employed for compressive strength development at different ages. On the other hand, the smaller-the better S/N equation (Eq. (4.2)) was used to investigate the admixture demand, marsh cone flow, and mini-slump spread loss.

4.2.2 Materials and test procedures

The SCEP mixtures investigated were proportioned using a general use cement (GU) complying with ASTM C150 specifications. The GU cement has a specific gravity of 3.15 and specific surface area of 0.3 m^2/g. Clay Type I consists of kaolinite with a specific surface area and specific gravity of 15 m^2/g and 2.73, respectively. Clay Type II is composed of 50% kaolinite and 50% attapulgite. The specific surface area and specific gravity of attapulgite are 155 m^2/g and 2.75, respectively. The silt powder used is composed of quartz grains of 2 to 75 µm and specific gravity of 2.69. The chemical compositions of the binders are summarized in Table 4.2. On the other hand, NaHMP with purity of 96% was used as solution in water with a solid content of 37.1%. Moreover, NaSil solution composed of water, 10.6% Na_2O, and 26.5% SiO_2 was used as inorganic deflocculant.

PCE, PNS, and NE-PC with solid contents of 40%, 39.25%, and 36.44%, respectively, were used as high-range water-reducer (HRWR) admixtures.

Table 4.2. Chemical composition of the binders used in this study.

Chemical composition (% wt.)	Binder type			
	GU cement	Kaolinite	Attapulgite	Quartz silt
CaO	62.50	0.10	2.92	0.01
SiO_2	19.30	46.10	66.20	99.02
Al_2O_3	4.80	38.10	11.71	0.64
Fe_2O_3	3.00	0.50	4.02	0.22
MgO	2.70	0.10	9.70	0.01
SO_3	4.10	0.04	-	-
Others	1.40	1.56	1.47	0.10
LOI*	2.20	13.50	3.98	-

LOI*: Loss of ignition

The aim of this study was to investigate the workability, workability loss, and compressive strength of the investigated SCEP mixtures proportioned with their novel ternary binder systems. The paste mixtures corresponding to 50 different earth types were investigated with a wide range of Atterberg limits to ensure a broad investigation of existing soils. Atterberg limits of the corresponding earth mixtures, consisting in clay, silt and sand finer than 425 μm, were measured as soil characterization parameters according to ASTM D4318 [37]. These include the liquid (LL) and plastic limits (PL). The numerical difference of LL and PL was also calculated as the plasticity index (PI). The paste mixtures were mixed in batches of 1.5 L using a planetary Hobart mixer according to ASTM C305 specifications [48]. Workability of the investigated SCEP mixtures was investigated using the mini-slump flow (MSF) [49] and marsh cone flow time (MCT) [50]. MCT corresponds to the required time to pass 500 mL of paste through a circular nozzle measuring 8-mm in diameter. The test consists of pouring 1000 mL of sample in the cone to determine the flow time of 500 mL passing through the nozzle. Higher flow time reflects low fluidity of the mixture. The mixtures investigated were designed to achieve the targeted mini-slump spread of 280 ± 20 mm to ensure a highly flowable and stable SCEP mixture. Furthermore, MSF loss values at 15- and 30-min intervals after the first contact between water and binder were also determined to evaluate the efficiency of admixtures over time. In addition to flow properties, for each mixture, different 50 × 50 × 50 mm^3 cubes were sampled to determine the compressive strength at 1, 7, and 28 days of curing in accordance with the ASTM C109 specifications [51].

4.2.3 SCEP mixture proportions

The mixture proportions summarized in Table 4.4 were established based on the levels of control factors in the L50 orthogonal array given in Table 4.1. As can be observed, for each level of a particular factor, all levels of each of the other factors are tested at least once.

Table 4.3. Absolute values of the 7 modelled factors according to L50 Orthogonal array

Experiment No.	Factors investigated							Experiment No.	Factors investigated						
	Clay type	Cement content (kg/m^3)	V_P (%)	W/P	Ce/Cl	S/A	Admixture		Clay type	Cement content (kg/m^3)	V_P (%)	W/P	Ce/Cl	S/A	Admixture
1			45	0.30	0.5	0.5	NaHMP	26			45	0.30	1.25	0.9	PNS
2			48	0.35	0.75	0.6	NaSil	27			48	0.35	1.5	0.5	NE-PC
3		60	51	0.40	1	0.7	PCE	28		60	51	0.40	0.5	0.6	NaHMP
4			54	0.45	1.25	0.8	PNS	29			54	0.45	0.75	0.7	NaSil
5			57	0.50	1.5	0.9	NE-PC	30			57	0.50	1	0.8	PCE
6			45	0.35	1	0.8	NE-PC	31			45	0.35	0.5	0.7	PCE
7			48	0.40	1.25	0.9	NaHMP	32			48	0.40	0.75	0.8	PNS
8		90	51	0.45	1.5	0.5	NaSil	33		90	51	0.45	1	0.9	NE-PC
9			54	0.50	0.5	0.6	PCE	34			54	0.50	1.25	0.5	NaHMP
10			57	0.30	0.75	0.7	PNS	35			57	0.30	1.5	0.6	NaSil
11			45	0.40	1.5	0.6	PNS	36			45	0.40	1	0.5	NaSil
12			48	0.45	0.5	0.7	NE-PC	37			48	0.45	1.25	0.6	PCE
13	I	120	51	0.50	0.75	0.8	NaHMP	38	II	120	51	0.50	1.5	0.7	PNS
14			54	0.30	1	0.9	NaSil	39			54	0.30	0.5	0.8	NE-PC
15			57	0.35	1.25	0.5	PCE	40			57	0.35	0.75	0.9	NaHMP
16			45	0.45	0.75	0.9	PCE	41			45	0.45	1.5	0.8	NaHMP
17			48	0.50	1	0.5	PNS	42			48	0.50	0.5	0.9	NaSil
18		150	51	0.30	1.25	0.6	NE-PC	43		150	51	0.30	0.75	0.5	PCE
19			54	0.35	1.5	0.7	NaHMP	44			54	0.35	1	0.6	PNS
20			57	0.40	0.5	0.8	NaSil	45			57	0.40	1.25	0.7	NE-PC
21			45	0.50	1.25	0.7	NaSil	46			45	0.5	0.75	0.6	NE-PC
22			48	0.30	1.5	0.8	PCE	47			48	0.3	1	0.7	NaHMP
23		180	51	0.35	0.5	0.9	PNS	48		180	51	0.35	1.25	0.8	NaSil
24			54	0.40	0.75	0.5	NE-PC	49			54	0.4	1.5	0.9	PCE
25			57	0.45	1	0.6	NaHMP	50			57	0.45	0.5	0.5	PNS

Table 4.4. Mixture proportions of the investigated SCEP based on L50 Orthogonal array.

Mix No.	Cement (kg/m^3)	Water (kg/m^3)	Clay Type I (kg/m^3)	Silt (kg/m^3)	W/P	Mix No.	Cement (kg/m^3)	Water (kg/m^3)	Clay Type II (kg/m^3)	Silt (kg/m^3)	W/P
P1	133.3	450.4	231.1	1136.9	0.30	P26	133.3	450.1	92.4	1274.4	0.30
P2	125.0	488.6	144.4	1126.6	0.35	P27	125.0	488.4	72.2	1198.3	0.35
P3	117.6	521.9	102.0	1085.1	0.40	P28	117.6	522.2	203.9	983.9	0.40
P4	111.1	551.1	77.0	1036.6	0.45	P29	111.1	551.3	128.4	985.6	0.45
P5	105.3	577.0	60.8	988.0	0.50	P30	105.3	577.1	91.2	957.8	0.50
P6	200.0	490.7	173.3	1028.5	0.35	P31	200.0	491.1	346.7	856.5	0.35
P7	187.5	523.9	130.0	992.4	0.40	P32	187.5	524.2	216.7	906.3	0.40
P8	176.5	553.2	102.0	950.8	0.45	P33	176.5	553.3	152.9	900.2	0.45
P9	166.7	579.7	288.9	703.7	0.50	P34	166.7	579.1	115.6	876.0	0.50
P10	157.9	450.9	182.5	1162.5	0.30	P35	157.9	450.6	91.2	1253.0	0.30
P11	266.7	526.2	154.1	894.9	0.40	P36	266.7	526.5	231.1	818.4	0.40
P12	250.0	556.3	433.3	553.0	0.45	P37	250.0	555.6	173.3	811.3	0.45
P13	235.3	581.7	271.9	656.3	0.50	P38	235.3	581.3	135.9	791.4	0.50
P14	222.2	452.5	192.6	1093.4	0.30	P39	222.2	452.9	385.2	902.3	0.30
P15	210.5	490.9	146.0	1046.0	0.35	P40	210.5	491.1	243.3	949.4	0.35
P16	333.3	558.7	385.2	523.0	0.45	P41	333.3	558.1	192.6	714.3	0.45
P17	312.5	584.1	270.8	584.9	0.50	P42	312.5	585.0	541.7	315.8	0.50
P18	294.1	454.2	203.9	1016.0	0.30	P43	294.1	454.6	339.9	881.2	0.30
P19	277.8	492.7	160.5	969.4	0.35	P44	277.8	492.9	240.7	889.7	0.35
P20	263.2	527.0	456.1	598.2	0.40	P45	263.2	526.2	182.5	869.9	0.40
P21	400.0	586.9	277.3	496.4	0.50	P46	400.0	587.5	462.2	312.7	0.50
P22	375.0	456.2	216.7	929.1	0.30	P47	375.0	456.5	325.0	821.6	0.30
P23	352.9	495.8	611.8	452.0	0.35	P48	352.9	494.9	244.7	816.3	0.35
P24	333.3	528.8	385.2	603.4	0.40	P49	333.3	528.2	192.6	794.6	0.40
P25	315.8	557.8	273.7	650.1	0.45	P50	315.8	558.6	547.4	378.3	0.45

4.3 Results and discussions

This study focused on the workability and compressive strength of SCEP mixtures to investigate the main challenges regarding clay dispersion and setting of the material. Fig. 4.1 represents the sequence of discussions established in this study. As shown in Fig. 4.1, first, the effect of binder composition and W/P ratio on workability, workability loss, and compressive strength of the paste mixtures incorporating different types of admixtures were evaluated. The signal-to-noise ratio (S/N) analysis was then conducted for all the investigated SCEP mixtures to identify the optimum levels of each factor to achieve the targeted properties. The contribution of each factor was then determined using the analysis of variance (ANOVA). Once the key factors showing the highest contribution were identified, several empirical models were proposed to predict the workability of the investigated SCEP mixtures as a function of the influencing factors. Finally, guidelines were recommended for proportioning SCEP mixtures considering different types of earth.

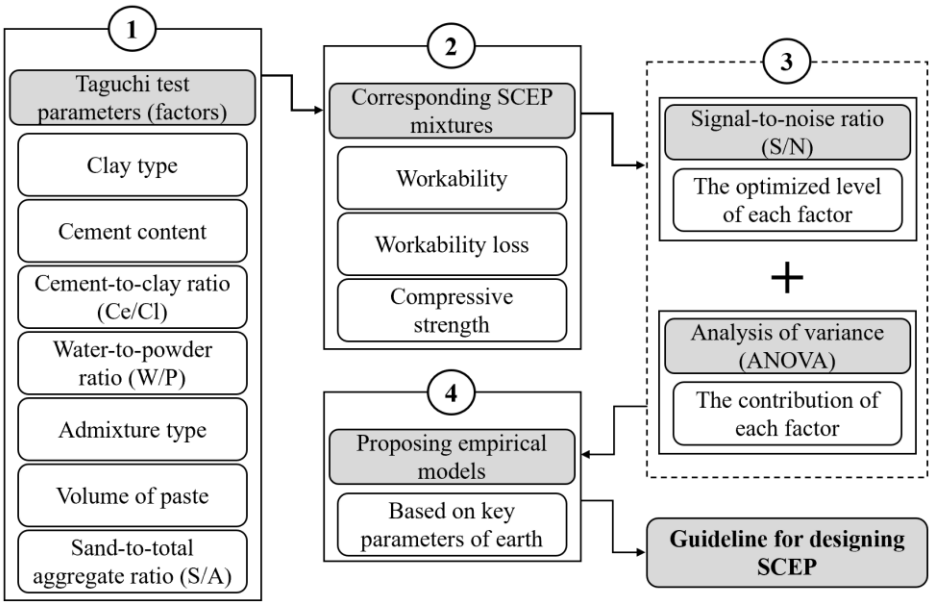

Fig. 4.1. Guideline for designing SCEP.

4.3.1 Effect of admixture and clay type on workability and compressive strength of SCEP mixtures

The workability and compressive strength values of the SCEP mixtures made with clay types I and II, as well as different admixtures, including NaHMP, NaSil, PCE, PNS, and NE-PC, are presented in Figs. 4.2-4.11, respectively. It is worth mentioning that the MSF and MCT evolutions were presented with the introduction of admixtures to achieve the targeted MSF value. The dosage of admixtures was determined as the ratio of the solid content of admixtures to the powder content (i.e., total content of cement, clay, and silt). Moreover, MSF loss was evaluated at 0, 15 (MSF $loss_{15\ min}$), and 30 min (MSF $loss_{30\ min}$) after achieving the targeted MSF. The compressive strength values correspond to the samples cast after achieving the targeted MSF. The dry density of the SCEP mixtures was in the range of 1750-1950 kg/m^3, which is lower than their corresponding cement paste due to the lower specific gravity of clay and silt than cement.

As can be observed in Fig. 4.2a and 4.3a for the mixtures containing NaHMP, a coupled effect of W/P and Ce/Cl ratios was observed on the admixture demand. For example, although P13 was proportioned with higher W/P compared to the P7 mixture (W/P of 0.5 vs. 0.4), P13 required higher NaHMP dosage than P7 (0.49% vs. 0.35%) to achieve the targeted MSF. This can be due to higher clay content in P13 compared to that of P7 (272 vs. 130 kg/m^3). The results of the

mixtures proportioned with Clay Type I revealed that the lowest and highest NaHMP demands were obtained for P7 and P19 mixtures with Ce/Cl of 1.25 and 1.5, and W/P of 0.40 and 0.35, respectively. In the case of the mixtures made with Clay Type II, P34 (Ce/Cl = 1.25 and W/P = 0.5) and P47 (Ce/Cl = 1.00 and W/P = 0.3) required the lowest and highest NaHMP dosages, respectively, to achieve the targeted MSF. As can be observed, Clay Type II required significantly higher NaHMP dosages compared to Clay Type I to achieve a given flowability. This can be due to the higher specific surface area (SSA) of Clay Type II which is in accordance with the literature [52,53].

As can be observed in Fig. 4.2b and 4.3b, the paste mixtures made with Clay Type II showed more viscosity reflected by significantly higher MCT values compared to those proportioned with Clay Type I [52]. It should be noted that marsh cone results could not be measured at specific lower dosages, due to blockage in the funnel. Accordingly, the P7 and P25 mixtures made with Clay Type I, and P34 and P47 with Clay Type II exhibited the lowest and highest MCT results, respectively. Significant MSF losses were obtained for both Clay Type I and II systems containing NaHMP, as shown in Fig. 4.2c and 4.3c. This increased with clay content. This proves that NaHMP can enhance the shape stability of the matrix, which can be favorable for concrete 3D printing applications. Indeed, in a layer-by-layer printing process, a high rate of structural build-up is of particular interest for improving shape stability of printed objects.

	Cement content (kg/m^3)	W/P	Ce/Cl
P1	60	0.30	0.50
P7	90	0.40	1.25
P13	120	0.50	0.75
P19	150	0.35	1.50
P25	180	0.45	1.00

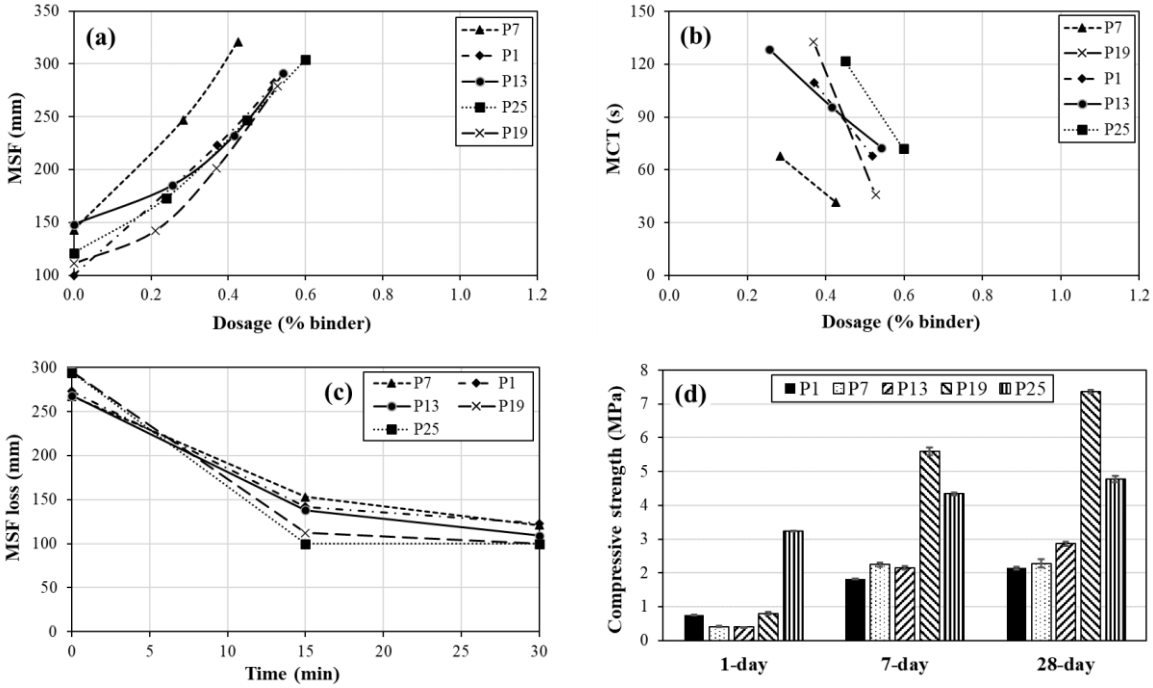

Fig. 4.2. Variations of (a) MSF, (b) MCT, (c) MSF loss, and (d) compressive strength of the SCEP mixtures containing NaHMP admixture and Clay Type I.

In the case of compressive strength, the mixtures containing Clay Type I and NaHMP, corresponding to P1, P7, and P13, exhibited comparable compressive strengths at 1 ($f'_{c\text{-}1d}$), 7 ($f'_{c\text{-}7d}$), and 28 ($f'_{c\text{-}28d}$) days after casting, Fig. 4.2d and 4.3d. Moreover, P19 made with a cement content of 150 kg/m^3, exhibited lower $f'_{c\text{-}1d}$ but higher $f'_{c\text{-}7d}$ and $f'_{c\text{-}28d}$ values compared to the P25 mixture containing 180 kg/m^3 cement content. It is worthy to mention that P19 was proportioned with lower W/P compared to P25. Regarding Clay Type II mixtures, a coupled effect of cement content and W/P ratio is observed. All mixtures made with NaHMP cannot satisfy the $f'_{c\text{-}1d}$ values higher than 1 MPa, except P25 and P47 mixtures. This means that a high cement content is required in the presence of NaHMP to increase the early-age compressive strength required for formwork removal.

	Cement content (kg/m^3)	W/P	Ce/Cl
P28	60	0.40	0.50
P34	90	0.50	1.25
P40	120	0.35	0.75
P41	150	0.45	1.50
P47	180	0.30	1.00

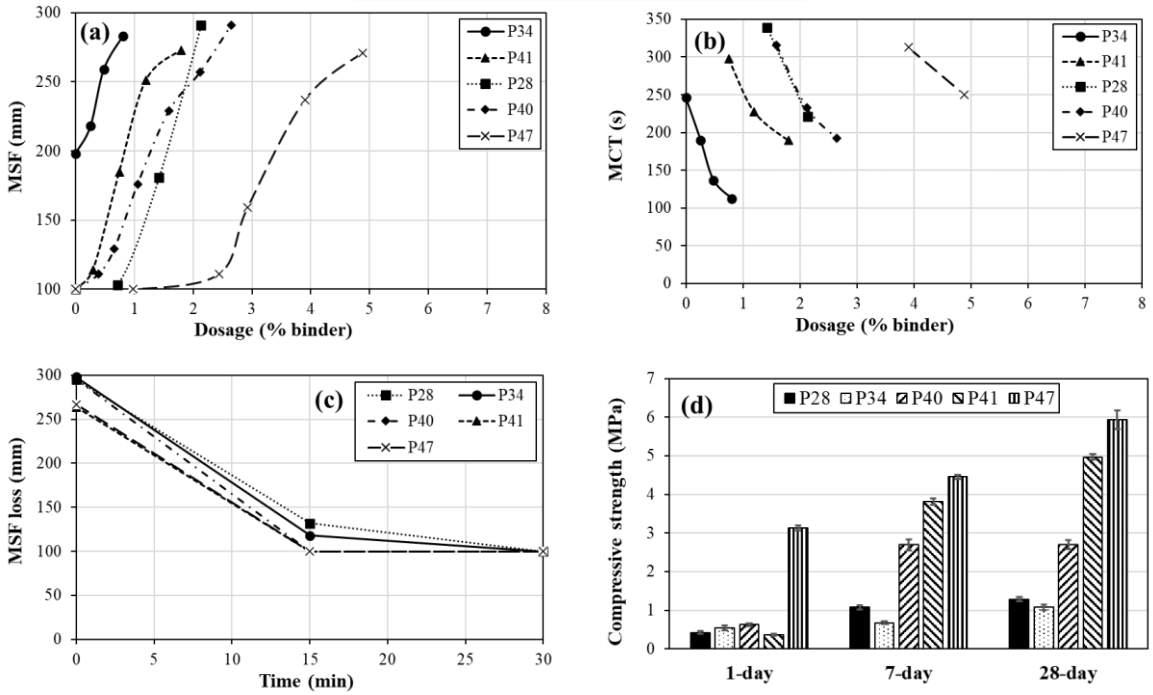

Fig. 4.3. Variations of (a) MSF, (b) MCT, (c) MSF loss, and (d) compressive strength of the SCEP mixtures containing NaHMP admixture and Clay Type II.

As shown in Fig. 4.4 and 4.5, SCEP mixtures proportioned with two different types of clay and NaSil admixture, P8 and P20 made with Ce/Cl of 1.5 and 0.5, and W/P of 0.45 and 0.4, required the lowest and highest NaSil demands, respectively, to achieve the targeted MSF value. Moreover, P29 and P42 mixtures made with Clay Type II, Ce/Cl of 0.75 and 0.5, and W/P of 0.45 and 0.5, respectively, exhibited the lowest and highest demand to achieve the targeted MSF value. Furthermore, even by introducing high NaSil dosage, P42 could not reach the targeted MSF value and, therefore, it was not achieved. On the other hand, the highest and lowest MCT results were obtained for P8 and P20 mixtures containing Clay Type I, and P29 and P36 mixtures made with Clay Type II, respectively. It is worth mentioning that P42 mixture was completely blocked through the marsh cone funnel. Furthermore, all the mixtures exhibited significant MSF losses which can be attributed to the admixture type and clay content. It can be concluded that inorganic deflocculants (i.e., NaHMP and NaSil) can lead to significant shape stability in the ternary binder system of SCEP.

	Cement content (kg/m^3)	W/P	Ce/Cl
P2	60	0.35	0.75
P8	90	0.45	1.50
P14	120	0.30	1.00
P20	150	0.40	0.50
P21	180	0.50	1.25

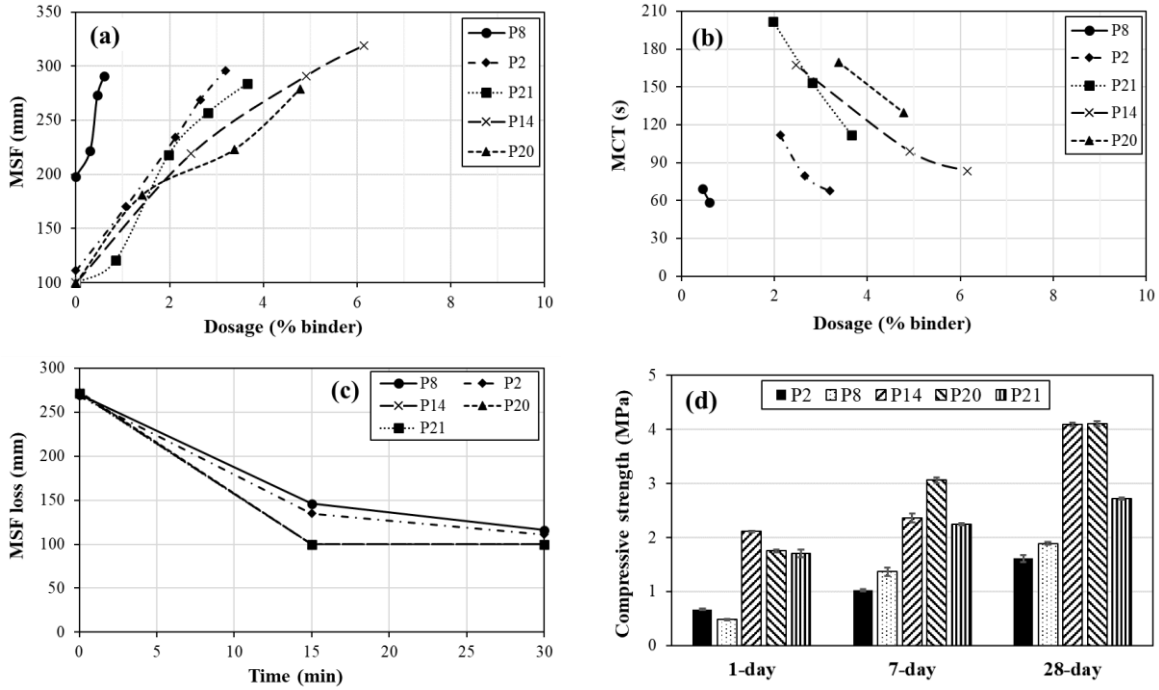

Fig. 4.4. Varations of (a) MSF, (b) MCT, (c) MSF loss, and (d) compressive strength of the SCEP mixtures containing NaSil admixture and Clay Type I.

Regarding the compressive strength, P14, P20, and P21 mixtures containing Clay Type I, as well as P35, P36, and P48 made with Clay Type II achieved $f'_{c\text{-}1d}$ values higher than 1 MPa. This can ensure the minimum compressive strength required for demolding [9] and is highly dependent on the cement content and W/P. Accordingly, P14 and P20 mixtures containing Clay Type I, as well as P48 mixture proportioned with Clay Type II showed the highest compressive strength. The coupled effect of cement content and W/P ratio on compressive strength results, at different ages, is observed.

	Cement content (kg/m^3)	W/P	Ce/Cl
P29	60	0.45	0.75
P35	90	0.30	1.50
P36	120	0.40	1.00
P42	150	0.50	0.50
P48	180	0.35	1.25

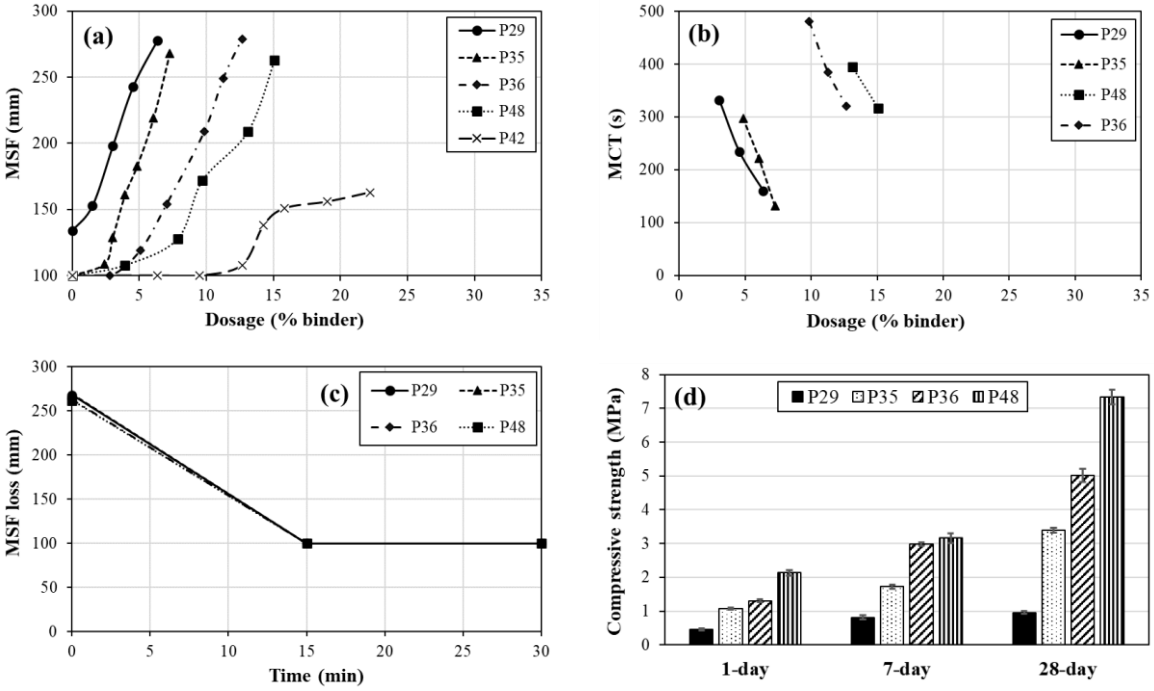

Fig. 4.5. Varations of (a) MSF, (b) MCT, (c) MSF loss, and (d) compressive strength of the SCEP mixtures containing NaSil admixture and Clay Type II.

The workability and mechanical performance of the SCEP mixtures made with PCE, PNS, and NE-PC admixtures are shown in Figs. 4.6-4.11, respectively. As can be observed in Fig. 4.6a and 4.7a, although P16 was made with higher W/P than P22, it required a relatively higher PCE dosage to achieve the targeted MSF, which can be due to its higher clay content. This reveals that type and content of clay can dictate the admixture demand to increase flowability more than water content. As can be observed in Fig. 4.6b and 4.7b, in the case of the SCEP mixtures proportioned with Clay Types I and II, P3 and P30 mixtures showed the lowest PCE demand, while P16 and P43 exhibited the highest MCT. Clay contents of P3, P30, P16, and P43 mixtures were 102, 91, 385, and 340 kg/m^3, respectively. It can be concluded that the viscosity of SCEP mixtures is highly dependent on the type and content of clay. According to the MCT results, higher clay content and SSA leads to higher viscosity of SCEP. Moreover, the MSF loss values obtained using PCE were not as significant as those of the mixtures containing NaHMP and NaSil types. However, higher MSF loss values were obtained for Clay Type II compared to those of type-I systems. The P16 and

P49 mixtures exhibited the highest MSF loss values for the mixtures made with Clay Type I and II, respectively. MSF loss values of SCEP mixtures with PCE are not as significant as NaHMP and NaSil. This may be due to the synergy of PCE with the powder constituents. As shown in Fig. 4.6c and 4.7c, in the case of PCE mixtures, the compressive strength values are highly dependent on the cement content. However, the P43 mixture showed lower $f'_{c\text{-}1d}$ values compared to P37 and P49 ones. This can be attributed to its higher PCE demand, which can delay the strength development at an early age (1 day). Therefore, the use of high admixture dosage, despite the effect of cement content and W/P ratio, can decrease the early-age compressive strength results.

	Cement content (kg/m^3)	W/P	Ce/Cl
P3	60	0.40	1.00
P9	90	0.50	0.50
P15	120	0.35	1.25
P16	150	0.45	0.75
P22	180	0.30	1.50

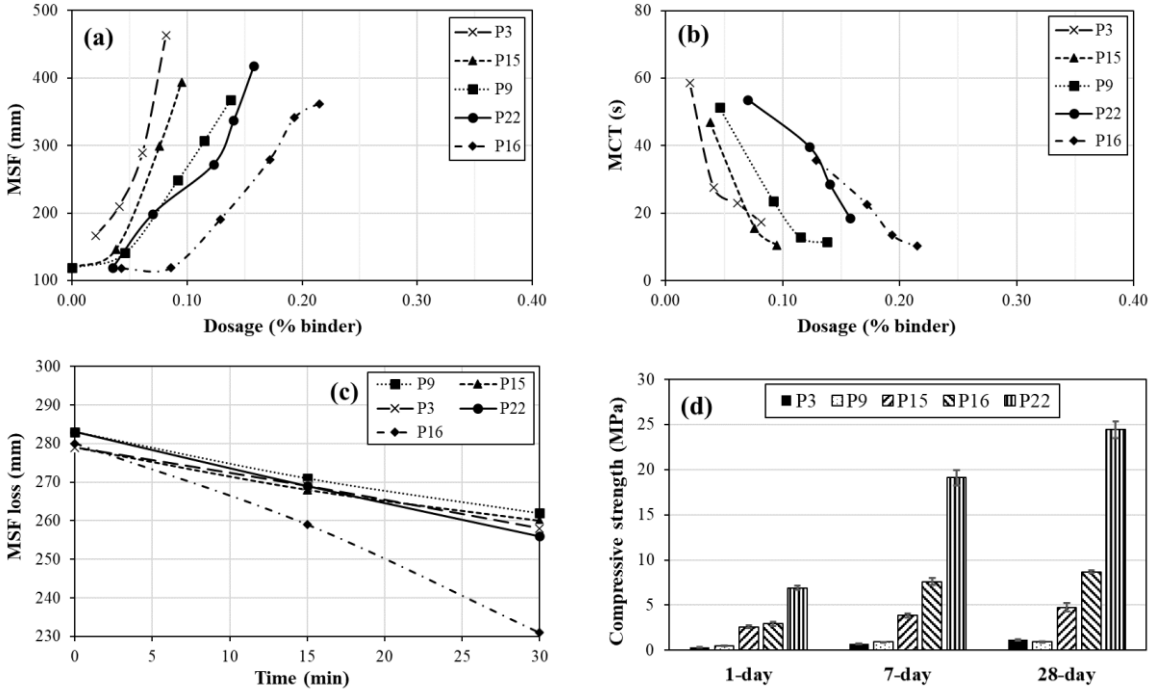

Fig. 4.6. Variations of (a) MSF, (b) MCT, (c) MSF loss, and (d) compressive strength of the SCEP mixtures containing PCE admixture and Clay Type I.

	Cement content (kg/m^3)	W/P	Ce/Cl
P30	60	0.50	1.00
P31	90	0.35	0.50
P37	120	0.45	1.25
P43	150	0.30	0.75
P49	180	0.40	1.50

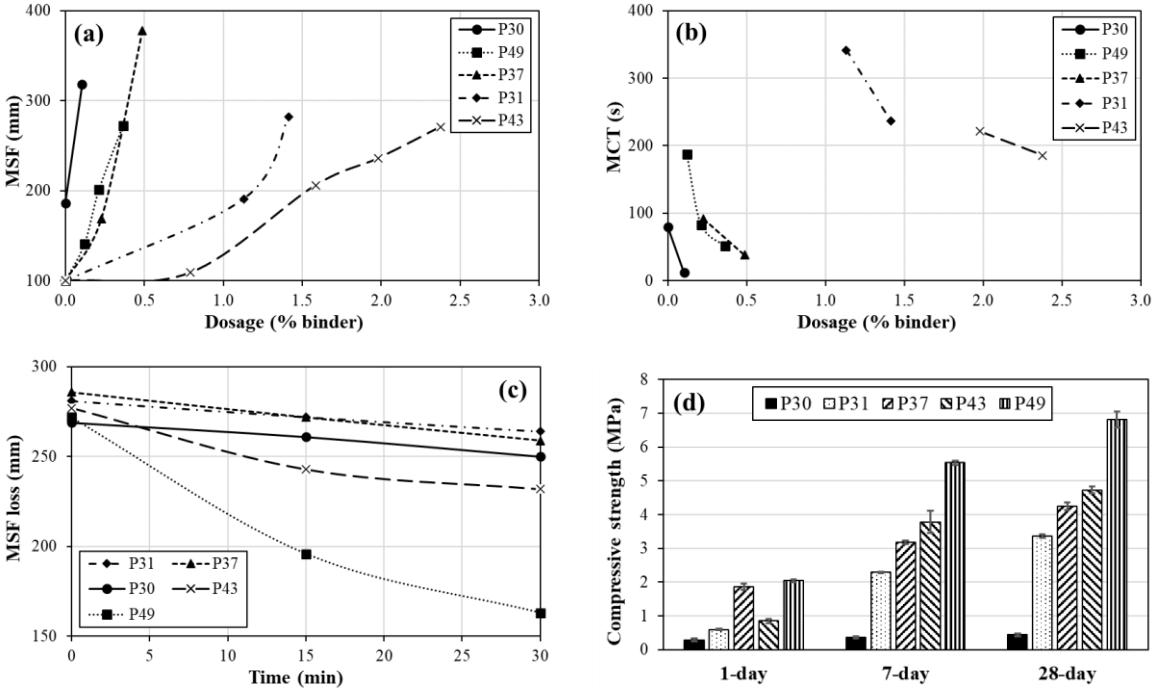

Fig. 4.7. Variations of (a) MSF, (b) MCT, (c) MSF loss, and (d) compressive strength of the SCEP mixtures containing PCE admixture and Clay Type II.

As shown in Fig. 4.8a and 4.9a, the P4 and P23 mixtures made with Clay Type I, and P38 and P50 containing Clay Type II required the lowest and highest MCT values and PNS dosages to achieve the targeted MSF value, respectively. Moreover, the P4 and P23 mixtures contain Clay Type I, and P38 and P50 mixtures made with Clay Type II demonstrated the lowest and highest MSF losses, respectively. This can be due to the clay content of Clay Type I (clay contents of P4 and P23 are 77 and 612 kg/m^3). Regarding Clay Type II, the clay contents were 136 and 547 kg/m^3 for P38 and P50, respectively. The P26 mixture had a lower clay content compared to P38 (92 kg/m^3); however, the water content was much lower than P38 (450 kg/m^3 vs. 581 kg/m^3). This proves the significance of the coupled effect of clay fraction and water content on MSF loss. Regarding the compressive strength results, the P23 and P44 mixtures showed the highest values for Clay Type I and II systems, respectively. The cement content and W/P showed a coupled effect on the compressive strength development. Seven out of 10 SCEP mixtures satisfy the 1-day compressive strength of more than 1 MPa, which is required for demolding.

	Cement content (kg/m^3)	W/P	Ce/Cl
P4	60	0.45	1.25
P10	90	0.30	0.75
P11	120	0.40	1.50
P17	150	0.50	1.00
P23	180	0.35	0.50

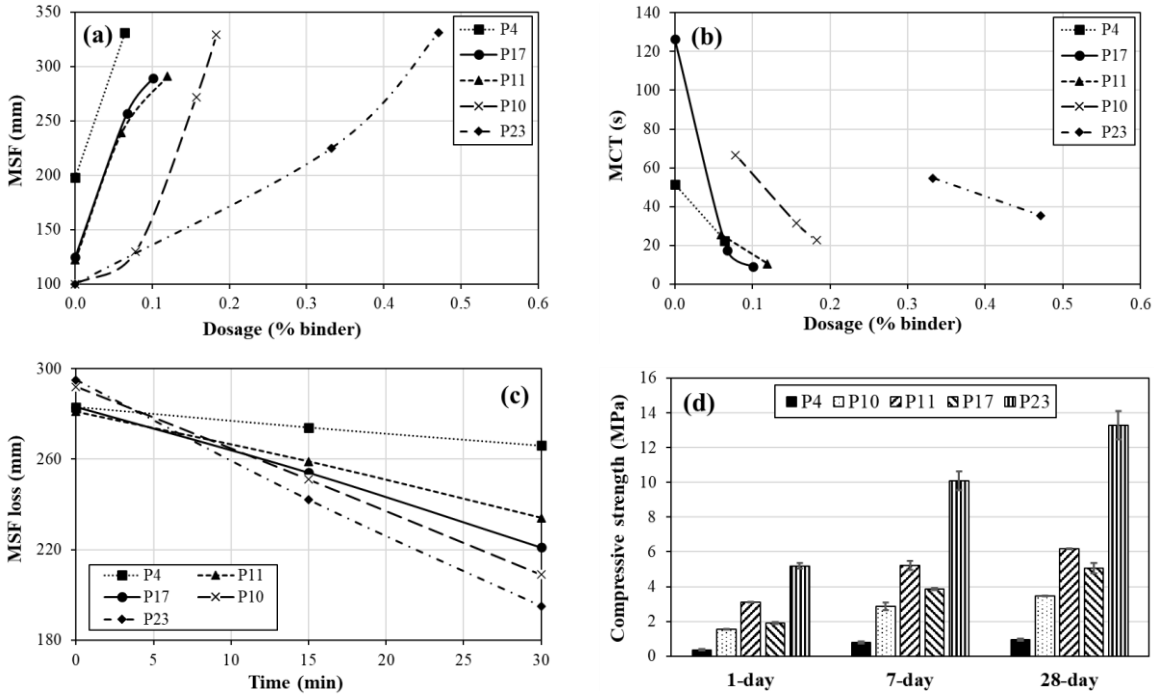

Fig. 4.8. Variations of (a) MSF, (b) MCT, (c) MSF loss, and (d) compressive strength of the SCEP mixtures containing PNS admixture and Clay Type I.

	Cement content (kg/m^3)	W/P	Ce/Cl
P26	60	0.30	1.25
P32	90	0.40	0.75
P38	120	0.50	1.50
P44	150	0.35	1.00
P50	180	0.45	0.50

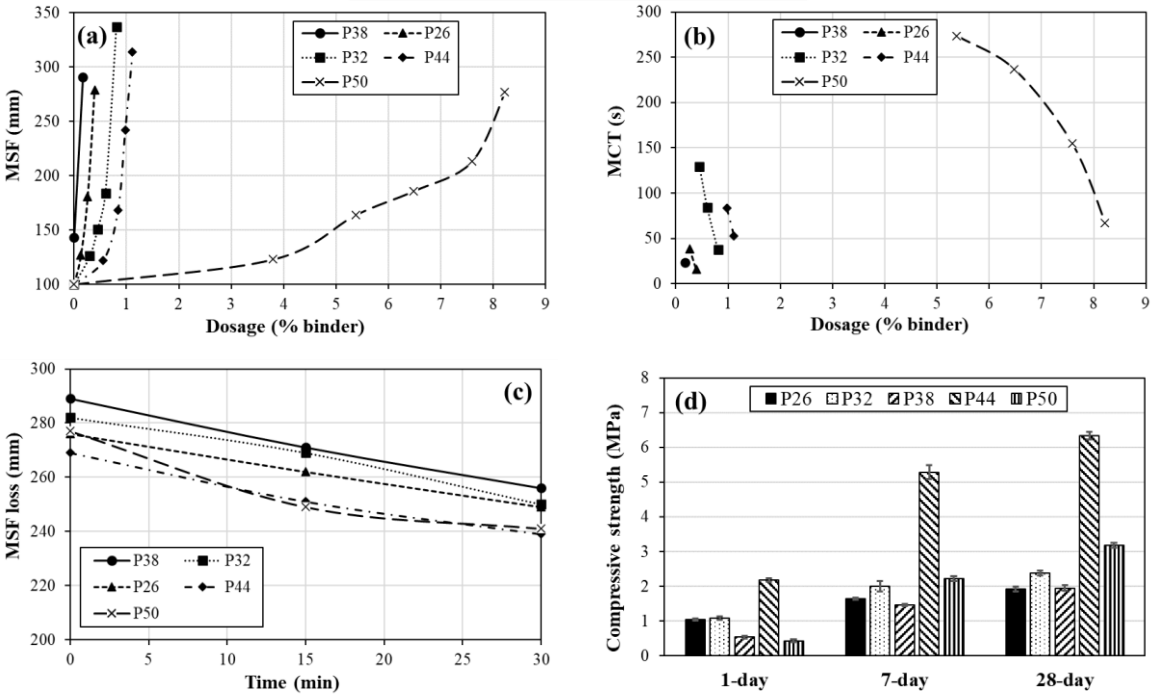

Fig. 4.9. Variations of (a) MSF, (b) MCT, (c) MSF loss, and (d) compressive strength of the SCEP mixtures containing PNS admixture and Clay Type II.

As can be observed in Fig. 4.10a and 4.11a, the lowest and highest NE-PC demands were obtained for P5 and P12 mixtures made with Clay Type I and P27 and P46 mixtures containing Clay Type II systems, respectively. It should be noted that the P39 mixture could not reach the targeted MSF value by introducing higher NE-PC dosages. As presented in Fig. 4.10b and 4.11b, the lowest and highest MCT values were obtained for P5 and P24 (Clay Type I), as well as P27 and P46 (Clay Type II) mixtures, respectively. The high clay content of P46 (462 kg/m^3) dictates the significantly high dosage for the targeted MSF and its corresponding MCT value. Moreover, this significantly high content leads to high MSF loss. As can be observed in Fig. 4.10c and 4.11c, the minimum and maximum MSF loss values were obtained for P5 and P24 mixtures containing Clay Type I, as well as P33 and P46 for Clay Type II suspensions, respectively. The compressive strength of NE-PC-contained SCEP mixtures is illustrated in Fig. 4.10d and 4.11d. The P18 and P45 mixtures exhibited the highest compressive strength values, while P46 showed lower compressive strength

values compared to P45, due to a higher W/P ratio (0.5 vs. 0.4) while the cement content was higher. Similarly, P24 resulted in lower compressive strength compared to P18.

	Cement content (kg/m^3)	W/P	Ce/Cl
P5	60	0.50	1.50
P6	90	0.35	1.00
P12	120	0.45	0.50
P18	150	0.30	1.25
P24	180	0.40	0.75

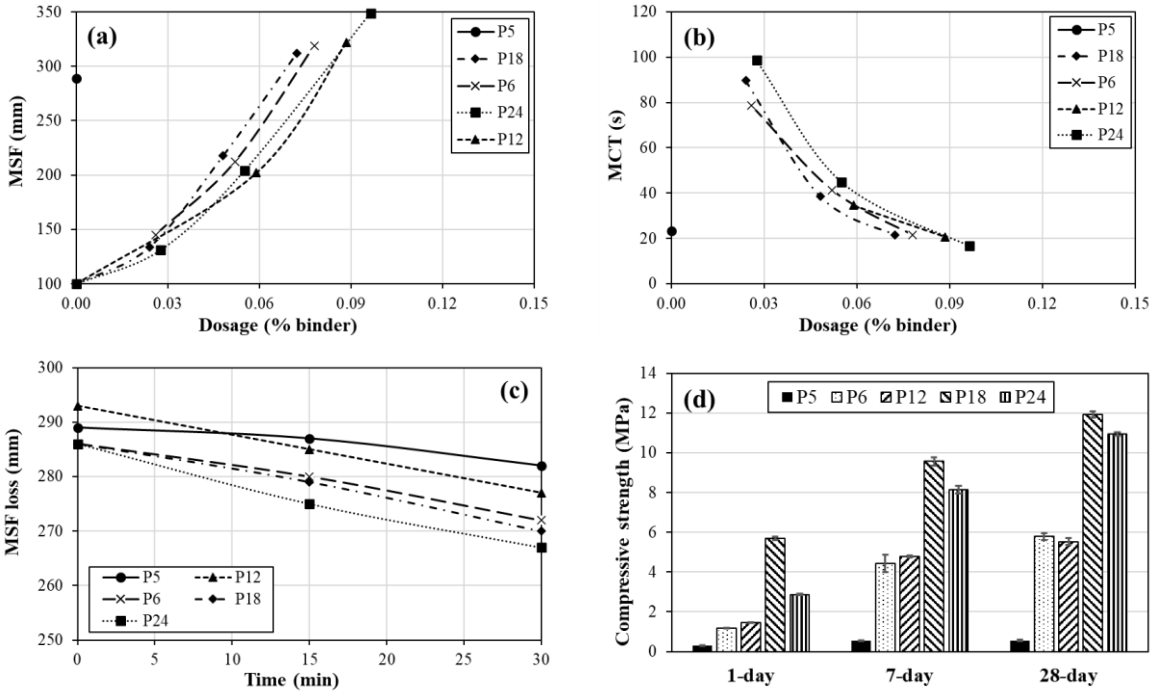

Fig. 4.10. Variations of (a) MSF, (b) MCT, (c) MSF loss, and (d) compressive strength of the SCEP mixtures containing NE-PC admixture and Clay Type I.

	Cement content (kg/m^3)	W/P	Ce/Cl
P27	60	0.35	1.50
P33	90	0.45	1.00
P45	150	0.40	1.25
P46	180	0.50	0.75

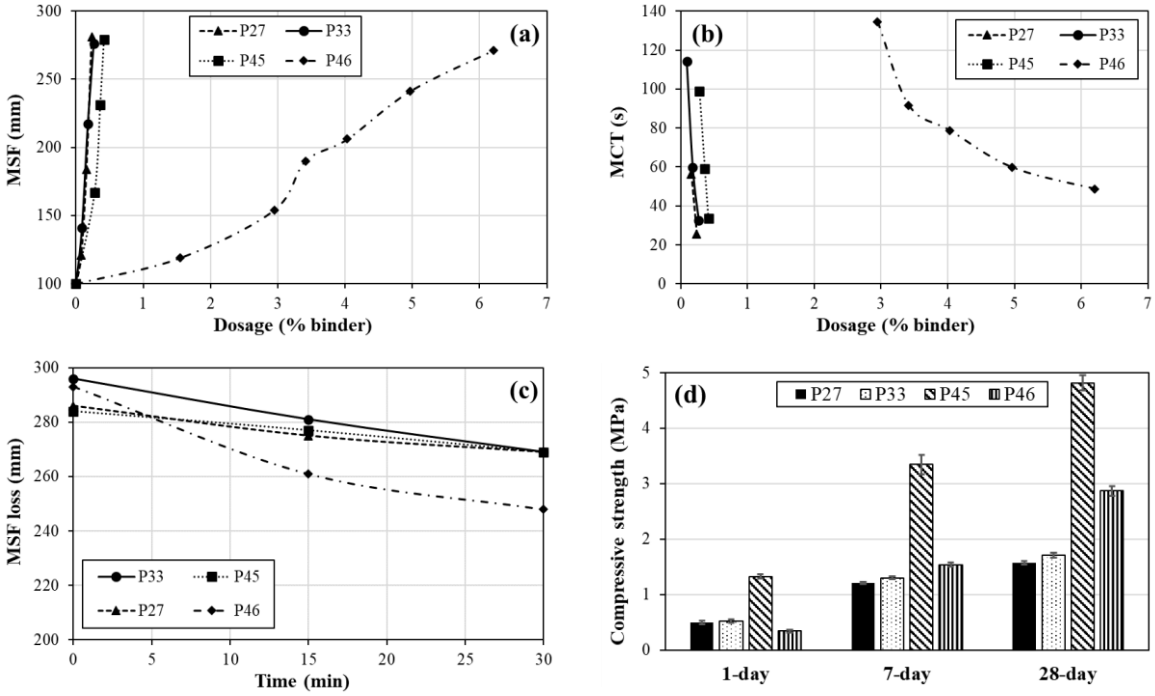

Fig. 4.11. Variations of (a) MSF, (b) MCT, (c) MSF loss, and (d) compressive strength of the SCEP mixtures containing NE-PC admixture and Clay Type II.

The reported workability and compressive strength results revealed the influence of different parameters and their coupled effects on the workability and compressive strength of SCEP mixtures. Therefore, analyzing signal-to-noise (S/N) ratio and variance (ANOVA) is necessary to evaluate the significance of control factors on the modelled properties.

4.3.2 Compatibility of admixtures with single-powder systems

The five selected admixtures were used with each type of powder (i.e., cement, clay, and silt) in single-powder suspension proportioned with a W/P of 0.40 to evaluate their compatibility. Accordingly, PT1, PT2, PT3, and PT4 paste mixtures were prepared with cement, Clay Type I, Clay Type II, or silt, respectively. The MSF values of these mixtures are summarized in Fig. 4.12. As can be observed, the admixtures did not show any effect on MSF values of the mixture containing silt, thus reflecting poor dispersion. Moreover, NaHMP exhibited insignificant effect on dispersing cement and silt particles, while PCE did not show any efficiency in dispersing clay particles. This is consistent with previous findings [9,13]. NaHMP admixture showed the highest

effect on flowability of paste mixtures made with clay particles (Type I and II). This is in agreement to the results reported by Andreola et al. [15] on the efficiency of sodium hexametaphosphate on the dissolution of kaolinite. On the other hand, PNS and NE-PC exhibited acceptable compatibility with clay and cement particles. In the case of NaSil admixture, similarly to ternary powder systems, relatively higher dosages were necessary to induce changes in the fluidity of the investigated paste mixtures, regardless of powder types. This high demand is contrary to the findings by Landrou et al. [13] on significant reduction in the yield stress of earth, consisting of clay minerals of predominantly smectite and quartz by the addition of small dosages of NaSil.

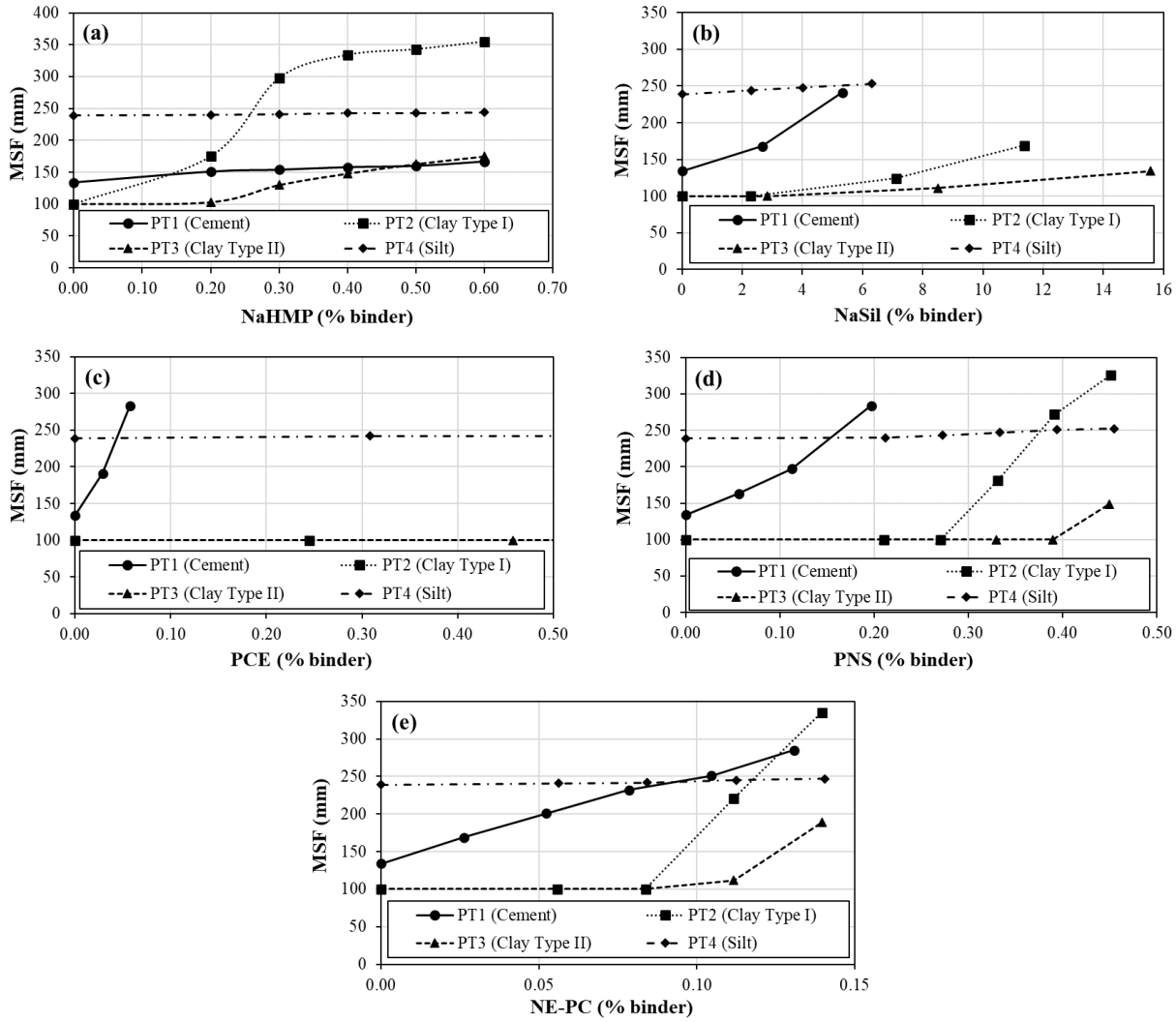

Fig. 4.12. Mini-slump flow of the single-powder pastes proportioned with (a) NaHMP, (b) NaSil, (c) PCE, (d) PNS, and (e) NE-PC admixtures.

4.3.3 Atterberg limits and experimental results

Atterberg limits including LL, PL, and PI were evaluated for each of the 50 mixtures, excluding cement. They can be used for classification of soils based on their binder type and fraction. For each of the mixtures investigated, the admixture demand, expressed as a percentage of mass of binder required to achieve the targeted MSF value, was recorded. Moreover, the flowability loss after 15 min, referred to MSF $loss_{15\ min}$ (in %), was also evaluated. Furthermore, the interpolated MCT value of the SCEP mixtures for the targeted MSF were evaluated. The experimental results, including admixture demand, MCT, MSF $loss_{15\ min}$, compressive strength, and LL and PI Atterberg limits, are summarized in Table 4.5. MSF loss values are summarized only in 15-mins intervals due to the insignificant loss variation trend afterward.

As can be observed, the P5 and P50 mixtures showed the lowest (12.5%) and highest LL (77.4%) values as well as the lowest Clay Type I content (60.8 kg/m^3) and highest Clay Type II content (547.4 kg/m^3), respectively. It proves that the variation of LL is dependent on the clay fraction and type. Similarly, P5 and P50 resulted in the lowest (0.5%) and highest PI (40.7%) values, respectively. That satisfies the key part of this study to investigate a wide range of soil types based on their characteristic parameters.

Table 4.5. Experimental results of the investigated SCEP mixtures.

Mix No.	Admixture demand (%binder)	MCT (s)	MSF $loss_{15\ min}$ (%)	$f'_{c\text{-}1d}$ (MPa)	$f'_{c\text{-}7d}$ (MPa)	$f'_{c\text{-}28d}$ (MPa)	LL (%)	PI (%)	Mix No.	Admixture demand (%binder)	MCT (s)	MSF $loss_{15\ min}$ (%)	$f'_{c\text{-}1d}$ (MPa)	$f'_{c\text{-}7d}$ (MPa)	$f'_{c\text{-}28d}$ (MPa)	LL (%)	PI (%)
P1	0.51	72	47.99	0.8	1.8	2.1	20.3	3.7	P26	0.40	16	5.07	1.0	1.6	1.9	21.5	3.2
P2	2.70	75	49.63	0.7	1.0	1.6	15.3	1.2	P27	0.24	26	3.85	0.5	1.2	1.6	22.5	3.4
P3	0.065	22	3.58	0.3	0.7	1.1	14.3	1.0	P28	2.10	222	55.25	0.4	1.1	1.3	32.7	10.2
P4	0.05	32	3.18	0.4	0.8	0.9	13.2	0.7	P29	6.50	160	62.69	0.5	0.8	1.0	28.3	6.4
P5	0	23	0.69	0.3	0.5	0.6	12.5	0.5	P30	0.09	13	2.97	0.3	0.4	0.4	28.1	5.4
P6	0.07	27	2.10	1.2	4.4	5.8	15.7	1.2	P31	1.40	237	3.20	0.6	2.3	3.4	37.5	14.7
P7	0.35	53	42.70	0.4	2.3	2.3	14.6	0.9	P32	0.75	45	4.61	1.1	2.0	2.4	30.8	7.2
P8	0.60	59	45.93	0.5	1.4	1.9	14.8	1.1	P33	0.28	32	5.07	0.5	1.3	1.7	28.2	5.9
P9	0.11	15	4.24	0.5	0.9	0.9	19.8	3.9	P34	0.70	112	60.40	0.5	0.7	1.1	29.6	7.5
P10	0.17	29	14.04	1.6	2.9	3.5	18.6	1.7	P35	7.50	130	62.83	1.1	1.7	3.4	26.8	5.1
P11	0.12	11	7.83	3.1	5.2	6.2	18.1	1.5	P36	12.00	321	61.98	1.3	3.0	5.0	34.5	12.0
P12	0.08	25	2.73	1.5	4.8	5.5	20.1	5.5	P37	0.39	56	4.90	1.9	3.2	4.2	32.8	11.0
P13	0.49	78	48.51	0.4	2.1	2.9	19.1	3.3	P38	0.10	24	6.23	0.5	1.5	2.0	29.3	8.9
P14	4.00	121	63.24	2.1	2.4	4.1	17.4	1.5	P39	-	blocked	-	-	-	-	40.6	17.3
P15	0.075	17	3.94	2.6	3.9	4.8	17.5	1.3	P40	2.60	201	66.22	0.6	2.7	2.7	32.7	10.4
P16	0.175	21	7.50	2.9	7.6	8.7	18.9	4.0	P41	1.80	189	62.12	0.4	3.8	5.0	30.9	10.1
P17	0.10	11	10.25	1.9	3.9	5.1	19.5	3.8	P42	-	blocked	-	-	-	-	58.9	33.7
P18	0.07	26	2.45	5.7	9.6	11.9	19.9	3.6	P43	2.40	186	12.27	0.9	3.8	4.7	43.1	17.1
P19	0.52	49	62.03	0.8	5.6	7.4	18.5	1.6	P44	1.05	61	6.69	2.2	5.3	6.3	36.5	13.3
P20	4.80	130	63.37	1.8	3.1	4.1	21.3	6.8	P45	0.42	34	2.46	1.3	3.3	4.8	34.6	11.8
P21	3.60	118	63.10	1.7	2.2	2.7	19.4	4.4	P46	6.40	48	10.92	0.3	1.5	2.9	57.5	30.2
P22	0.13	36	4.95	6.9	19.1	24.4	18.9	3.1	P47	4.90	250	62.55	3.1	4.5	5.9	38.5	15.6
P23	0.43	41	17.97	5.2	10.1	13.3	21.5	6.7	P48	15.00	316	61.83	2.1	3.2	7.3	33.1	11.1
P24	0.08	28	3.85	2.9	8.1	10.9	21.6	7.1	P49	0.38	51	27.94	2.0	5.5	6.8	31.5	11.0
P25	0.55	81	65.99	3.2	4.3	4.8	20.5	4.9	P50	8.30	119	10.11	0.4	2.2	3.2	77.4	40.7

4.3.4 Analysis of the signal-to-noise (S/N) ratio

The coupled effects of different mixture parameters on the workability, workability loss, and compressive strength of the investigated mixtures were evaluated. Further analysis was thus required to clarify the significance of each parameter on the targeted responses. Regarding the workability of the paste mixtures, lower admixture demand and loss values of MCT and MSF are favorable. In the case of compressive strength responses, higher value is desirable. Therefore, the smaller-the better S/N ratio (Eq. 4.2) was employed for workability evaluation, while the larger-the better S/N ratio (Eq. 4.1) was used for compressive strength response. As can be observed in Figs. 4.13-4.16, S/N values were calculated to identify the effect of each controlling factor on the workability and compressive strength development of the SCEP mixtures investigated. This can help to identify the optimum level of controlling factors to achieve the targeted properties. It should be noted that higher mean values of the S/N ratio represent the best level for each factor based on the required performance (whether smaller-the better or larger-the better).

As can be observed in Fig. 4.13, optimum levels of the modelled factors to minimize the admixture demand are, in order of importance, NE-PC admixture, cement content of 60 kg/m^3, W/P of 0.50, Ce/Cl of 1.5, and Clay Type I. This can clearly reflect the importance of the compatibility of admixture type (NE-PC), which showed the highest contribution to minimizing the admixture demand, in the case of the ternary-powder system in SCEP mixtures. Moreover, as expected, higher W/P (0.50) and Ce/Cl ratios contributed to lower admixture demand to achieve the targeted MSF.

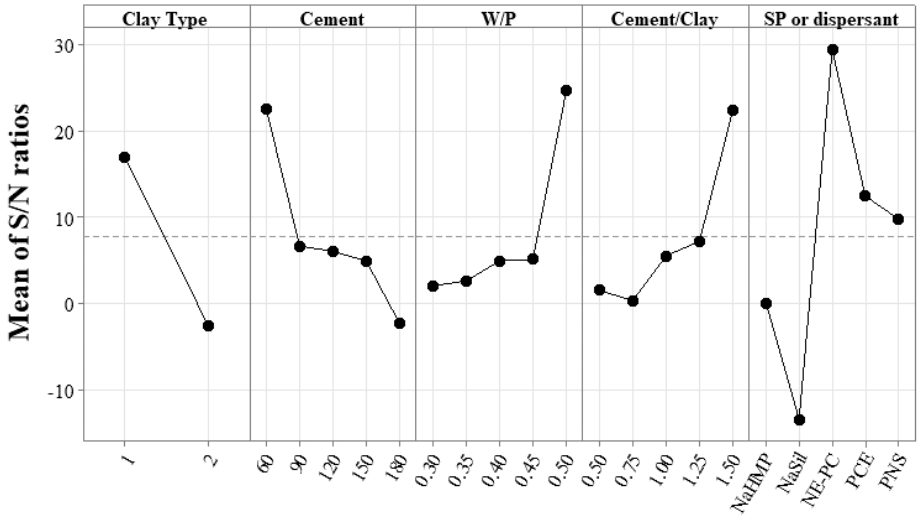

Fig. 4.13. Mean of the smaller-the better S/N ratios for admixture demand to achieve the targeted MSF values

Similarly, the S/N ratios for each level of the controlling factors to secure a minimum MCT are presented in Fig. 4.14. In the case of admixture type, NE-PC and PNS showed almost the same effect to minimize MCT values, higher than PCE and much higher than NaHMP and NaSil. This can be due to their different synergies with the ternary-powder systems investigated. Furthermore, lower cement content (60 kg/m^3), in addition to higher W/P and Ce/Cl ratios resulted in lower MCT values. Accordingly, SCEP mixtures with Clay Type II were found to possess higher MCT values. This proves that finer content of powder exhibited higher MCT values, which causes higher plastic viscosity. This is in accordance with the findings of previous studies [52,53].

As can be observed in Fig. 4.15, minimizing the MSF loss is highly dependent on the admixture type. NaHMP and NaSil were the least effective at minimizing the MSF loss. However, NE-PC, PCE, and PNS contributed the most to minimizing MSF loss, in a descending order of importance. Lower MSF loss was observed for SCEP mixtures with higher W/P ratios. Regarding mixture constituents, Clay Type II with finer particles and higher clay content, controlled by the cement content and Ce/Cl ratio, resulted in greater MSF loss. This proves the significance of powders on MSF loss values of SCEP mixtures.

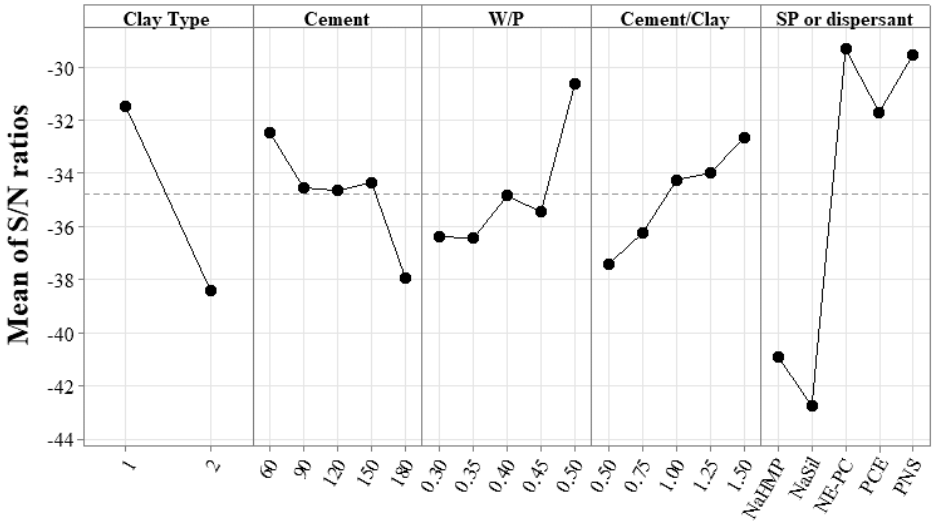

Fig. 4.14. Mean of S/N ratios for MCT results with the smaller-the better performance.

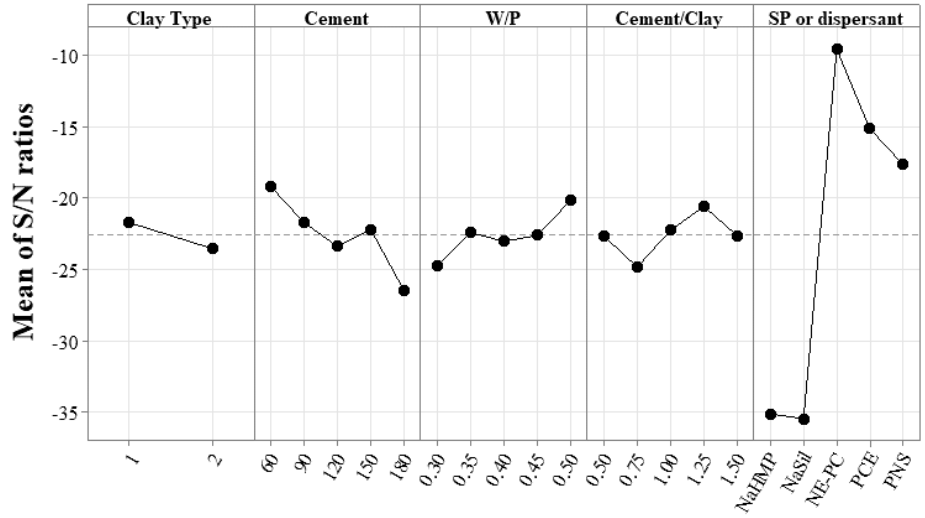

Fig. 4.15. Mean of S/N ratios for MSF loss relative to the targeted MSF with the smaller-the better performance.

In the case of 1-, 7- and 28-day compressive strength values (Fig. 4.10), Clay Type I exhibited higher contribution on strength development. This can be due to high admixture demand of Clay Type II, which consequently may require additional water to achieve a given workability. As expected, it can be observed that increasing cement content and decreasing W/P can maximize the compressive strength values. However, the effect of Ce/Cl on compressive strength was not found to be significant. On the other hand, the effect of admixture type on compressive strength values was found to vary depending on the age of testing. Accordingly, in the case of $f'_{c\text{-}7d}$ and $f'_{c\text{-}28d}$,

NaHMP and NaSil showed the least contribution in achieving the maximum values, while PCE, PNS, and NE-PC resulted in almost identical contributions. However, as can be observed in Fig. 4.10a, PNS, PCE, and NaSil demonstrated higher contributions to enhance the $f'_{c\text{-}1d}$ compressive strength results in order of significance. It should be noted that NaSil led to higher $f'_{c\text{-}1d}$, even though a very high dosage was required to achieve the targeted MSF value, thus resulting in adding more water to the mixture.

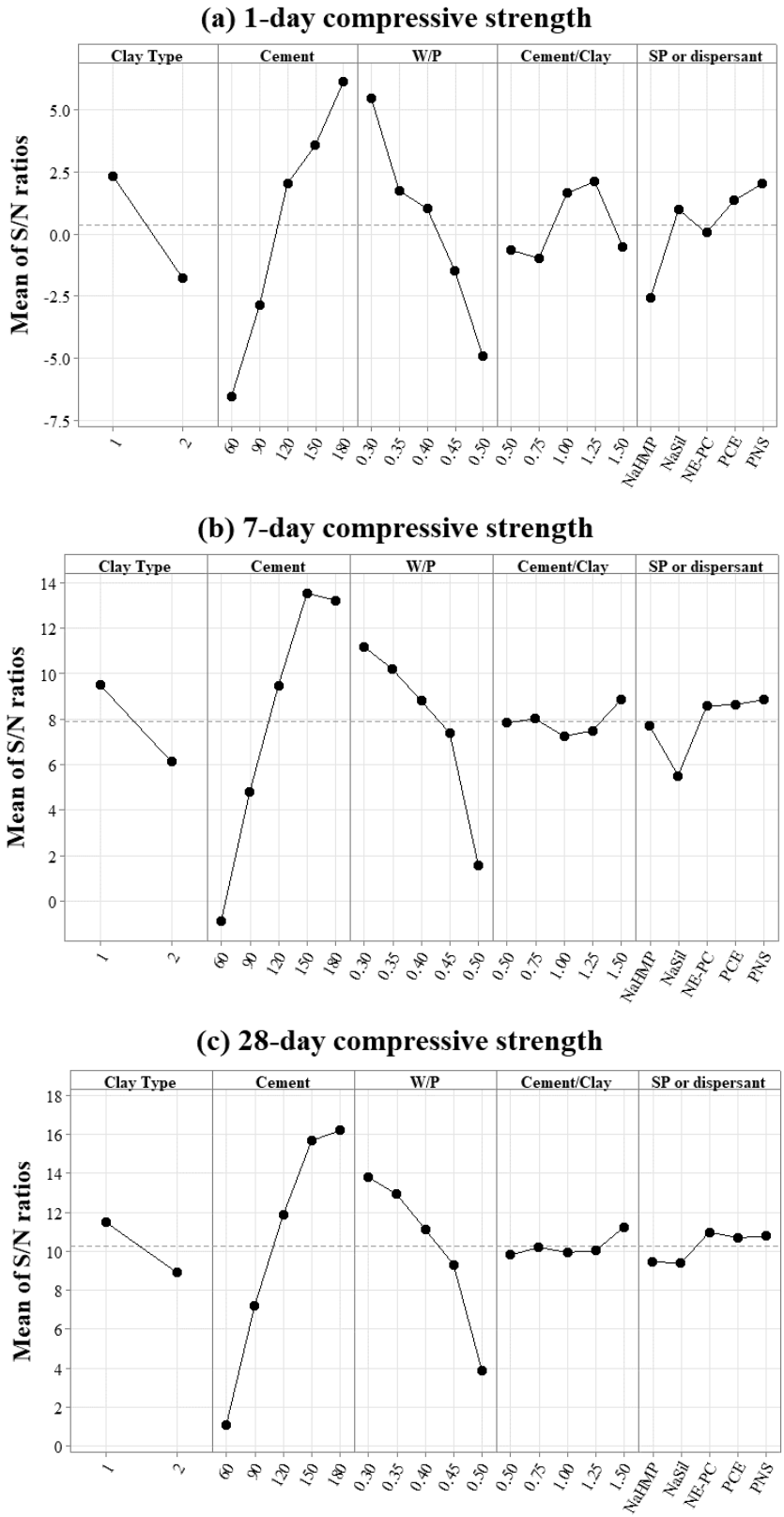

Fig. 4.16. Taguchi analysis (the larger-the better) based on the mean of S/N ratios of control factors for (a) $f'_{c\text{-}1d}$, (b) $f'_{c\text{-}7d}$, and (c) $f'_{c\text{-}28d}$ values.

4.3.5 Analysis of variation (ANOVA)

The two-way analysis of variance (ANOVA) was carried out to evaluate the significance of controlling factors on the modelled responses, including MSF, MCT, MSF loss, and compressive strength at different ages, by considering a 95% confidence level. The results of the ANOVA analysis for workability results of the investigated SCEP mixtures are summarized in Table 4.6.

Table 4.6. Results of ANOVA analysis for admixture demand, MCT, and MSF loss values.

Responses	Source	DF	Seq SS	Contribution	Adj SS	Adj MS	F-Value	P-Value
Admixture demand to achieve the targeted MSF value	Clay type	1	1.2209	22.51%	1.36967	1.36967	86.18	0.000
	Cement content	4	0.4971	9.17%	0.52556	0.13139	8.27	0.000
	W/P	4	0.2412	4.45%	0.09425	0.02356	1.48	0.232
	Ce/Cl	4	0.3939	7.26%	0.45869	0.11467	7.22	0.000
	SP or dispersant	4	2.5939	47.82%	2.59386	0.64847	40.80	0.000
	Error	30	0.4768	8.79%	0.47677	0.01589		
	Total	47	5.4237	100.00%				
MCT	Clay type	1	7.604	18.12%	8.332	8.3319	36.09	0.000
	Cement content	4	2.026	4.83%	2.071	0.5177	2.24	0.088
	W/P	4	2.642	6.30%	1.383	0.3459	1.50	0.228
	Ce/Cl	4	2.127	5.07%	2.452	0.6130	2.65	0.052
	SP or dispersant	4	20.632	49.17%	20.632	5.1581	22.34	0.000
	Error	30	6.927	16.51%	6.927	0.2309		
	Total	47	41.958	100.00%				
MSF loss	Clay type	1	1.242	0.37%	1.476	1.4761	3.73	0.063
	Cement content	4	8.896	2.62%	8.721	2.1803	5.51	0.002
	W/P	4	3.703	1.09%	0.183	0.0457	0.12	0.976
	Ce/Cl	4	1.976	0.58%	1.968	0.4920	1.24	0.313
	SP or dispersant	4	311.363	91.84%	311.363	77.8407	196.88	0.000
	Error	30	11.861	3.50%	11.861	0.3954		
	Total	47	339.041	100.00%				

As can be observed in Table 4.6, admixture and clay types showed the highest contributions to admixture demand. This reflects the importance of the compatibility of admixtures with the binder system of the SECP mixtures investigated. As presented in section 4.3.1, it is obvious that the admixture type effect is highly significant on admixture demand. This is due to the higher demands of inorganic deflocculants compared to common superplasticizers used in concrete. This higher demand can be attributed to the chemical effect of dispersants on clay particles in a ternary powder system. The common superplasticizers used in concrete industry, especially in SCC, are significantly more efficient in the ternary powder system of SCEP. Furthermore, low and high contributions of W/P ratio and clay type, respectively, can illustrate the importance of powder constituent on admixture demand. Very fine particles of Clay Type II, slightly dependent on W/P ratio, demand a higher dosage of admixture. Lower admixture demand will consequently reduce

the cost of SCEP mixtures. The presence of very fine particles significantly increases admixture demand, which leads to higher production cost.

The admixture and clay type showed the most significant contribution on MCT. This suggests that the viscosity of SCEP mixtures, reflected by MCT values, is mostly affected by powder composition and its synergy with the admixtures. The presence of finer particles of clay leads to higher MCT and, consequently, higher viscosity. Accordingly, inorganic deflocculants lead to higher MCT values which may result from their chemical effect on clay particles in the ternary powder system of SCEP. Again, the impact of W/P ratio was found negligible compared to the type of admixture and clay used.

Finally, according to the results presented in Table 4.6, MSF loss values were mostly controlled by the admixture type (F-value of 91.8%). This is due to the significant MSF loss of mixtures dispersed by NaHMP and NaSil. It can be concluded that the flowability of SCEP mixtures significantly decreases over time by inorganic deflocculants used in the clay industry. These admixtures lead to dispersion of clay particles by electrostatic repulsion mechanism, which is not effective over time and results in high MSF loss values. Therefore, the types of admixtures and clay were found to be the most influencing factors on the workability of SCEP mixtures. It proves the importance of the compatibility of chemical admixture with clay particles on the workability of SCEP mixtures, more than other parameters.

ANOVA was applied to investigate the coupled effect of different controlling factors on compressive strength results of the SCEP mixtures investigated. The ANOVA analyses of $f'_{c\text{-}1d}$, $f'_{c\text{-}7d}$, and $f'_{c\text{-}28d}$ values are summarized in Table 4.7. According to the established ANOVA analyses, the most significant factors affecting the compressive strength of SCEP are due to the coupled effect of cement content and W/P. This is also consistent with was discussed in section 4.3.1 as well. Accordingly, after only 1-day, the contribution of cement content and W/P were reflected by F-values of 38.1% and 20.2%, respectively. The coupled effect of cement content and W/P ratio on compressive strength was observed after 1, 7, and 28 days. It is worthy to mention that these contributions increased over time to 59.2% and 19.7% after 7 days, and 63% and 21.2% after 28 days, respectively. Furthermore, clay and admixture types, as well as clay content did not significantly affect the compressive strength development. It can be concluded that the selection

of cement content and W/P, controls the mechanical performance of SCEP mixtures. Therefore, as mentioned for the higher contribution of finer clay particles on admixture demand compared to the W/P ratio, selecting low W/P ratios can lead to achieve a SCEP matrix with appropriate compressive strength, without significantly increasing the admixture demand.

Table 4.7. Results of ANOVA analysis for 1-day, 7-day and 28-day compressive strength values.

Response	Source	DF	Seq SS	Contribution	Adj SS	Adj MS	F-Value	P-Value
$f'_{c\text{-}1d}$	Clay type	1	2.706	7.68%	2.518	2.5184	8.14	0.008
	Cement content	4	13.436	38.14%	13.115	3.2788	10.60	0.000
	W/P	4	7.107	20.17%	7.040	1.7600	5.69	0.002
	Ce/Cl	4	1.069	3.04%	1.062	0.2655	0.86	0.500
	SP or dispersant	4	1.633	4.63%	1.633	0.4082	1.32	0.285
	Error	30	9.277	26.33%	9.277	0.3092		
	Total	47	35.229	100.00%				
$f'_{c\text{-}7d}$	Clay type	1	1.8172	5.67%	1.7023	1.70231	14.53	0.001
	Cement content	4	18.9912	59.22%	17.8010	4.45025	37.97	0.000
	W/P	4	6.3099	19.68%	6.8278	1.70694	14.57	0.000
	Ce/Cl	4	0.2007	0.63%	0.2051	0.05128	0.44	0.780
	SP or dispersant	4	1.2325	3.84%	1.2325	0.30813	2.63	0.054
	Error	30	3.5157	10.96%	3.5157	0.11719		
	Total	47	32.0673	100.00%				
$f'_{c\text{-}28d}$	Clay type	1	1.0605	3.23%	0.9316	0.93157	8.02	0.008
	Cement content	4	20.6606	62.98%	19.7032	4.92580	42.39	0.000
	W/P	4	6.9533	21.20%	7.2246	1.80615	15.54	0.000
	Ce/Cl	4	0.1559	0.48%	0.1568	0.03919	0.34	0.851
	SP or dispersant	4	0.4869	1.48%	0.4869	0.12173	1.05	0.399
	Error	30	3.4863	10.63%	3.4863	0.11621		
	Total	47	32.8035	100.00%				

4.3.6 Effect of specific surface area of binder, liquid limit, and plasticity index of earth on admixture demand

As discussed in the previous section, MSF loss and MCT values of SCEP mixtures are highly dependent on their powder system. In this section, the coupled effect of different characteristics of the powder portion on admixture demand, to achieve the targeted MSF value, was evaluated. The characteristics include SSA and the Atterberg limits of earth, which are found in wide ranges of aggregates and binders with different characteristics. The soil type can be represented using the Atterberg limits, including liquid limit (LL) and plasticity index (PI), reflecting the sensitivity of the soil to water. The LL and PI parameters can characterize the binding portion of earth. Accordingly, these parameters were evaluated for the binder portion of the SCEP mixtures investigated, excluding cement. Various correlations were thus established between the soil

characteristics (LL and PI) and workability of the SCEP mixtures investigated. As shown in Fig. 4.17, the admixture demands to achieve MSF value were correlated to three additional factors, including log(SSA/(W/P)), LL/(W/P), and PI/(W/P) for each of the admixtures investigated.

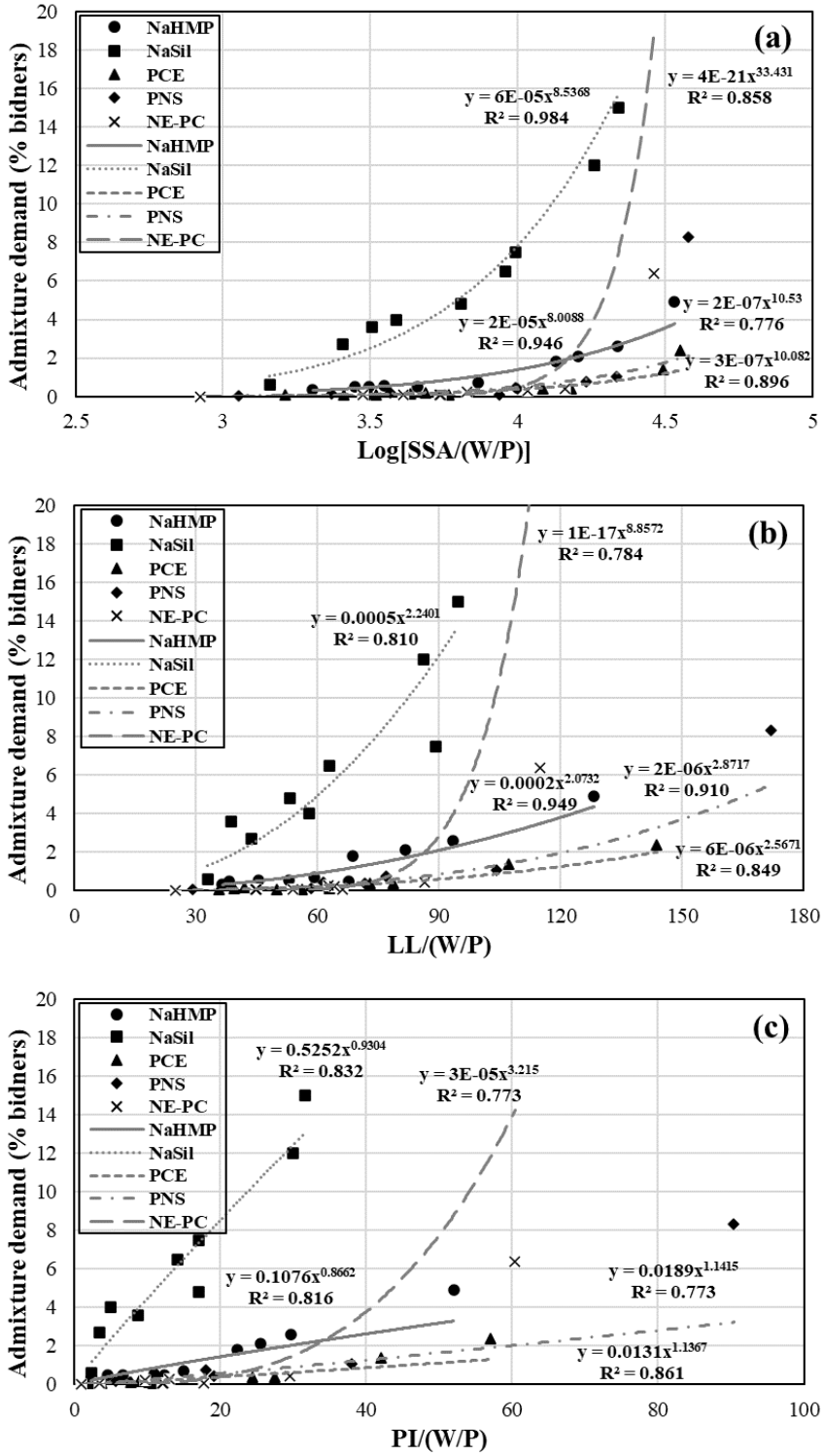

Fig. 4.17. Correlation of admxiture demand to achieve the targeted MSF value with (a) log(SSA/(W/P)), (b) LL/(W/P) and (c) PI/(W/P) values.

As can be observed in Fig. 4.17a, NaSil and PCE types showed the highest and lowest demand, respectively. Moreover, low dosages of NE-PC admixture are required for log(SSA/(W/P)) values less than 4; however, its demand increases significantly in higher values (> 4). On the other hand, PNS demand was found comparable with PCE admixture. It is worthy to mention that the PCE used costs almost 3 times more than the incorporated PNS. Therefore, PNS showed promising efficiency in SCEP mixtures from an economical point of view. The same trends were also observed with LL and PI of the earth binders, as presented in Fig. 4.17b and 4.17c. High R^2 values confirm that LL and PI are the key characterizing parameters of earth to dictate the admixture demand of SCEP mixtures.

In order to evaluate the coupled effect of powder characteristics and W/P ratio on admixture demand of the investigated SCEP mixtures, the following correlation was established:

$$\text{Admixture demand (\% binder)} = \alpha \times SSA^{\beta} \times LL^{\gamma} \times PI^{\delta} / (W/P)^{\varepsilon} + \zeta \quad (4.4)$$

where α, β, γ, δ, ε, and ζ are the adjustment factors to be determined for each admixture type, reflecting the contribution of SSA, LL, PI, and W/P on admixture demand. These adjustment factors were obtained for each admixture using a developed Microsoft Excel solver, as summarized in Table 4.8.

Table 4.8. Adjustment factors of the established admixture demand correlations (Eq. 4.4) for different types of admixtures.

Admixture	α	β	γ	δ	ε	ζ
NaHMP	2.3E-04	0.939	1.83E-09	1.01E-09	0.921	7.61E-10
NaSil	2.54E-03	0.84	2.18E-05	0	1.086	0.066
PCE	3.6E-06	0.269	0.056	3.758	0	0.092
PNS	1.6E-05	0.491	0.76	1.185	0.838	0.122
NE-PC	7.9E-09	4.91E-09	5.04E-09	6.015	8.48E-10	0.118

The SSA showed the highest contribution in increasing NaHMP and NaSil demands compared to LL and PI (higher adjustment factor β). Moreover, NaHMP and NaSil demands decrease with W/P ratio values, which is reflected by the high adjustment factors ε of 0.921 and 1.086, respectively. However, in the case of PCE, PI exhibited the most dominant effect on the admixture demand compared to SSA and LL. Moreover, a power index ε of 0 was obtained for the W/P ratio which refers to no sensitivity of PCE demands to W/P variations (in the range used in this study). Similarly, PI showed the highest contribution to increase the PNS demand. However, SSA, LL,

and W/P exhibited stronger effects on PNS demand compared to those obtained for PCE. In the case of NE-PC admixture, PI was found as the only significant parameter, while the effect of SSA, LL, and W/P was negligible (very low adjustment factors).

As illustrated in Fig. 4.18, the experimental admixture demands for the targeted MSF values are compared to those obtained using the empirical correlations (Eq. 4.4) for all types of the investigated admixtures (Table 4.8). As can be observed in Fig. 4.18, the established correlations (Eq. 4.4 and Table 4.8) are in very good agreement with the experimental results with high R^2 (more than 0.987) and low root-mean-squared error (RMSE) values (lower than 0.21%). Therefore, the proposed empirical correlations can be used to predict the admixture demands as functions of the main controlling factors, including SSA, LL, PI, and W/P ratio.

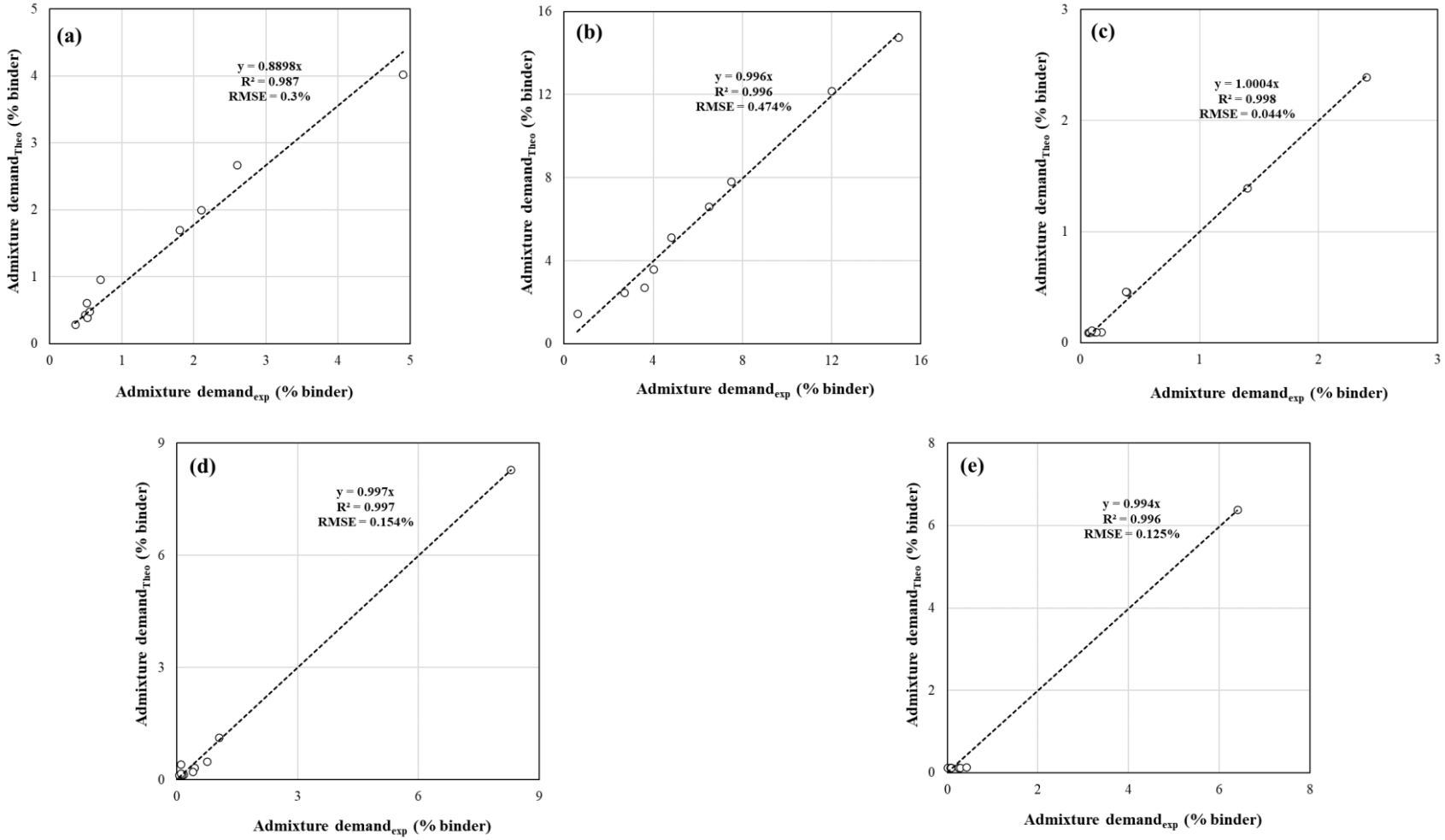

Fig. 4.18. Comparison between the experimental admixture demand and those obtained using the empirical correlations (Eq. 4.4 and Table 4.8) for (a) NaHMP, (b) NaSil, (c) PCE, (d) PNS, and (e) NE-PC admixtures.

4.3.7 Effect of specific surface area of binder, and liquid limit and plasticity index of earth on MCT

The effect of powder characteristics on MCT results, corresponding to the targeted MSF, are evaluated in this section. Le Roy and Roussel [54] classified the flow of cement pastes through the marsh cone in three different categories as "normal flow", "difficult flow", and "no flow". Similarly, according to the results shown in Table 4.9, the flow of the investigated SCEP mixtures through the marsh cone was classified in four different categories, including "good flow", "moderate flow", "difficult flow", and "no flow".

Table 4.9. Flowability classification of the SCEP mixtures investigated based on the MCT values.

MCT (s)	Flowability range
0-30	Good flow
30-50	Moderate flow
50-100	Difficult flow
> 100	No flow

The MCT results of the SCEP mixtures investigated were then correlated to their corresponding powder characteristics, including SSA, LL, and PI values, as shown in Fig. 4.19. As can be observed, increasing SSA, LL, and PI resulted in higher MCT, regardless of different admixture types. Moreover, NaSil and NaHMP admixtures resulted in significantly higher MCT values, especially for high SSA powders, compared to other admixtures. According to the classifications presented in Table 4.9, the mixtures containing NaSil and NaHMP lie within the range of difficult and no flow. For a given SSA, LL, and PI of powder, SCEP mixtures containing NaSil and NE-PC resulted in the highest and lowest MCT results, respectively. On the other hand, SCEP mixtures dispersed with conventional superplasticizers used in SCC are within good and moderate flow, except for the very high SSA values which led to difficult and no flow ranges. Furthermore, stronger correlations (higher R^2 values) were obtained for NaSil, NaHMP, and NE-PC admixtures compared to those obtained for PCE and PNS types. It is worthy to mention that very high LL and PI values are not favorable for designing SCEP mixtures. The recommended LL and PI should be lower than 40 and 25, respectively.

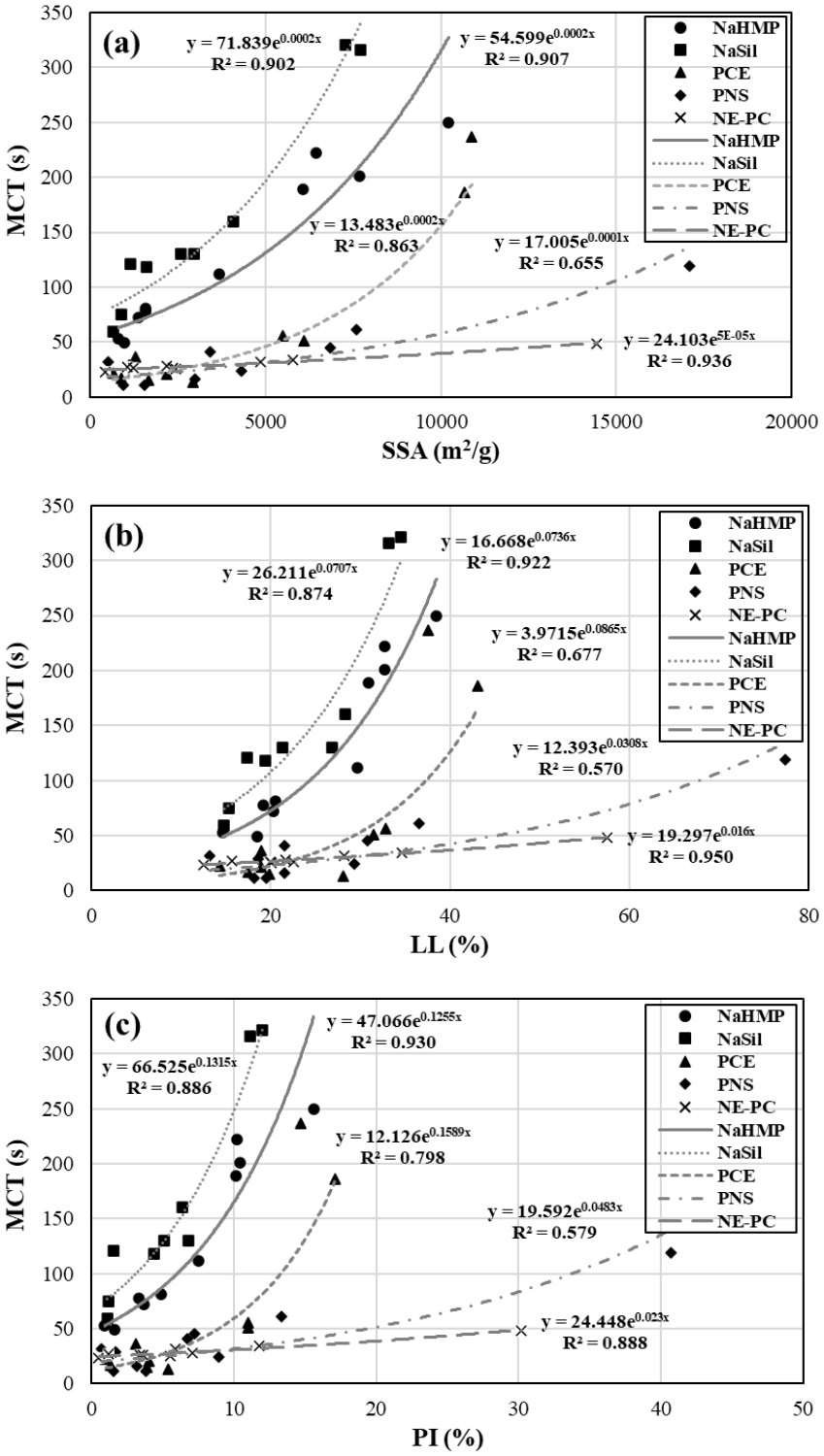

Fig. 4.19. Correlation of MCT values of the mixtures investigated versus (a) log(SSA/(W/P)), (b) LL/(W/P) and (c) PI/(W/P) values.

To evaluate the coupled effect of different powder characteristics on MCT values, the following correlation Eq. (4.5) was then established:

$$MCT\ (s) = \alpha \times SSA^{\beta} \times LL^{\gamma} \times PI^{\delta} + \zeta \quad (4.5)$$

where the adjustment factors α, β, γ, δ, and ζ were obtained for different types of admixtures and summarized in Table 4.10. According to the established correlations and adjustment factors, in the case of NaHMP, NaSil, PCE, and PNS admixtures, SSA of powders exhibited the highest contribution on MCT. Moreover, no effects of LL and low contribution of PI on MCT of the mixtures containing NaHMP and PNS were observed. Furthermore, SSA was found as the only factor controlling the MCT of SCEP mixtures dispersed with NaSil and PCE types. On the other hand, LL of powders showed higher contribution on MCT of SCEP mixtures dispersed with NE-PC compared to SSA.

Table 4.10. Adjustment factors of MCT correlations (Eq. 4.5) for different types of admixtures.

Admixture	α	β	γ	δ	ζ
NaHMP	0.709	0.635	0	0.012	0
NaSil	0.539	0.71	0	0	1.65E-04
PCE	5.6E-09	2.613	2E-10	2.4E-12	17.966
PNS	2.39E-04	1.313	0	0.046	17.927
NE-PC	0.029	0.285	1.011	0	21.45

The experimental MCT values of the SCEP mixtures investigated are compared to those obtained using the established correlations, summarized in Eq. 4.5 and Table 4.10 and presented in Fig. 4.20. As can be observed, the established empirical correlations showed good precision in evaluating the coupled effect of powder characteristics on MCT results, reflected by high R^2, estimation indices close to unity, and low RMSE values. The established correlations can then be used to optimize the powder characteristics and enhance the flowability of SCEP mixtures.

4.3.8 Dismantling the formwork

As explained earlier, a compressive strength higher than 1 MPa can guarantee successful demolding of the formworks [9]. According to the ANOVA analysis summarized in Table 4.7, cement content and W/P ratio exhibited the highest contribution to enhance the 1-d compressive strength of SCEP. The contour plot of 1-day compressive strength versus cement content and W/P ratios presented in Fig. 4.21a can be employed to evaluate the coupled effect of cement content and W/P on 1-d compressive strength and determine a formwork removal criterion. As can be

observed, cement content of 60 kg/m^3 cannot satisfy the minimum $f'_{c\text{-}1d}$ of 1 MPa to dismantle the formwork. In the case of cement content of 90 kg/m^3, SCEP mixtures made with a low W/P ratio of 0.30 could achieve a $f'_{c\text{-}1d}$ of 1 to 3 MPa. However, this content is not satisfactory for higher W/P ratios. By increasing cement content up to 120 kg/m^3, SCEP mixtures satisfied the demolding requirement, except in the case of a high W/P ratio of 0.5. The SCEP mixtures made with cement contents higher than 120 kg/m^3 could achieve the targeted minimum 1-d compressive strength of 1 MPa, regardless of W/P ratio. Relatively high ranges of $f'_{c\text{-}1d}$ of 3 to 5 MPa were achieved for the SCEP mixtures containing 150 kg/m^3 cement and a W/P of 0.30, and 180 kg/m^3 cement and a W/P of 0.30 and 0.35. The 7- and 28-day compressive strength contours as a function of W/P and cement content (Fig. 4.21b and 4.21c) can be used as a mechanical performance criterion to optimize SCEP mixture proportioning. Accordingly, appropriate W/P and cement content can be selected to achieve a required mechanical performance.

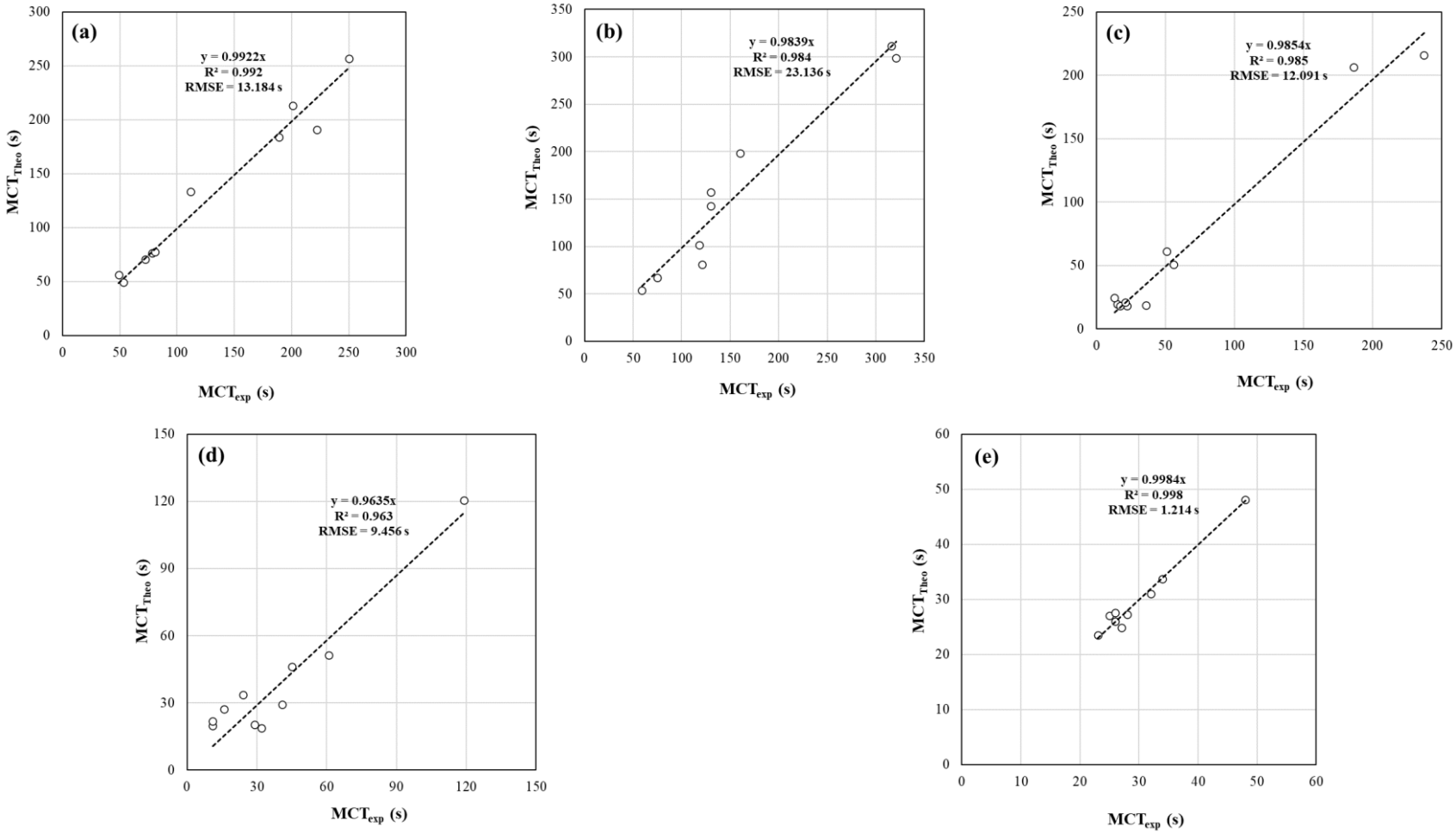

Fig. 4.20. Comparison between the experimental MCT results and those obtained using the empirical correlations Eq. (4.5) and Table 4.10 for (a) NaHMP, (b) NaSil, (c) PCE, (d) PNS, and (e) NE-PC admixtures.

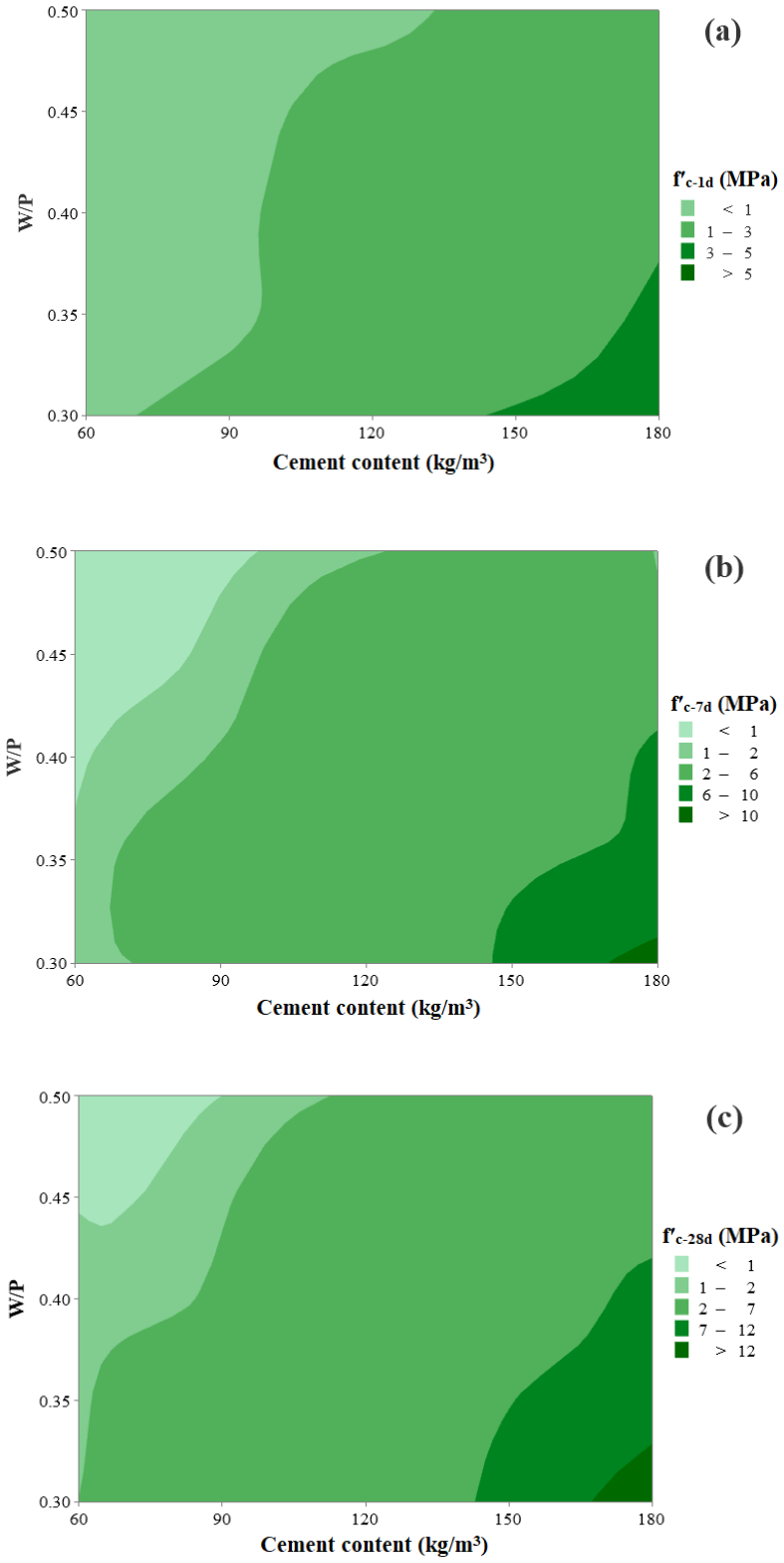

Fig. 4.21. Contour plot of (a) $f'_{c\text{-}1d}$, (b) $f'_{c\text{-}7d}$ in and (c) $f'_{c\text{-}28d}$ in respect to cement content and W/P.

4.3.9 Designing proper SCEP mixtures

According to the reported results obtained for wide ranges of powder characteristics, W/P ratios, cement and clay contents, and admixture types, a new approach for proportioning SCEP mixtures is proposed. The proposed approach is based on the empirical models (Eqs. 4.4 and 4.5) established in this study, as illustrated in Fig. 4.22. As can be observed, the particle-size distribution (PSD), LL, and PI of the available soil are the inputs of the proposed proportioning model (step #1). As reported earlier, it is highly recommended to select soils with LL and PI values lower than 40 and 25, respectively. Moreover, the cement content and W/P ratio can be selected using the compressive strength contour plots shown in Fig. 4.21 for $f'_{c\text{-}1d}$ and $f'_{c\text{-}28d}$ values given the required compressive strength for formwork removal ($f'_{c\text{-}1d} > 1$ MPa) and targeted $f'_{c\text{-}28d}$ (steps #2-1 and #2-2). Then, the clay content can be calculated using the specific gravity values of cement and clay in a unit volume of SCEP mixture. The admixture type is usually selected based on the application, local availability, and cost (step #3). Once the soil is selected, the SSA is thus determined (step #4). The empirical model in Eq. 4.4 along with the adjustment factors presented in Table 4.8 are then used to determine the required admixture dosage (step #5). Workability of the trail SCEP mixture can then be verified by determining the MCT values using the established correlation in Eq. 4.5 and corresponding factors presented in Table 4.10 (step #6-1). The predicted MCT value is then compared with the proposed classification in Table 4.9 (step #6-2). The selected cement content, W/P, and clay type can then be modified according to the flowability verification carried out at step #6.

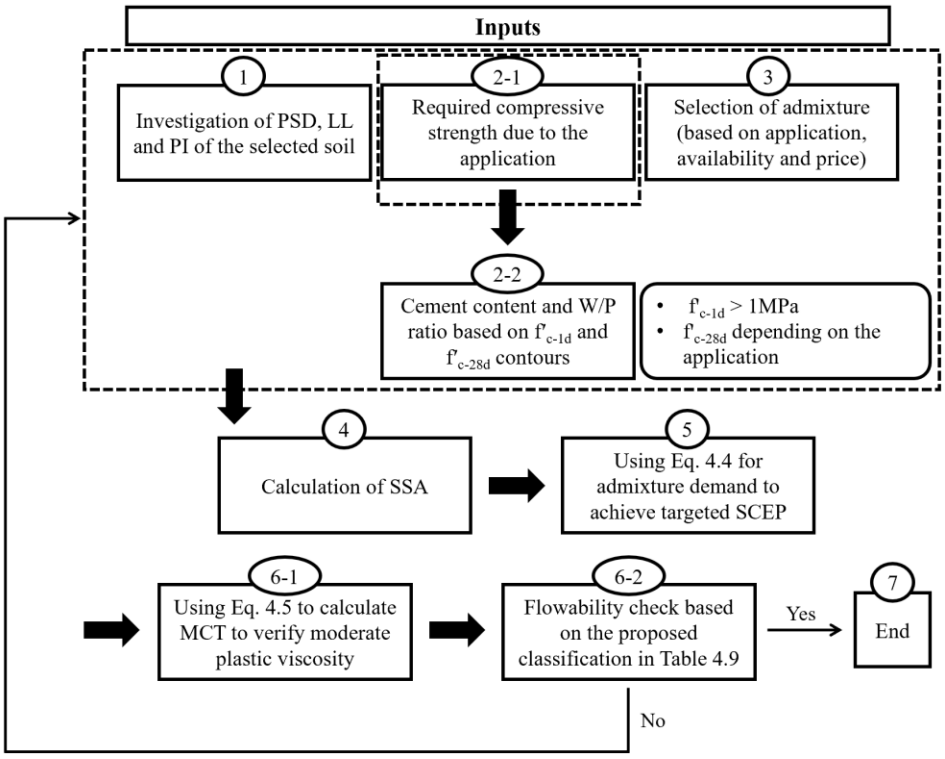

Fig. 4.22. Schematics of the proposed proportioning approach for SCEP mixtures.

4.4 Conclusions

Recently, there has been an increasing interest in sustainable construction materials to reduce the environmental impact of the construction industry. Development and use of SCEC, as a novel environment-friendly material, can facilitate casting and speed up the construction process. In this study, workability characteristics and compressive strength performance of SCEP mixtures were investigated. The effect of different admixture and clay types, cement content, fineness of powder constituents, and W/P on the targeted responses was investigated using the Taguchi DOE. Using the Atterberg limits and specific surface area of the earth, a proportioning approach to design SCEP mixtures was proposed to facilitate the design protocol given diverse earth types. According to the experimental results presented in this study, the following concluding remarks can be pointed out:

- Workability of SCEP mixtures was mainly controlled by the fineness of powders and W/P, while cement content and W/P showed the highest contribution on compressive strength values. Clay Type II consisting of 50% kaolinite and 50% attapulgite and low W/P (0.30) resulted in the highest admixture demand to achieve targeted workability characteristics.

- Using signal-to-noise analysis, the highest admixture demand and workability loss were attributed to NaSil and NaHMP, respectively. However, the use of NE-PC demand was the lowest among all admixture types with the minimum MSF loss. Regarding marsh cone test (MCT) results, NE-PC and PNS resulted in the lowest values. Based on S/N ratios, Clay Type I (100% kaolinite), lower cement content, and higher W/P and Ce/Cl resulted in lower MCT values, corresponding to lower plastic viscosity of SCEP mixtures.

- Adequate clay dispersion can be achieved using NaHMP, while the use of PCE was only efficient in the presence of cement. Moreover, NE-PC and PNS showed good compatibility with both clay and cement particles. The effect of NaSil on flowability of single-powder systems was negligible.

- The PNS, PCE, and NaSil admixture types showed the highest contribution on early compressive strength development. However, the contribution of PNS, PCE and NE-PC on 7- and 28-day compressive strength values was comparable.

- Increasing the specific surface area of binder compositions, and liquid limit and plasticity index of earth led to higher admixture demand and marsh cone values. These parameters were also well correlated with the workability of SCEP mixtures to propose more accurate theoretical models. LL and PI values lower than 40 and 25, respectively, were recommended to achieve SCEP mixtures.

- A new proportioning approach to design SCEP mixtures with targeted workability and compressive strength was proposed.

4.5 Declaration of competing interest

The authors declare that they have no known competing financial interests or personal relationships that could have appeared to influence the work reported in this paper.

4.6 Acknowledgement

The authors wish to thank the financial support of the National Science and Engineering Research Council of Canada (NSERC) and the eight industrial partners participating in the NSERC Chair on Development of Flowable Concrete with Adapted Rheology and their Application in Concrete Infrastructures, held by Professor Ammar Yahia at the Université de Sherbrooke.

REFERENCES

[1] M.K. Dixit, Life cycle recurrent embodied energy calculation of buildings: A review, J. Clean. Prod. 209 (2019) 731–754. https://doi.org/10.1016/J.JCLEPRO.2018.10.230.

[2] E.M. Gartner, D.E. MacPhee, A physico-chemical basis for novel cementitious binders, Cem. Concr. Res. 41 (2011) 736–749. https://doi.org/10.1016/J.CEMCONRES.2011.03.006.

[3] F. Pacheco-Torgal, S. Jalali, Earth construction: Lessons from the past for future eco-efficient construction, Constr. Build. Mater. 29 (2012) 512–519. https://doi.org/10.1016/j.conbuildmat.2011.10.054.

[4] P.G. McHenry, Adobe and Rammed Earth Buildings: Design and Construction, University of Arizona Press, Arizona, 1989.

[5] R. Bahar, M. Benazzoug, S. Kenai, Performance of compacted cement-stabilised soil, Cem. Concr. Compos. 26 (2004) 811–820. https://doi.org/10.1016/j.cemconcomp.2004.01.003.

[6] M. Hall, Y. Djerbib, Rammed earth sample production: Context, recommendations and consistency, Constr. Build. Mater. 18 (2004) 281–286. https://doi.org/10.1016/j.conbuildmat.2003.11.001.

[7] A. Coelho, Preliminary study for self-sufficiency of construction materials in a Portuguese region - Évora, J. Clean. Prod. 112 (2016) 771–786. https://doi.org/10.1016/j.jclepro.2015.06.113.

[8] H. Van Damme, H. Houben, Earth concrete. Stabilization revisited, Cem. Concr. Res. 114 (2018) 90–102. https://doi.org/10.1016/J.CEMCONRES.2017.02.035.

[9] C.M. Ouellet-Plamondon, G. Habert, Self-Compacted Clay based Concrete (SCCC): Proof-of-concept, J. Clean. Prod. 117 (2016) 160–168. https://doi.org/10.1016/j.jclepro.2015.12.048.

[10] P. Walker, R. Keable, J. Martin, V. Maniatidis, Rammed earth: design and construction guidelines, IHS BRE, 2005.

[11] N. Kumari, C. Mohan, Basics of Clay Minerals and Their Characteristic Properties, in: Clay Clay

Miner., 2021.

[12] Y. Qian, G. De Schutter, Enhancing thixotropy of fresh cement pastes with nanoclay in presence of polycarboxylate ether superplasticizer (PCE), Cem. Concr. Res. 111 (2018) 15–22. https://doi.org/10.1016/J.CEMCONRES.2018.06.013.

[13] G. Landrou, C. Brumaud, F. Winnefeld, R.J. Flatt, G. Habert, Lime as an anti-plasticizer for self-compacting clay concrete, Materials (Basel). 9 (2016). https://doi.org/10.3390/ma9050330.

[14] F. Andreola, E. Castellini, J.M.F. Ferreira, S. Olhero, M. Romagnoli, Effect of sodium hexametaphosphate and ageing on the rheological behaviour of kaolin dispersions, Appl. Clay Sci. 31 (2006) 56–64. https://doi.org/10.1016/j.clay.2005.08.004.

[15] F. Andreola, E. Castellini, T. Manfredini, M. Romagnoli, The role of sodium hexametaphosphate in the dissolution process of kaolinite and kaolin, J. Eur. Ceram. Soc. 24 (2004) 2113–2124. https://doi.org/10.1016/S0955-2219(03)00366-2.

[16] K.O. Adebowale, I.E. Unuabonah, B.I. Olu-Owolabi, Adsorption of some heavy metal ions on sulfate- and phosphate-modified kaolin, Appl. Clay Sci. 29 (2005) 145–148. https://doi.org/10.1016/j.clay.2004.10.003.

[17] F. Andreola, E. Castellini, G. Lusvardi, L. Menabue, M. Romagnoli, Release of ions from kaolinite dispersed in deflocculant solutions, Appl. Clay Sci. 36 (2007) 271–278. https://doi.org/10.1016/j.clay.2006.10.002.

[18] E. Castellini, C. Berthold, D. Malferrari, F. Bernini, Sodium hexametaphosphate interaction with 2:1 clay minerals illite and montmorillonite, Appl. Clay Sci. 83–84 (2013) 162–170. https://doi.org/10.1016/j.clay.2013.08.031.

[19] H.M.M. Diz, B. Rand, The mechanism of deflocculation of kaolinite by polyanions, Br. Ceram. Trans. 89 (1990) 77–82.

[20] J.L. Amorós, V. Beltrán, V. Sanz, J.C. Jarque, Electrokinetic and rheological properties of highly concentrated kaolin dispersions: Influence of particle volume fraction and dispersant concentration, Appl. Clay Sci. 49 (2010) 33–43. https://doi.org/10.1016/j.clay.2010.03.020.

[21] F. Andreola, M. Romagnoli, E. Castellini, G. Lusvardi, L. Menabue, Role of the surface treatment in the deflocculation of kaolinite, J. Am. Ceram. Soc. 89 (2006) 1107–1109. https://doi.org/10.1111/j.1551-2916.2005.00814.x.

[22] D. Penner, G. Lagaly, Influence of anions on the rheological properties of clay mineral dispersions D., Appl. Clay Sci. 19 (2001) 131–142.

[23] B.M. Aïssoun, S.-D. Hwang, K.H. Khayat, Influence of aggregate characteristics on workability of superworkable concrete, Mater. Struct. 49 (2016) 597–609.

[24] B.I.O. Koura, M. Hosseinpoor, A. Yahia, Coupled effect of fine mortar and granular skeleton characteristics on dynamic stability of self-consolidating concrete as a diphasic material, Constr. Build. Mater. 263 (2020) 120131. https://doi.org/10.1016/j.conbuildmat.2020.120131.

[25] B.I. Ouro Koura, M. Hosseinpoor, A. Yahia, E.H. Kadri, A. Kaci, A new proportioning approach of low and normal binder self-consolidating concrete based on the characteristics of fine mortar and granular skeleton, Constr. Build. Mater. 239 (2020) 117892. https://doi.org/10.1016/j.conbuildmat.2019.117892.

[26] M. Hosseinpoor, B.I. Ouro Koura, A. Yahia, Rheo-morphological investigation of static and dynamic stability of self-consolidating concrete: A biphasic approach, Cem. Concr. Compos. 121 (2021) 104072. https://doi.org/10.1016/j.cemconcomp.2021.104072.

[27] C. Galán-Marín, C. Rivera-Gómez, J. Petric, Clay-based composite stabilized with natural polymer and fibre, Constr. Build. Mater. 24 (2010) 1462–1468. https://doi.org/10.1016/J.CONBUILDMAT.2010.01.008.

[28] M. Achenza, L. Fenu, On Earth Stabilization with Natural Polymers for Earth Masonry Construction, Mater. Struct. 39 (2006) 21–27.

[29] C.A. Dove, F.F. Bradley, S. V. Patwardhan, Seaweed biopolymers as additives for unfired clay bricks, Mater. Struct. 49 (2016) 4463–4482.

[30] T. Funami, Y. Fang, S. Noda, S. Ishihara, M. Nakauma, K.I. Draget, K. Nishinari, G.O. Phillips, Rheological properties of sodium alginate in an aqueous system during gelation in relation to supermolecular structures and Ca2+ binding, Food Hydrocoll. 23 (2009) 1746–1755. https://doi.org/10.1016/J.FOODHYD.2009.02.014.

[31] F. Winnefeld, B. Lothenbach, Hydration of calcium sulfoaluminate cements — Experimental findings and thermodynamic modelling, Cem. Concr. Res. 40 (2010) 1239–1247. https://doi.org/10.1016/J.CEMCONRES.2009.08.014.

[32] S. Guiheneuf, Formulation et renforts de blocs en matériau terre pour une utilisation structurelle, INSA de Rennes, 2020. https://tel.archives-ouvertes.fr/tel-03194559.

[33] A.W. Skempton, The Colloidal activity of clays, in: 3rd Int. Conf. Soil Mech. Found. Eng., London, 1953: pp. 47–61.

[34] B. Voight, Correlation between Atterberg plasticity limits and residual shear strength of natural soils, Géotechnique. 23 (1973) 265–267.

[35] A. Laskar, S.K. Pal, Geotechnical characteristics of two different soils and their mixture and relationships between parameters, Electron. J. Geotech. Eng. 17 (2012) 2821–2832.

[36] P.P. Raj, Soil Mechanics and Foundation Engineering, Dorling Kindersley, (India) Pvt. Ltd., New Delhi, 2012.

[37] ASTM D4318 − 17, Standard Test Methods for Liquid Limit, Plastic Limit, and Plasticity Index of Soils, ASTM Stand. (2017).

[38] S. Panda, P. Sarkar, Abrasion resistance of copper slag aggregate concrete designed by Taguchi method, Mater. Today Proc. (2022). https://doi.org/10.1016/J.MATPR.2022.02.545.

[39] T. Fantous, A. Yahia, Effect of viscosity and shear regime on stability of the air-void system in self-consolidating concrete using Taguchi method, Cem. Concr. Compos. 112 (2020) 103653. https://doi.org/10.1016/J.CEMCONCOMP.2020.103653.

[40] M.S. Phadke, Quality Engineering using Robust Design, Prentice Hall, New Jersey, 1989.

[41] P. Dhemla, P. Somani, B.L. Swami, A. Gaur, Optimizing the design of sintered fly ash light weight concrete by Taguchi and ANOVA analysis, Mater. Today Proc. (2022). https://doi.org/10.1016/J.MATPR.2022.03.573.

[42] J. Esmaeili, K. Andalibi, O. Gencel, Mechanical characteristics of experimental multi-scale steel

fiber reinforced polymer concrete and optimization by Taguchi methods, Constr. Build. Mater. 313 (2021) 125500. https://doi.org/10.1016/J.CONBUILDMAT.2021.125500.

[43] R.K. Roy, A Primer on the Taguchi Method, Competitive Manufacturing Series, 1990.

[44] G.S. Peace, Taguchi Method, Corporate and Professional Publishing Group, 1993.

[45] O. Gencel, O. Yavuz Bayraktar, G. Kaplan, A. Benli, G. Martínez-Barrera, W. Brostow, M. Tek, B. Bodur, Characteristics of hemp fibre reinforced foam concretes with fly ash and Taguchi optimization, Constr. Build. Mater. 294 (2021) 123607. https://doi.org/10.1016/J.CONBUILDMAT.2021.123607.

[46] S. V. Dave, A. Bhogayata, The strength oriented mix design for geopolymer concrete using Taguchi method and Indian concrete mix design code, Constr. Build. Mater. 262 (2020) 120853. https://doi.org/10.1016/J.CONBUILDMAT.2020.120853.

[47] P. Walker, The Australian earth building handbook, Sydney : Standards Australia International, 2002.

[48] ASTM C305-20, Standard Practice for Mechanical Mixing of Hydraulic Cement Pastes and Mortars of Plastic Consistency, ASTM Int. (2020) 1–3. https://doi.org/10.1520/C0305-20.2.

[49] N. Roussel, C. Stefani, R. Leroy, From mini-cone test to Abrams cone test: Measurement of cement-based materials yield stress using slump tests, Cem. Concr. Res. 35 (2005) 817–822. https://doi.org/10.1016/j.cemconres.2004.07.032.

[50] BS EN 445, Grout for prestressing tendons. Test methods, 2007.

[51] ASTM C109-20, Standard test method for compressive strength of hydraulic cement mortars (using 2-in. or [50-mm] cube specimens), ASTM Int. (2020). https://doi.org/10.1520/C0109_C0109M-20B.

[52] J.J. Chen, B.H. Li, P.L. Ng, A.K.H. Kwan, Adding granite polishing waste as sand replacement to improve packing density, rheology, strength and impermeability of mortar, Powder Technol. 364 (2020) 404–415.

[53] S.K. Ling, A.K.H. Kwan, Adding ground sand to decrease paste volume, increase cohesiveness and improve passing ability of SCC, Constr. Build. Mater. 84 (2015) 46–53.

[54] R. Le Roy, N. Roussel, The marsh cone as a viscometer: Theoretical analysis and practical limits, Mater. Struct. 38 (2005) 25–30. https://doi.org/10.1007/bf02480571.

CHAPTER 5. Multiscale investigation of self-consolidating earthen materials using a novel concrete-equivalent mortar approach

Authors and affiliations

Mojtaba Kohandelnia: Ph.D. candidate, Cement and Concrete Research Group, Department of Civil and Building Engineering, Université de Sherbrooke, Sherbrooke, Québec, Canada, J1K 2R1.

Masoud Hosseinpoor: Post-Doc, Cement and Concrete Research Group, Department of Civil and Building Engineering, Université de Sherbrooke, Sherbrooke, Québec, Canada, J1K 2R1.

Ammar Yahia: Professor, Cement and Concrete Research Group, Department of Civil and Building Engineering, Université de Sherbrooke, Sherbrooke, Québec, Canada, J1K 2R1.

Rafik Belarbi, Professor, LaSIE UMR CNRS 7356, La Rochelle Université, La Rochelle, France.

Article Status: Published
Journal: Construction and Building Materials - Elsevier
Reference: M. Kohandelnia, M. Hosseinpoor, A. Yahia, R. Belarbi, Multiscale investigation of self-consolidating earthen materials using a novel concrete-equivalent mortar approach, Constr. Build. Mater. 370 (2023) 130700. https://doi.org/10.1016/J.CONBUILDMAT.2023.130700.
Titre française: Étude multi-échelle des matériaux terreux autoplaçants à l'aide d'une nouvelle approche de mortier équivalent au béton.

Abstract

Earth-based materials have been used since ancient times due to their low environmental impact and superior thermal performance. The rammed earth (RE) method, as a common earthen construction, consists in casting the material layer-by-layer, which is time-consuming, labor-intensive, and energy consuming. Designing self-consolidating earth concrete (SCEC) can speed up the construction process and overcome the disadvantages of conventional RE and enhance its performance. Achieving high fluidity and adequate compressive strength for early demolding is challenging because of the presence of clay and low cement content, respectively. Moreover, diversity of existing soil types does not allow to propose a universal mixture proportioning approach. In this study, workability, drying shrinkage, and compressive strength of SCEC mixtures were evaluated using a new concrete-equivalent mortar (CEM) approach. The approach is mainly based on optimizing the excess paste (EP) thickness. The mixture parameters included the water-to-powder ratio (W/P), volumetric sand-to-total aggregate (S/A) ratio, and the excess paste thickness. Good correlations between the investigated CEMs and their corresponding concrete mixtures were established. According to the carried-out ANOVA analysis, the main influencing parameters on workability, drying shrinkage, and compressive strength of SCEC include the specific surface area and Atterberg limits of the ternary binder system, W/P, paste volume, and EP thickness.

Keywords: Self-consolidating earth concrete (SCEC), Workability, Concrete-equivalent mortar (CEM), Rammed earth (RE), Clay.

5.1 Introduction

Cement, as the key component of concrete, leads to high amount of CO_2 emission compared to other construction materials [1]. Lowering the use of cement by incorporating other sustainable materials can lead to greener construction [2]. Rammed earth (RE), one of the common earthen construction methods proportioned with no or low amount of cement, is an ancient construction method commonly used in wall applications. The most important advantages of RE are its low environmental impact due to lower consumption of industrial materials, better thermal performance, and superior indoor air quality compared to conventional concrete [3,4]. However,

unlike cement-based mortar and concrete, RE construction has not been comprehensively investigated in literature for a long time despite of the great interest in earthen materials in recent years [5].

Regardless of all aforementioned advantages, the process of RE construction is time-consuming and labor intensive with layer-by-layer deficiencies [6]. Self-consolidating earth concrete (SCEC) can be an alternative to facilitate and speed-up the construction process yet keeping the advantages of earthen materials. However, designing SCEC is challenging because of the earth composition and presence of clay. The earth consists in sand and gravel as aggregates, as well as clay and silt as binders [7]. Clay particles are finer than 2 μm with high specific surface area (SSA), hence leading to high plastic viscosity and yield stress of clay-based suspensions [8,9]. Therefore, the first challenge to develop SCEC is to improve its flowability due to the presence of clay particles, sometimes in high quantity in soil composition [10]. The compatibility and interaction of superplasticizer admixtures with ternary clay, cement, and silt binder system is fundamental to achieve SCEC [11]. Polycarboxylate-ether based (PCE) superplasticizers used in conventional SCC can significantly decrease the yield stress of earth-based suspensions, but only in presence of cement [7,12]. Moreover, clay particles can be dispersed in presence of inorganic dispersants, including sodium hexametaphosphate and sodium silicate, hence leading to a significant reduction in the yield stress of earth [12]. However, a comparative study on the significance of high-range water reducer (HRWR) admixtures and clay dispersants on performance of ternary binder system of SCEC can broaden the application of this new construction material.

The second challenge to develop highly flowable earth concrete mixtures, such as SCEC, is the delayed setting of the matrix due to low amount of cement, hence leading to low early-age compressive strength. This latter can be used as quality control index for demolding process [7]. In addition, the packing density and quantity of fine particles are key factors influencing the rheological properties, stability, and compressive strength of SCEC [13–16]. A proper optimization of all these factors can contribute in designing SCEC and proper setting and rheological properties. An adequate selection of the soil type is also essential given the various available types with variable properties. Because of these challenges, it is difficult to recommend a universal mixture proportioning method regardless of the diverse soil types. Therefore, evaluating the feasibility of using various soil types and taking into account their key

characteristics and classifications is of particular interest to enhance designing SCEC. The Atterberg limits are the key parameters, mostly affected by clay fraction, often used to describe the properties of soils given their constituents in the presence of water [17–20].

Flow properties of concrete can be modelled using the concrete-equivalent mortar (CEM) method. In this approach, the coarse aggregate fraction is replaced by sand of equal surface area, aiming to keep a constant total surface area of aggregate covered with cement paste [21]. The CEM method was successfully used to investigate the effect of binder-admixture interaction, packing density of the binder composition, robustness of the fresh properties, and rheological behavior of the suspending phase on the fresh and hardened properties of SCC [22]. Schwartzentruber and Catherine [21] employed the CEM approach to optimize the dosage of HRWR admixtures to achieve the targeted workability. Strong correlations were reported between the fresh properties of CEM and concrete mixtures. Assaad et al. [23] investigated the relationships between the fresh and hardened properties of concrete and their corresponding CEM mixtures. Erdem [24] reported satisfactory relationship between the rheological properties of SCC and their corresponding CEM. However, considering equal surface area can neglect the variation of packing density of the granular skeleton. On the other hand, Kabagire et al. [25] introduced the excess paste theory to improve the agreements between the fresh properties of SCC and their corresponding CEM mixtures. Indeed, in addition to the portion of cement paste required to fill the interparticle voids of aggregate, the excess paste volume (excess paste EP) covers the aggregate surface area. More recently, Lee et. al [26] employed the EP theory to propose a correlation between yield stress of concrete and its corresponding CEM. The authors successfully predicted the yield stress of concrete by establishing a relationship between the PCE dosage and the EP thickness in CEM. Therefore, EP thickness seems to be a key factor which is dependent on packing density of granular skeleton.

In this study, a new CEM approach considering a constant EP thickness was proposed to investigate the effect of different types of superplasticizers, mixture constituents, and soil characteristics on workability of SCEC and its variation with time. Moreover, the compressive strength and drying shrinkage of the investigated mixtures were evaluated at different ages. Five different dispersion agents, including two used in clay industry and three common HRWR admixtures for concrete industry, as well as two clay types were evaluated. Based on the obtained

results, a performance-based classification of SCEC was proposed to achieve adequate workability, mechanical, and shrinkage properties. Finally, the proposed CEM approach was validated using the workability, compressive strength, and shrinkage results of SCEC mixtures.

5.2 New CEM approach

In this study, the workability, dying shrinkage, and mechanical performance of various SCEC mixtures were evaluated using their corresponding CEM. As mentioned earlier, the conventional CEM method was established to simulate the workability and mechanical performance of its corresponding concrete by keeping the total surface area of aggregate constant [23,25]. However, the variation of packing density of the granular skeleton was neglected. This can therefore induce change in the thickness of EP, which can impact on the correlation between the workability of concrete and its corresponding CEM. A schematic of a unit volume of concrete consisting in compacted aggregate and excess paste volume is shown in Fig. 5.1. Lower aggregate content than its maximum packing ($\varphi < \varphi_{max}$) may require low paste volume, namely compacted paste volume (V_{CP}), to fill the existing interparticle voids between the compacted aggregate (V_{CA}) and achieve the highest packing density (φ_{max}). The remaining paste volume, which is referred to the EP volume ($V_{EP} = 1- \frac{\varphi}{\varphi_{max}}$), can contribute to reducing the internal frictions between the aggregate, thus enhancing the flowability of the mixture. The excess paste volume is a function of the volumetric content-to-maximum packing density of aggregate ratio, namely the relative solid packing fraction ($\frac{\varphi}{\varphi_{max}}$) [27].

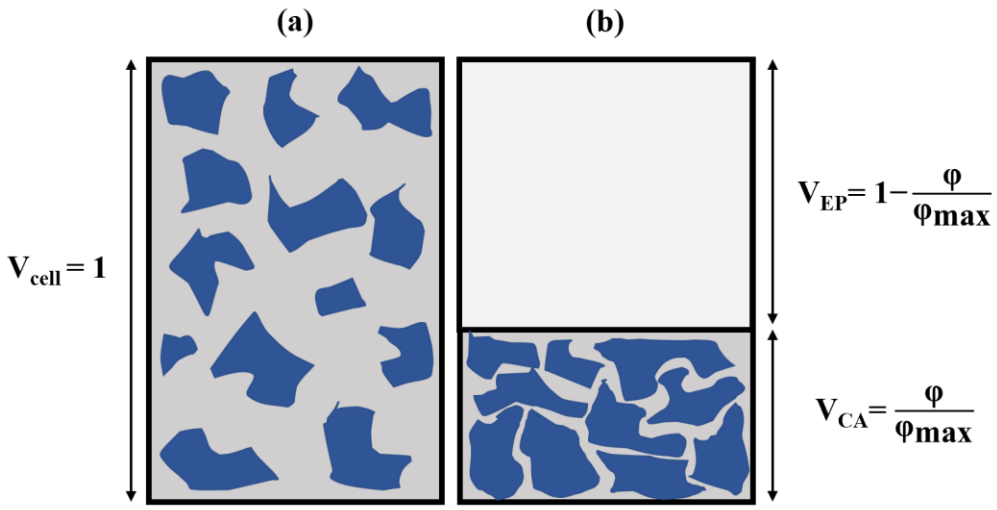

Fig. 5.1. (a) Schematic of a unit volume of concrete (V_{cell} = 1) as a suspension of aggregate in paste and (b) excess paste volume (V_{EP}) and compacted aggregate (V_{CA}).

The average EP thickness (e_{EP}) can then be estimated by the ratio of the VEP-to-the total surface area of aggregate ($e_{EP} = V_{EP} / A_{Aggregate}$). In order to achieve comparable workability of concrete and its corresponding CEM, the coarse aggregate was replaced by sand while targeting an equal e_{EP}, as follows:

$$e_{EP} = \frac{1 - \frac{\varphi_{sand+gravel}}{\varphi_{max:sand+gravel}}}{A_{sand+gravel}} = \frac{1 - \frac{\varphi_{eq:sand}}{\varphi_{max:sand}}}{A_{eq:sand}} \quad (5.1)$$

where $\varphi_{sand+gravel}$, $\varphi_{eq:sand}$, $\varphi_{max:sand+gravel}$, $\varphi_{max:sand}$, $A_{sand+gravel}$, and $A_{eq:sand}$ are the volumetric contents, packing density, and surface area of sand and gravel in SCEC mixture, as well as sand in corresponding CEM mixtures, respectively. It is worthy to mention that in order to obtain 3D surface area-to-volume ratio (A_{3D}/V) of the aggregate particles coarser and finer than 1.25 mm, the Max3D laser scanner (Fig. 5.2a) and X-ray micro-CT scanner (Fig. 5.2b) were employed, respectively [16,28,29]. Different subclasses of particles of the sand and coarse aggregate, corresponding to different standard sieves, were scanned. The A_{3D}/V values of the investigated sand and coarse aggregate were then calculated using the volumetric-weighted arithmetic mean of A_{3D}/V values of their corresponding subclasses, given their particle-size distributions (PSD) (Table 5.1).

Fig. 5.2. (a) MAXscan 3D laser scanner and (b) X-ray micro-CT scanner.

5.3 Experimental program

5.3.1 Materials and test procedures

A natural river sand (0-5 mm) and crushed limestone coarse aggregate (5-10 mm) were used. The PSD, A_{3D}/V, density, and water absorption of the aggregate are summarized in Table 5.1.

Table 5.1. Cumulative passing, 3D-surface area-to-volume ratio, density, and water absorption of sand and coarse aggregate.

Sieve size range (mm)	Sand, Nominal: 0-5 mm (%)	Coarse Aggregate, Nominal: 5-10 mm (%)
20-28	-	-
14-20	-	-
10-14	-	18.3
5-10	4.45	71.2
2.5-5	10.41	5.4
1.25-2.5	14.32	5.1
0.630-1.25	19.03	-
0.315-0.630	27.45	-
0.160-0.315	18.44	-
0.080-0.160	5.78	-
0-0.080	0.12	-
A_{3D}/V (m^2/m^3)	21583.4	859.8
Density (kg/m^3)	2670	2720
Water absorption (%)	1.09	0.42

In this study, five different volumetric sand-to-total aggregate ratios (S/A) of 0.5, 0.6, 0.7, 0.8, and 0.9 were selected to evaluate the effect of packing density on concrete performance. The packing densities of the investigated sand ($\varphi_{max:sand}$) and granular ($\varphi_{max:sand+gravel}$) skeletons were then determined using the intensive compaction tester (ICT) device [30], [31]. It consists in applying

50 gyratory cycles at an angle of 40 mrad and a normal pressure of 20 kPa. These testing parameters were recommended to prevent crushing of aggregate [16] (Table 5.2).

Table 5.2. Packing density of the investigated sand ($\varphi_{max:sand}$) and gravel skeletons ($\varphi_{max:sand+gravel}$).

S/A	0.5	0.6	0.7	0.8	0.9	1 ($\varphi_{max:\ sand}$)
$\varphi_{max:\ sand\ +\ gravel}$	0.788	0.797	0.786	0.770	0.753	0.739

The binder of the investigated SCEC mixtures were proportioned using a quartz-silt powder of 2–75 μm size and specific gravity of 2.69, a GU Portland cement with specific gravity of 3.15, and two types of clay, including 100% kaolinite (Clay Type I) and 50% kaolinite and 50% attapulgite (Clay Type II). The investigated kaolinite and attapulgite have specific surface areas of 15 and 155 m^2/g and specific gravities of 2.73 and 2.75, respectively. Moreover, two inorganic deflocculants were used, including sodium hexametaphosphate (NaHMP) and sodium silicate (NaSil) solution. The NaHMP (96% pure) powders were dispersed in water with a solid concentration of 37.1%, by mass. On the other hand, the NaSil is composed of 10.6% Na_2O, 26.5% SiO_2, % by mass, and water. Three common HRWR admixtures, including polycarboxylate-ether (PCE), sodium polynaphtalene (PNS), and non-esterified polycarboxylate (NE-PC) types, were evaluated with solid contents of 40%, 39.25%, and 36.44%, by mass, respectively.

A L50 orthogonal Taguchi array was used to investigate the influence of seven mixture parameters, including one 2-levels and six 5-levels factors. As can be observed in Table 5.3, the types of clay (types I and II) are modelled to assess the efficiency of mineralogy and constituent of fine particles existing in the earth. According to available literature on cement-stabilized earth concrete, five different levels of 60, 90, 120, 150, and 180 kg/m^3 were selected for cement content [10,32]. In addition, 5 different levels of paste volume (V_P) corresponding to 45%, 48%, 51%, 54%, and 57% were investigated. It is worthy to mention that V_P corresponds to total volume of air, water, and powders, including clay, silt, and cement. The water-to-powder (W/P) ratios was evaluated at five levels of 0.30, 0.35, 0.40, 0.45, and 0.50. Furthermore, the volumetric cement-to-clay ratio (Ce/Cl) was evaluated at five levels of 0.50, 0.75, 1.00, 1.25, and 1.50 to assess different binder packing. Furthermore, as mentioned earlier, five different S/A ratios of 0.5, 0.6, 0.7, 0.8, and 0.9 and five different admixture types, including NaHMP, NaSil, PCE, PNS, and NE-PC, were investigated as well.

Table 5.3. Modelled factors and their corresponding levels.

Levels	Factors						
	Clay type	Cement content (kg/m^3)	V_P (%)	W/P	Ce/Cl	S/A	Admixture type
1	Type I	60	45	0.30	0.50	0.5	NaHMP
2	Type II	90	48	0.35	0.75	0.6	NaSil
3	-	120	51	0.40	1.00	0.7	PCE
4	-	150	54	0.45	1.25	0.8	PNS
5	-	180	57	0.50	1.50	0.9	NE-PC

Initially, the paste mixtures, namely self-consolidating earth pastes (SCEP), were prepared in batches of 1.5 L using a planetary Hobart mixer according to the ASTM C305 specifications [33] for paste. The admixture dosages were optimized to achieve a targeted mini-slump flow (MSF) [34] of 280 ± 20 mm. This value was selected to ensure highly flowable and stable (i.e., no bleeding) SCEP mixtures. The admixture demands and MSF values were used as comparative measurements. Furthermore, nine cubic specimens (50 × 50 × 50 mm3) were sampled and used to determine the compressive strength at 1 day of age in accordance with ASTM C109 specifications [35].

On the other hand, the CEM mixtures were made in batches of 6 L according to the ASTM C305 specifications [33] for mortar. The MSF [34] and mini V-Funnel (MVF) [36] tests were carried out at 0, 30, and 60 min immediately after mixing to evaluate the flowability and workability loss of the investigated mortar mixtures. In the case of MVF, the funnel was filled, and the bottom outlet was then opened to allow the mortar to flow out. The required time to empty the cone was recorded as the MVF time. In the case of mortar mixtures, the compressive strength was evaluated at different ages of 1, 7, and 28 days of age according to the ASTM C109 specifications [35]. Drying shrinkage of the CEM mixtures was measured according to the ASTM C596 specifications [37]. Moreover, the Atterberg limits [38], including the liquid (LL) and plastic limits (PL), of clay, silt, and sand (< 425 μm) in each soil were determined. It is important to mention that the LL is defined as the moisture content above which the soil behaves as a liquid, and PL is the moisture content beyond which the soil behaves plastic. The plasticity index (PI) was also calculated as the difference between LL and PL values (PI = LL - PL).

All the SCEC mixtures were prepared in batches of 60 L using a rotating drum mixer. The mixing sequence consisted in homogenizing the aggregate (sand + coarse aggregate) for 90 s, then 1/3 of the mixing water was introduced and mixed for 60 s. The powder (silt, clay, and cement) was then added and mixed for 30 s. The second 1/3 of the mixing water and HRWR or dispersant admixture

were added and mixed for an additional 60 s. The remaining 1/3 of water was then added and the mixing was resumed for another 90 s. After 120 s of rest, the mixing was presumed for an additional 180 s. Immediately after mixing, the slump flow (SF) [36] and V-Funnel [39] tests were carried out to evaluate the flowability of the investigated SCEC mixtures. Moreover, the compressive strength of the investigated concrete mixtures was determined at 1, 7, and 28 days of age using cylindrical specimens of 100-mm diameter and 200-mm height conforming to the ASTM C39 standard [40]. Drying shrinkage of the investigated SCEC and their corresponding CEM mixtures were also evaluated at 7, 14, 21, 28, and 90 days of age according to the ASTM C157 specifications [41].

5.3.2 Paste, CEM, and concrete mixture proportions

The mixtures necessary to carry out the L50 orthogonal array are summarized in Table 5.4. The admixture demand to achieve the targeted MSF and $f'_{c\text{-}1d}$ of the 50 investigated SCEP mixtures are also summarized in Table 5.5 [11]. A minimum $f'_{c\text{-}1d}$ of 1 MPa was selected to ensure the feasibility of demolding after 24 hours of casting [7]. As can be observed in Fig. 5.3, the 50 paste mixtures were evaluated based on their MSF and 1-day compressive strength to ensure good compatibility between admixture and ternary binder system and adequate strength for formwork removal. The paste mixtures satisfying these criteria were then selected for further workability, compressive strength, and drying shrinkage investigation on their CEM scale. CEM mixtures with optimum admixture dosage, 1-day compressive strength, and 28-day drying shrinkage were selected for investigation in concrete scale. Finally, key parameters were selected to predict CEM and concrete performance based on paste and CEM mixtures, respectively.

The mixtures with $f'_{c\text{-}1d}$ greater than 1 MPa were chosen to carry out the mortar tests. Although P14, P20, P21, P35, P36, P47, and P48 mixtures satisfied the required compressive strength values, but they were not chosen due to their significantly high admixture demand. In total, eighteen CEM mixtures were therefore selected for further investigation. The mixture proportioning of the investigated CEM mixtures and their corresponding excess paste thicknesses (e_{EP}) are summarized in Table 5.6.

According to the 1-day compressive strength results of the investigated CEMs presented in Table 5.6, three concrete C16, C22 and C37 mixtures proportioned with PCE type were selected (

Table **5.7**). The selection criteria were based on their corresponding CEM mixtures achieving the targeted MSF of 280 ± 20 mm and the $f'_{c\text{-}1d}$ values higher than 1 MPa. Moreover, a cement-based reference mixture C_{ref} (i.e. without any clay) and its corresponding CEM (M_{ref}) and paste (P_{ref}) mixtures were proportioned with PCE, W/P of 0.40, VP of 0.45, and S/A of 0.5, as presented in Table **5.7**.

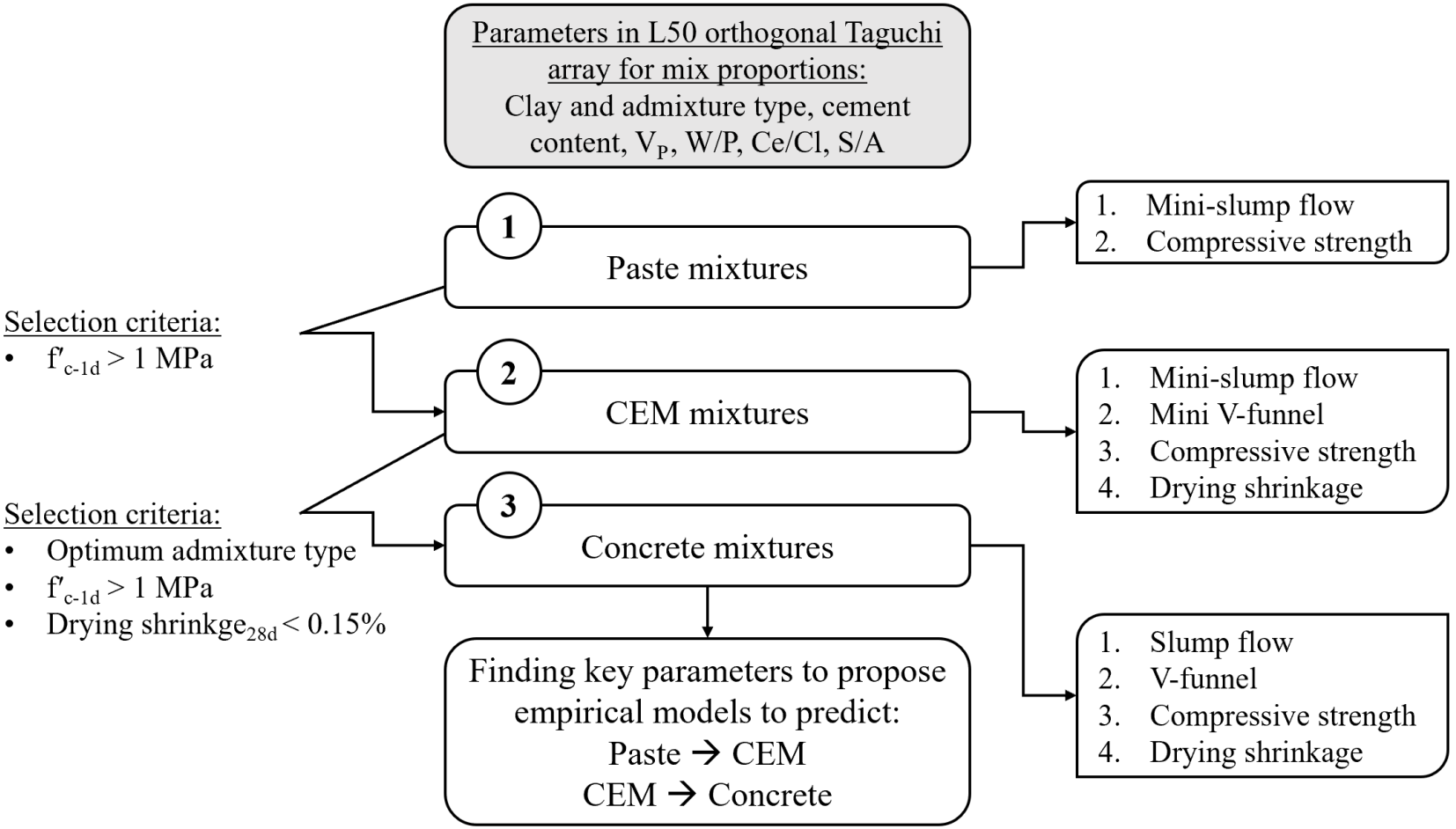

Fig. 5.3. Schematic sequence of the study carried out on paste, CEM, and concrete mixtures.

Table 5.4. Mixture proportions of the L50 Orthogonal array considering the seven investigated factors [11].

Experiment No.	Investigated factors							Experiment No.	Investigated factors						
	Clay type	Cement content (kg/m^3)	V_P (%)	W/P	Ce/Cl	S/A	Admixture		Clay type	Cement content (kg/m^3)	V_P (%)	W/P	Ce/Cl	S/A	Admixture
1			45	0.3	0.5	0.5	NaHMP	26		60	45	0.3	1.25	0.9	PNS
2			48	0.35	0.75	0.6	NaSil	27			48	0.35	1.5	0.5	NE-PC
3		60	51	0.4	1	0.7	PCE	28			51	0.4	0.5	0.6	NaHMP
4			54	0.45	1.25	0.8	PNS	29			54	0.45	0.75	0.7	NaSil
5			57	0.5	1.5	0.9	NE-PC	30			57	0.5	1	0.8	PCE
6			45	0.35	1	0.8	NE-PC	31		90	45	0.35	0.5	0.7	PCE
7			48	0.4	1.25	0.9	NaHMP	32			48	0.4	0.75	0.8	PNS
8		90	51	0.45	1.5	0.5	NaSil	33			51	0.45	1	0.9	NE-PC
9			54	0.5	0.5	0.6	PCE	34			54	0.5	1.25	0.5	NaHMP
10			57	0.3	0.75	0.7	PNS	35			57	0.3	1.5	0.6	NaSil
11			45	0.4	1.5	0.6	PNS	36		120	45	0.4	1	0.5	NaSil
12			48	0.45	0.5	0.7	NE-PC	37			48	0.45	1.25	0.6	PCE
13	I	120	51	0.5	0.75	0.8	NaHMP	38	II		51	0.5	1.5	0.7	PNS
14			54	0.3	1	0.9	NaSil	39			54	0.3	0.5	0.8	NE-PC
15			57	0.35	1.25	0.5	PCE	40			57	0.35	0.75	0.9	NaHMP
16			45	0.45	0.75	0.9	PCE	41		150	45	0.45	1.5	0.8	NaHMP
17			48	0.5	1	0.5	PNS	42			48	0.5	0.5	0.9	NaSil
18		150	51	0.3	1.25	0.6	NE-PC	43			51	0.3	0.75	0.5	PCE
19			54	0.35	1.5	0.7	NaHMP	44			54	0.35	1	0.6	PNS
20			57	0.4	0.5	0.8	NaSil	45			57	0.4	1.25	0.7	NE-PC
21			45	0.5	1.25	0.7	NaSil	46		180	45	0.5	0.75	0.6	NE-PC
22			48	0.3	1.5	0.8	PCE	47			48	0.3	1	0.7	NaHMP
23		180	51	0.35	0.5	0.9	PNS	48			51	0.35	1.25	0.8	NaSil
24			54	0.4	0.75	0.5	NE-PC	49			54	0.4	1.5	0.9	PCE
25			57	0.45	1	0.6	NaHMP	50			57	0.45	0.5	0.5	PNS

Table 5.5. Proportioning, admixture demand, and $f'_{c\text{-}1d}$ of the investigated SCEP mixtures [11].

Mix No.	Cement (kg/m^3)	Water (kg/m^3)	Clay type I (kg/m^3)	Silt (kg/m^3)	W/P	Admixture demand (% binder)	$f'_{c\text{-}1d}$ (MPa)	Mix No.	Cement (kg/m^3)	Water (kg/m^3)	Clay type II (kg/m^3)	Silt (kg/m^3)	W/P	Admixture demand (% binder)	$f'_{c\text{-}1d}$ (MPa)
P1	133.3	450.4	231.1	1136.9	0.30	0.510	0.75 (0.01)	P26	133.3	450.1	92.4	1274.4	0.30	0.400	1.04 (0.02)
P2	125.0	488.6	144.4	1126.6	0.35	2.700	0.67 (0.01)	P27	125.0	488.4	72.2	1198.3	0.35	0.240	0.50 (0.03)
P3	117.6	521.9	102.0	1085.1	0.40	0.065	0.32 (0.01)	P28	117.6	522.2	203.9	983.9	0.40	2.100	0.42 (0.04)
P4	111.1	551.1	77.0	1036.6	0.45	0.050	0.37 (0.01)	P29	111.1	551.3	128.4	985.6	0.45	6.500	0.46 (0.02)
P5	105.3	577.0	60.8	988.0	0.50	0.000	0.31 (0.02)	P30	105.3	577.1	91.2	957.8	0.50	0.090	0.29 (0.04)
P6	200.0	490.7	173.3	1028.5	0.35	0.071	1.17 (0.01)	P31	200.0	491.1	346.7	856.5	0.35	1.400	0.59 (0.02)
P7	187.5	523.9	130.0	992.4	0.40	0.350	0.41 (0.02)	P32	187.5	524.2	216.7	906.3	0.40	0.750	1.09 (0.04)
P8	176.5	553.2	102.0	950.8	0.45	0.600	0.48 (0.01)	P33	176.5	553.3	152.9	900.2	0.45	0.280	0.53 (0.03)
P9	166.7	579.7	288.9	703.7	0.50	0.110	0.51 (0.01)	P34	166.7	579.1	115.6	876.0	0.50	0.700	0.54 (0.07)
P10	157.9	450.9	182.5	1162.5	0.30	0.170	1.56 (0.04)	P35	157.9	450.6	91.2	1253.0	0.30	7.500	1.07 (0.04)
P11	266.7	526.2	154.1	894.9	0.40	0.120	3.11 (0.04)	P36	266.7	526.5	231.1	818.4	0.40	12.000	1.30 (0.04)
P12	250.0	556.3	433.3	553.0	0.45	0.081	1.46 (0.02)	P37	250.0	555.6	173.3	811.3	0.45	0.390	1.86 (0.09)
P13	235.3	581.7	271.9	656.3	0.50	0.490	0.40 (0.01)	P38	235.3	581.3	135.9	791.4	0.50	0.100	0.54 (0.04)
P14	222.2	452.5	192.6	1093.4	0.30	4.000	2.11 (0.01)	P39	222.2	452.9	385.2	902.3	0.30	NA*	-
P15	210.5	490.9	146.0	1046.0	0.35	0.075	2.60 (0.12)	P40	210.5	491.1	243.3	949.4	0.35	2.600	0.63 (0.04)
P16	333.3	558.7	385.2	523.0	0.45	0.175	2.94 (0.24)	P41	333.3	558.1	192.6	714.3	0.45	1.800	0.36 (0.03)
P17	312.5	584.1	270.8	584.9	0.50	0.100	1.91 (0.01)	P42	312.5	585.0	541.7	315.8	0.50	NA*	-
P18	294.1	454.2	203.9	1016.0	0.30	0.068	5.69 (0.09)	P43	294.1	454.6	339.9	881.2	0.30	2.400	0.85 (0.06)
P19	277.8	492.7	160.5	969.4	0.35	0.520	0.80 (0.04)	P44	277.8	492.9	240.7	889.7	0.35	1.050	2.19 (0.05)
P20	263.2	527.0	456.1	598.2	0.40	4.800	1.75 (0.03)	P45	263.2	526.2	182.5	869.9	0.40	0.420	1.33 (0.04)
P21	400.0	586.9	277.3	496.4	0.50	3.600	1.71 (0.07)	P46	400.0	587.5	462.2	312.7	0.50	6.400	0.34 (0.02)
P22	375.0	456.2	216.7	929.1	0.30	0.130	6.92 (0.21)	P47	375.0	456.5	325.0	821.6	0.30	4.900	3.13 (0.06)
P23	352.9	495.8	611.8	452.0	0.35	0.430	5.20 (0.09)	P48	352.9	494.9	244.7	816.3	0.35	15.000	2.14 (0.09)
P24	333.3	528.8	385.2	603.4	0.40	0.079	2.86 (0.04)	P49	333.3	528.2	192.6	794.6	0.40	0.380	2.04 (0.04)
P25	315.8	557.8	273.7	650.1	0.45	0.550	3.24 (0.02)	P50	315.8	558.6	547.4	378.3	0.45	8.300	0.43 (0.04)

* NA: Targeted MSF value not achieved; (): standard deviation

Table 5.6. Proportioning and e_{EP} of the investigated CEM mixtures.

Mix No.	Cement (kg/m^3)	Water (kg/m^3)	Clay type I (kg/m^3)	Clay type II (kg/m^3)	Silt (kg/m^3)	W/P	Sand (kg/m^3)	e_{EP} (μm)	$f'_{c\text{-}1d}$ (MPa)
M6	100.0	245.3	86.7	-	514.2	0.35	1197.2	40.2	-
M10	101.6	290.1	117.4	-	748.0	0.30	815.6	88.4	1.3 (0.04)
M11	149.3	294.6	86.2	-	500.9	0.40	1038.0	56.0	2.3 (0.08)
M12	139.6	310.7	242.0	-	308.8	0.45	1041.6	55.6	1.3 (0.04)
M15	147.0	342.8	101.9	-	730.4	0.35	669.6	121.4	1.7 (0.05)
M16	157.7	264.3	182.2	-	247.4	0.45	1268.7	34.4	2.8 (0.10)
M17	192.8	360.4	167.1	-	360.9	0.50	885.6	76.5	1.6 (0.04)
M18	181.5	280.4	125.9	-	627.2	0.30	885.1	76.5	4.6 (0.10)
M22	198.7	241.7	114.8	-	492.2	0.30	1117.7	47.6	5.6 (0.12)
M23	188.1	264.3	326.1	-	240.9	0.35	1109.1	48.4	3.6 (0.08)
M24	224.1	355.5	259.0	-	405.7	0.40	738.4	104.2	2.3 (0.14)
M25	212.0	374.5	183.7	-	436.4	0.45	741.4	103.5	0.5 (0.02)
M26	63.1	212.9	-	43.7	602.9	0.30	1268.7	34.4	-
M32	99.3	277.7	-	114.8	480.2	0.40	1117.7	47.6	-
M37	147.2	327.2	-	102.1	477.8	0.45	960.3	65.6	1.5 (0.02)
M44	179.1	317.8	-	155.2	573.6	0.35	812.1	89.1	-
M45	169.3	338.6	-	117.4	559.7	0.40	815.6	88.4	0.5 (0.02)
M49	187.6	297.3	-	108.4	447.2	0.40	1030.1	56.9	2.5 (0.04)

(): standard deviation

Table 5.7. Mixture proportions of the investigated SCEC mixtures, as well as reference CEM and paste ones.

Mix No.	Cement (kg/m^3)	Water (kg/m^3)	Clay type I (kg/m^3)	Clay type II (kg/m^3)	Silt (kg/m^3)	W/P	Sand (kg/m^3)	Gravel (kg/m^3)	e_{EP} (μm)
C16	150.0	251.4	173.3	-	235.3	0.45	1197.0	136.0	34.4
C22	180.0	219.0	104.0	-	445.9	0.30	1000.2	255.7	47.6
C37	120.0	266.7	-	83.2	389.4	0.45	750.1	511.4	65.6
C_{ref}	627.2	250.9	-	-	0	0.40	665.0	680.0	65.1
M_{ref}	818.7	327.5	-	-	0	0.40	964.5	0	65.1
P_{ref}	1393.8	557.5	-	-	0	0.40	0	0	-

5.4 Result and discussion

5.4.1 CEM mixtures

The properties of the 18 investigated CEM mixtures, including admixture demands to achieve the targeted MSF of 280 ± 20 mm, MSF, and MVF values, the compressive strength (f'_c), the dry density (ρ) at 1, 7, and 28 days of age, the drying shrinkage, and the Atterberg limits of the earth used are summarized in Table 5.8. As can be observed, the LL, PL and PI values of the corresponding earth ranged from 15.7 to 36.5% and 1.2 to 13.3%, respectively. These wide ranges can guarantee a thorough investigation on different soil types. Despite of the high admixture dosages, the M6, M26, M32, and M44 CEM mixtures did not achieved the targeted MSF values. In the case of M6, this can be due to the very low contents of cement and clay, hence resulting in inadequate binding and instability even for lower MSF values than the targeted MSF. Moreover, in the case of M26, M32, and M44 mixtures made with PNS, the lack in fluidity can be attributed to the inefficiency of PNS to disperse the Clay Type II particles in the CEM mixtures. On the other hand, high NaHMP demands are reported in the case of the Clay Type II systems.

5.4.1.1 Mini-slump flow (MSF)

The evolution of MSF values with admixture dosage is presented in Fig. 5.4. As can be observed in Fig. 5.4a, the use of Clay Type II resulted in higher PCE demand compared to Clay Type I. Moreover, among the different Clay Type I systems, the mixture M16 (W/P of 0.45) required the highest PCE dosage compared to M15 and M22 (0.35 and 0.30). This is due to its higher clay content (182 vs. 102 and 115 kg/m^3). This reflects the significant negative effect of clay content on flowability of the mixtures compared to the positive influence of W/P ratio. Furthermore, the mixture M37 proportioned with higher W/P ratio and lower clay content required lower PCE dosage compared to M49 to achieve a given flowability level.

As can be observed in Fig. 5.4b, none of the CEM mixtures proportioned with Clay Type II and PNS type could reach the targeted MSF value. This is probably due to the low synergy of PNS with the attapulgite clay particles in the Clay Type II in CEM phase. On the other hand, among the CEM mixtures proportioned with 100% kaolinite Clay Type I, the mixture M23 containing the highest clay content (326 kg/m^3) and relatively low W/P of 0.35 exhibited the highest PNS demand. Moreover, the opposite effects of clay content and W/P ratio led to comparable PNS demands in the case of M10, M11, and M17 mixtures to achieve the targeted MSF value.

In the case of the CEM mixtures incorporating NE-PC admixture (Fig. 5.4c), the M45 mixture proportioned with Clay Type II required significantly higher dosage compared to the other mixtures containing Clay Type I. Similar to PCE and PNS, the combined effect of clay content and W/P ratio governed the NE-PC demand of the CEM mixtures made with Clay Type I. Finally, the highest admixture demand was observed for the mixture M25 containing NaHMP, as shown in Fig. 5.4d. This can be attributed to the low efficiency of NaHMP with the ternary powder system of SCEC (i.e., clay, cement, and silt) since it only disperses clay particles.

Table 5.8. Properties of the investigated CEM mixtures.

Mix No.	Admixture demand (% binder)	MSF (mm)			MVF (s)			ρ (kg/m^3)			f'_c (MPa)			Drying shrinkage (%)					Atterberg limits (%)		
		0 min	30 min	60 min	0 min	30 min	60 min	1d	7d	28d	1d	7d	28d	7d	14d	21d	28d	90d	LL	PL	PI
M6	NA*	-	-	-	-	-	-	-	-	-	-	-	-	-	-	-	-	-	15.7	14.5	1.2
M10	0.28	265	222	155	7.1	11.5	18.2	2263	2244	2266	1.3	2.5	3.2	0.08	0.08	0.08	0.09	0.09	18.6	16.9	1.7
M11	0.29	269	236	193	3.2	3.9	4.4	2281	2330	2300	2.3	4.4	5.4	0.05	0.06	0.06	0.06	0.07	18.1	16.6	1.5
M12	0.27	266	259	238	1.5	1.9	2.4	2254	2248	2346	1.3	3.3	4.4	0.20	0.21	0.21	0.22	0.22	20.1	14.6	5.5
M15	0.10	279	243	211	2.4	3.1	3.7	2186	2237	2230	1.7	3.3	4.2	0.08	0.08	0.08	0.08	0.09	17.5	16.2	1.3
M16	0.28	272	236	189	3.0	3.6	4.1	2314	2321	2341	2.8	5.8	7.3	0.07	0.08	0.09	0.09	0.09	18.9	14.9	4.0
M17	0.25	263	223	156	1.0	1.7	2.1	2148	2178	2175	1.6	3.6	4.5	0.11	0.12	0.12	0.13	0.14	19.5	15.7	3.8
M18	0.20	265	261	248	9.9	11.0	13.5	2233	2353	2307	4.6	8.6	10.4	0.07	0.07	0.07	0.08	0.08	19.9	16.3	3.6
M22	0.21	282	264	249	7.5	7.9	8.3	2354	2354	2359	5.6	13.8	16.9	0.02	0.03	0.06	0.07	0.09	18.9	15.8	3.1
M23	0.65	264	232	171	3.3	4.3	10.9	2282	2324	2389	3.6	7.1	9.0	0.17	0.21	0.21	0.21	0.22	21.5	14.8	6.7
M24	0.18	281	267	246	3.1	4.0	5.2	2279	2277	2238	2.3	7.0	8.7	0.09	0.10	0.10	0.10	0.11	21.6	14.5	7.1
M25	1.89	263	100	100	2.0	blocked	blocked	2193	2193	2189	0.5	4.6	4.6	0.64	0.65	0.66	0.67	0.68	20.5	15.6	4.9
M26	NA*	-	-	-	-	-	-	-	-	-	-	-	-	-	-	-	-	-	21.5	18.3	3.2
M32	NA*	-	-	-	-	-	-	-	-	-	-	-	-	-	-	-	-	-	30.8	23.6	7.2
M37	0.55	286	209	171	2.5	3.6	4.2	2187	2232	2263	1.5	3.4	4.7	0.14	0.15	0.15	0.15	0.15	32.8	21.8	11.0
M44	NA*	-	-	-	-	-	-	-	-	-	-	-	-	-	-	-	-	-	36.5	23.2	13.3
M45	1.15	264	250	247	2.7	3.7	4.3	2219	2233	2247	0.5	5.1	6.1	1.11	1.12	1.13	1.13	1.13	34.6	22.8	11.8
M49	0.79	270	201	184	2.2	5.6	8.4	2186	2195	2193	2.5	6.2	7.8	0.11	0.12	0.12	0.12	0.13	31.5	20.5	11.0

*NA: Targeted MSF value not achieved

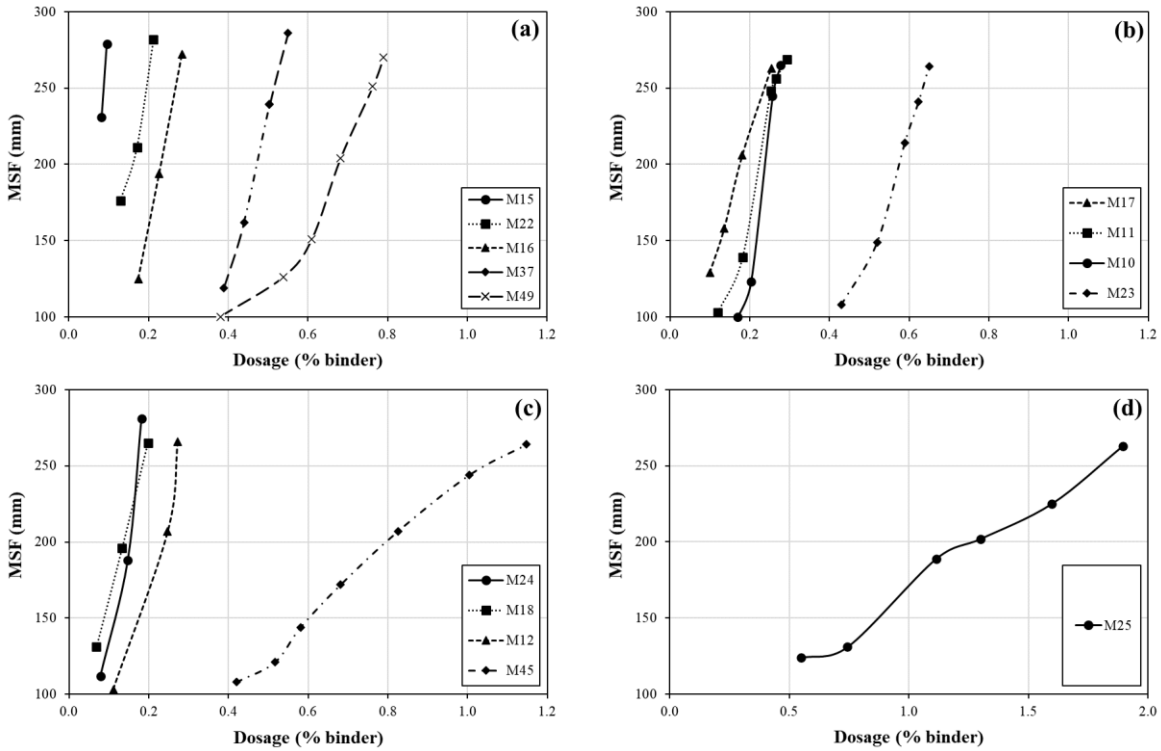

Fig. 5.4. Mini-slump flow of CEM mixtures containing (a) PCE, (b) PNS, (c) NE-PC, and (d) NaHMP admixtures.

The results presented in Fig. 5.4 confirmed the significant coupled effect of binder constituents and W/P ratio on admixture demand. The effect of binder constituents can be reflected using the SSA of powders and PI of soils. As shown in Fig. 5.5a and 5.5b, the PCE, PNS, and NE-PC admixture demands to achieve the targeted MSF of 280 ± 20 mm are well correlated to PI/(W/P) and SSA/(W/P) ratios of the investigated CEM mixtures (leading to R^2 values close to unity (> 0.944)).

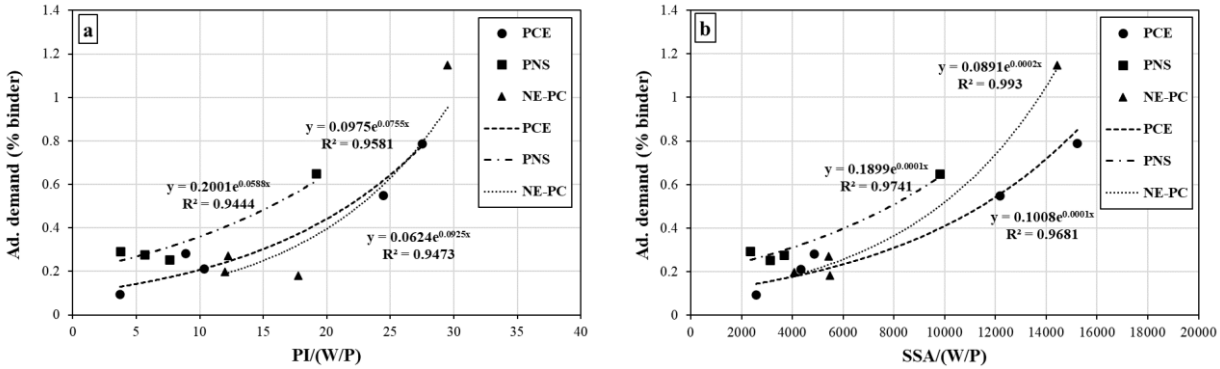

Fig. 5.5. Relationship between the admixture demands and (a) PI/(W/P) and (b) SSA/(W/P) of the investigated CEM mixtures.

Moreover, a Microsoft Excel solver was developed to evaluate the coupled effect of characteristics of different mixture constituents, including the Atterberg limits (LL and PI) of the soil, paste volume (V_P), W/P ratio, and excess paste thickness (e_{EP}) on PCE, PNS, and NE-PC admixture demands of the investigated CEM mixtures using the following equation:

$$\text{Ad. demand (\% binder)} = \alpha + \beta \times \frac{LL^{\gamma} \times PI^{\delta}}{V_P{}^{\varepsilon} \times \left(\frac{W}{P}\right)^{\zeta} \times e_{EP}{}^{\eta}} \quad (5.2)$$

where α, β, γ, δ, ε, ζ, and η are the adjustment factors and power indices determined for each admixture type, referring the contribution of LL, PI, V_P, W/P, and e_{EP} on admixture demand, respectively. The value of these parameters are summarized in Table 5.9. The established correlations are compared to the experimental PCE, PNS, and NE-PC admixture demands, as presented in Fig. 5.6a, 5.6b, and 5.6c, respectively. As can be observed, the admixture demands are well correlated to the characteristics of CEM mixtures constituents, leading to high R^2 of 1.0 and low root-mean squared-error (RMSE) of 0.001%. According to the obtained power indices (Table 5.9), the CEM mixtures proportioned with soils exhibiting lower LL and PI, as well as higher V_P, W/P, and e_{EP} required lower admixture dosage to achieve the targeted MSF value to fulfill the self-consolidation criterion. Moreover, the PCE, PNS, and NE-PC demands are mostly controlled by the e_{EP}, W/B ratio, and LL values, respectively, as reflected by the highest power indices. Furthermore, among the solid characteristics, LL showed more dominant effect on PNS and NE-PC demands rather than the PI values. However, the PCE demands of the CEM mixtures were found more influenced by the PI values rather than the LL of their corresponding soils.

Table 5.9. Adjustment factors of the established admixture demand correlations (Eq. 5.2).

Admixture	Adjustment factors (Eq. (2))						
	α	β	γ	δ	ε	ζ	η
PCE	0.093	0.986	0.905	1.689	0.208	1.640	2.027
PNS	0.196	1.133	1.449	0.518	0.435	2.252	1.805
NE-PC	0.094	1.559	2.938	1.607	1.725	2.455	2.241

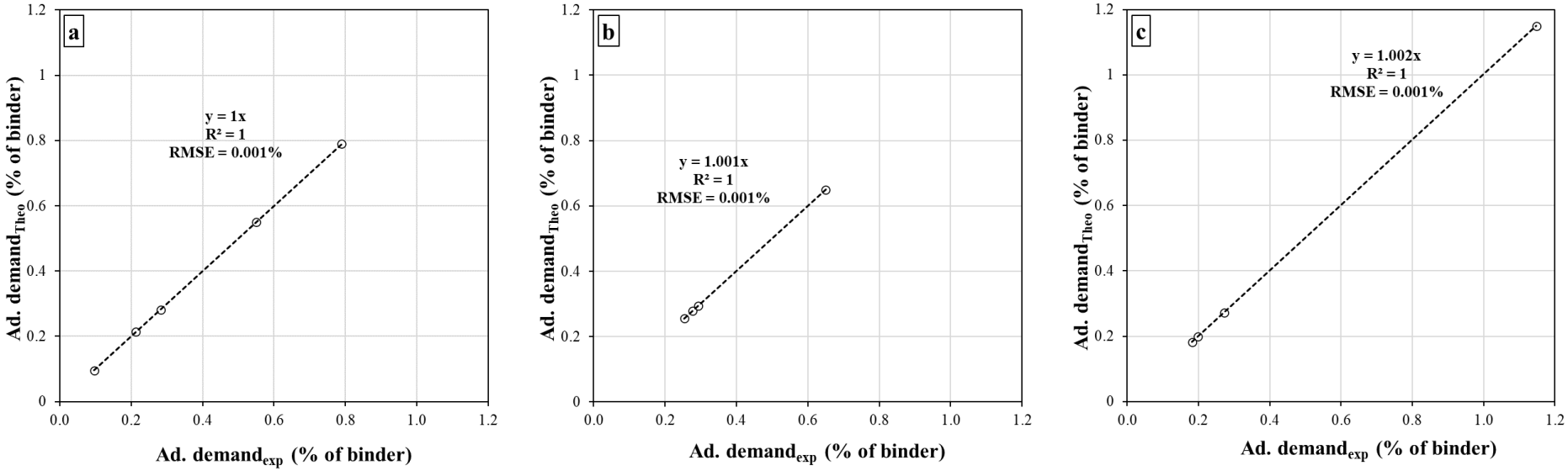

Fig. 5.6. Comparison between the experimental (a) PCE, (b) PNS, and (c) NE-PC admixture demands of the investigated CEM mixtures and those obtained using Eq. 5.2 and Table 5.9.

The MSF results of the investigated CEM mixtures obtained at 0, 30, and 60 min after mixing are presented in Fig. 5.7 for different admixtures. As can be observed, for the PCE-based mixtures (Fig. 5.7a), Clay Type II led to the highest MSF loss values over time. On the other hand, among the CEM mixtures proportioned with Clay Type I, the M16 mixture containing the highest clay content and W/P ratio, and the lowest V_P, exhibited the highest MSF loss compared to the mixtures M15 and M22. In the case of mixtures containing PNS type, the M11 mixture made with the lowest clay content and V_P exhibited the lowest MSF loss, as illustrated in Fig. 5.7b. The clay, W/P ratio, and V_P showed a coupled effect on MSF loss. Moreover, the CEM mixtures containing NE-PC exhibited the lowest MSF loss values compared to those made with other admixture types, as shown in Fig. 5.7c. This can demonstrate the efficiency of the NE-PC admixture in the presence of both clay types, hence leading to low MSF loss over time. However, the highest MSF loss was observed for the M25 mixture containing NaHMP admixture (Fig. 5.7d), leading to no flow after 30 min of age (i.e., MSF of 100 mm). Such behavior can be favorable for 3D-printing applications where quick structural-build up is required. According to the obtained results, the NaHMP and NE-PC admixtures confirmed the highest and lowest contributions of admixture types on MSF loss over time.

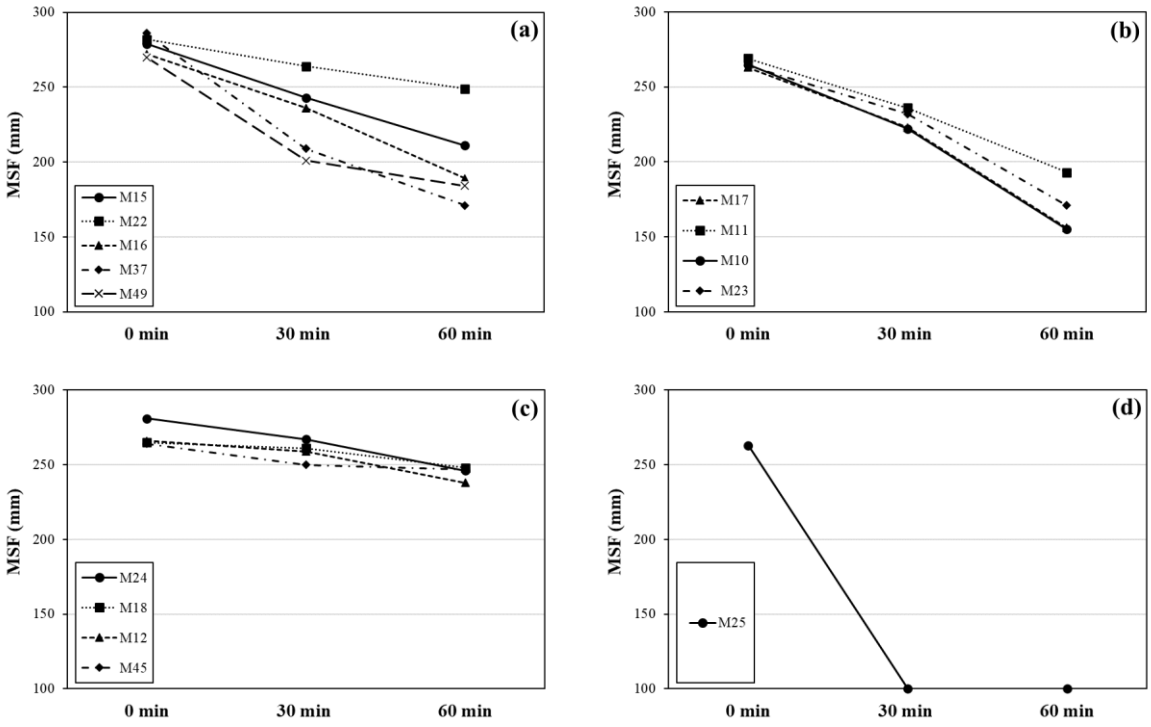

Fig. 5.7. MSF loss values (after 30 and 60 min) of the investigated CEM mixtures made with (a) PCE, (b) PNS, (c) NE-PC, and (d) NaHMP admixtures.

5.4.1.2 Mini V-funnel (MVF)

The MVF results of the investigated CEM mixtures measured at 0, 30, and 60 min after mixing are illustrated in Fig. 5.8. It is important to mention that according to the European guidelines for SCC [36] that recommend a MSF of 280 to 340 mm, Domone [42] proposed a MVF of 1 to 7.5 s to achieve SCC with satisfactory fresh properties. The MVF results of the CEM mixtures containing PCE are presented in Fig. 5.8a. As can be observed, the M22 mixture proportioned with the lowest W/P ratio of 0.30 showed the most viscous behavior reflected by the highest MVF values over time. However, the highest MVF-increasing rate was obtained for the mixture M49 containing Clay Type II. It is worthy to mention that the M37 mixture made with comparable contents of Clay Type II (102 and 108 kg/m3) showed lower MVF increasing rate due to its higher W/P ratio compared to the M49 mixture (0.45 vs. 0.40). This suggests the dominant contribution of W/P ratio on MVF of the PCE-based CEM mixtures compared to the clay content. Among the CEM mixtures containing PNS (Fig. 5.8b), the M17 mixture exhibited the lowest MVF values due to its highest W/P ratio (0.50). The mixtures M11, M23, and M10 proportioned with W/P ratios of 0.40, 0.35, and 0.30, respectively, exhibited higher MVF values. This highlights the significant effect of W/P ratio on viscosity of the PNS-based CEM mixtures, rather than the clay content and V_P.

Similarly, the MVF values of the CEM mixtures containing NE-PC are mainly controlled by W/P ratios, as shown in Fig. 5.8c. For example, the mixtures M24 (259 kg/m^3 of Clay Type I) and M45 (117 kg/m^3 of Clay Type II) proportioned with an equal W/P exhibited comparable MVF values due to their same W/P ratios. On the other hand, as shown in Fig. 5.8d, the incorporation of NaHMP led to a relatively low initial MVF value of 2 s for the mixture M25, immediately after mixing, but no flowability was observed after 30 min. This can be due to the synergy of NaHMP with the ternary binder system of SCEC mixtures. The accelerated structural build-up observed with the NaHMP admixture is favorable for 3D-printing applications.

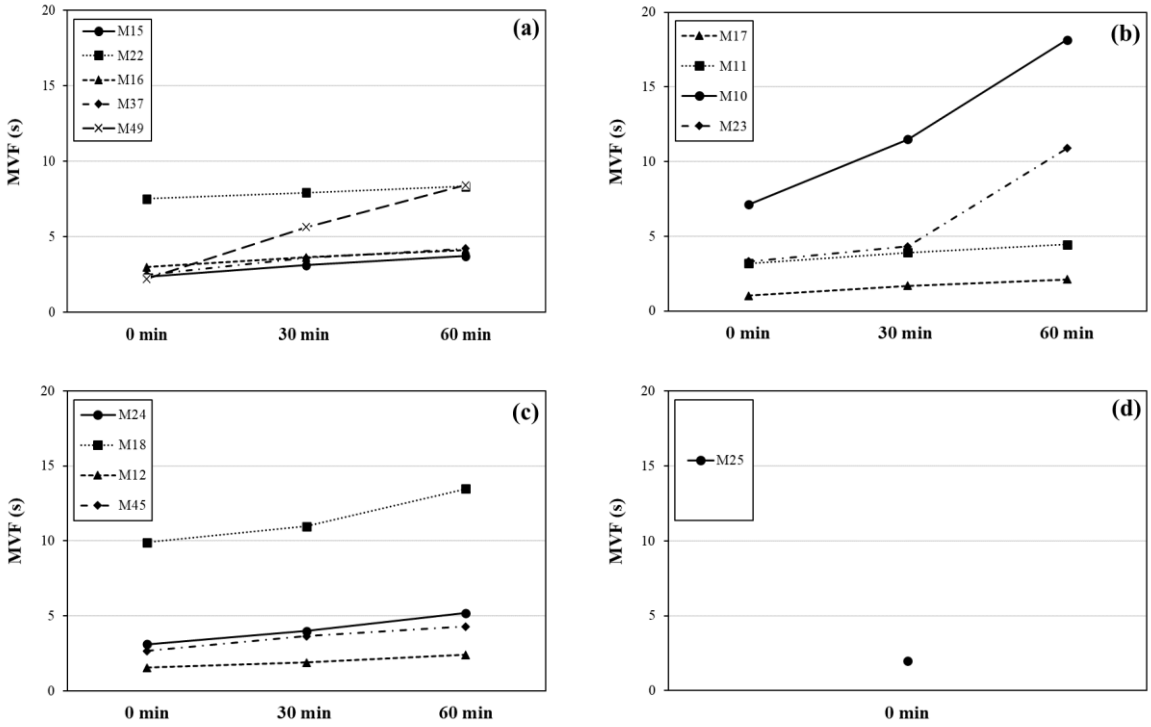

Fig. 5.8. MVF of the investigated CEM mixtures proportioned with (a) PCE, (b) PNS, (c) NE-PC, and (d) NaHMP admixtures over time (0, 30, and 60 min after mixing).

A Microsoft Excel solver was then developed to correlate the initial MVF values determined immediately after mixing to the characteristics of the mixture constituents, as follows:

$$\text{MVF (s)} = \alpha + \beta \times \frac{e_{EP}{}^{\varepsilon}}{V_P{}^{\gamma} \times \left(\frac{W}{P}\right)^{\delta}} \quad (5.3)$$

where α, β, γ, δ, and ε are the adjustment factors and power indices reflecting the contributions of V_P, W/P, and e_{EP} on MVF values, respectively. The established correlations are presented in Table 5.10 and Fig. 5.9. As can be observed in Fig. 5.9, the MVF values of the investigated CEM mixtures are in very good agreement with the characteristics of the mixture constituents, reflected by high R^2 of 1.0 and RMSE values lower than 0.264 s. According to the obtained power indices, increasing the paste content and W/P ratio led to lower MVF values, hence reflecting low viscosity. On the other hand, the W/P showed the most dominant effect on MVF values compared to the paste characteristics (i.e., V_P and e_{EP}). It signifies the high effect of solid fraction on viscosity, followed by paste volume.

Table 5.10. Adjustment factors of the established correlations of MVF (Eq. 5.3).

Admixture	Adjustment factors				
	α	β	γ	δ	ε
PCE	2.494	7.902	8.482	26.008	0.276
PNS	0	3291.47	3.750	4.744	0.739
NE-PC	0	1.204	1.409	4.333	0.560

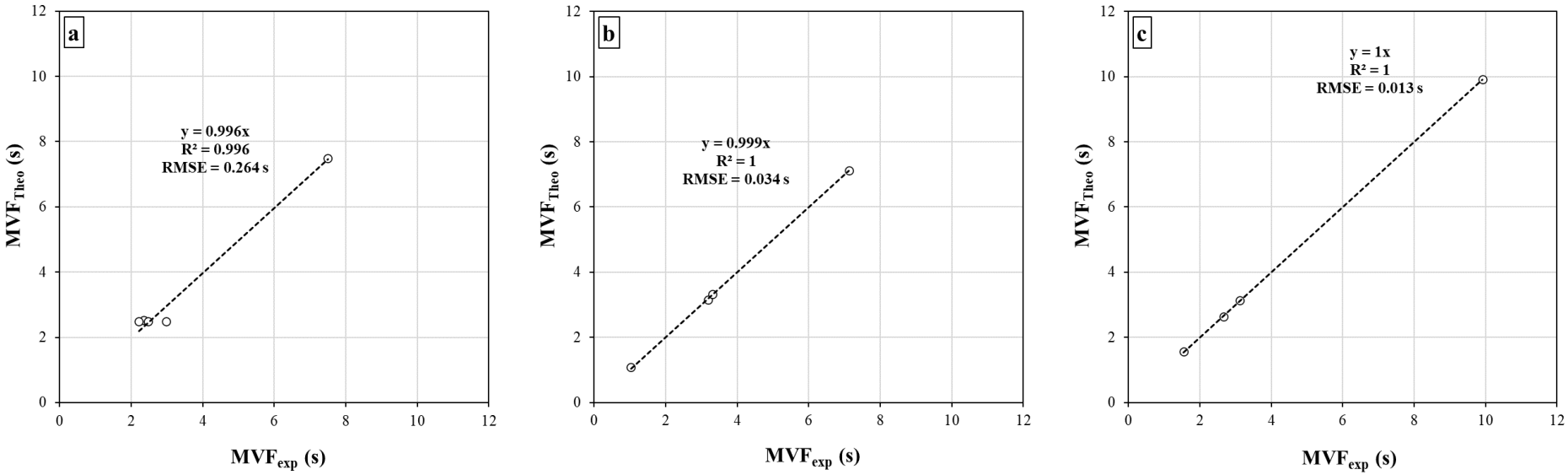

Fig. 5.9. Comparison between the experimental MVF values of the investigated CEM mixtures and those obtained using Eq. 5.3 and Table 5.10, including (a) PCE, (b) PNS, and (c) NE-PC admixtures.

5.4.1.3 Compressive strength

The evolution of the compressive strength of the investigated mixtures at 1, 7, and 28 days of age is presented in Fig. 5.10 for different types of admixtures. As can be observed in Fig. 5.10a, the mixture M22 showed the highest compressive strength, regardless of the age (~17 MPa in 28 days) compared to the mixtures containing PCE types. This is due to its highest cement content and lowest W/P ratio. The compressive strength of the CEM mixtures was mostly governed by the cement content, W/P ratios, and V_P. In the case of PNS systems (Fig. 5.10b), the highest compressive strength values were obtained for M23 made with the highest cement content, followed by M11, M17, and M10, respectively. It is important to mention that despite of its lower cement content, the M11 mixture exhibited higher compressive strength than the mixture M17, which is due to its lower W/P ratio (0.40 vs. 0.50).

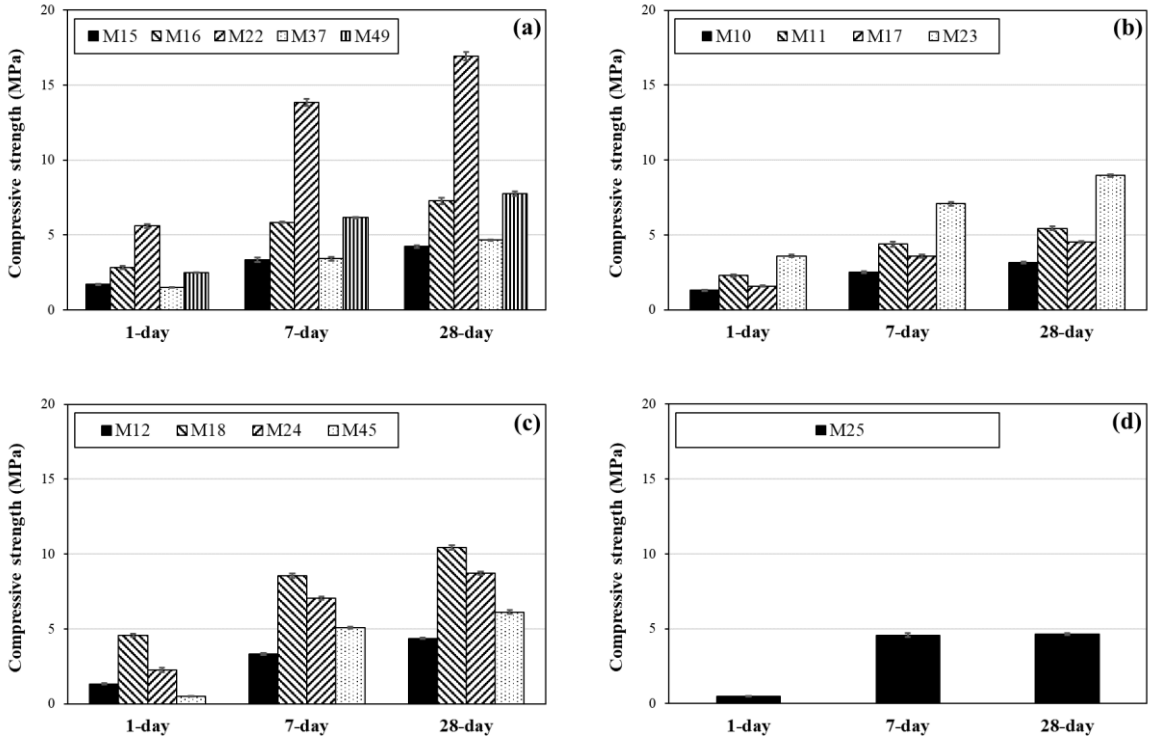

Fig. 5.10. Compressive strength of the investigated CEM mixtures made with (a) PCE, (b) PNS, (c) NE-PC, and (d) NaHMP admixtures.

Furthermore, as can be observed in Fig. 5.10c, the mixtures M18 and M24 exhibited the highest compressive strength, regardless of the age. On the other hand, the M25 mixture made with NaHMP developed very low 1-d compressive strength of 0.5 MPa. However, after 7 days of age, it developed 4.6 MPa, but no change was observed afterwards up to 28 days of age (Fig. 5.10d).

This highlights the negative effect of NaHMP-binder combination on compressive strength development of the CEM mixtures. As can be observed in Fig. 5.11, the compressive strengths are in good agreements with cement content and W/P ratios, reflecting their significant effects on mechanical properties of earth-based mortars. It is worth mentioning that the lower R^2 obtained for the $f'_{c\text{-}1d}$ can reflect its dependency to other factors, such as binder constituents which can hinder the formation of C-S-H gels.

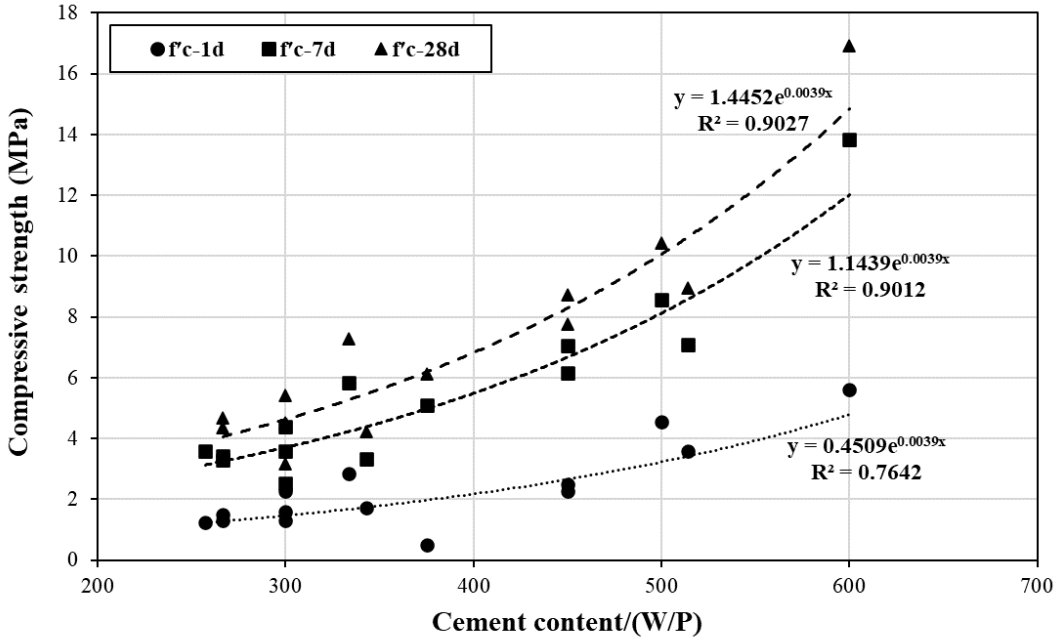

Fig. 5.11. Relationship between the compressive strengths of the investigated CEM mixtures at different ages and their corresponding cement contents and W/P ratios.

Therefore, the following correlation was established using a Microsoft Excel solver to assess the contribution of different mixture constituent factors on the $f'_{c\text{-}1d}$ values of the investigated CEM mixtures:

$$f'_{c\text{-}1d}\ (\text{MPa}) = \alpha + \beta \times \frac{CC^{\varepsilon}}{LL^{\gamma} \times \left(\frac{W}{P}\right)^{\delta}} \tag{5.4}$$

where α, β, γ, δ and ε are the adjustment factors and power indices reflecting the contribution of LL, W/P, and cement content (CC in kg/m^3) on $f'_{c\text{-}1d}$, respectively. The values of these parameters are summarized in Table 5.11. As shown in Fig. 5.12, the established correlations can predict the 1-d compressive strengths of the investigated mixtures (R^2 more than 0.997 and RMSE less than 0.183 MPa). According to the established correlations, the CEM mixtures proportioned with higher cement content, soils (clay, silt, and sand) with lower LL, and lower W/P ratios can exhibit higher

compressive strength values at 24 hours of age, which can be useful for early formwork removal. On the other hand, the obtained power indices (Table 5.11) revealed that cement content and W/P ratio showed the highest and lowest contribution on $f'_{c\text{-}1d}$ values of the PCE-based CEM mixtures, respectively. Moreover, the LL of the soils used mostly controls the early-age mechanical properties of the CEM mixtures containing PNS. However, cement content was found more effective on the $f'_{c\text{-}1d}$ values of mortar mixtures made with PNS compared to W/P ratio. Furthermore, the compressive strength of the CEM mixtures proportioned with NE-PC admixture is controlled by the LL values of the used soil and W/P ratio.

Table 5.11. Adjustment factors of the established $f'_{c\text{-}1d}$ correlations (Eq. 5.4).

Admixture	Adjustment factors				
	α	β	γ	δ	ε
PCE	0.856	7.26E-07	1.951	0.103	4.099
PNS	0	64.320	8.180	2.593	3.753
NE-PC	0	3.754	2.795	2.358	1.141

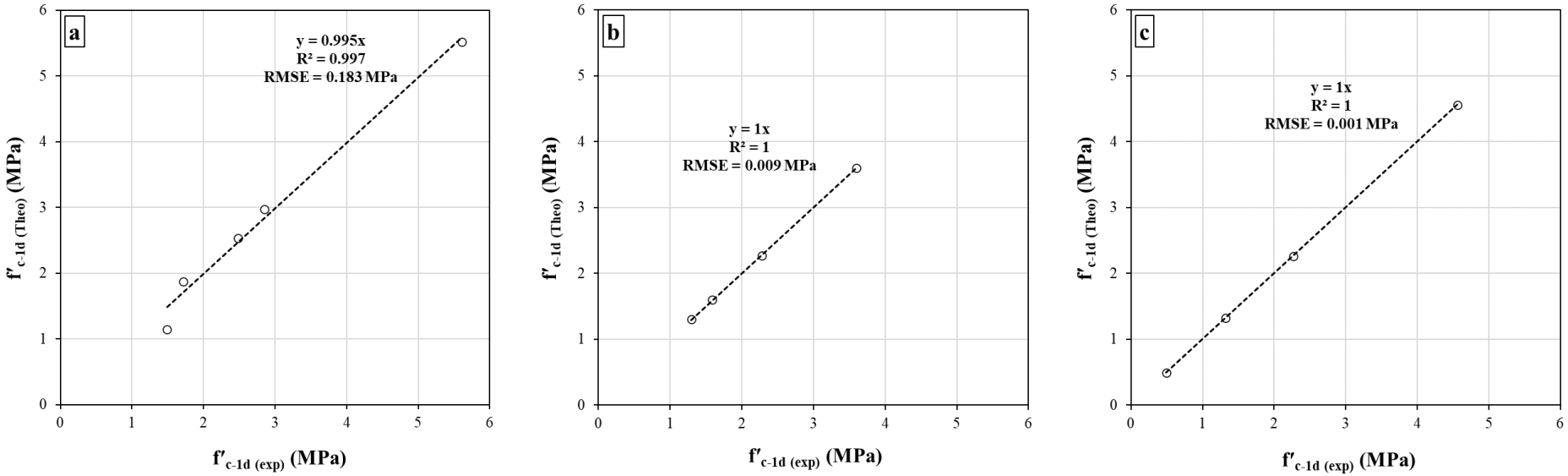

Fig. 5.12. Comparison between the experimental $f'_{c\text{-}1d}$ values of the investigated CEM mixtures and those obtained using Eq. 5.4 for (a) PCE, (b) PNS, and (c) NE-PC admixtures.

5.4.1.4 Drying shrinkage

The drying shrinkage measurements of the investigated CEM mixtures are presented in Fig. 5.13. Walker et al. [10] recommended an acceptable upper limit of 0.5% for drying shrinkage of earth-based construction materials. The M25 and M45 mixtures made with NaHMP and NE-PC types, respectively, exhibited higher drying shrinkage than the recommended value of 0.5%. Also, these mixtures required the highest admixture demands (more than 1% of the binder content) compared to other mixtures. This may be due to the relatively high content of Clay Type II (M45) and the admixture type. The mixtures proportioned with low W/P ratio and high clay content required high admixture demand, hence leading to high drying shrinkage. Among the PCE-based mixtures (Fig. 5.13a), the M37 and M49 mixtures containing soils with high LL of 32.8% and 31.5%, respectively, exhibited the highest drying shrinkage. Moreover, the M22 mixture made with the lowest W/P ratio of 0.30 showed the lowest shrinkage among the mixtures containing Clay Type I. Regarding the mixtures dispersed with PNS (Fig. 5.13b), the M23 mixture exhibited the highest drying shrinkage given its relatively high LL (21.5%) and PI (6.7%) values compared to other mixtures. The M17, M10, and M11 mixtures made with the soils having LL values of 19.5%, 18.6%, and 18.1%, respectively, showed lower drying shrinkage. In the case of the CEM mixtures proportioned with NE-PC (Fig. 5.13c), it was revealed that despite off the comparable LL values of their corresponding soils, higher W/P ratio (0.45) of the M12 mixture led to the highest drying shrinkage rather than the M18 and M24 mixtures.

As can be observed in Fig. 5.14, the 7-days drying shrinkage of the investigated mixtures are in good agreement with their corresponding early-age compressive strength values ($f'_{c\text{-}1d}$). For instance, the M25 and M45 mixtures with low $f'_{c\text{-}1d}$ less than 1 MPa exhibited very high drying shrinkage after 7 days of age. According to the obtained results, it can be concluded that a satisfactory compressive strength for formwork removal after 24 hours (i.e., $f'_{c\text{-}1d} > 1$ MPa) can ensure the 7-days drying shrinkage values of less than 0.2%.

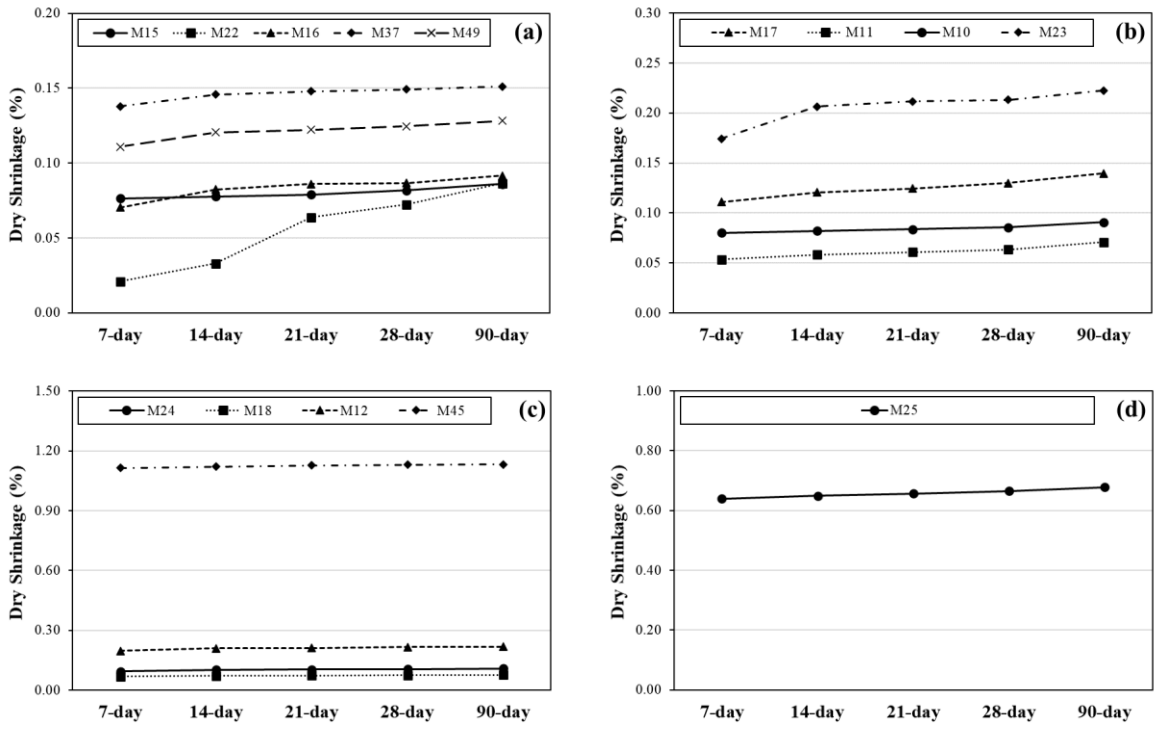

Fig. 5.13. Evolution of dry shrinkage (up to 90 days) of the investigated CEM mixtures proportioned with (a) PCE, (b) PNS, (c) NE-PC, and (d) NaHMP admixtures.

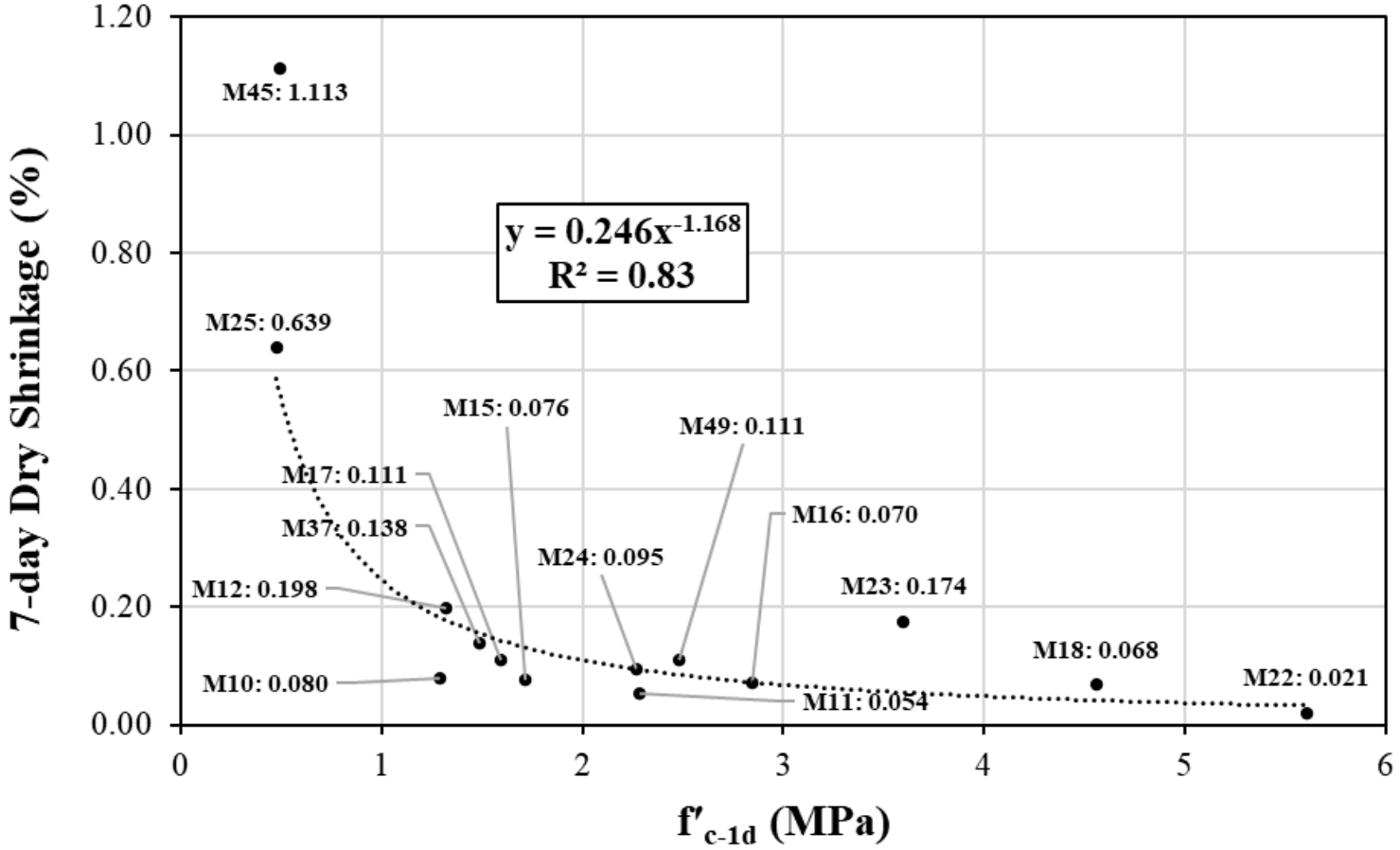

Fig. 5.14. Relationship between the 7-days drying shrinkage and 1-day compressive strength values of the investigated CEM mixtures

The 7-day drying shrinkage values of the investigated CEM mixtures were then correlated to different characteristics of the mixture constituents, in terms of PI of soil, paste volume, W/P ratio, and cement content, as follows:

$$\text{Drying shrinkage}_{7d}\ (\%) = \alpha + \beta \times \frac{PI^{\gamma} \times V_P{}^{\delta} \times \left(\frac{W}{P}\right)^{\varepsilon}}{CC^{\zeta}} \quad (5.5)$$

where α, β, γ, δ, ε and ζ are the adjustment factors and power indices reflecting the contribution of PI, V_P, W/P, and cement content (CC), respectively, on 7-days drying shrinkage values of the investigated mixtures (Table 5.12). As can be observed in Fig. 5.15, the shrinkage values are in very good agreements with the PI, V_P, W/P, and CC values (high R^2 of 1.0 and RMSE values less than 0.007%). According to the established correlations, the drying shrinkage of the PCE-based mortar mixtures was mostly controlled by their corresponding V_P and W/P. However, drying shrinkage of PCE-contained mixtures was found less sensitive to the soil characteristics (PI). On the other hand, the shrinkage properties of the PNS-based mixtures were found influenced by the PI of the used soil and cement content. Furthermore, drying shrinkage of the CEM mixtures containing NE-PC type was found more significantly affected by the paste volume and cement content values rather than PI of the soils and W/P ratio.

Table 5.12. Adjustment factors of the established drying shrinkage$_{7d}$ correlations (Eq. 5.5)

Admixture	Adjustment factors					
	α	β	γ	δ	ε	ζ
PCE	0	7.64E-06	0.232	4.016	3.120	0.796
PNS	0.012	7.007	1.236	0	0	1.179
NE-PC	0.055	1.521	3.516	5.064	2.868	5.366

5.4.1.5 Analysis of variance (ANOVA)

In order to evaluate the sensitivity of the flow and mechanical performances, as well as drying shrinkage of the investigated CEM mixtures due to variation of different mixture constituents, including W/P ratio, paste volume V_P, and admixture type, analyses of variance (ANOVA) were carried out, as shown in Table 5.13 and 5.14, respectively. The ANOVA analyses are presented in terms of contribution and p-value of each of the influencing factors. As shown in Table 5.13, the investigated characteristics at fresh state included the admixture demand to achieve the targeted MSF of 280 ± 20 mm, MSF losses and MVF increments between 0 to 30 min ($\Delta MSF_{0\text{-}30\ min}$ and $\Delta MVF_{0\text{-}30\ min}$) and 30 to 60 min ($\Delta MSF_{30\text{-}60\ min}$ and $\Delta MVF_{30\text{-}60\ min}$) after mixing, and initial MVF

values measured immediately after mixing (MVF_0). On the other hand, the compressive strengths at 1 ($f'_{c\text{-}1d}$), 7 ($f'_{c\text{-}7d}$), and 28 ($f'_{c\text{-}28d}$) days of age, as well as the drying shrinkage at 7 and 28 days were investigated using ANOVA analyses for hardened state, as summarized in Table 5.14.

As can be observed in Table 5.13, the paste volume showed higher contribution on the admixture demand compared to W/P and admixture type, which showed comparable influences (33.34% vs. 25.38% and 25.3%). Moreover, the initial MVF_0 values were controlled by W/P ratios of the mixtures compared to V_P and admixture type. On the other hand, the workability-loss after 30 min ($MSF_{0\text{-}30\ min}$ and $MVF_{0\text{-}30\ min}$) is more influenced by the admixture type compared to W/P ratio and V_P. However, in the case of workability loss at 30 and 60 min, the admixture type is more effective on MSF losses ($MSF_{30\text{-}60\ min}$), while the W/P influenced $MVF_{30\text{-}60\ min}$ rather than the admixture type. Furthermore, the admixture type and paste volume exhibited the lowest and highest contributions on the characteristics of CEM in hardened states (compressive strength and shrinkage), respectively. It is worth mentioning that contributions of V_P and W/P on the early-age characteristics of the investigated CEM mixtures ($f'_{c\text{-}1d}$ and 7-day drying shrinkage) were stronger than those observed at longer ages.

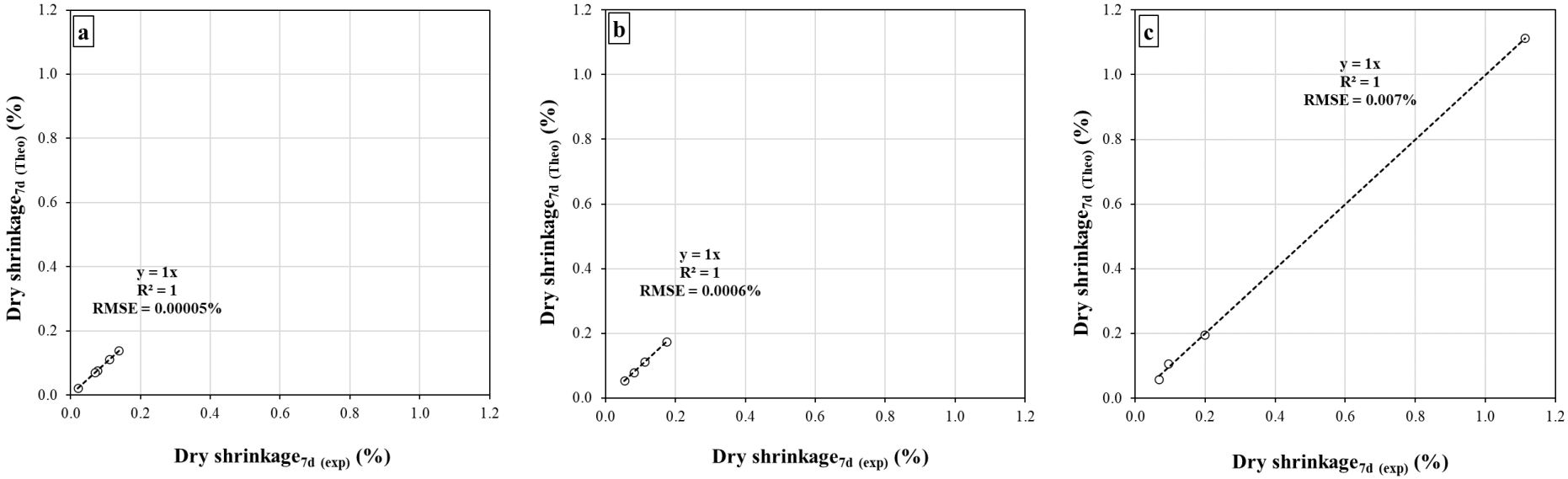

Fig. 5.15. Comparison between the experimental 7-days drying shrinkage values of the investigated CEM mixtures and those obtained using the established correlation Eq. 5.5, incluidng (a) PCE, (b) PNS, and (c) NE-PC admixtures.

Table 5.13. ANOVA analysis for the CEM fresh properties, including the admixture demand, MSF loss, MVF_0, and MVF increase.

Source	Admixture demand		MSF loss				MVF_0		MVF increment			
			$\Delta MSF_{0\text{-}30\ min}$		$\Delta MSF_{30\text{-}60\ min}$				$\Delta MVF_{0\text{-}30\ min}$		$\Delta MVF_{30\text{-}60\ min}$	
	Contribution (%)	P-Value	Contribution (%)	P-Value	Contribution (%)	P-Value	Contribution (%)	P-Value	Contribution (%)	P-Value	Contribution (%)	P-Value
W/P	25.4	0.322	9.6	0.254	36.8	0.162	91.9	0.034	15.1	0.768	36.5	0.663
V_P	33.3	0.381	11.8	0.267	16.3	0.338	5.9	0.305	29.3	0.544	20.1	0.499
Admixture type	25.4	0.386	73.9	0.059	44.9	0.042	1.0	0.564	38.3	0.311	30.7	0.292
Error	15.9		4.6		2.0		1.2		17.2		12.7	
Total	100.0		100.0		100.0		100.0		100.0		100.0	

Table 5.14. ANOVA analysis for the CEM hardened properties, including the compressive strength and drying shrinkage.

Source	Compressive strength						Drying shrinkage			
	$f'_{c\text{-}1d}$		$f'_{c\text{-}7d}$		$f'_{c\text{-}28d}$		7-d shrinkage		28-d shrinkage	
	Contribution (%)	P-Value	Contribution (%)	P-Value	Contribution (%)	P-Value	Contribution (%)	P-Value	Contribution (%)	P-Value
W/P	35.3	0.141	28.8	0.471	27.1	0.482	17.3	0.450	16.3	0.500
V_P	52.4	0.109	36.4	0.536	39.2	0.519	65.3	0.374	63.8	0.423
Admixture type	9.0	0.265	16.7	0.519	15.9	0.529	3.4	0.805	3.5	0.826
Error	3.2		18.0		17.8		14.0		16.5	
Total	100.0		100.0		100.0		100.0		100.0	

5.4.2 Concrete mixtures

The fresh and hardened properties of four different concrete mixtures, including 3 SCEC mixtures C16, C22, and C37, and a no-clay reference mixture C_{ref} were investigated, as shown in Fig. 5.16. It is important to mention that the investigated concrete mixtures were proportioned with the same dosage of PCE admixtures of their corresponding CEM mixtures to achieve a MSF of 280 ± 20 mm. The workability of the investigated concrete mixtures was evaluated in terms of the slump flow (SF) and V-Funnel (VF) values immediately after mixing, 30, and 60 min of age (Fig. 5.16a and 5.16b). Moreover, the drying shrinkage was evaluated at 7, 14, 21, 28, and 90 days of age (Fig. 5.16c). The compressive strength of the investigated mixtures determined at 1, 7, and 28 days of age are presented in Fig. 5.16d.

According to the European guideline (EFNARC) [36], the SF and VF values between 650 to 800 mm and 6 to 12 s, respectively, were recommended to ensure adequate workability criteria for SCC. As can be observed in Fig. 5.16a, the initial SF values of the investigated mixtures achieved the recommended SF range for SCC. However, significant SF loss was observed in the case of the mixture C37 containing the Clay Type II. This reflects the significant effect of the binder constituents and fineness on SF loss compared to the other influencing parameters. The mixture C22 showed the highest initial VF values, hence reflecting the highest initial viscosity (Fig. 5.16b). This is probably due to its lowest W/P ratio (0.30) compared to other mixtures. However, the highest increase in the VF values was obtained for C37, which can be attributed to incorporation of the finer Clay Type II which hinders the filling ability over time. It is worth mentioning that negligible increasing rates of VF was observed in the case of the mixtures C16 and C22 made with Clay Type I. The lowest VF values over time were obtained for C16 mixture due to its highest W/P ratio. This proves the significant influence of solid fraction and finer particles in increasing the viscosity.

As can be observed in Fig. 5.16c, the reference mixture C_{ref} made without clay exhibited the lowest drying shrinkage. For example, its 28-day dry shrinkage was 0.04% while it ranged between 0.07% and 0.11% for the other three SCEC mixtures. The presence of clay particles induces high shrinkage, which needs special consideration. Among the investigated SCEC mixtures, C37 made with Clay Type II showed the highest drying shrinkage. This is due to the relatively higher fineness of Clay Type II compared to that of Clay Type I. On the other hand, the C16 mixture proportioned

with relatively high W/P and Clay Type I content exhibited higher shrinkage values than C22. As expected, C_{ref} exhibited the highest compressive strength, regardless of the age, followed by C22, C16, and C37 mixtures, respectively (Fig. 5.16d). the compressive strength results emphasized the coupled effect of cement content and W/P ratio on compressive strength of SCEC mixtures, regardless of clay type.

Fresh density and air content of the investigated concrete mixtures measured immediately after mixing are illustrated in Fig. 5.16e. As can be observed, increasing the cement content with higher specific gravity than Clay Types I and II led to higher fresh density of concrete. Accordingly, the C_{ref} and C37 mixtures showed the highest and lowest fresh density values of 2340 and 2200 kg/m^3, respectively. Moreover, the C_{ref} and C37 mixtures exhibited the lowest air content compared to C16 and C22, which can be attributed to their higher packing density of aggregate (Table 5.2). However, the mixture C22 showed the highest air content (4%) which can be due to its low water content in presence of PCE admixture. Moreover, as shown in Fig. 5.17, no visual segregation was observed for all the investigated concrete mixtures (Visual segregation index VSI = 0).

In order to better understand the behavior of highly flowable earth-based mixtures (HFEBM) several correlations were established between the properties of the investigated paste, CEM, and concrete mixtures. Indeed, precise predictions of the workability and mechanical performance of the HFEBM mixtures can lead to an economic and sustainable optimization.

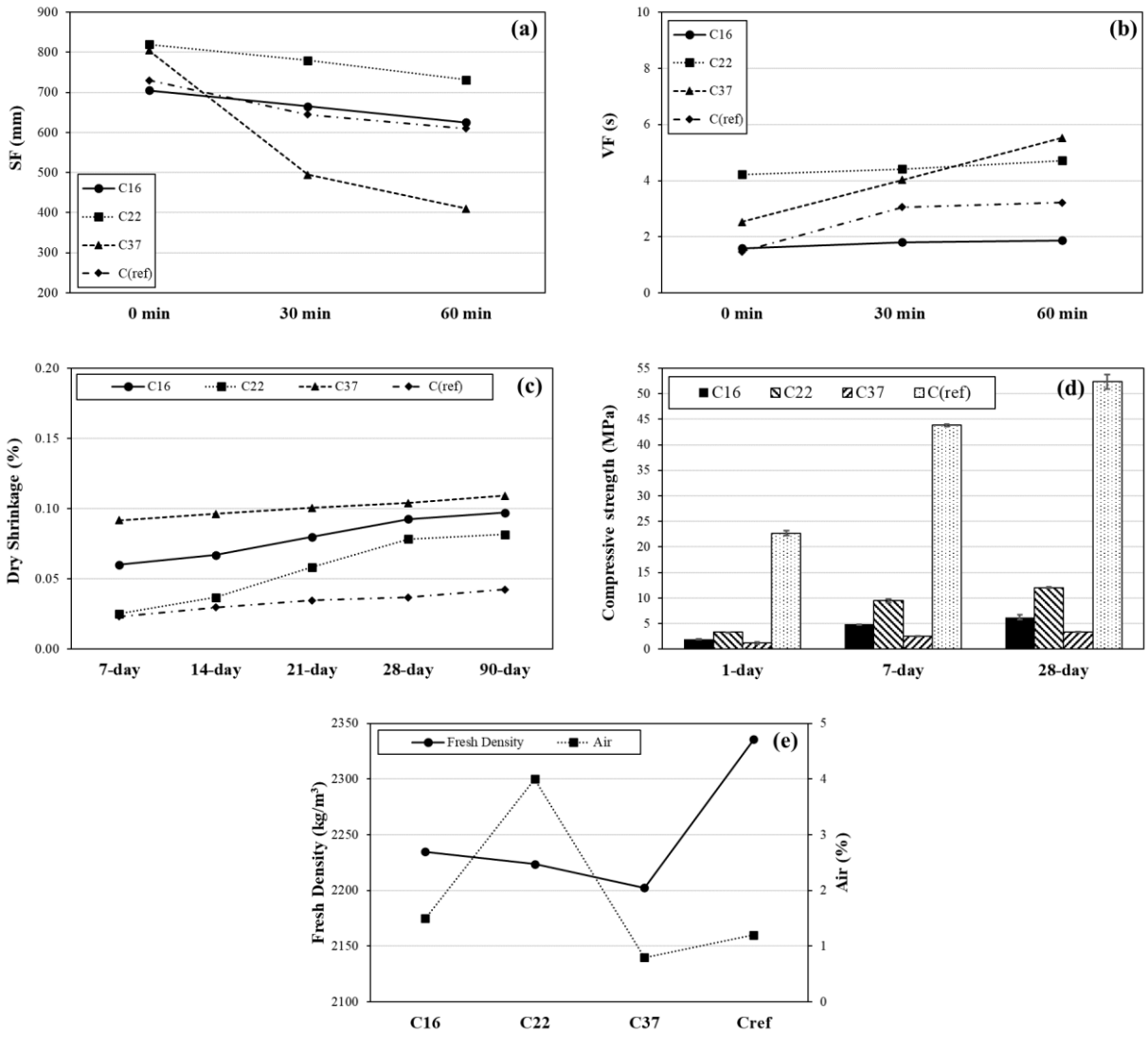

Fig. 5.16. Properties of the investigated concrete mixtures, including (a) SF, (b) VF, (c) drying shrinkage, (d) compressive strength, and (e) fresh density and air content.

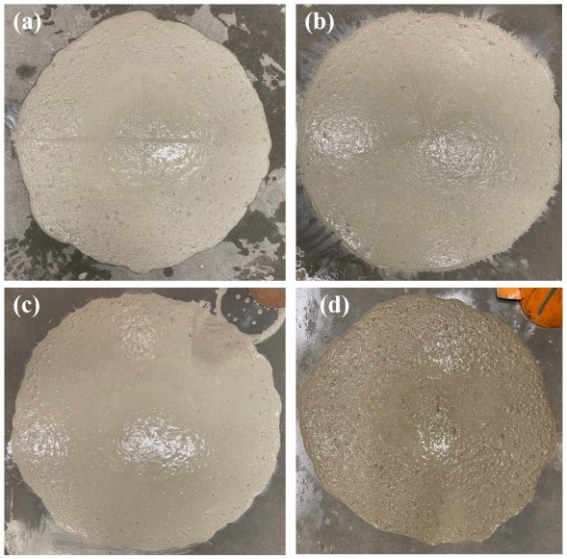

Fig. 5.17. Slump-flow spreads of (a) C16, (b) C22, (c) C37, and (d) C_{ref} mixtures.

5.4.3 CEM-to-paste correlations

The properties of the investigated CEM mixtures, including the admixture demand to achieve a MSF of 280 ± 20 mm (Ad. demand), and MSF loss up to 30 min ($\Delta MSF_{0\text{-}30\ min}$) relative to those of their corresponding pastes were correlated. The characteristics of the mixture constituents, including the Atterberg limits of the used soil (LL or PI), V_P, W/P, and e_{EP}, are considered. In the case of the "Ad. demand" ratio, the following correlation was established:

$$\text{Ad. demand ratio} = \frac{\text{Ad. demand (CEM)}}{\text{Ad. demand (paste)}} = \alpha + \beta \times PI^{\gamma} \times {V_P}^{\delta} \times \left(\frac{W}{P}\right)^{\varepsilon} \times {e_{EP}}^{\zeta} \quad (5.6)$$

where α, β, γ, δ, ε and ζ are the adjustment factors and power indices corresponding to contribution of PI, V_P, W/P, and EP thickness, respectively. The determined coefficients are summarized in Table 5.15. As can be observed in Fig. 5.18, the admixture demand of the investigated CEM is well predicted to those of their corresponding paste mixtures (Eq. 5.6 and Table 5.15). According to the adjustment factors presented in Table 5.15, the PCE and NE-PC admixture demands of the CEM mixtures relative to their pastes increased with paste volume and PI of the soil. However, the admixture demand decreased with W/P ratio and excess paste thickness. The investigated CEM mixtures required higher PNS dosages compared to their corresponding pastes by using low PI-soils and incorporating high V_P, W/P, and e_{EP} values. According to the obtained power indices, the

W/P ratio showed higher contribution on the relative admixture demands, while e_{EP} was more effective on those of the NE-PC-based mixtures.

Table 5.15. Adjustment factors of the established relative admixture-demand ratio correlation (Eq. 5.6).

Admixture	Adjustment factors					
	α	β	γ	δ	ε	ζ
PCE	1.28	4.166	2.557	2.516	-5.910	-5.749
PNS	1.482	2.161	-1.803	1.505	7.227	0.202
NE-PC	0.821	6.017	0.061	0.825	-0.332	-1.101

The following correlation was then established between the ratio of $\Delta MSF_{0\text{-}30\ min}$ values of the investigated CEM mixtures to those of their corresponding pastes and mixture constituents:

$$\text{MSF loss ratio} = \frac{\Delta MSF_{0-30\ min}\ (\text{CEM})}{\Delta MSF_{0-30\ min}\ (\text{paste})} = \alpha + \beta \times LL^{\gamma} \times PI^{\delta} \times \left(\frac{W}{P}\right)^{\varepsilon} \times e_{EP}{}^{\zeta} \quad (5.7)$$

where α, β, γ, δ, ε and ζ are the adjustment factors and power indices reflecting the contribution of LL and PI of the used soil, W/P ratio, and EP thickness, respectively. The obtained coefficients are summarized in Table 5.16. As can be observed in Fig. 5.19, the relative MSF losses of the investigated CEM and paste mixtures are well correlated (high $R^2 \approx 1.0$ and RMSE < 0.047) to the characteristics of the mixture constituents using Eq. 5.7 and Table 5.16. The power indices summarized in Table 5.16 revealed that W/P ratio showed more significant effect on the relative MSF-loss ratios of the investigated CEM and paste mixtures proportioned with PCE and NE-PC admixtures compared to the soil characteristics and excess paste thickness. On the other hand, the MSF-loss ratios of the mixtures containing PNS are mostly influenced by the LL of the used soil compared to W/P ratio and excess paste thickness.

Table 5.16. Adjustment factors of the established correlation of the relative MSF loss (Eq. 5.7).

Admixture	Adjustment factors					
	α	β	γ	δ	ε	ζ
PCE	0.672	5.26E-08	0	0	23.592	8.695
PNS	0	21201.862	-3.489	0	0.742	0.127
NE-PC	1.68E-07	0.028	0	0.768	1.097	0.598

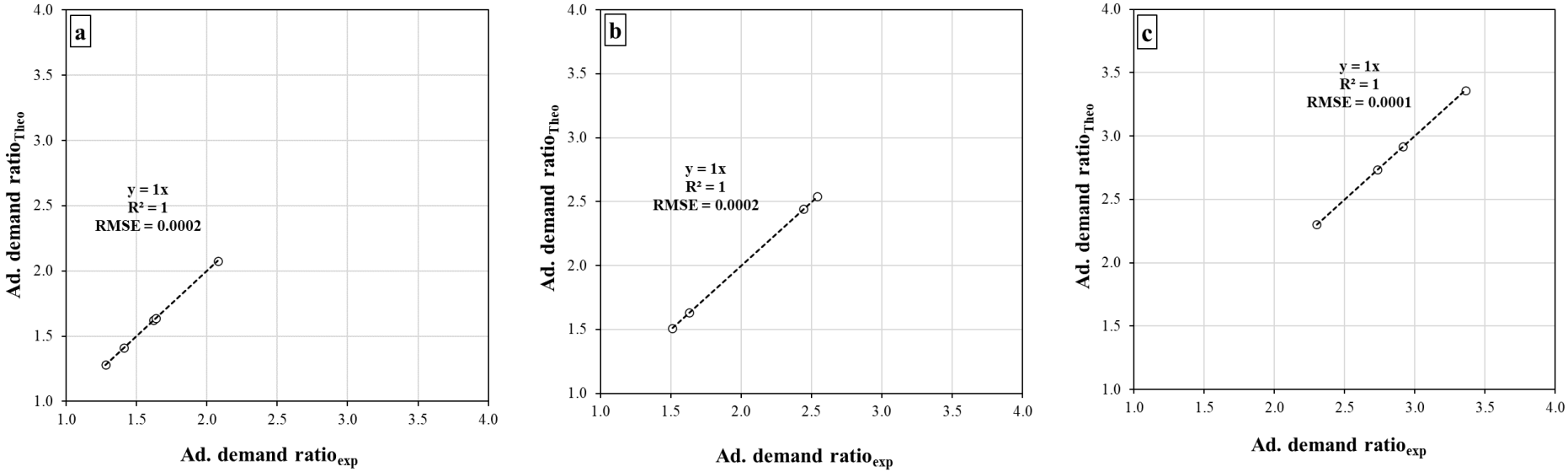

Fig. 5.18. Comparison between the experimental CEM-to-paste Ad. demand ratios and those obtained using the established correlation Eq. 5.6 and Table 5.15, including (a) PCE, (b) PNS, and (c) NE-PC admixtures.

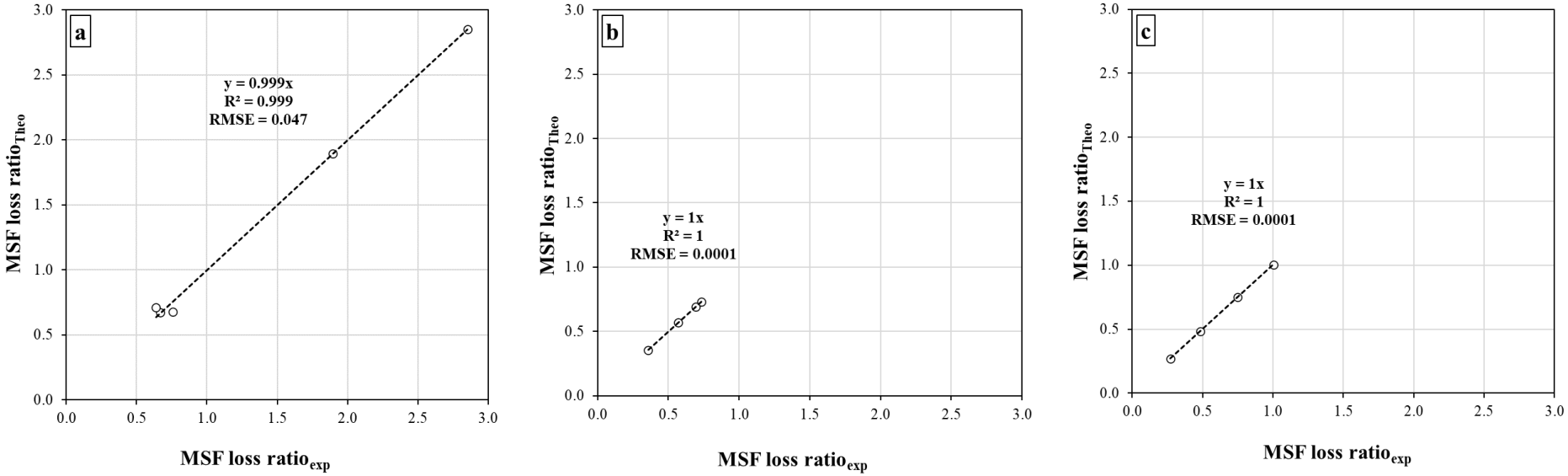

Fig. 5.19. Comparison between the experimental CEM-to-paste MSF-loss ratios and those obtained using the established correlation Eq. 5.7, including (a) PCE, (b) PNS, and (c) NE-PC admixtures.

5.4.4 Validation of the new proposed CEM approach: Concrete-to-CEM correlations

The accuracy of the proposed CEM approach to predict the characteristics of the corresponding concrete given the influencing parameters is evaluated in this section. It is worthy to mention that the validation was only carried out on mixtures made with PCE since their corresponding CEM mixtures that achieved targeted workability, drying shrinkage, and compressive strength. Accordingly, the relative admixture demand, SF, and MSF losses up to 30 min, VF and MVF increase up to 30 min, 28-day drying shrinkage, and 28-days compressive strength ($f'_{c\text{-}28d}$) of the investigated concrete mixtures-to-their corresponding CEM mixtures were investigated. The established concrete-to-CEM relative properties were then correlated to the mixture constituents, including W/P, e_{EP}, and S/A, as follows:

$$\text{Concrete-to-CEM relative measure} = \alpha + \beta \times \left(\frac{W}{P}\right)^{\gamma} \times {e_{EP}}^{\delta} \times \left(\frac{S}{A}\right)^{\varepsilon} \quad (5.8)$$

where α, β, γ, δ and ε are the adjustment factors and power indices reflecting the effect of W/P, e_{EP}, and S/A ratio, respectively. The obtained coefficients are summarized in Table 5.17. As can be observed in Fig. 5.20, the characteristics, including admixture demand, workability loss, compressive strength, and drying shrinkage of the investigated mixtures are in perfect agreements (R^2 = 1.0, 0.995 < estimation indices < 1.003, and RMSE < 0.022) with those of their corresponding CEM mixtures. The established relationships can be employed to accurately predict the fresh and hardened properties of concrete using those of the corresponding CEM mixtures. This can reduce the number of trial batches and facilitate the design process.

According to the established correlations, the relative admixture demand depends on the three affecting parameters to the same extent, while workability loss (SF and VF) values of the investigated concrete and their corresponding CEM mixtures showed greater sensitivity to the excess paste thickness variations rather than W/P and S/A ratios. Furthermore, the S/A and W/P ratios did not show a significant effect on the relative VF variation and compressive strengths of concrete and CEM mixtures, respectively. Similar to the workability loss values, the drying shrinkage of the investigated concrete and CEM mixtures were mostly controlled by the excess paste thickness.

Table 5.17. Adjustment factors of the established correlations (Eq. 5.8)

Concrete-to-CEM relative measures	Adjustment factors				
	α	β	γ	δ	ε
$\frac{\text{Ad. demand (Concrete) (\%)}}{\text{Ad. demand (CEM) (\%)}}$	0.149	4.680	-0.923	-0.776	-0.998
$\frac{\Delta SF_{0\text{-}30min}\text{ (Concrete) (mm)}}{\Delta MSF_{0\text{-}30min}\text{(CEM) (mm)}}$	0	2.41E-05	0.475	2.927	1.727
$\frac{\Delta VF_{0\text{-}30min}\text{ (Concrete) (s)}}{\Delta MVF_{0\text{-}30min}\text{(CEM) (s)}}$	0.023	0.012	0.301	1.175	0
$\frac{f'_{c\text{-}28d}\text{ (Concrete) (MPa)}}{f'_{c\text{-}28d}\text{(CEM) (MPa)}}$	0	24.769	0	-0.983	-1.088
$\frac{\text{Drying shrinkage}_{28d}\text{ (Concrete) (\%)}}{\text{Drying shrinkage}_{28d}\text{(CEM) (\%)}}$	0	37.612	-0.745	-1.199	-0.857

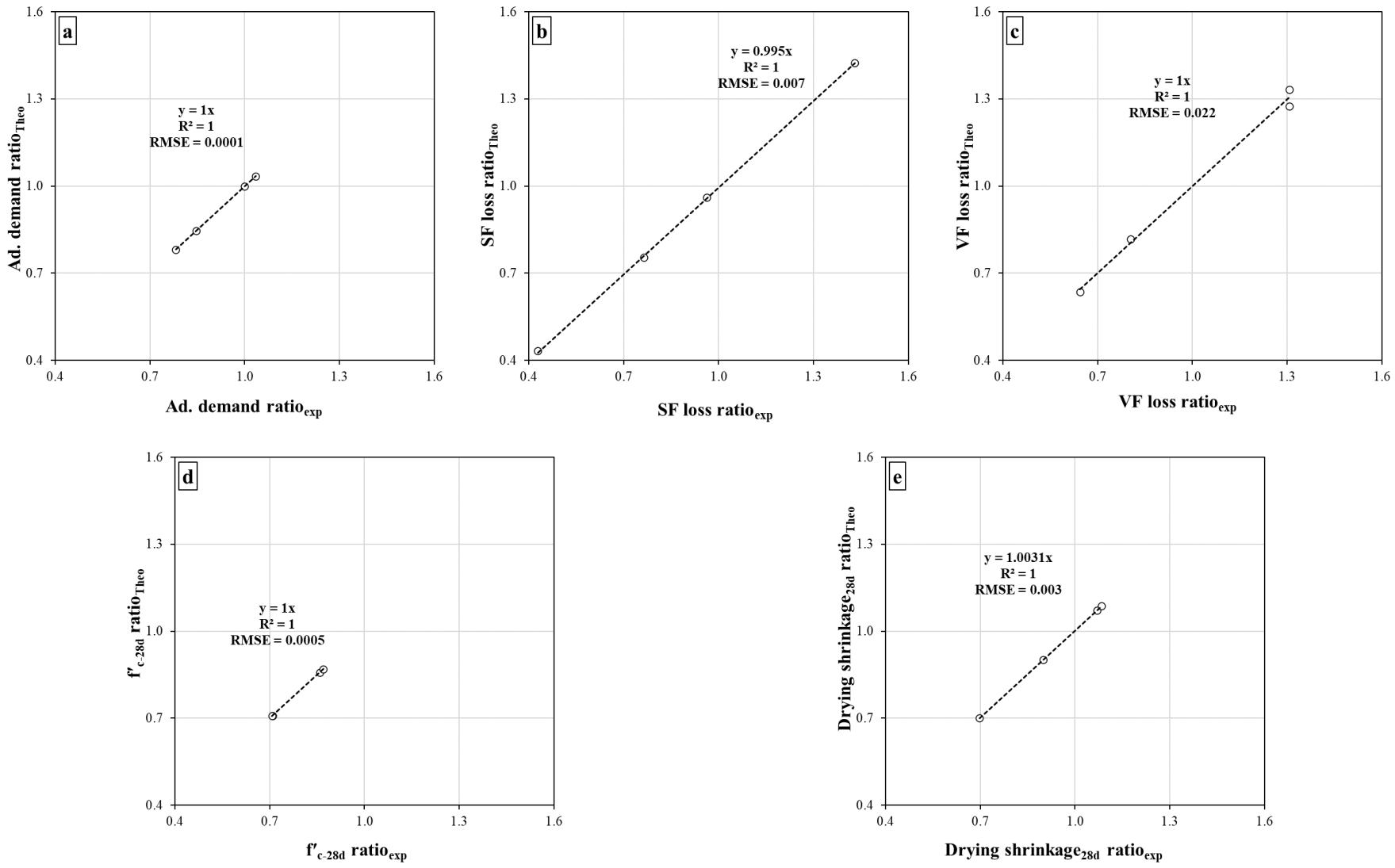

Fig. 5.20. Comparisons between the proprties of concrete and CEM mixtures, including (a) admixture demand, (b) SF loss, and (c) VF increment up to 30 min after mixing, (d) 28-days compressive strength $f'_{c\text{-}28d}$, (e) and 28-day drying shrinkage, and those obtained using the established correlations Eq. 5.8.

5.5 Conclusions

In this study, a new proposed concrete-equivalent mortar (CEM) approach to design self-consolidating earth concrete (SCEC) mixtures was proposed and validated. This approach consisted in proportioning the CEM mixtures using the same excess paste thickness in the SCEC reference. The coupled effect of characteristics of the mixture constituents, including clay and admixture types, water-to-powder ratio (W/P), volumetric cement-to-clay ratio (Ce/Cl), and volumetric sand-to-total aggregate ratio (S/A) ratios, as well as cement content on fresh and hardened properties of the investigated mixtures was evaluated. According to the obtained results, the following conclusions can be pointed out:

- CEM approach used in this study was successfully used and validated to assess workability and dry shrinkage of the corresponding concrete mixtures. These properties are highly dependent on the W/P, EP thickness, and S/A. However, relative compressive strength of concrete to CEM ratio was found to be only dependent on the EP thickness and sand-to-total aggregate ratio

- Workability of the investigated CEM mixtures can be predicted using their corresponding paste mixtures depending on the used soil characteristics, V_P, W/P, and excess-paste thickness.

- Workability of the investigated SCEC mixtures were affected by the combined effect of W/P ratio and binder constituents. The PI/(W/P) and SSA/(W/P) parameters were the most influencing parameters on the admixture demand to achieve the targeted workability. Admixture demand was proportional to LL and PI, and inversely proportional to V_P, W/P, and e_{EP}.

- ANOVA analysis revealed that the MSF loss was highly dependent on the admixture type, followed by W/P ratio. The NE-PC and NaHMP types exhibited the lowest and highest MSF loss values, respectively, compared to PNS and PCE ones.

- Viscosity values mostly decreased due to higher W/P ratios and V_P, but not affected by the binder characteristics. However, mini V-Funnel (MVF) increase was found to be highly dependent on the admixture type. The NaHMP mixtures showed high shape stability and gaining viscosity over time.

- The 7- and 28-day compressive strength ($f'_{c\text{-}7d}$ and $f'_{c\text{-}28d}$) values were highly dependent on the cement content and W/P ratio, while $f'_{c\text{-}1d}$ was also dependent on the binder characteristics (LL), especially in the presence of PNS admixture.

- Dry shrinkage properties were found in good agreement with the early-age compressive strength values, showing very high values in the case of $f'_{c\text{-}1d}$ less than 1 MPa. It was also revealed that the drying shrinkage values were highly dependent on V_P, followed by W/P ratio.

5.6 Declaration of competing interest

The authors declare that they have no known competing financial interests or personal relationships that could have appeared to influence the work reported in this paper.

5.7 Acknowledgement

The authors wish to thank the financial support of the National Science and Engineering Research Council of Canada (NSERC) and the eight industrial partners participating in the NSERC Chair on Development of Flowable Concrete with Adapted Rheology and their Application in Concrete Infrastructures, held by Professor Ammar Yahia at the Université de Sherbrooke.

REFERENCES

[1] International Energy Agency, The Reduction of Greenhouse Gas Emissions From The Cement Industry, Report PH3/7, Paris, France, 1999.

[2] F. Pacheco-Torgal, S. Jalali, Earth construction: Lessons from the past for future eco-efficient construction, Constr. Build. Mater. 29 (2012) 512–519. https://doi.org/10.1016/j.conbuildmat.2011.10.054.

[3] R. Bahar, M. Benazzoug, S. Kenai, Performance of compacted cement-stabilised soil, Cem. Concr. Compos. 26 (2004) 811–820. https://doi.org/10.1016/j.cemconcomp.2004.01.003.

[4] M. Hall, Y. Djerbib, Rammed earth sample production: Context, recommendations and consistency, Constr. Build. Mater. 18 (2004) 281–286. https://doi.org/10.1016/j.conbuildmat.2003.11.001.

[5] P.G. McHenry, Adobe and Rammed Earth Buildings: Design and Construction, University of Arizona Press, Arizona, 1989.

[6] L. Miccoli, U. Müller, P. Fontana, Mechanical behaviour of earthen materials: A comparison between earth block masonry, rammed earth and cob, Constr. Build. Mater. 61 (2014) 327–339. https://doi.org/10.1016/j.conbuildmat.2014.03.009.

[7] C.M. Ouellet-Plamondon, G. Habert, Self-Compacted Clay based Concrete (SCCC): Proof-of-concept, J. Clean. Prod. 117 (2016) 160–168. https://doi.org/10.1016/j.jclepro.2015.12.048.

[8] J.J. Chen, B.H. Li, P.L. Ng, A.K.H. Kwan, Adding granite polishing waste as sand replacement to improve packing density, rheology, strength and impermeability of mortar, Powder Technol. 364 (2020) 404–415.

[9] S.K. Ling, A.K.H. Kwan, Adding ground sand to decrease paste volume, increase cohesiveness and improve passing ability of SCC, Constr. Build. Mater. 84 (2015) 46–53.

[10] P. Walker, R. Keable, J. Martin, V. Maniatidis, Rammed earth: design and construction guidelines, IHS BRE, 2005.

[11] M. Kohandelnia, M. Hosseinpoor, A. Yahia, R. Belarbi, A new approach for proportioning self-consolidating earth paste (SCEP) using the Taguchi method, Constr. Build. Mater. 347 (2022) 128579. https://doi.org/10.1016/J.CONBUILDMAT.2022.128579.

[12] G. Landrou, C. Brumaud, F. Winnefeld, R.J. Flatt, G. Habert, Lime as an anti-plasticizer for self-compacting clay concrete, Materials (Basel). 9 (2016). https://doi.org/10.3390/ma9050330.

[13] B.M. Aïssoun, S.-D. Hwang, K.H. Khayat, Influence of aggregate characteristics on workability of superworkable concrete, Mater. Struct. 49 (2016) 597–609.

[14] B.I.O. Koura, M. Hosseinpoor, A. Yahia, Coupled effect of fine mortar and granular skeleton characteristics on dynamic stability of self-consolidating concrete as a diphasic material, Constr. Build. Mater. 263 (2020) 120131. https://doi.org/10.1016/j.conbuildmat.2020.120131.

[15] B.I. Ouro Koura, M. Hosseinpoor, A. Yahia, E.H. Kadri, A. Kaci, A new proportioning approach of low and normal binder self-consolidating concrete based on the characteristics of fine mortar and granular skeleton, Constr. Build. Mater. 239 (2020) 117892. https://doi.org/10.1016/j.conbuildmat.2019.117892.

[16] M. Hosseinpoor, B.-I.O. Koura, A. Yahia, Rheo-morphological investigation of Reynolds dilatancy and its effect on pumpability of self-consolidating concrete, Cem. Concr. Compos. 117 (2021).

[17] A.W. Skempton, The Colloidal activity of clays, in: 3rd Int. Conf. Soil Mech. Found. Eng., London, 1953: pp. 47–61.

[18] B. Voight, Correlation between Atterberg plasticity limits and residual shear strength of natural

soils, Géotechnique. 23 (1973) 265–267.

[19] A. Laskar, S.K. Pal, Geotechnical characteristics of two different soils and their mixture and relationships between parameters, Electron. J. Geotech. Eng. 17 (2012) 2821–2832.

[20] P.P. Raj, Soil Mechanics and Foundation Engineering, Dorling Kindersley, (India) Pvt. Ltd., New Delhi, 2012.

[21] A. Schwartzentruber, C. Catherine, Method of Concrete Equivalent Mortar—A Novel Tool to Help in Formulation of Concrete with Admixtures, Mater. Struct. 33 (2000) 475–482.

[22] K.H. Khayat, S.-D. Hwang, Effect of High-Range Water- Reducing Admixture Type on Performance of Self-Consolidating Concrete, in: Eighth CANMET/ACI Int. Conf. Superplast. Other Chem. Admixtures Concr., American Concrete Institute, Farmington Hills, MI, 2006: pp. 185–200.

[23] J.J. Assaad, J. Harb, E. Chakar, Relationships between Key ASTM Test Methods Determined on Concrete and Concrete-Equivalent-Mortar Mixtures, J. ASTM Int. 6 (2008).

[24] T.K. Erdem, K.H. Khayat, A. Yahia, Correlating Rheology of Self-Consolidating Concrete to Corresponding Concrete-Equivalent Mortar, ACI Mater. J. (2009).

[25] D. Kabagire, P. Diederich, A. Yahia, New insight into the equivalent concrete mortar approach for self-consolidating concrete, J. Sustain. Cem. Mater. 4 (2015) 215–224. https://doi.org/10.1080/21650373.2015.1018983.

[26] J.H. Lee, J.H. Kim, J.Y. Yoon, Prediction of the yield stress of concrete considering the thickness of excess paste layer, Constr. Build. Mater. 173 (2018) 411–418. https://doi.org/10.1016/j.conbuildmat.2018.03.124.

[27] M. Hosseinpoor, B.I. Ouro Koura, A. Yahia, E.H. Kadri, Diphasic investigation of the visco-elastoplastic characteristics of highly flowable fine mortars, Constr. Build. Mater. 270 (2021) 121425. https://doi.org/10.1016/J.CONBUILDMAT.2020.121425.

[28] M. Hosseinpoor, B.I. Ouro Koura, A. Yahia, Rheo-morphological investigation of static and dynamic stability of self-consolidating concrete: A biphasic approach, Cem. Concr. Compos. 121 (2021) 104072. https://doi.org/10.1016/j.cemconcomp.2021.104072.

[29] M. Hosseinpoor, B.I.O. Koura, A. Yahia, New diphasic insight into the restricted flowability and granular blocking of self-consolidating concrete: Effect of morphological characteristics of coarse aggregate on passing ability of SCC, Constr. Build. Mater. 308 (2021) 125001. https://doi.org/10.1016/J.CONBUILDMAT.2021.125001.

[30] Nordtest, Concrete, fresh: Compactibility with ic-tester (intensive compaction tester) (NT BUILD 427), 1994.

[31] B.M. Aïssoun, Study of the Influence of Aggregate Characteristics on the Rheology of Fluid Concrete with Adapted Rheology (in French), Université de Sherbrooke, 2011.

[32] P. Walker, The Australian earth building handbook, Sydney : Standards Australia International, 2002.

[33] ASTM C305-20, Standard Practice for Mechanical Mixing of Hydraulic Cement Pastes and Mortars of Plastic Consistency, ASTM Int. (2020) 1–3. https://doi.org/10.1520/C0305-20.2.

[34] N. Roussel, C. Stefani, R. Leroy, From mini-cone test to Abrams cone test: Measurement of cement-based materials yield stress using slump tests, Cem. Concr. Res. 35 (2005) 817–822.

https://doi.org/10.1016/j.cemconres.2004.07.032.

[35] ASTM C109-20, Standard test method for compressive strength of hydraulic cement mortars (using 2-in. or [50-mm] cube specimens), ASTM Int. (2020). https://doi.org/10.1520/C0109_C0109M-20B.

[36] EFNARC, Specification and Guidelines for Self-Compacting Concrete, (2002).

[37] ASTM C596-18, Standard Test Method for Drying Shrinkage of Mortar Containing Hydraulic Cement, ASTM Int. (2018). https://doi.org/10.1520/C0596-18.

[38] ASTM D4318 − 17, Standard Test Methods for Liquid Limit, Plastic Limit, and Plasticity Index of Soils, ASTM Stand. (2017).

[39] H. Okamura, M. Ouchi, Self-Compacting Concrete, J. Adv. Concr. Technol. 1 (2003) 5–15.

[40] ASTM C39, Standard Test Method for Compressive Strength of Cylindrical Concrete Specimens, ASTM Stand. (2021).

[41] ASTM C157, Standard Test Method for Length Change of Hardened Hydraulic-Cement Mortar and Concrete, ASTM Stand. (2017).

[42] P. Domone, Mortar Tests for Self-Consolidating Concrete: Simple evaluation of materials and mixture proportions, Concr. Int. ACI. (2006) 39–45.

CHAPTER 6. New insight on rheology of self-consolidating earth concrete (SCEC)

Authors and affiliations

Mojtaba Kohandelnia: Ph.D. candidate, Cement and Concrete Research Group, Department of Civil and Building Engineering, Université de Sherbrooke, Sherbrooke, Québec, Canada, J1K 2R1.

Masoud Hosseinpoor: Post-Doc, Cement and Concrete Research Group, Department of Civil and Building Engineering, Université de Sherbrooke, Sherbrooke, Québec, Canada, J1K 2R1.

Ammar Yahia: Professor, Cement and Concrete Research Group, Department of Civil and Building Engineering, Université de Sherbrooke, Sherbrooke, Québec, Canada, J1K 2R1.

Rafik Belarbi, Professor, LaSIE UMR CNRS 7356, La Rochelle Université, La Rochelle, France.

Article Status: Submitted
Journal: Powder Technology - Elsevier
Initial date of submission: October 30th, 2022
Titre française: Nouvelles connaissances sur la rhéologie du béton de terre autoplaçant (BTAP)

Abstract

Self-consolidating earth concrete (SCEC) is a novel alternative to facilitate the earth-based construction. A new concrete-equivalent mortar (CEM) approach was proposed to evaluate the rheological and thixotropic properties of various SCEC mixtures proportioned with different kaolinite and attapulgite clay and superplasticizer types. The CEM mixtures were designed to achieve an equal excess-paste (EP) thickness of their corresponding SCEC mixtures. According to the experimental results, the use of non-esterified polycarboxylate (NE-PC) superplasticizer and sodium polynaphtalene systems in combination with a finer clay type led to a thixotropic behavior. The rheological properties of the investigated mixtures were mainly controlled by the admixture type, followed by the type and content of the clay used. The use of sodium hexametaphosphate resulted in significantly higher yield stress and plastic viscosity values. Empirical models were proposed to evaluate the coupled effect of mixture constituents on rheology of earth-based paste, CEM, and SCEC mixtures were then established.

Keywords: Clay; Concrete-equivalent mortar; Rheology; Self-consolidating earth concrete; Thixotropy.

6.1 Introduction

Earth construction goes back to 100 centuries ago and is still used worldwide under different climate conditions [1]. This technique includes cob, mud and adobe masonry bricks, and rammed-earth construction. Environmental-friendly earth construction can be a solution to address the global climate-change concern, because of their availability, durability, economic, and thermal comfort [2]. Cement-stabilized earth or soil, mostly used for wall applications, is widely used as layer-by-layer casting and renowned as rammed-earth (RE) with favorable performance [3]. However, RE construction process which necessitate application of mechanical consolidation to achieve targeted performance is time-consuming along with deficiencies due to its layer-by-layer nature [4]. Self-consolidating earth concrete (SCEC) can be an alternative to address these abovementioned defects while preserving the advantages of RE technique.

Self-consolidating concrete (SCC) is typically proportioned with relatively higher volume of paste (V_P) than conventional concrete to improve workability. Supplementary cementitious materials are therefore used to partially replace cement and reduce the clinker factor of SCC. In the case of

SCEC, the binder system consist generally in a ternary mixture of very fine clay and silt particles contained in earth, in addition to cement [5–7]. Different test measurements are employed to identify the key characteristics of clay and silt constituents of the binder to help classifying soils given the application on hand. The Atterberg limits of soil are highly influenced by the type and content of clay which can be useful in classifying soil behaviors in presence of water [8–11]. Suspensions containing high volumetric content of fine particles generally exhibit high yield stress and plastic viscosity values due to high interparticle frictions [12–14]. The use of high-range water-reducer (HRWR) is therefore necessary to achieve good deformability of SCEC mixtures containing fine clay particles. Ensuring good compatibility between the HRWR and ternary binder system in SCEC matrix is essential to ensure proper dispersion of fine particles [7] and achieve adequate workability. The efficiency of polycarboxylate-ether (PCE) based superplasticizers on ternary binder system of SCEC has been reported in literature [6]. On the other hand, inorganic dispersing agents, such as sodium hexametaphosphate (NaHMP), were also found very effective to disperse clay particles by electrostatic repulsion forces [15–17]. Therefore, evaluating rheology of SCEC mixtures proportioned with different types and content of clay, as well admixture types can be of interest to achieve adapted rheology given the application on hand.

Various rheometric approaches were proposed to evaluate the rheological properties and structural build-up of cementitious materials [18,19]. These measurements are affected by various physicochemical synergies, including flocculation of the binder particles and nucleation of hydration products. These are dependent on the binder compositions, solid concentration, existence of colloidal particles, as well as the type and dosage of admixtures [18]. In the case of mortar and concrete mixtures, the volumetric content and particle-size distribution (PSD) of aggregate can significantly affect the rheological measurements [20]. The effect of these influencing parameters can be reflected by the viscoplastic properties, including yield stress and plastic viscosity. The evaluation of static yield stress of cementitious materials is challenging due to the effect of the adopted testing protocol, shear history, elapsed time, and ambient conditions [21]. In the case of ternary binder system of SCEC, the applied shear protocol is even more important due to the risk of liquid phase migration [22]. The growth of static yield stress, namely thixotropic coefficient A_{thix}, was employed to evaluate the structuration [18,23,24]. This is defined by the area between the ascending and descending flow curves, obtained using the hysteresis loops (rebuilding energy) at various intervals, and used as an indication of structuration kinetics [25,26].

Moreover, selection of the geometry is critical to limit wall-slip and liquid phase migration risks [27,28]. Using coaxial geometry limits the maximum aggregate size, while the results of parallel-plates rheometry is questionable due to the evaporation and wall-slip risk [29,30]. However, regarding the shortcomings of coaxial geometry, using parallel-plates can be more favorable to measure the rheological properties of earth-based suspensions due to the presence of silt particles (up to 75 μm).

The concrete equivalent mortar (CEM) approach has been widely used to predict the performance of its corresponding concrete. The CEM mixtures are proportioned to achieve the same surface area of coarse and fine aggregate existing in its corresponding concrete mixture [31]. The CEM approach was widely used to simulate different properties of concrete in fresh and hardened states. This approach was successfully used to simulate the interaction between the binders and admixtures, and evaluate the robustness of the workability and rheological properties of SCC mixtures [32]. Strong relationships between the fresh and hardened properties of CEM and concrete were proposed [31,33,34]. The established correlations can facilitate the optimization process and reduce the number of trial batches and materials. Although in the conventional CEM approach the surface area of aggregate is maintained constant, the EP thickness can change due to packing density of coarse and fine aggregate. This can therefore negatively affect the accuracy of the conventional CEM to reproduce the workability and rheology of concrete mixtures. The excess paste (EP) concept was also introduced to improve the capability of CEM to predict the properties of concrete [35,36]. Therefore, CEM approach can be beneficial to be considered from two different perspectives, including (i) conformity of this approach in the case of SCEC and (ii) rheology of each CEM mixture can be considered as an independent representative of another SCEC mixture, since earth particles are commonly consisted in finer particles compared to conventional concrete.

In this context, a new CEM approach that considers the EP thickness is proposed in this study. Accordingly, the coupled effect of binder constituents, including type and content of clay, cement content, water-to-powder ratio, volume of paste, EP thickness, volumetric sand-to-total aggregate ratio, and admixture type on rheology and thixotropy of paste, CEM, and SCEC mixtures is investigated using the proposed CEM approach. The significance of key parameters affecting the rheological behavior of multiscale self-consolidating earthen-cementitious suspensions was

highlighted. Various empirical models were established to predict the rheological behavior of self-consolidating earth-based paste mixtures from their workability parameters. Accordingly, the rheological properties of the CEM and SCEC mixtures were predicted as functions of the characteristics of their corresponding paste and CEM mixtures, respectively.

6.2 Methodology

6.2.1 Materials and testing methods

Two different clay types were used, including a pure kaolinite with specific surface area (SSA) of 15 m^2/g and specific gravity of 2.73 (Type I), and a combination of 50% kaolinite and 50% attapulgite (wt. % by mass) having SSA of 155 m^2/g and specific gravity of 2.75 (Type II). A general use Portland cement (GU) and quartz silt powder (2 to 75 µm) with specific gravities of 3.15 and 2.69, respectively, were used. Two common inorganic dispersant agents in clay industry were used, including high purity sodium hexametaphosphate (NaHMP) with solid ratio of 37.1% and sodium silicate solution (NaSil) with 10.6% Na_2O, 26.5% SiO_2, and 72.9% H_2O (wt.% by mass). Three commonly used HRWR admixtures in concrete industry, including polycarboxylate ether (PCE), sodium polynaphtalene (PNS), and non-esterified polycarboxylate (NE-PC) were also employed. The aggregate used to proportion the investigated SCEC mixtures included natural river sand (0-5 mm) and crushed limestone gravel (5-10 mm) with specific gravities of 2.67 and 2.72 and water absorptions of 1.09% and 0.42%, respectively. The PSDs of the aggregates are presented in Fig. 6.1.

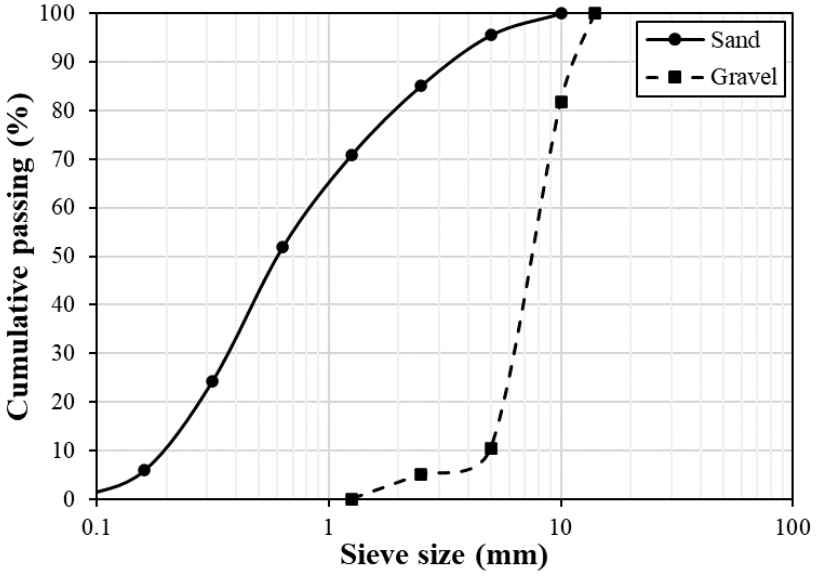

Fig. 6.1. Particle-size distributions of the sand and gravel.

The rheological behavior of the investigated SCEC mixtures was investigated using the proposed concrete-equivalent mortar (CEM) approach. As mentioned earlier, in the case of conventional CEM method, only the total surface area of aggregate is constant [33,35], while the change in packing density of granular skeleton (sand and gravel) to that of sand has been neglected. As can be observed in Fig. 6.2, for a unit volume of concrete, only a given paste volume, namely compacted volume of paste (V_{CP}), is required to fill the voids between the compacted aggregate (V_{CA}), since the volumetric fraction of aggregates (φ) in concrete is lower than its packing density (φmax). The remaining paste, referred to the excess volume of paste (V_{EP}), contributes to improving the flowability of the mixture by reducing the interparticle frictions. The excess volume of paste ($V_{EP} = 1- \frac{\varphi}{\varphi_{max}}$) can be calculated using the ratio of the volumetric content of aggregates-to-their packing density ($\frac{\varphi}{\varphi_{max}}$), namely relative-solid packing fraction [37]. The required sand content to proportion the new proposed CEM mixture with similar excess paste thickness (e_{EP}) to that of its corresponding concrete mixture can be calculated as follow:

$$e_{EP\text{-}CEM} = e_{EP\text{-}Concrete} \Longrightarrow \frac{V_{EP\text{-}CEM}}{A_{eq:\,sand}} = \frac{V_{EP\text{-}Concrete}}{A_{sand+gravel}} \Longrightarrow \frac{1-\frac{\varphi_{eq:sand}}{\varphi_{max:sand}}}{A_{eq:sand}} = \frac{1-\frac{\varphi_{sand+gravel}}{\varphi_{max:sand+gravel}}}{A_{sand+gravel}} \quad (6.1)$$

where $\varphi_{sand+gravel}$, $\varphi_{eq:sand}$, $\varphi_{max:sand+gravel}$, $\varphi_{max:sand}$, $A_{sand+gravel}$, and $A_{eq:sand}$ are the volumetric content, packing density, and surface area of aggregate in SCEC (sand and gravel) and its corresponding CEM mixture (sand), respectively. In order to ensure higher accuracy of the aggregates' morphology, the 3D surface area-to-volume ratio (A_{3D}/V) of sand and gravel particles was evaluated using Max3D laser scanner and X-ray micro-CT scanner for different aggregate subclasses of sand and gravel, corresponding to the standard sieves, larger and smaller than 1.25 mm, respectively. According to the image analyses results, the A_{3D}/V ratios of 21583.4 and 859.8 m^2/m^3 were obtained for the sand and gravel particles used in this study, respectively.

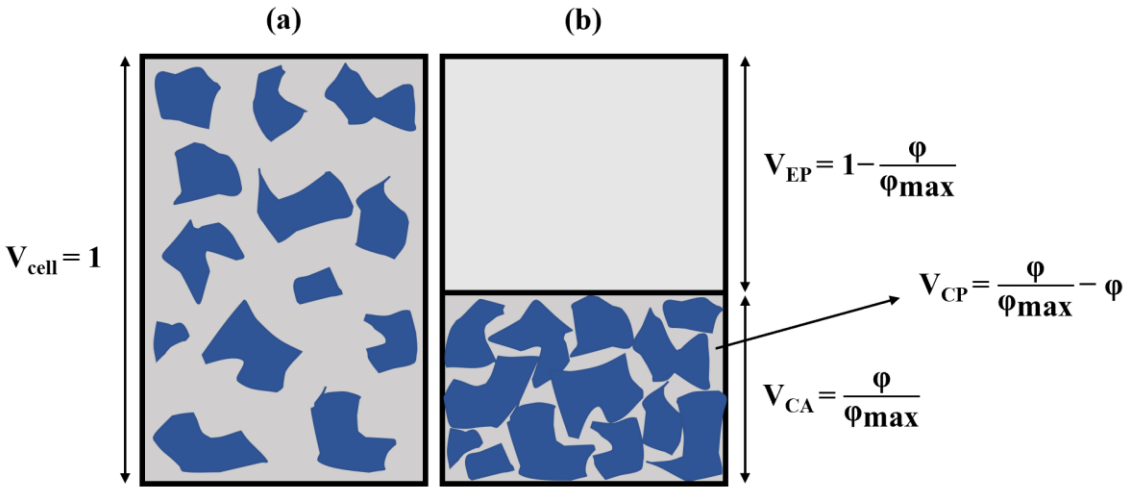

Fig. 6.2. (a) Schematic of a unit volume of concrete (V_{cell} = 1) as a suspension of sand and gravel particles in paste and (b) excess volume of paste (V_{EP}), compacted aggregates (V_{CA}), and compacted paste volume (V_{CP}).

The paste and mortar mixtures were prepared using a planetary Hobart mixer conforming to the ASTM C305 specifications [38]. The mini-slump flow (MSF) [39] of paste and CEM mixtures was assessed at 0, 30, and 60 min after mixing. Mini-V-funnel (MVF) [40] and marsh cone (MCT) [41] tests were also employed to evaluate the flowability of the investigated mortar and paste mixtures, respectively. Workability of concrete mixtures were evaluated using the slump flow (SF) [40] and V-Funnel [42] tests. The Atterberg limit tests, including the liquid limit (LL), plastic limit (PL), and plasticity index (PI = LL - PL), were carried out according to the ASTM D4318 specifications [43] to characterize the soil (i.e., clay, silt, and sand < 425 µm). Rheometric tests were conducted on the investigated paste mixtures using the Anton Paar MCR 302 rheometer with parallel-plates geometry, as shown in Fig. 6.3. It should be noted that coaxial geometry could not be employed due to the presence of silt particles up to 75 µm. The viscoplastic properties of the paste mixtures were measured using a shearing protocol that consists in applying a pre-shearing of 150 s^{-1} for 120 s, followed by stepwise descending regime to a shear rate of 1 s^{-1} during 105 s, as shown in Fig. 6.4a.

Moreover, a hysteresis-loop shearing protocol was applied to evaluate the thixotropy of the paste mixtures, as shown in Fig. 6.4b. This consists in applying a pre-shearing of 50 s^{-1} for 30 s, followed by a 30-s resting period (0 s^{-1}). After the resting period, the shear rate values increased step-wise from 0.1 s^{-1} to 150 s^{-1} during 90 s, followed by a step-wise shear-rate reduction to its initial value 0.1 s^{-1} for another 90-s period [44–46]. The enclosed area between the increasing (Up) and

decreasing (Down) shear stress-shear rate curves was then calculated and used to assess the breakdown and thixotropy of the investigated paste mixtures [47]. On the other hand, the ConTec 5 and 6 viscometers were used to evaluate the rheological properties of the investigated concrete mixtures and their corresponding CEMs, respectively. The Bingham and Herschel-Bulkley models were applied to estimate the rheological parameters of the investigated mixtures, as follow:

$$\text{Bingham model: } \tau = \tau_0 + \mu_p \times \dot{\gamma} \quad (6.2)$$

$$\text{Herschel-Bulkley model: } \tau = \tau_0 + k \times \dot{\gamma}^n \quad (6.3)$$

where τ, τ_0, μ_p, $\dot{\gamma}$, k, and n are shear stress, yield stress, plastic viscosity, shear rate, consistency, and pseudoplastic indices, respectively. It must be also noted that the viscoplastic and thixotropic measurements were carried out at 0, 30, and 60 min after mixing.

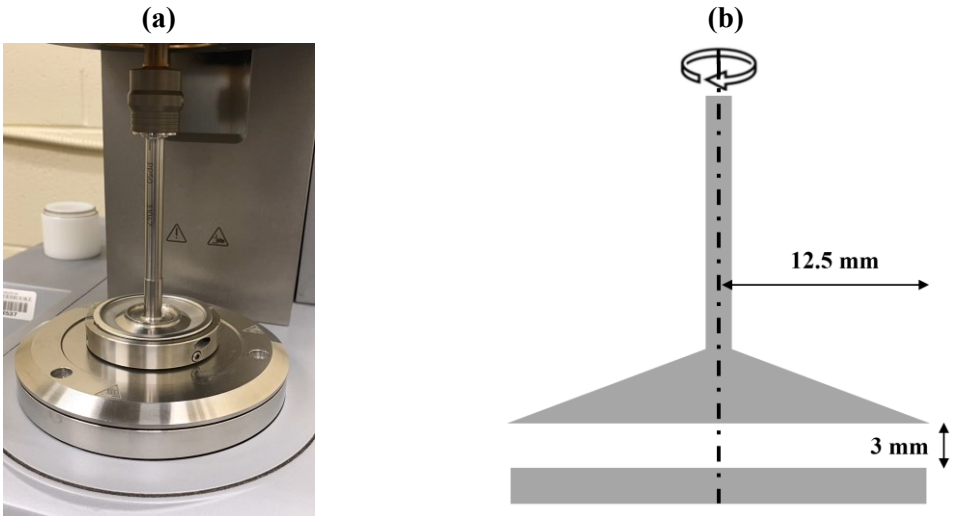

Fig. 6.3. (a) AntonPaar rheometer with parallel-plate geometry and (b) schematics of the parallel-plates system geometry.

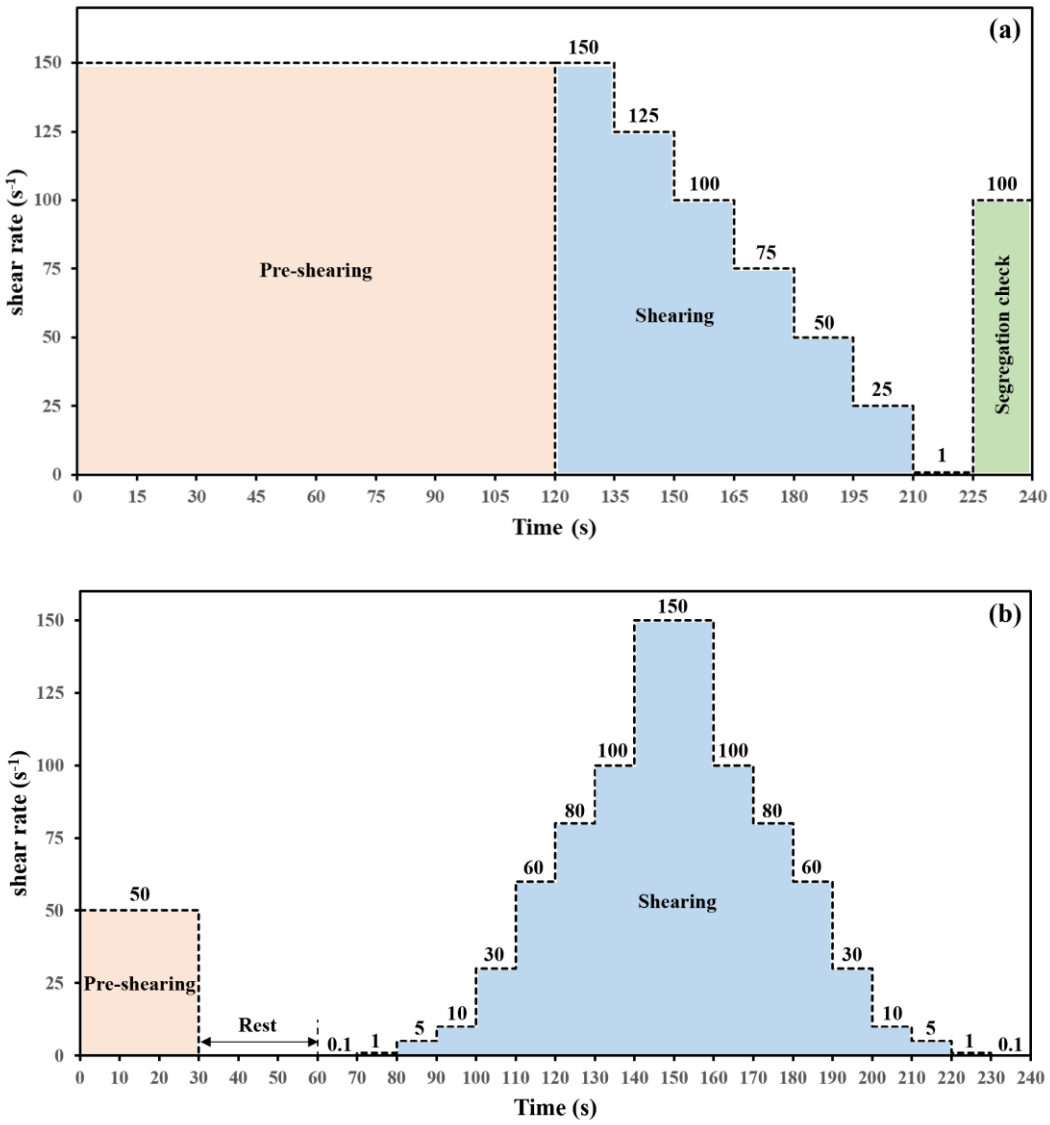

Fig. 6.4. Shear protocol employed to assess (a) viscoplastic properties and (b) thixotropy of the investigated paste mixtures.

6.2.2 Materials and testing methods

As summarized in Table 6.1, 5 different cement contents, paste volumes (V_P), water-to-powder (W/P), cement-to-clay (Ce/Cl, by mass), and volumetric sand-to-total aggregate (S/A) ratios, and 5 different types of admixtures were investigated in this study. Moreover, two clay types with highly different fineness were selected to cover a wide range of soil types. As can be observed in Table 6.1, the investigated V_P values are relatively higher than those in conventional SCC mixtures to simulate the presence of ternary binder system existing in the earth concrete (clay, cement, and silt). Moreover, wide ranges of W/P (0.30 to 0.50) and Ce/Cl (0.50 to 1.50) were investigated.

Furthermore, different S/A ratios of 0.5 to 0.9 were selected to investigate the effect of aggregate packing on rheological properties of the SCEC mixtures. The synergy of the binders used with two inorganic dispersants and three common superplasticizers on rheology of the investigated mixtures was studied. Based on the Taguchi orthogonal array L50 ($2^1 \times 5^6$), 50 experiments were conducted to evaluate the coupled effect of the abovementioned factors on rheological behavior of the investigated SCEC mixtures.

Table 6.1. Investigated parameters and their corresponding levels to proportion the investigated SCEC mixtures [7].

Levels	Factors						
	Clay type	Cement content (kg/m^3)	V_P (%)	W/P	Ce/Cl	S/A	Admixture type
1	Type I	60	45	0.30	0.50	0.5	NaHMP
2	Type II	90	48	0.35	0.75	0.6	NaSil
3	-	120	51	0.40	1.00	0.7	PCE
4	-	150	54	0.45	1.25	0.8	PNS
5	-	180	57	0.50	1.50	0.9	NE-PC

First, eighteen paste mixtures were selected out of the 50 investigated mixtures [7] to proportion the CEM mixtures, based on their 1-day compressive strength (> 1 MPa) and admixture demand to achieve a targeted MSF of 280 ± 20 mm. Similarly, the MSF values of the 18 selected CEM mixtures were assessed to secure the targeted MSF of 280 ± 20 mm. Finally, according to the CEM results, three SCEC mixtures were selected. It is worthy to mention that only the SCEC mixtures proportioned with PCE were chosen to avoid complexity of admixture-type effect on the rheological results. Moreover, a reference concrete mixture (C_{ref}) and its corresponding CEM (M_{ref}) were also investigated. These mixtures were proportioned with PCE and without any clay content. The mixture proportioning of the investigated paste (P), CEM (M), and SCEC (C) mixtures are summarized in Table 6.2.

6.3 Results and discussion

6.3.1 Rheology of paste mixtures

The Atterberg limits of the investigated soils (clay, silt, and sand < 425 μm) and thixotropy indices of their corresponding paste mixtures are summarized in Table 6.3. Atterberg limits were used as an indication of the binder contribution on soil behavior. Wide ranges of LL (15.7%–36.5%), PL (14.5%–23.6%), and PI (1.2%–13.3%) ensured a comprehensive investigation of various earth types. On the other hand, the evolution rate of the static yield stress, reflected by the thixotropic coefficient A_{thix}, was used to assess the kinetics of structuration [18,24]. For instance, the hysteresis loops of the mixtures P44 and P49, determined immediately after mixing (i.e., t = 0), are illustrated

in Fig. 6.5a and 6.5b, respectively. As can be observed, in the case of P44, the descending shear stress values were lower than the ascending ones, hence reflecting a thixotropic behavior. However, in the case of P49, a rheopectic behavior, reflected by higher descending shear stresses compared to the ascending ones, was observed. The enclosed area between the upward and downward steps was calculated for all the investigated mixtures. It should be noted that positive and negative values refer to thixotropic and rheopectic behaviors, respectively.

Table 6.2. Proportioning of the investigated paste, CEM, and SCEC mixtures.

	Mix No.	Admixture type	Cement (kg/m³)	Water (kg/m³)	Clay (kg/m³)		Silt (kg/m³)	W/P	V_P (%)	Sand (kg/m³)	Gravel (kg/m³)	S/A	e_{EP} (μm)
					Type I	Type II							
Paste	P6	NE-PC	200.0	490.7	173.3	-	1028.5	0.35	-	-	-	-	-
	P10	PNS	157.9	450.9	182.5	-	1162.5	0.30	-	-	-	-	-
	P11	PNS	266.7	526.2	154.1	-	894.9	0.40	-	-	-	-	-
	P12	NE-PC	250.0	556.3	433.3	-	553.0	0.45	-	-	-	-	-
	P15	PCE	210.5	490.9	146.0	-	1046.0	0.35	-	-	-	-	-
	P16	PCE	333.3	558.7	385.2	-	523.0	0.45	-	-	-	-	-
	P17	PNS	312.5	584.1	270.8	-	584.9	0.50	-	-	-	-	-
	P18	NE-PC	294.1	454.2	203.9	-	1016.0	0.30	-	-	-	-	-
	P22	PCE	375.0	456.2	216.7	-	929.1	0.30	-	-	-	-	-
	P23	PNS	352.9	495.8	611.8	-	452.0	0.35	-	-	-	-	-
	P24	NE-PC	333.3	528.8	385.2	-	603.4	0.40	-	-	-	-	-
	P25	NaHMP	315.8	557.8	273.7	-	650.1	0.45	-	-	-	-	-
	P26	PNS	133.3	450.1	-	92.4	1274.4	0.30	-	-	-	-	-
	P32	PNS	187.5	524.2	-	216.7	906.3	0.40	-	-	-	-	-
	P37	PCE	250.0	555.6	-	173.3	811.3	0.45	-	-	-	-	-
	P44	PNS	277.8	492.9	-	240.7	889.7	0.35	-	-	-	-	-
	P45	NE-PC	263.2	526.2	-	182.5	869.9	0.40	-	-	-	-	-
	P49	PCE	333.3	528.2	-	192.6	794.6	0.40	-	-	-	-	-
CEM	M6	NE-PC	100.0	245.3	86.7	-	514.2	0.35	45	1197.2	-	1	40.2
	M10	PNS	101.6	290.1	117.4	-	748.0	0.30	57	815.6	-	1	88.4
	M11	PNS	149.3	294.6	86.2	-	500.9	0.40	45	1038.0	-	1	56.0
	M12	NE-PC	139.6	310.7	242.0	-	308.8	0.45	48	1041.6	-	1	55.6
	M15	PCE	147.0	342.8	101.9	-	730.4	0.35	57	669.6	-	1	121.4
	M16	PCE	157.7	264.3	182.2	-	247.4	0.45	45	1268.7	-	1	34.4
	M17	PNS	192.8	360.4	167.1	-	360.9	0.50	48	885.6	-	1	76.5
	M18	NE-PC	181.5	280.4	125.9	-	627.2	0.30	51	885.1	-	1	76.5
	M22	PCE	198.7	241.7	114.8	-	492.2	0.30	48	1117.7	-	1	47.6
	M23	PNS	188.1	264.3	326.1	-	240.9	0.35	51	1109.1	-	1	48.4
	M24	NE-PC	224.1	355.5	259.0	-	405.7	0.40	54	738.4	-	1	104.2
	M25	NaHMP	212.0	374.5	183.7	-	436.4	0.45	57	741.4	-	1	103.5
	M26	PNS	63.1	212.9	-	43.7	602.9	0.30	45	1268.7	-	1	34.4
	M32	PNS	99.3	277.7	-	114.8	480.2	0.40	48	1117.7	-	1	47.6
	M37	PCE	147.2	327.2	-	102.1	477.8	0.45	48	960.3	-	1	65.6
	M44	PNS	179.1	317.8	-	155.2	573.6	0.35	54	812.1	-	1	89.1
	M45	NE-PC	169.3	338.6	-	117.4	559.7	0.40	57	815.6	-	1	88.4
	M49	PCE	187.6	297.3	-	108.4	447.2	0.40	54	1030.1	-	1	56.9
	M_{ref}	PCE	818.7	327.5	-	-	-	0.40	45	964.5	-	1	65.1
SCEC	C16	PCE	150.0	251.4	173.3	-	235.3	0.45	45	1197.0	136.0	0.9	34.4
	C22	PCE	180.0	219.0	104.0	-	445.9	0.30	48	1000.2	255.7	0.8	47.6
	C37	PCE	120.0	266.7	-	83.2	389.4	0.45	48	750.1	511.4	0.6	65.6
	C_{ref}	PCE	627.2	250.9	-	-	-	0.40	45	665.0	680.0	0.5	65.1

Table 6.3. Atterberg limits of the earths used (clay, silt, and sand < 425 μm) and thixotropy indices of the investigated paste mixtures.

Mix No.	Clay type	Admixture type	Atterberg limits			A_{thix} (Pa/s)		
			LL (%)	PL (%)	PI (%)	0 min	30 min	60 min
P6	Type I	NE-PC	15.7	14.5	1.2	153	242	151
P10		PNS	18.6	16.9	1.7	-47	-96	-674
P11		PNS	18.1	16.6	1.5	-371	-501	-607
P12		NE-PC	20.1	14.6	5.5	174	200	176
P15		PCE	17.5	16.2	1.3	-145	-117	-77
P16		PCE	18.9	14.9	4	-100	-109	-90
P17		PNS	19.5	15.7	3.8	-602	-642	-711
P18		NE-PC	19.9	16.3	3.6	214	112	120
P22		PCE	18.9	15.8	3.1	223	241	272
P23		PNS	21.5	14.8	6.7	-76	-118	-109
P24		NE-PC	21.6	14.5	7.1	101	78	68
P25		NaHMP	20.5	15.6	4.9	-1138	-1003	-1517
P26	Type II	PNS	21.5	18.3	3.2	636	710	1296
P32		PNS	30.8	23.6	7.2	182	-242	-2375
P37		PCE	32.8	21.8	11	-1628	-1664	-1967
P44		PNS	36.5	23.2	13.3	1123	1322	1413
P45		NE-PC	34.6	22.8	11.8	604	469	440
P49		PCE	31.5	20.5	11	-2629	-2695	-2740

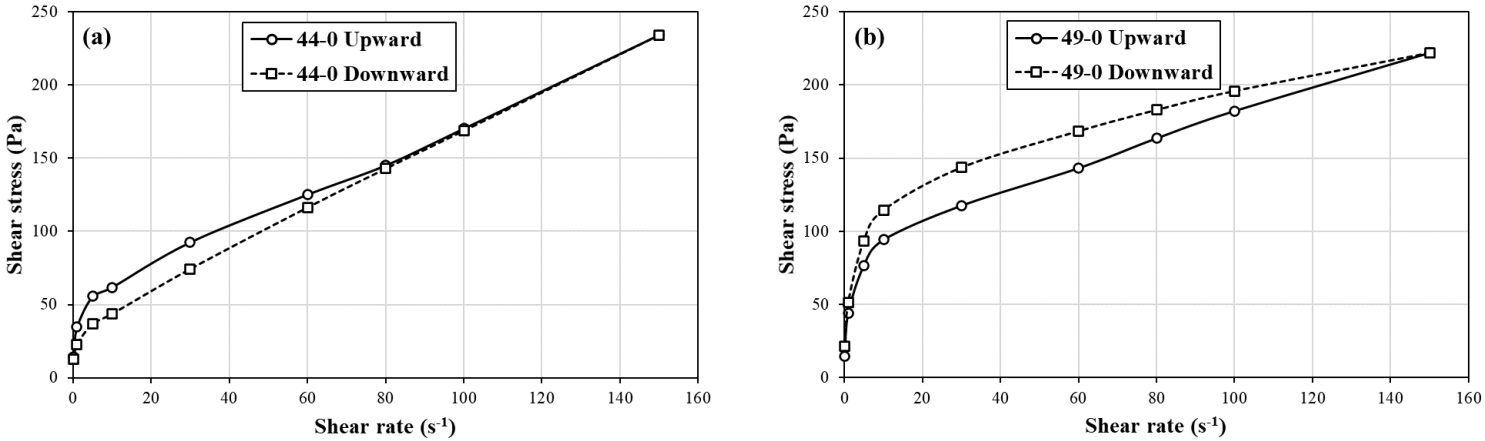

Fig. 6.5. The hysteresis loops observed for (a) P44 (thixotropy) and (b) P49 (rheopexy) paste mixtures at t = 0.

According to the obtained A_{thix} values, the thixotropic and rheopectic behaviors of the investigated mixtures were mostly dictated by the admixture type. Accordingly, all the NE-PC-based mixtures showed thixotropic behavior ($A_{thix} > 0$). Moreover, in addition to the mixture P22, proportioned with the lowest W/P ratio and containing PCE admixture, all the mixtures proportioned with PNS admixture and Clay Type II showed thixotropic behavior. The mixture P44, containing the highest content of Clay Type II, showed the highest thixotropy response, while the highest rheopectic response was observed for the P49 mixture followed by the P37 and P25 mixtures. In fact, the P49 and P37 paste mixtures made with PCE and Clay Type II, while the mixture P25 was the only system dispersed with NaHMP. Furthermore, the Clay Type II having higher Atterberg limits exhibited higher magnitude of thixotropic/rheopectic response. It is worth mentioning that the behavior of P32 changed over time from thixotropic to highly rheopectic. This mixture was proportioned with the highest W/P ratio among the thixotropic PNS-based mixtures. This suggests that the type of admixture and its synergy with clay type had a dominant effect on the structuration of earth-based paste mixtures, followed by the W/P ratio.

The thixotropy indices of the investigated paste mixtures are presented in Fig. 6.6 for different types of admixtures. As can be observed in Fig. 6.6a, all the PCE-contained paste mixtures showed a rheopectic behavior (negative A_{thix} values), excluding P22 proportioned with the lowest W/P ratio of 0.30. This suggests that low W/P ratio can lead to thixotropic behavior in presence of PCE admixture. Moreover, the mixtures contained Clay Type II showed significantly higher A_{thix} values due to their higher specific surface area. On the other hand, as shown in Fig. 6.6b, the PNS-based paste mixtures proportioned with Clay Types I and II showed rheopectic and thixotropic behaviors, respectively. Moreover, the mixtures P10 and P23 showed the lowest rheopexy values due to their low W/P ratios among the PNS-Clay Type I-based paste mixtures. Among the mixtures proportioned with Clay Type II and PNS admixture, the thixotropic behavior of the mixture P32 turned to rheopectic over time. This can be due to its higher W/P ratio compared to the mixtures P26 and P44, despite its comparable clay content. Furthermore, the highest A_{thix} rates over time were obtained for the mixtures P10 and P26 proportioned with the lowest W/P ratio of 0.30.

As can be observed in Fig. 6.6c, all the NE-PC-based paste mixtures showed lower thixotropic indices (A_{thix} values) compared to those made with PCE and PNS. Among the NE-PC mixtures, the highest A_{thix} value was obtained for the mixture P45, as the only mixture proportioned with

Clay Type II. However, the consistency of A_{thix} magnitude over time remained questionable and needs to be further investigated. The only system dispersed with NaHMP (P25) showed a highly rheopectic behavior comparable to that of the PCE-based paste mixtures proportioned with Clay Type II. The high rheopectic behavior observed for the mixture P25 can be attributed to the synergy between the NaHMP and Clay Type I.

The workability and rheological results of the investigated paste mixtures are summarized in Table 6.4. The flow curves were evaluated using both Bingham and Herschel-Bulkley models. As can be observed, all the investigated earth-based paste mixtures exhibited shear-thinning behavior, reflected by pseudoplastic indices "n" lower than 1, excluding the mixture P23 proportioned with the highest content of Clay Type I ($n_{P23} = 1.06$). However, it must be noted that the use of Bingham model led to coefficient of determinations R^2 higher than 0.94, excluding the mixtures P17, P25, P37, and P49 which showed the highest rheopectic behavior. Moreover, relatively high consistency indices "k" were obtained for these mixtures. The Bingham parameters were used to assess the evolution of viscoplastic properties (yield stress and plastic viscosity) of all the investigated mixtures because of its conformity with the majority of mixtures. Furthermore, significantly high yield stress and plastic viscosity values were obtained for the mixture P25 made with NaHMP. This can be attributed to the synergy between NaHMP and the ternary binder system (cement, clay, and silt). The clay type showed the second degree of significance on rheological parameters. Accordingly, high viscoplastic properties were obtained for the mixtures proportioned with the Clay Type II.

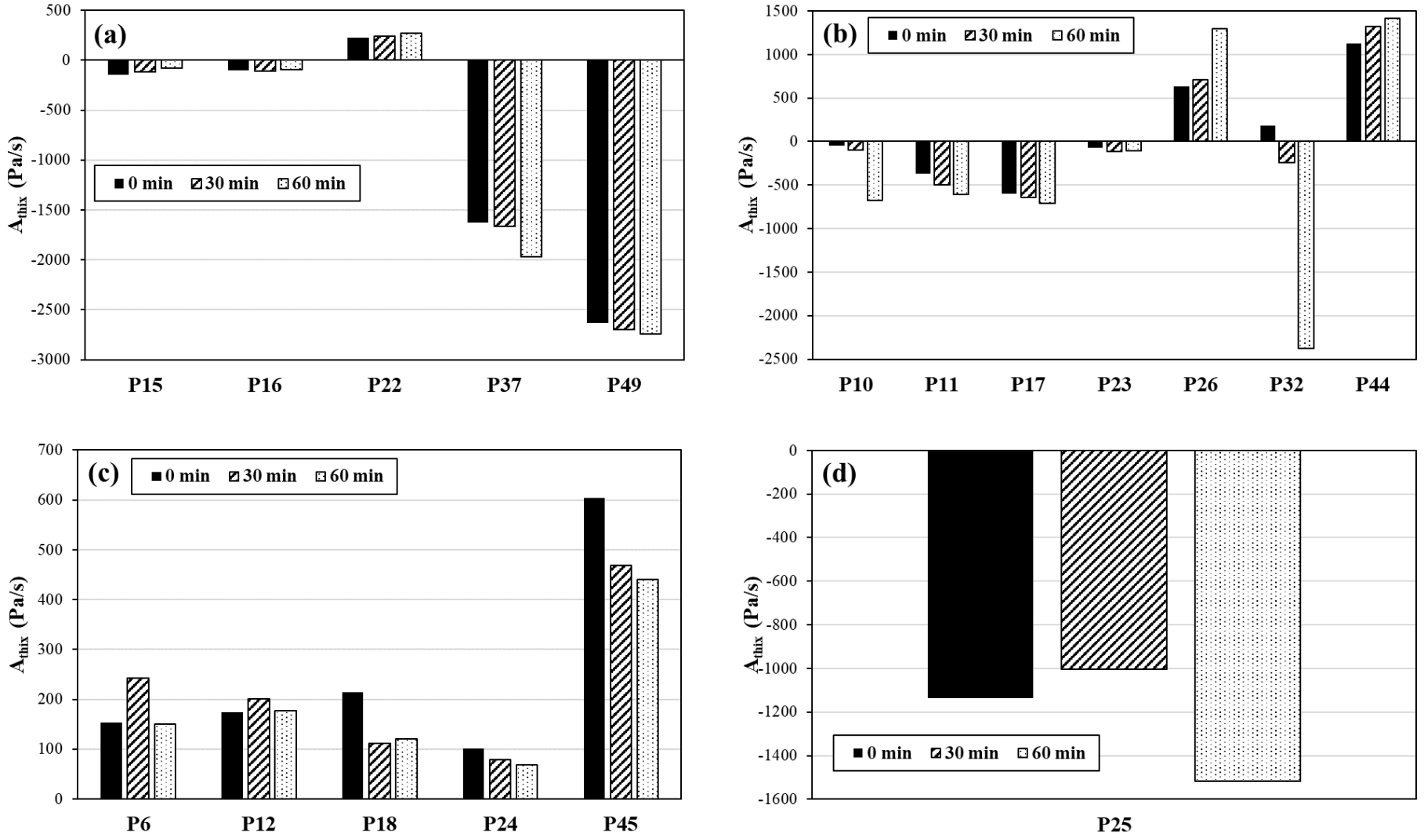

Fig. 6.6. A_{thix} values of the investigated paste mixtures proportioned with (a) PCE, (b) PNS, (c) NE-PC, and (d) NaHMP admixtures.

Table 6.4. Workability and rheological properties of the investigated paste mixtures.

Mix No.	Clay type	Admixture type	MSF (mm)			MCT (s)	Bingham model						Herschel-Bulkley model								
							0 min		30 min		60 min		0 min			30 min			60 min		
			0 min	30 min	60 min	0 min	τ_0 (Pa)	μ_p (Pa.s)	τ_0 (Pa)	μ_p (Pa.s)	τ_0 (Pa)	μ_p (Pa.s)	τ_0 (Pa)	k (Pa.s^n)	n	τ_0 (Pa)	k (Pa.s^n)	n	τ_0 (Pa)	k (Pa.s^n)	n
P6	Type I	NE-PC	286	272	267	27	3.8	0.42	3.3	0.42	4.0	0.42	2.2	0.68	0.91	1.9	0.63	0.92	2.2	0.69	0.90
P10		PNS	292	209	189	29.0	9.9	0.87	18.9	0.97	31.9	1.19	4.2	1.83	0.85	8.4	3.02	0.78	13.2	5.47	0.71
P11		PNS	281	234	205	11.0	18.2	0.29	22.8	0.32	29.5	0.38	8.4	3.64	0.52	8.8	5.90	0.45	1.0	15.51	0.32
P12		NE-PC	293	277	261	25.0	14.0	0.17	15.6	0.18	19.5	0.19	11.6	0.70	0.73	13.1	0.73	0.73	15.8	1.11	0.66
P15		PCE	279	260	248	17.0	10.8	0.43	14.1	0.46	18.0	0.53	6.1	1.37	0.78	7.6	1.86	0.73	8.5	2.82	0.68
P16		PCE	280	231	213	21.0	17.0	0.18	19.5	0.20	22.4	0.22	13.1	1.21	0.63	14.8	1.52	0.61	16.9	1.84	0.59
P17		PNS	283	221	209	11.0	43.8	0.29	48.2	0.37	61.6	0.46	0.0	29.08	0.21	0.0	30.29	0.24	0.0	39.16	0.23
P18		NE-PC	286	270	252	26.0	6.5	0.80	6.6	0.80	8.6	0.87	2.7	1.38	0.89	2.9	1.38	0.89	3.6	1.68	0.87
P22		PCE	283	256	238	36.0	10.0	0.65	11.0	0.71	13.1	0.75	2.9	2.04	0.78	7.5	1.27	0.89	8.6	1.49	0.87
P23		PNS	295	195	148	41.0	3.9	0.53	8.0	0.58	10.1	0.67	5.1	0.40	1.06	4.8	1.11	0.87	10.8	0.58	1.03
P24		NE-PC	286	267	238	28.0	11.6	0.23	13.2	0.24	16.5	0.26	9.7	0.56	0.83	10.9	0.67	0.80	13.7	0.83	0.78
P25		NaHMP	294	100	100	81.0	114.6	0.97	123.9	1.32	127.9	1.43	0.0	70.28	0.25	0.0	71.85	0.29	0.0	73.06	0.29
P26	Type II	PNS	276	249	219	16.0	7.4	1.18	10.6	1.28	21.9	1.50	1.7	2.08	0.89	3.7	2.39	0.88	8.4	3.97	0.81
P32		PNS	282	250	216	45.0	33.4	0.67	65.0	0.80	133.1	1.06	22.0	3.37	0.69	31.4	13.78	0.47	0.0	88.57	0.22
P37		PCE	286	259	237	56.0	60.3	0.59	74.7	0.73	94.6	0.88	0.0	36.88	0.26	0.0	45.72	0.26	0.0	58.89	0.25
P44		PNS	269	239	219	61.0	26.1	1.40	34.8	1.47	51.6	1.57	17.7	2.79	0.87	24.6	3.22	0.85	37.0	4.29	0.81
P45		NE-PC	284	269	250	34.0	16.2	0.58	13.2	0.58	13.3	0.61	10.7	1.61	0.80	8.3	1.46	0.82	8.4	1.49	0.83
P49		PCE	272	163	138	51.0	76.3	0.84	113.5	1.21	131.1	1.37	0.0	44.60	0.29	0.0	67.17	0.28	0.0	78.23	0.28

Flow curves of the investigated paste mixtures with the non-linear viscoplastic behavior are presented in Fig. 6.7. Despite of the comparable mixture constituents, the mixtures P25 (NaHMP admixture) and P17 (PNS admixture) exhibited the highest and lowest rheological parameters, respectively. The presence of PNS in the mixture P17 proportioned with the highest water content can lead to non-linear viscoplastic behavior. It is worth mentioning that the mixture P17 made with Clay Type I having low PI value of 3.8%. This suggests that the observed non-linearity is not due to the type and content of clay used. However, the clay type and content significantly affected the rheological behavior of the PCE mixtures. Accordingly, the mixtures P37 and P49, exhibiting the highest PI values (11% for both) among the PCE-based mixtures, showed significant nonlinear viscoplastic behavior, even more than the mixture P17. The high PI can reflect the high specific surface area of their incorporated earth, which induces higher water absorption, nucleation promotion, and flocculation [24]. This must also be noted that the effect of very fine particles on stiffening can be attenuated due to the breakage of the flocs [48]. Therefore, the admixture type and its sensitivity to clay or water content dictate the rheological behavior of the self-consolidating paste mixtures.

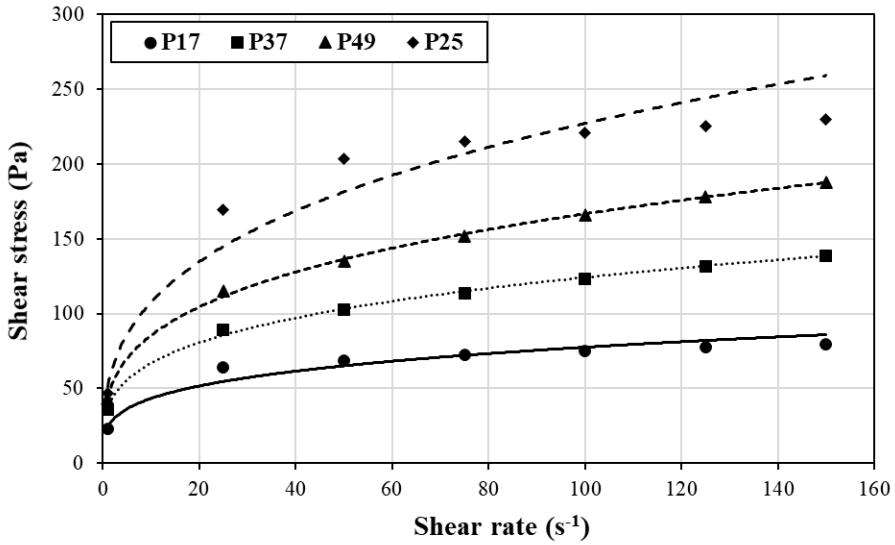

Fig. 6.7. Flow curves of the paste mixtures P17, P37, P49, and P25.

It is worth mentioning that all the rheological measurements were carried out on the paste mixtures having a MSF of 280 ± 20 mm. The Bingham yield stress and plastic viscosity of the PCE paste mixtures are presented in Fig. 6.8. As can be observed, the mixtures P37 and P49 made with Clay

Type II showed the highest yield stress values due to the significant effect of Clay Type II. Although the use of Herschel-Bulkley model resulted in better fitting, the Bingham parameters were discussed here for comparison purposes. The PI values of the incorporated earths showed a significant effect on yield stress values of the PCE-based mixtures. For example, the mixture made with Clay Type I and in presence of PCE HRWR exhibited comparable yield stress values for the PCE-systems proportioned with Clay Type I which have shown comparable PI values. All these mixtures exhibited yield stress values less than 20 Pa and low increasing rate. However, the highest yield stress value among the PCE-Clay Type I-based mixtures was obtained for the mixture P16 with relatively higher PI value than the P15 and P22 mixtures. On the other hand, the plastic viscosity values were found highly affected by W/P ratio. As can be observed in Fig. 6.8, among the PCE mixtures proportioned with Clay Types I and II, the P16 and P22 (Clay Type I), and P37 and P49 (Clay Type II) showed the lowest and highest plastic viscosity values, respectively, which is probably due to the W/P ratios. Hence, this can be concluded that the yield stress and plastic viscosity of the mixtures containing PCE mostly governed by clay type/content (PI values) and W/P ratio, respectively.

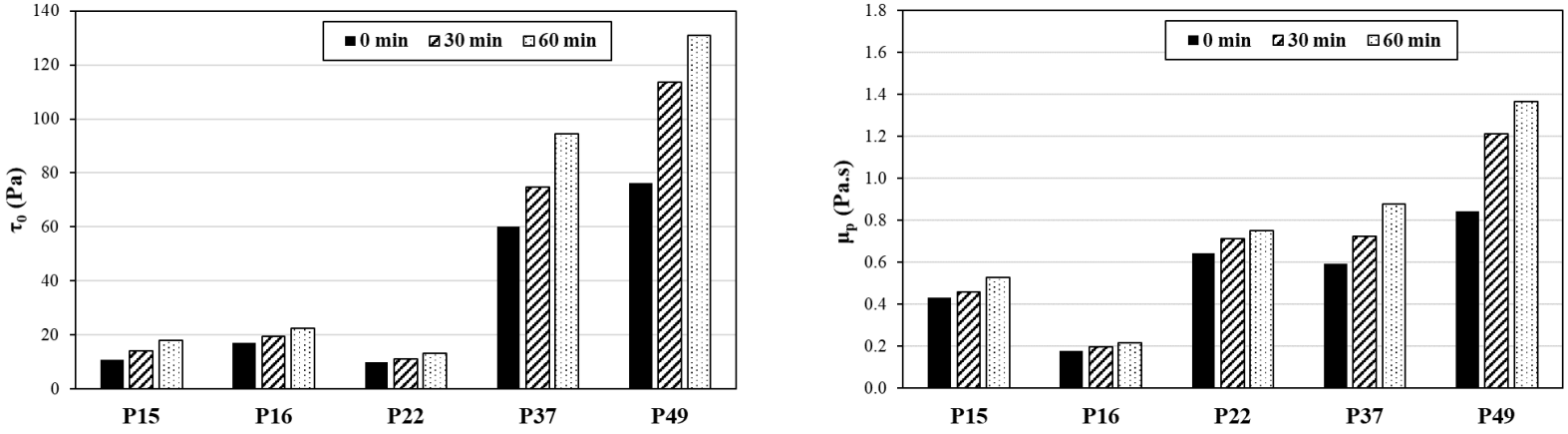

Fig. 6.8. Bingham rheological parameters of the PCE paste mixtures, including (a) yield stress and (b) plastic viscosity.

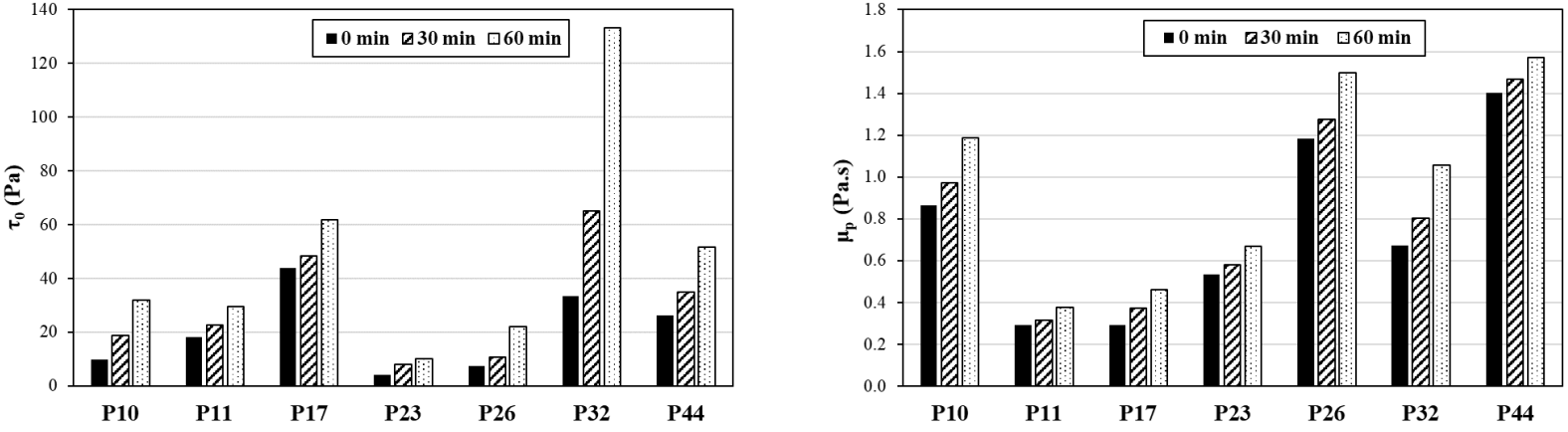

Fig. 6.9. Bingham rheological parameters of the PNS paste mixtures, including (a) yield stress and (b) plastic viscosity.

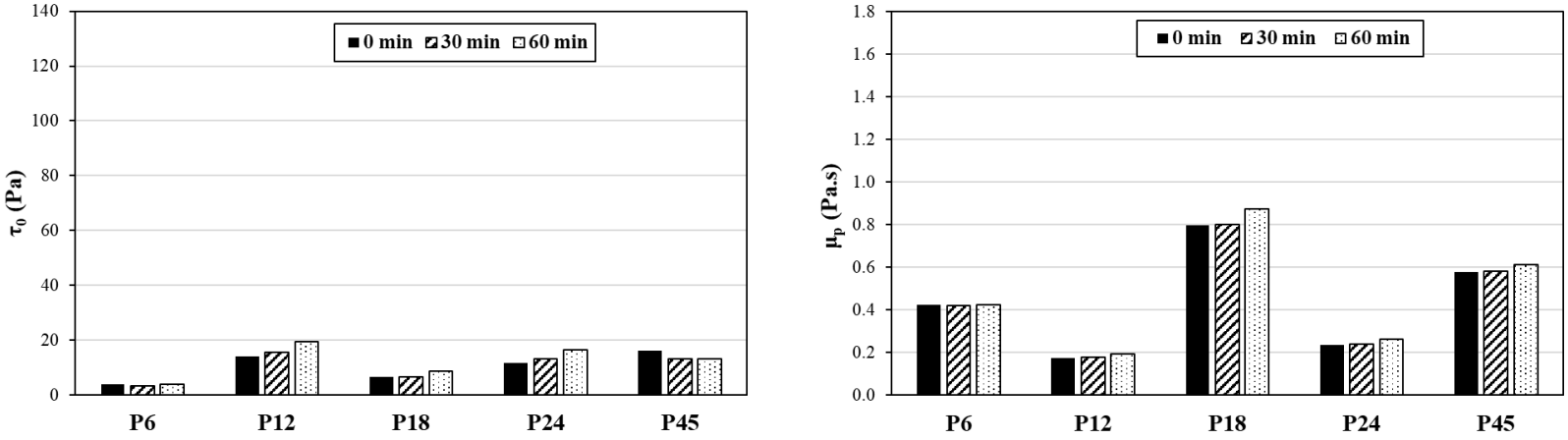

Fig. 6.10. Bingham rheological parameters of the NE-PC paste mixtures, including (a) yield stress and (b) plastic viscosity.

As shown in Fig. 6.9, the yield stress of the paste mixtures proportioned with the PNS admixture were found to be dependent on both the clay content and W/P ratio. As can be observed, despite its higher W/P ratio, the mixture P32 exhibited the highest yield stress values and increasing rate over time rather than the mixtures P44 and P26. This can confirm the coupled contribution of clay and water on yield stress of the mixtures containing PNS. It must be noted that applying the Bingham model for the P17 mixture (Fig. 6.9), resulted in untrustworthy results compared to other mixtures (low R^2 value of 0.63). Therefore, among the paste mixtures proportioned with PNS and Clay Type I, excluding P17, the mixture P11 showed the highest yield stress value despite its relatively higher W/P ratio of 0.4 compared to the P10 and P23 mixtures. However, unlike the yield stress values, lower plastic viscosity values were obtained for the paste mixtures proportioned with higher W/P ratios. Accordingly, among the Clay Type I-based paste mixtures, the mixture P10 gained the highest plastic viscosity due to its lowest W/P ratio of 0.3. Similarly for the Clay Type II-based mixtures, the lowest plastic viscosity value was obtained for the mixture P32 made with the highest W/P ratio. Hence, it can be concluded that the yield stress values of the PNS-dispersed pastes were more influenced due to the water content compared to those proportioned with the PCE admixture. However, the plastic viscosity values of the PCE- and PNS-based mixtures showed comparable sensitivities due to W/P variations.

As can be observed in Fig. 6.10, the use of NE-PC led to significantly lower values and increasing rates of yield stress over time (less than 20 Pa after 60 min) rather than those obtained using the PCE and PNS admixtures. Among the NE-PC-contained paste mixtures, the mixture P6 gained the lowest yield stress which is due to its lowest clay content. However, similar to other admixtures, the plastic viscosity values of the NE-PC-based pastes were mostly controlled by the W/P ratio. Accordingly, the mixture P18 exhibited the highest plastic viscosity value due to its lowest W/P ratio of 0.30. On the other hand, although the mixtures P24 and P45 were proportioned with the same W/P of 0.40, the mixture P45 showed higher plastic viscosity than P24 which can be explained due to its higher PI value (11.8% vs. 7.1%). This can be attributed to the effect of clay type on plastic viscosity values. Due to the presence of coupled effect of influencing parameters affecting the rheological parameters, further investigation was required to understand the significance of each factor.

6.3.2 Rheology of CEM mixtures

The results of the workability and rheological measurements of the investigated CEM mixtures are summarized in Table 6.5. As can be observed, simultaneous incorporation of Clay Type II and PNS admixture led to MSF values lower than the targeted value 280 ± 20 mm (low flowability). This can reflect the incompatibility between the PNS admixture and Clay Type II. Furthermore, the mixture M6, contained high content of silt, showed extensive segregations prior achieving the targeted MSF. It is worth mentioning that all the mixtures were well-fitted with the Bingham model, excluding the mixture M25. As can be observed, the mixture M25, proportioned with NaHMP admixture, showed quite high shape stability, reflected by significantly higher values and increasing rates of yield stress and plastic viscosity over time, rather than other mixtures. Accordingly, no flow was recorded for the mixture M25 through the MVF (blockage) and MSF (no spread) tests. Such shape stability is highly favorable for concrete 3D-printing applications.

The Bingham yield stress and plastic viscosity of the CEM mixtures dispersed with the PCE admixture are presented in Fig. 6.11. As can be observed, the results of the PCE-based CEM mixtures were comparable to their corresponding paste mixtures in which M49 followed by M37 showed the highest yield stress values (more than 40 Pa at t = 0). As discussed earlier, this is due to their high contents of Clay Type II and their corresponding PI values. On the other hand, the mixtures containing the Clay Type I exhibited almost comparable yield stress values (less than 40 Pa at t = 0). This can be due to the coupled effect of clay content, W/P ratio, and EP thickness on yield stress of the PCE-based mortar mixtures. However, immediately after mixing, among all the PCE-based CEM mixtures, the mixture M22 showed the highest plastic viscosity value which can be due to its lowest W/P ratio of 0.3. It can confirm higher contribution of W/P ratios on plastic viscosity of the PCE-based mixtures, rather than binder composition. Moreover, higher increasing rates of plastic viscosity values obtained for the mixture P49 can be explained due to its lower W/P ratio and e_{EP}, compared to the mixture P37.

Table 6.5. The workability and rheological properties of the investigated CEM mixtures over time.

Mix No.	Clay type	Admixture type	MSF (mm)			MVF (s)			Bingham parameters					
									0 min		30 min		60 min	
			0 min	30 min	60 min	0 min	15 min	30 min	τ_0 (Pa)	μ_p (Pa.s)	τ_0 (Pa)	μ_p (Pa.s)	τ_0 (Pa)	μ_p (Pa.s)
M6	Type I	NE-PC	NA	-	-	-	-	-	-	-	-	-	-	-
M10		PNS	265	222	155	7.1	11.5	18.2	15.3	5.26	42.6	11.51	75.7	22.43
M11		PNS	269	236	193	3.2	3.9	4.4	35.8	3.69	52.6	4.77	66.6	6.18
M12		NE-PC	266	259	238	1.5	1.9	2.4	17.0	1.11	22.0	1.86	26.2	3.31
M15		PCE	279	243	211	2.4	3.1	3.7	21.8	1.42	29.8	2.80	36.9	3.96
M16		PCE	272	236	189	3.0	3.6	4.1	22.1	2.85	31.8	3.67	48.8	4.80
M17		PNS	263	223	156	1.0	1.7	2.1	37.9	1.02	56.2	1.68	71.6	2.99
M18		NE-PC	265	261	248	9.9	11.0	13.5	12.4	7.09	16.5	11.16	23.5	21.12
M22		PCE	282	264	249	7.5	7.9	8.3	31.4	7.41	46.4	9.15	54.9	10.80
M23		PNS	264	232	171	3.3	4.3	10.9	41.6	3.12	68.4	5.02	82.8	12.67
M24		NE-PC	281	267	246	3.1	4.0	5.2	21.4	3.19	27.3	5.02	32.9	6.42
M25		NaHMP	263	100	100	2.0	blocked	blocked	182.1	9.53	744.9	38.24	849.4	42.56
M26	Type II	PNS	NA	-	-	-	-	-	-	-	-	-	-	-
M32		PNS	NA	-	-	-	-	-	-	-	-	-	-	-
M37		PCE	286	209	171	2.5	3.6	4.2	47.7	5.17	81.9	6.01	121.9	8.15
M44		PNS	NA	-	-	-	-	-	-	-	-	-	-	-
M45		NE-PC	264	250	247	2.7	3.7	4.3	53.0	5.57	62.5	6.85	68.3	9.04
M49		PCE	270	201	184	2.2	5.6	8.4	85.2	4.82	102.5	8.83	149.1	15.93
M_{ref}	-	PCE	273	240	195	2.9	5.3	5.8	24.6	3.58	29.5	4.78	38.5	6.12

NA: Not achieved to the targeted MSF of 280 ± 20 mm

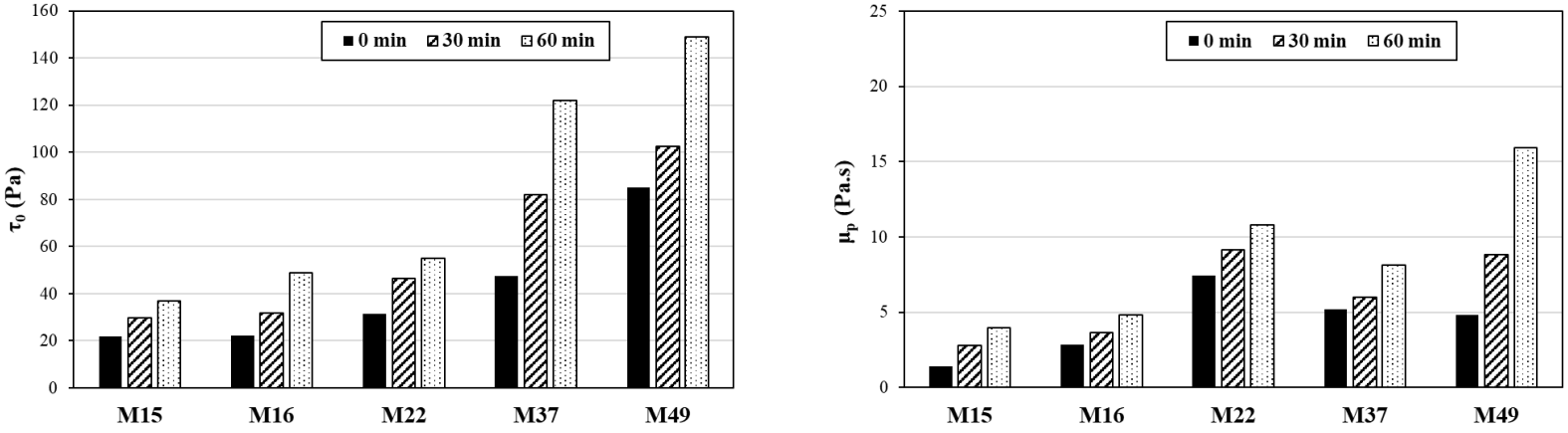

Fig. 6.11. Bingham (a) yield stress and (b) plastic viscosity of the PCE-contained CEM mixtures.

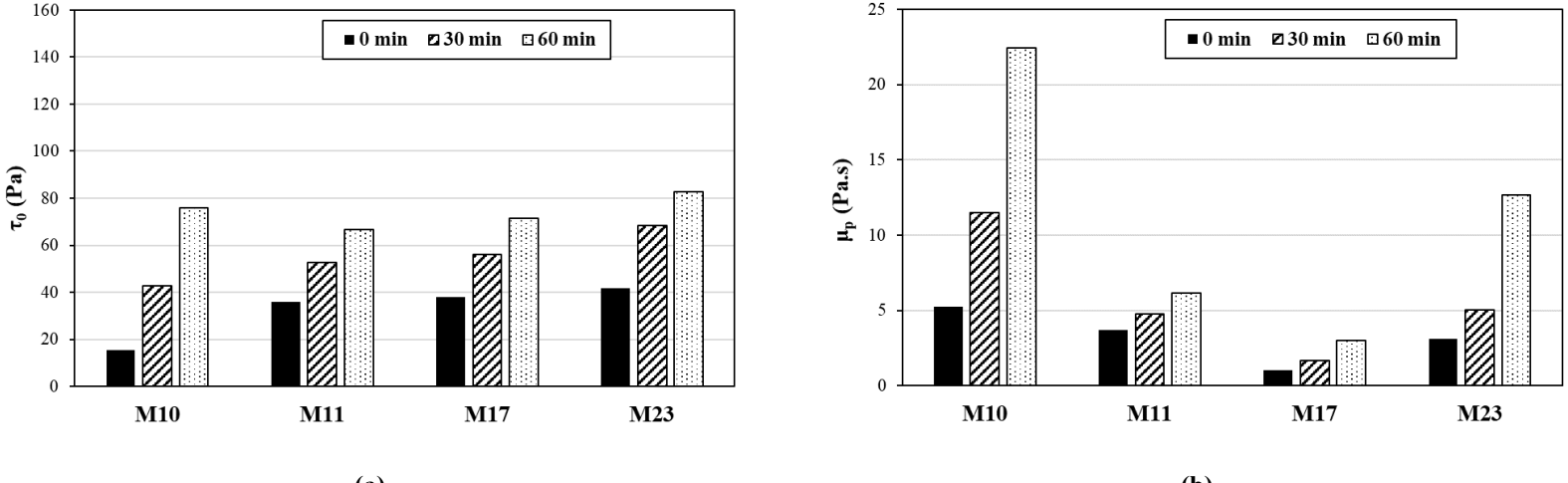

Fig. 6.12. Bingham (a) yield stress and (b) plastic viscosity of the PNS-contained CEM mixtures.

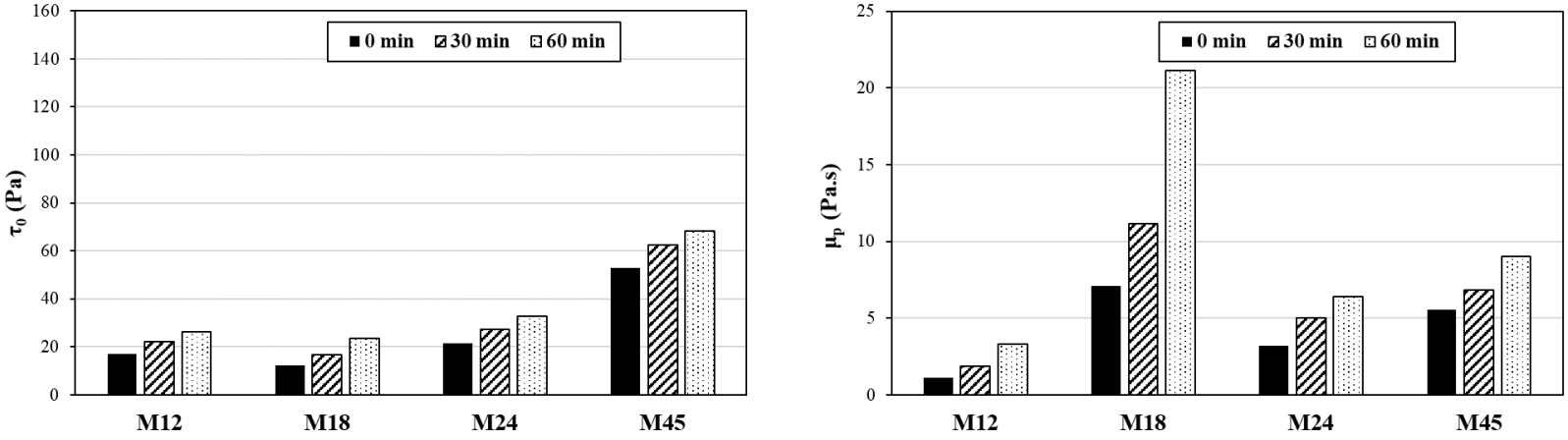

Fig. 6.13. Bingham (a) yield stress and (b) plastic viscosity of the NE-PC-contained CEM mixtures.

Fig. 6.12 illustrates the Bingham yield stress and plastic viscosity of the PNS-contained CEM mixtures over time. As mentioned earlier, the PNS-Clay Type II-contained CEM mixtures could not achieve the targeted MSF of 280 ± 20 mm. Therefore, only the results of the PNS-Clay Type I-based CEM mixtures were discussed in this section. As can be observed, all these mixtures showed the initial yield stress values lower than 40 Pa at t = 0. However, a combined effect of clay content, W/P ratio, and EP thickness on the yield stress values of the PNS-based CEM mixtures was observed which will be further discussed in section 3.2. However, the plastic viscosity values of the PNS-based CEM mixtures were found to be mainly governed by W/P ratio. Accordingly, among all the PNS-Clay Type I-based CEM mixtures, the mixtures M10 and M17 showed the highest and lowest plastic viscosity values due to their lowest and highest W/P ratios of 0.30 and 0.50, respectively. Moreover, similarly to the PCE-dispersed CEM mixtures, the highest increasing rate of plastic viscosity values were obtained for the mixtures M10 and M23 proportioned with the lowest W/P ratios of 0.30 and 0.35, respectively.

As can be observed in Fig. 6.13, the mixture M45 exhibited the highest yield stress value among all the NE-PC-based CEM mixtures due to its finer Clay Type II. This can be generally concluded that regardless of the admixture type, all the CEM mixtures proportioned with the Clay Types I and II obtained the initial yield stress values lower and higher than 40 Pa at t = 0, respectively. Moreover, the values and increasing rates of the yield stress of the CEM mixtures dispersed with the NE-PC admixture over time were found relatively lower than those obtained by incorporating the PNS and PCE admixtures. This can be referred to the synergy of this linear type of PC with powder constituents of the earth binders. The coupled effect of the mixture constituents on the yield stress values of the NE-PC-based CEM mixtures are further discussed in section 3.2. Moreover, similarly to other types of admixtures, the plastic viscosity of the NE-PC-based CEM mixtures was found to be highly dependent on the W/P ratio. Accordingly, the mixtures M12 and M18 showed the lowest and highest plastic viscosity values due to their highest (0.45) and lowest (0.30) W/P ratios, respectively.

6.3.3 Rheology of SCEC mixtures

The rheometry results revealed that the Bingham model was well fitted to the shear stress-shear rate data of the investigated SCEC mixtures. The workability and rheological properties of the four investigated SCEC mixtures proportioned with PCE, are summarized in Table 6.6 in terms of V-

Funnel and slump flow results, as well as the Bingham yield stress and plastic viscosity values over time.

Table 6.6. Experimental results of the investigated concrete mixtures.

Mix No.	Admixture type	Slump flow (mm)			V-Funnel (s)			Bingham model					
								0 min		30 min		60 min	
		0 min	30 min	60 min	0 min	30 min	60 min	τ_0 (Pa)	μ_p (Pa.s)	τ_0 (Pa)	μ_p (Pa.s)	τ_0 (Pa)	μ_p (Pa.s)
C16	PCE	705	665	625	1.6	1.8	1.9	30.7	3.31	37.9	4.71	54.6	5.51
C22	PCE	820	780	732	4.2	4.4	4.7	49.5	9.95	57	10.10	64.6	12.18
C37	PCE	805	495	410	2.5	4.0	5.5	49.9	6.10	98.8	7.04	154.3	9.74
C_{ref}	PCE	730	645	610	1.5	3.1	3.2	34.1	5.74	39.9	6.05	51.1	7.09

The Bingham yield stress and plastic viscosity values of the investigate SCEC mixtures are presented in Fig. 6.14. As can be observed, despite completely different binder constituents, the mixtures C16 and C_{ref} showed comparable yield stress values. This can highlight the coupled effect of different influencing parameters, including the S/A and W/P ratios, V_P, and content and type of the used clay. Moreover, although the mixtures C22 and C37 exhibited comparable initial yield stress values after mixing (t = 0), due to its finer clay particles and higher W/P ratio, the yield stress values of the mixture C37 showed significantly higher increase rate over time. Furthermore, similarly to the investigated paste and CEM mixtures, W/P ratio was found as the most influencing factor on plastic viscosity values of the investigated PCE-based SCEC mixtures. Accordingly, the mixture C22 with the lowest W/P ratio of 0.30 showed the highest plastic values among all the investigated SCEC mixtures.

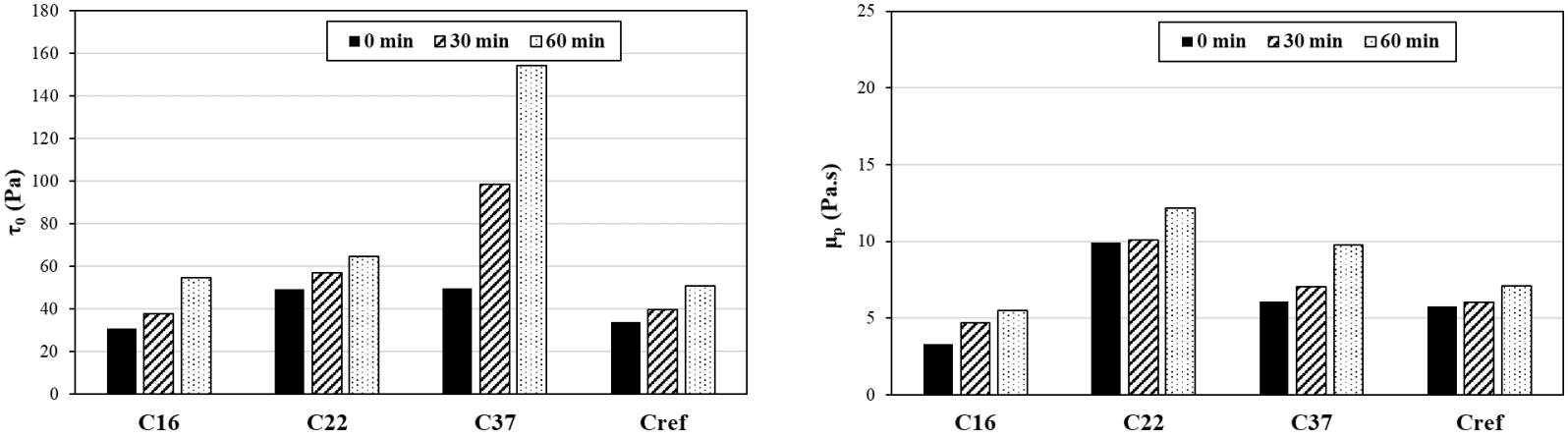

(a) **(b)**

Fig. 6.14. Bingham (a) yield stress and (b) plastic viscosity of the investigated SCEC mixtures.

6.3.4 Multiscale approach to control rheology of SCEC

As discussed earlier, the rheology of the self-consolidating earth-based cementitious suspensions is tricky due to the presence of clay and silt particles. In order to facilitate the control, prediction, and optimization of the rheological parameters, it is important to investigate the main influencing parameters on rheology of these materials. Also, it is useful to establish relationships between workability and rheology of SCEC to facilitate its design to achieve adequate rheological properties. In this section, the coupled effect of different characteristics of mixture constituents on rheological properties of the investigated SCEC, CEM, and paste mixtures was evaluated. Accordingly, the following correlation was established between different workability and rheological properties of the investigated mixtures (Response) and the main influencing parameters (ai), indicated in the last section:

$$\text{Response} = \alpha + \beta \times \prod_{i=1}^{n}(a_i{}^{m_i}) \quad (6.4)$$

where n is the number of influencing parameters a_i =1 to n, and α, β, and m_i = 1 to n are the adjustment factors which were determined for each "Response" using a developed Microsoft Excel solver. The 5 influencing parameters a_i= 1 to 5 included the PI and W/P ratio in the paste mixtures, in addition to the V_P and e_{EP} in the CEM mixtures, and S/A ratio in the investigated SCEC mixtures. It is worthy to mention that the effect of the type and content of the clay type used on rheological properties of the investigated mixtures was reflected using the PI values of the soil (clay, silt, and sand < 425 μm). The results of the established correlations are summarized in Table 6.7, in terms of the obtained adjustment factors (α, β, and mi = 1 to 5). Moreover, the precision of the established predictions was evaluated by considering the estimation index (EI), R^2, and root-mean-square error (RMSE) values, as presented in Table 6.7. The EI indices were defined as the mean value of the ratio between the predicted and experimental values. It is important to mention that R^2 and EI values closer to unity and lower RMSE values correspond to stronger agreement between the investigated flow performance responses and mixture constituent parameters. The investigated "Responses" included the characteristics of the investigated mixtures in different scales, as follow:

(i) Paste scale: The Bingham yield stress and plastic viscosity values, as well as the ratio of the rheology-to-workability immediately after mixing (t = 0) of the investigated paste mixtures containing different types of admixtures.

(ii) CEM scale: The Bingham yield stress and plastic viscosity of the investigated CEM mixtures immediately after mixing (t = 0), relative to those of their corresponding paste mixtures.

(iii) SCEC scale: The Bingham yield stress and plastic viscosity of the investigated SCEC mixtures immediately after mixing (t = 0), relative to those of their corresponding CEM mixtures.

As can be observed in Table 6.7, the yield stress of the paste mixtures dispersed with the PCE and PNS admixtures are in good agreements with the PI of their earth and W/P ratio. According to the obtained adjustment factors, the yield stress values of the PCE- and PNS-contained pastes were found to be more controlled by the PI and W/P ratio, respectively. Moreover, the yield stress values of the NE-PC-based mixtures were found highly dependent on the PI values. This can reveal the significant effect of the type and content of the used clay, whereas W/P showed no contribution on the yield stress values of the NE-PC-based mixtures. However, the W/P ratio showed the most dominant effect on plastic viscosity values of the investigated pastes, regardless of their admixture types.

The prediction of the rheological properties using the workability measurements can lead to easier rheological evaluation rather than using the sophisticated and expensive commercial rheometers [49]. As can be observed in Table 6.7, the yield stress values of the investigated paste mixtures can be well predicted using their corresponding MSF values as a function of the PI values, reflecting the characteristics of the binder constituents, and W/P ratio. The yield stress-MSF relationship of the PCE-contained paste mixtures was found highly dependent on the powder constituents, reflected by high adjustment factor obtained for PI, whereas W/P ratio showed no contribution. However, W/P showed more significant effect on the yield stress-to-MSF ratios of the pastes proportioned with the PNS and NE-PC admixtures, rather than PI of the used earths. On the other hand, the plastic viscosity of the investigated paste mixtures proportioned with different types of admixtures were found in good agreements with their corresponding MCT values with a significant contribution of W/P ratio, regardless of the PI values of their corresponding earths.

Moreover, the yield stress of the investigated CEM mixtures relative to those of their corresponding paste mixtures were well correlated to W/P, e_{EP}, and PI values, in a descending order of significance. On the other hand, the relative plastic viscosity values of the CEM mixtures to their corresponding pastes were found highly governed by V_P values, followed by W/P ratio and EP thickness, whereas the PI values, as an indication of the binder compositions, showed no contribution. On the other hand, as shown in Table 6.7, the rheological properties of the investigated SCEC mixtures can be well predicted using those of their corresponding CEM mixtures proportioned using the proposed approach. The established predictions were found in very good agreements with the e_{EP} and S/A values, in a descending order of significance (R^2 and EI values close to unity and low RMSE). This suggests the high potential of the new proposed CEM approach to simulate the rheological properties of the SCEC mixtures.

Table 6.7. Adjustment factors and prediction precisions of the established correlations (Eq. 6.4).

	Response	Adjustment factors							Precision		
		α	β	m_i							
				PI (%)	W/P	V_P (%)	e_{EP} (µm)	S/A	EI	R^2	RMSE
Paste	$\tau_{0\text{-PCE}}$ (Pa)	11.01	0.006	3.053	-2.168	-	-	-	0.995	0.997	2.315
	$\tau_{0\text{-PNS}}$ (Pa)	9.784	1927.6	2.507	10.599	-	-	-	0.949	0.953	5.535
	$\tau_{0\text{-NE-PC}}$ (Pa)	0	3.8593	0.594	0	-	-	-	0.976	0.979	1.769
	$\mu_{p\text{-PCE}}$ (Pa.s)	0.273	4.5E-5	1.683	-5.91	-	-	-	0.978	0.982	0.876
	$\mu_{p\text{-PNS}}$ (Pa.s)	0.342	7.8E-7	1.220	-10.386	-	-	-	0.974	0.979	0.136
	$\mu_{p\text{-NE-PC}}$ (Pa.s)	0	0.009	0.301	-3.403	-	-	-	0.96	0.971	0.100
	$\frac{\tau_{0\text{-PCE}}\ (\text{Pa})}{\text{MSF}_{0\text{-PCE}}\ (\text{mm})}$	0.034	0.001	2.298	0	-	-	-	0.98	0.972	0.023
	$\frac{\tau_{0\text{-PNS}}\ (\text{Pa})}{\text{MSF}_{0\text{-PNS}}\ (\text{mm})}$	0.035	7.13	2.663	10.965	-	-	-	0.95	0.963	0.020
	$\frac{\tau_{0\text{-NE-PC}}\ (\text{Pa})}{\text{MSF}_{0\text{-NE-PC}}\ (\text{mm})}$	0.001	0.064	0.522	1.562	-	-	-	0.997	0.992	0.002
	$\frac{\mu_{p\text{-PCE}}\ (\text{Pa.s})}{\text{MCT}_{0\text{-PCE}}\ (\text{s})}$	0	0.004	0	-1.417	-	-	-	0.932	0.951	0.004
	$\frac{\mu_{p\text{-PNS}}\ (\text{Pa.s})}{\text{MCT}_{0\text{-PNS}}\ (\text{s})}$	0.018	8.1E-8	0	-10.731	-	-	-	0.852	0.965	0.008
	$\frac{\mu_{p\text{-NE-PC}}\ (\text{Pa.s})}{\text{MCT}_{0\text{-NE-PC}}\ (\text{s})}$	0.001	3.8E-4	0	-3.594	-	-	-	0.971	0.969	0.003
CEM	$\frac{\tau_{0\text{-CEM}}\ (\text{Pa})}{\tau_{0\text{-paste}}\ (\text{Pa})}$	1.612	4.888	13.204	-52.576	0	-20.546	-	0.968	0.974	0.59
	$\frac{\mu_{p\text{-CEM}}\ (\text{Pa.s})}{\mu_{p\text{-paste}}\ (\text{Pa.s})}$	6.979	1.5E47	0	-4.331	-27.015	-2.004	-	0.922	0.916	2.015
SCEC	$\frac{\tau_{0\text{-concrete}}\ (\text{Pa})}{\tau_{0\text{-CEM}}\ (\text{Pa})}$	1.218	2.5E-10	0	0	0	6.288	15.159	0.995	0.991	0.161
	$\frac{\mu_{p\text{-concrete}}\ (\text{Pa.s})}{\mu_{p\text{-CEM}}\ (\text{Pa.s})}$	1.228	14.256	0	0	0	-7.170	-37.952	0.997	0.993	0.071

6.4 Conclusions

In this study, the rheological properties of the SCEC mixtures were investigated in three different scales of paste, CEM, and concrete. The coupled effect of different mixture constituents, including binder composition (type and content of clay, silt, and cement content), V_P, W/P and S/A ratios, EP thickness, and admixture type on rheological properties of the investigated paste, CEM, and SCEC mixtures were evaluated. Considering the effect of EP thickness, a new CEM approach was proposed to predict the characteristics of the SCEC mixtures in fresh state. The rheological measurements included the viscoplastic properties (yield stress and plastic viscosity) and thixotropy of the investigated mixtures. According to the experimental results, the following concluding remarks can be pointed out:

- Admixture type showed the major effect on the thixotropic or rheopectic behavior of the investigated self-consolidating earth paste mixtures. All the investigated paste mixtures showed rheopectic behavior except those proportioned with PNS admixture and Clay Type II, as well as the one dispersed using the NE-PC admixture.

- The highest thixotropy response was obtained for the paste mixture proportioned with the highest content of the finer Clay Type II. On the other hand, the highest rheopectic behavior was observed for the mixtures P49 and P37 proportioned with PCE admixture and Clay Type II, as well as the mixture P25 dispersed using the NaHMP.

- The admixture and clay types showed the most significant effect on viscoplastic properties of the investigated mixtures. The highest yield stress and plastic viscosity values were obtained for the mixtures proportioned with NaHMP dispersant and Clay Type II. Moreover, the paste and CEM mixtures contained the NE-PC admixture exhibited relatively lower values and increasing rates of yield stress over time, compared to those proportioned with the PNS and PCE admixtures.

- The yield stress of the investigated paste, CEM, and SCEC mixtures were influenced by the coupled effect of the content and type of the clay and W/P ratio. All the CEM mixtures proportioned with the Clay Types I and II exhibited initial yield stress values lower and higher than 40 Pa, respectively, except the one made with NaHMP. In concrete scale, the use of the Clay Type II led to higher values and increasing rates of yield stress over time. However, the plastic viscosity values were mostly governed by the W/P ratio according to an inverse proportional relationship.

- A multiscale approach was proposed to control the rheological properties of SCEC mixtures from of their corresponding paste and CEM matrices. The rheological properties of SCEC mixtures were successfully predicted using those of their corresponding CEM mixtures, EP thickness, and S/A ratio. The relative rheological properties of the investigated CEM mixtures to their corresponding paste mixtures were found in good agreements with the V_P and EP thickness values.

6.5 Declaration of competing interest

The authors declare that they have no known competing financial interests or personal relationships that could have appeared to influence the work reported in this paper.

6.6 Acknowledgement

The authors wish to thank the financial support of the National Science and Engineering Research Council of Canada (NSERC) and the eight industrial partners participating in the NSERC Chair on Development of Flowable Concrete with Adapted Rheology and their Application in Concrete Infrastructures, held by Professor Ammar Yahia at the Université de Sherbrooke.

REFERENCES

[1] F. Pacheco-Torgal, S. Jalali, Earth construction: Lessons from the past for future eco-efficient construction, Constr. Build. Mater. 29 (2012) 512–519. https://doi.org/10.1016/j.conbuildmat.2011.10.054.

[2] P. Walker, V. Maniatidis, A Review of Rammed Earth Construction, United Kingdom, 2003.

[3] R. Bahar, M. Benazzoung, S. Kenai, Performance of compacted cement stabilized soil, Cem. Concr. Compos. 26 (2004) 811–820.

[4] L. Miccoli, U. Müller, P. Fontana, Mechanical behaviour of earthen materials: A comparison between earth block masonry, rammed earth and cob, Constr. Build. Mater. 61 (2014) 327–339. https://doi.org/10.1016/j.conbuildmat.2014.03.009.

[5] D. Gélard, Identification and Characterization of Internal Cohesion of Earth Material in its Natural Condition (in French), in: INPG Grenoble, France, 2005.

[6] C.M. Ouellet-Plamondon, G. Habert, Self-Compacted Clay based Concrete (SCCC): Proof-of-concept, J. Clean. Prod. 117 (2016) 160–168. https://doi.org/10.1016/j.jclepro.2015.12.048.

[7] M. Kohandelnia, M. Hosseinpoor, A. Yahia, R. Belarbi, A new approach for proportioning self-consolidating earth paste (SCEP) using the Taguchi method, Constr. Build. Mater. 347 (2022) 128579. https://doi.org/10.1016/J.CONBUILDMAT.2022.128579.

[8] A.W. Skempton, The Colloidal activity of clays, in: 3rd Int. Conf. Soil Mech. Found. Eng., London, 1953: pp. 47–61.

[9] B. Voight, Correlation between Atterberg plasticity limits and residual shear strength of natural soils, Géotechnique. 23 (1973) 265–267.

[10] A. Laskar, S.K. Pal, Geotechnical characteristics of two different soils and their mixture and relationships between parameters, Electron. J. Geotech. Eng. 17 (2012) 2821–2832.

[11] P.P. Raj, Soil Mechanics and Foundation Engineering, Dorling Kindersley, (India) Pvt. Ltd., New Delhi, 2012.

[12] M. Westerholm, B. Lagerbald, J. Silfwerbrand, E. Forssberg, Influence of fine aggregate characteristics on the rheological properties of mortars, Cem. Concr. Compos. 30 (2008) 274–282.

[13] S.K. Ling, A.K.H. Kwan, Adding ground sand to decrease paste volume, increase cohesiveness and improve passing ability of SCC, Constr. Build. Mater. 84 (2015) 46–53.

[14] J.J. Chen, B.H. Li, P.L. Ng, A.K.H. Kwan, Adding granite polishing waste as sand replacement to improve packing density, rheology, strength and impermeability of mortar, Powder Technol. 364 (2020) 404–415.

[15] F. Andreola, E. Castellini, J.M.F. Ferreira, S. Olhero, M. Romagnoli, Effect of sodium hexametaphosphate and ageing on the rheological behaviour of kaolin dispersions, Appl. Clay Sci. 31 (2006) 56–64. https://doi.org/10.1016/j.clay.2005.08.004.

[16] F. Andreola, E. Castellini, T. Manfredini, M. Romagnoli, The role of sodium hexametaphosphate in the dissolution process of kaolinite and kaolin, J. Eur. Ceram. Soc. 24 (2004) 2113–2124. https://doi.org/10.1016/S0955-2219(03)00366-2.

[17] F. Andreola, E. Castellini, G. Lusvardi, L. Menabue, M. Romagnoli, Release of ions from kaolinite dispersed in deflocculant solutions, Appl. Clay Sci. 36 (2007) 271–278. https://doi.org/10.1016/j.clay.2006.10.002.

[18] A. Mostafa, A. Yahia, New approach to assess build-up of cement-based suspensions, Cem. Concr. Res. (2016) 174–182. https://doi.org/https://doi.org/10.1016/j. cemconres.2016.03.005.

[19] M.A. Moeini, M. Hosseinpoor, A. Yahia, Effectiveness of the rheometric methods to evaluate the build-up of cementitious mortars used for 3D printing, Constr. Build. Mater. 257 (2020) 119551. https://doi.org/10.1016/J.CONBUILDMAT.2020.119551.

[20] B. Panda, M.J. Tan, Experimental study on mix proportion and fresh properties of fly ash based geopolymer for 3D concrete printing, Ceram. Int. 44 (2018) 10258–10265. https://doi.org/10.1016/J.CERAMINT.2018.03.031.

[21] N. Roussel, Understanding the Rheology of Concrete, Woodhead Publishing Limited, 2012.

[22] M.A. Moeini, M. Hosseinpoor, A. Yahia, Yield stress of fine cement-based mortars: Challenges and potentials with rotational and compressional testing methods, Constr. Build. Mater. 314 (2022).

[23] A. Perrot, D. Rangeard, A. Pierre, Structural built-up of cement-based materials used for 3D-printing extrusion techniques, Mater. Struct. 49 (2016) 1213–1220.

[24] Y. Qian, G. De Schutter, Enhancing thixotropy of fresh cement pastes with nanoclay in presence of polycarboxylate ether superplasticizer (PCE), Cem. Concr. Res. 111 (2018) 15–22. https://doi.org/10.1016/J.CEMCONRES.2018.06.013.

[25] Y. Zhang, Y. Zhang, W. She, L. Yang, G. Liu, Y. Yang, Rheological and harden properties of the high-thixotropy 3D printing concrete, Constr. Build. Mater. 201 (2019) 278–285. https://doi.org/10.1016/J.CONBUILDMAT.2018.12.061.

[26] R. Ferron, A. Gregori, Z. Sun, S.P. Shah, Rheological method to evaluate structural buildup in self-consolidating concrete cement pastes, ACI Mater. J. 104 (2007) 242–250.

[27] A. Kaleta-Jurowska, S. Grzeszczyk, M. Dziubiński, Application of multiple step change in shear rate model for determination of thixotropic behaviour of cement pastes, J. Build. Eng. 32 (2020). https://doi.org/https://doi.org/10.1016/j.jobe.2020.101494.

[28] O. H.Wallevik, D. Feys, J.E. Wallevik, K.H. Khayat, Avoiding inaccurate interpretations of rheological measurements for cement-based materials, Cem. Concr. Res. 78 (2015) 100–109. https://doi.org/https://doi.org/10.1016/j.cemconres.2015.05.003.

[29] D. Feys, K.H. Khayat, Particle migration during concrete rheometry: How bad is it?, Mater. Struct. 50 (2017). https://doi.org/https://doi.org/10.1617/s11527-016-0992-4.

[30] J. Mewis, N.J. Wagner, Colloidal Suspension Rheology, Cambridge University Press, Cambridge, 2011.

[31] A. Schwartzentruber, C. Catherine, Method of Concrete Equivalent Mortar—A Novel Tool to Help in Formulation of Concrete with Admixtures, Mater. Struct. 33 (2000) 475–482.

[32] K.H. Khayat, S.-D. Hwang, Effect of High-Range Water- Reducing Admixture Type on Performance of Self-Consolidating Concrete, in: Eighth CANMET/ACI Int. Conf. Superplast. Other Chem. Admixtures Concr., American Concrete Institute, Farmington Hills, MI, 2006: pp.

185–200.

[33] J.J. Assaad, J. Harb, E. Chakar, Relationships between Key ASTM Test Methods Determined on Concrete and Concrete-Equivalent-Mortar Mixtures, J. ASTM Int. 6 (2008).

[34] T.K. Erdem, K.H. Khayat, A. Yahia, Correlating Rheology of Self-Consolidating Concrete to Corresponding Concrete-Equivalent Mortar, ACI Mater. J. (2009).

[35] D. Kabagire, P. Diederich, A. Yahia, New insight into the equivalent concrete mortar approach for self-consolidating concrete, J. Sustain. Cem. Mater. 4 (2015) 215–224. https://doi.org/10.1080/21650373.2015.1018983.

[36] J.H. Lee, J.H. Kim, J.Y. Yoon, Prediction of the yield stress of concrete considering the thickness of excess paste layer, Constr. Build. Mater. 173 (2018) 411–418. https://doi.org/10.1016/j.conbuildmat.2018.03.124.

[37] M. Hosseinpoor, B.I. Ouro Koura, A. Yahia, E.H. Kadri, Diphasic investigation of the visco-elastoplastic characteristics of highly flowable fine mortars, Constr. Build. Mater. 270 (2021) 121425. https://doi.org/10.1016/J.CONBUILDMAT.2020.121425.

[38] ASTM C305-20, Standard Practice for Mechanical Mixing of Hydraulic Cement Pastes and Mortars of Plastic Consistency, ASTM Int. (2020) 1–3. https://doi.org/10.1520/C0305-20.2.

[39] N. Roussel, C. Stefani, R. Leroy, From mini-cone test to Abrams cone test: Measurement of cement-based materials yield stress using slump tests, Cem. Concr. Res. 35 (2005) 817–822. https://doi.org/10.1016/j.cemconres.2004.07.032.

[40] EFNARC, Specification and Guidelines for Self-Compacting Concrete, (2002).

[41] BS EN 445, Grout for prestressing tendons. Test methods, 2007.

[42] H. Okamura, M. Ouchi, Self-Compacting Concrete, J. Adv. Concr. Technol. 1 (2003) 5–15.

[43] ASTM D4318 − 17, Standard Test Methods for Liquid Limit, Plastic Limit, and Plasticity Index of Soils, ASTM Stand. (2017).

[44] Y.A. Abebe, L. Lohaus, Rheological characterization of the structural breakdown process to analyze the stability of flowable mortars under vibration, Constr. Build. Mater. 131 (2017) 517–525. https://doi.org/10.1016/J.CONBUILDMAT.2016.11.102.

[45] R.S. Ahari, T.K. Erdem, K. Ramyar, Thixotropy and structural breakdown properties of self consolidating concrete containing various supplementary cementitious materials, Cem. Concr. Compos. 59 (2015) 26–37. https://doi.org/10.1016/J.CEMCONCOMP.2015.03.009.

[46] H.A. Barnes, Thixotropy—a review, J. Nonnewton. Fluid Mech. 70 (1997) 1–33. https://doi.org/10.1016/S0377-0257(97)00004-9.

[47] J.J. Assaad, K.H. Khayat, H.A. Mesbah, Assessment of Thixotropy of Flowable and Self-Consolidating Concrete, Aci Mater. J. 100 (2003) 99–107.

[48] S. Kawashima, P. Hou, D.J. Corr, S.P. Shah, Modification of cement-based materials with nanoparticles, Cem. Concr. Compos. 36 (2013) 8–15. https://doi.org/10.1016/J.CEMCONCOMP.2012.06.012.

[49] N. Roussel, P. Coussot, "Fifty-cent rheometer" for yield stress measurements: From slump to spreading flow, J. Rheol. (N. Y. N. Y). 49 (2005) 705–718.

https://doi.org/https://doi.org/10.1122/1.1879041.

CHAPTER 7. Hygrothermal and microstructural characterization of self-consolidating earth concrete (SCEC)

Authors and affiliations

Mojtaba Kohandelnia: Ph.D. candidate, Cement and Concrete Research Group, Department of Civil and Building Engineering, Université de Sherbrooke, Sherbrooke, Québec, Canada, J1K 2R1.

Masoud Hosseinpoor: Post-Doc, Cement and Concrete Research Group, Department of Civil and Building Engineering, Université de Sherbrooke, Sherbrooke, Québec, Canada, J1K 2R1.

Ammar Yahia: Professor, Cement and Concrete Research Group, Department of Civil and Building Engineering, Université de Sherbrooke, Sherbrooke, Québec, Canada, J1K 2R1.

Rafik Belarbi, Professor, LaSIE UMR CNRS 7356, La Rochelle Université, La Rochelle, France.

Article Status: Published
Journal: Journal of Building Engineering - Elsevier
Reference: M. Kohandelnia, M. Hosseinpoor, A. Yahia, R. Belarbi, Hygrothermal and microstructural characterization of self-consolidating earth concrete (SCEC), J. Build. Eng. 69 (2023) 106287. https://doi.org/10.1016/J.JOBE.2023.106287.
Titre française: Caractérisation hygrothermique et microstructurale du béton de terre autoplaçant (BTAP)

Abstract

The incorporation of earth-based materials offers superior hygrothermal performance to the construction industry, ensuring significant ecological and environmental benefits. The hygrothermal and microstructural characterization of self-consolidating earth concrete (SCEC) are investigated in this study. These include the sorption isotherm, permeability, heat capacity, thermal parameters (conductivity, diffusivity and effusivity), moisture buffer value (MBV), total porosity and pores distribution, and microstructural characteristics. The investigated SCEC mixtures gained lower water content than normal concrete, as reference mixture, comparable to that of clay bricks. They also showed higher permeability due to their higher porosity and connected pores. Thermal conductivity, diffusivity and effusivity of the investigated SCEC mixtures showed lower values than those of the reference mixture, similar to existing earthen materials in the literature. Since the diffusivity and effusivity of the earthen materials are higher than those of wood, SCEC mixtures can offer both low diffusivity and high effusivity among different construction materials. Furthermore, the investigated SCEC mixtures compared to the reference exhibited lower mass losses attributed to calcium silicate hydrate (CSH), dehydroxylation of portlandite, and decarbonation. The water vapor and gas permeability of SCEC were found in good agreements with cumulative pore volume in the ranges of 100–200 nm and 100–300 nm, respectively. Furthermore, the drying shrinkage and compressive strength values were dependent on the cumulative pore volume of pore sizes less than 1 μm.

Keywords: Clay; Hygrothermal properties; Microstructure; Porosity; Self-consolidating earth concrete (SCEC).

7.1 Introduction

The construction industry consumes substantial amount of energy and is responsible of considerable CO_2 emission due to the use of polluted materials, such as cement-based concrete [1]. The use of sustainable materials is necessary to decrease CO_2 footprint towards green construction [2]. New developments are required to reduce the high energy demand of construction industry [3]. One of the alternative construction methods which is progressively emerging is rammed earth (RE) [4,5]. Earth is a locally available material used extensively for traditional

houses. It can be found in very high quantity which is desirable for the context of sustainable development to reduce energy consumption [2,6]. Earth-based materials are widely used in different forms including cob, mud and block-masonry brick and RE [7]. These materials are used unstabilized or cement-stabilized given the application in demand.

Earth-based materials have lower environmental impact, better thermal performance, superior indoor air quality, and more diverse final textures compared to the conventional construction materials [8,9]. These advantages place it as an appropriate material for building envelopes. However, the earthen construction (especially in the case of RE) can be time-consuming and labor-intensive with deficiencies in layer interface [10]. Self-consolidating earth concrete (SCEC) can be used to speed up the construction process and enhance the performance, while keeping the advantages of earthen materials. For example, the incorporation of earthen materials in SCEC results in a novel microstructure system which can affect their hygrothermal properties. The main difference between SCEC and conventional self-consolidating concrete (SCC) is the presence of clay and silt, in addition to low cement content, forming its ternary binder system [11]. Several attempts undertaken to achieve SCEC faced potential challenges, including the difficulty in dispersing clay particles and delayed setting of the material due to the low cement content [11–13].

Porous structure of earthen materials allows the gas and liquid to diffuse through their network as a hygroscopic material [14]. On the other hand, hygroscopic materials, such as clay, can have a significant effect on the relative humidity level and variations of the indoor air, the quality of the air, and comfort of habitants [15]. A hygroscopic material (e.g., clay in SCEC) is a substance that is capable of absorbing/desorbing moisture from/to surrounding atmosphere. Sorption capacity is linked to the porous structure of the material. A high porous structure, mainly composed of mesopores [16] and a wide specific area [17], may favor moisture buffer. However, it should be noted that there should be an optimum porosity since higher porosity can decrease the mechanical properties of the materials. The porous structure leads to a material with low density and low thermal conductivity. In addition to the porous structure, other factors can also influence the buffering capacity. In the case of clay, its mineralogy is very important as well. For instance, kaolinite clay minerals show a lower surface affinity and surface area than montmorillonite types which have greater surface area due to their active interlayer space [18].

Thermal characteristics of earth-based materials were studied by many researchers. Tavil et al. [19] confirmed that the masonry walls, made by different insulating systems, can provide high thermal mass which is referred to the fewer exterior temperature fluctuations inside the residence, compared to other construction materials. Lovec et al. [20] reported that rammed earth walls showed low thermal conductivity, high heat capacity, and desirable thermal mass effect, as the key element of thermal stability. Moreover, thermal conductivity is affected by temperature, chemical composition of the constituents, porosity, humidity and microstructure [21]. Moreover, it was reported that a 60-cm thick cob wall can possess thermal insulation twice the minimum of UK thermal requirements for residence [22]. It was also revealed that straw constructions were chosen as a feasible option for UK based on thermal performance [23,24]. William et al. [25] reported that earth block masonry could meet UK requirements. Similarly in Portugal, corn cobs provided adequate thermal properties [26]. Soebarto [27] investigated the thermal performance of uninsulated and insulated rammed earths (insulator with thermal resistance of 2 $m^2.K.W^{-1}$) in summer and winter. It was reported that both rammed earth types exhibited comparable performance in summer, based on indoor temperature. However, the rammed earth led to 5°C lower indoor temperature than the insulated one in winter. Furthermore, RE materials were found to possess high thermo-buffering capacity as an alternative to masonry materials. Earth-based materials showed high capability to store heat with characteristics of latent heat storage [28]. Soudani et al. [28] reported that the earth materials, either dry, wet, or as solid brick, can present both low diffusivity and high effusivity properties, referred to as thermal mass parameters [28].

Moisture can play a significant role on energy efficiency due to its effect on the heat transfer of the building envelope. Therefore, the study of coupled heat and mass transfer in a porous media is essential. Hygrothermal performance of earth-based materials were proved to provide sufficient comfort for inhabitants. As exposed to variations of temperature and relative humidity, it is also critical to study the effect of temperature and water content. Giada et al. [29] reported the high thermal effusivity of raw earth composites, i.e., high thermal inertia to enhance thermal comfort and energy efficiency. The authors concluded that earth earthen materials show both good buffering capacities and hygrothermal inertia properties due to their low water vapor diffusion resistance and high hygroscopic nature [29]. This can explain the ability of earthen constructions to keep the interior temperatures almost constant and regulate indoor relative humidity. Therefore, it is

necessary to measure hygrothermal parameters to conduct a comprehensive comparative study of SCEC, as a novel earth-based material for green constructions.

Although broad investigation on hygrothermal and microstructural characterization of different earthen materials exists in literature, further investigation is required to explore the hygrothermal properties of SCEC with different earth compositions. In this context, the main objective of the present study is to characterize the hygrothermal properties of SCEC mixtures as function of their microstructure and assess their potential as building envelopes. Three SCEC mixtures with different earth compositions were investigated and their properties were compared to those of a reference conventionnel SCC mixture. The studied properties include sorption isotherm, water vapor and gas permeability, heat capacity, thermal conductivity, thermogravimetric analysis (TGA), total porosity, and pores distribution, as well as microstructure observations. The obtained results are compared with other earthen materials to evaluate the potential of SCEC. Furthermore, the correlations between pores distribution with permeability, drying shrinkage, and compressive strength are investigated.

7.2 Experimental program

7.2.1 Materials and mixtures proportioning

A natural river sand and crushed limestone coarse aggregate with specific gravity of 2.67 and 2.72, and water absorption of 1.09% and 0.42%, respectively, were used as aggregate in this study (Fig. 7.1). Two types of clay were used, including (1) Type I consisting of 100% kaolinite and (2) Type II consisting of 50% kaolinite and 50% attapulgite. The used kaolinite and attapulgite possessed specific gravities of 2.73 and 2.75 and specific surface areas of 15 and 155 m^2/g, respectively. A general use (GU) Portland cement was used with specific gravity of 3.15 and specific surface area of 0.3 m^2/g. As the third binder, quartz-silt powder of 2–75 μm size, and specific gravity of 2.69 was used. Chemical composition of the binders is presented in Table 7.1. A polycarboxylate-ether (PCE) based high-range water-reducer (HRWR) was used as the chemical admixture.

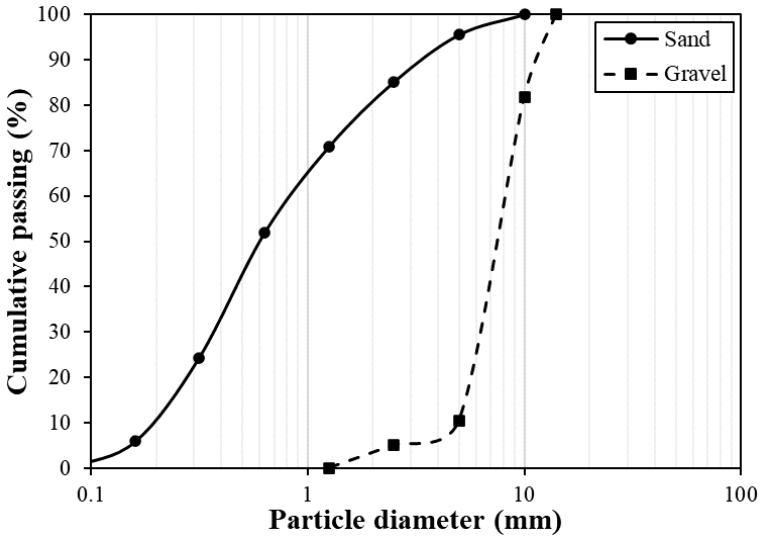

Fig. 7.1. Particle-size distribution of sand and gravel particles.

Table 7.1. Chemical composition of the binders used in this study.

Chemical composition (% wt.)	Binder type			
	GU cement	Kaolinite	Attapulgite	Quartz silt
CaO	62.50	0.10	2.92	0.01
SiO_2	19.30	46.10	66.20	99.02
Al_2O_3	4.80	38.10	11.71	0.64
Fe_2O_3	3.00	0.50	4.02	0.22
MgO	2.70	0.10	9.70	0.01
SO_3	4.10	0.04	-	-
Others	1.40	1.56	1.47	0.10
LOI*	2.20	13.50	3.98	-

LOI*: Loss of ignition

The mixture proportioning of the investigated concrete mixtures are summarized in Table 7.2. The three SCEC mixtures were carefully selected to achieve a minimum 1-day compressive strength of 1 MPa [30] and a slump flow of 700 mm with no visual segregation [31]. The investigated mixtures were proportioned with various clay types/contents covering large range of Atterberg limits [32], as summarized in Table 7.3. Due to plasticity of earth-based materials containing clay, Atterberg limits of the corresponding earths (i.e., clay, silt, and sand < 425 μm) were evaluated to obtain liquid limit (LL), plastic limit (PL), and plasticity index (PI). It should be noted that Atterberg limits are presented only for SCEC mixtures since there is no clay and silt in the reference conventionnel SCC mixture. The 28-day drying shrinkage of the investigated mixtures [33] are also presented in Table 7.3.

Table 7.2. Proportioning of the investigated mixtures.

Mix No.	Cement (kg/m^3)	Water (kg/m^3)	Clay Type I (kg/m^3)	Clay Type II (kg/m^3)	Silt (kg/m^3)	W/P	Sand (kg/m^3)	Gravel (kg/m^3)
C_{ref}	627.2	250.9	-	-	0	0.40	665.0	680.0
C120-II	120.0	266.7	-	83.2	389.4	0.45	750.1	511.4
C150-I	150.0	251.4	173.3	-	235.3	0.45	1197.0	136.0
C180-I	180.0	219.0	104.0	-	445.9	0.30	1000.2	255.7

Table 7.3. Atterberg limits of the three investigated earth mixtures.

Mix No.	Atterberg limits			Compressive strength (MPa)		28-day drying shrinkage (%)
	LL (%)	PL (%)	PI (%)	1-day	28-day	
C_{ref}	-	-	-	22.7	52.4	0.037
C120-II	32.8	21.8	11.0	1.2	3.3	0.104
C150-I	18.9	14.9	4.0	1.9	6.2	0.093
C180-I	18.9	15.8	3.1	3.3	12.0	0.078

7.2.2 Test methods

The investigated mixtures were prepared using a rotating drum mixer. The mixing procedure consisted of mixing sand and gravel particles for 90 s, followed by adding 1/3 of the mixing water and mixing for additional 60 s. The binders were then added and mixed for 30 s. Again, 1/3 of the mixing water and HRWR admixture were added and mixed for 60 s. Finally, the last 1/3 of mixing water was added and mixed for 90 s. After resting for 120 s, the mixing was resumed for an additional 180 s to finalize the mixing procedure. Hygrothermal and microstructural characterization of the samples were investigated after 28 days of curing at 23°C and 100% relative humidity, as follow:

7.2.2.1 Sorption isotherm

The sorption isotherm test, carried out in isothermal conditions, characterizes the relationship between water content and relative humidity of the surrounding environment in various moisture conditions ranging from 0 to 95%. The samples were first oven dried at 40°C for 24 h followed by air-vacuum drying before determining their dry masses. These values were then analyzed with the SPS ProUmid device using manometric method [34]. Cubic samples of 15 × 15 × 15 mm^3 dimensions were treated in adsorption-desorption isotherms. The changes in water-vapor volume adsorbed or desorbed were measured for each sample at a fixed temperature. The calculations were based on the adsorbed water by procurement of vapor pressure and perfect gas formula [35]. The

volumetric method was treated for water vapor sorption isotherms. In order to achieve more precise measurements, Belsorp aqua-3® device is equipped with three analysis ports to allow high output measurements. This method can attenuate possible inaccuracies used in the gravimetric methods by overcoming the sensitivity of the weighing devices.

7.2.2.2 Water vapor permeability

As one of the critical hygric properties, water vapor permeability test is essential for characterization of building materials by assessing migration of moisture in the samples. This migration is referred to vapor diffusion. The measurements were performed at 23°C using the cup method according to EN ISO 12572 standard [36]. The samples include cylinders of 78-mm diameter and 20-mm height. The test procedure consists in subjecting the sample to a pressure gradient. The gradient for dry cup consisted of 3% relative humidity inside the cup, and 50% outside. By using a Gravitest® device as a climatic chamber, each cup was automatically weighed with a high precision of 0.00001 g.

7.2.2.3 Gas permeability

Gas permeability of the mixtures was measured on cylindrical samples measuring 11-mm diameter and 50-mm thickness [37] using the Cembureau permeameter. The samples were preconditioned at 45°C temperature under vacuum until mass stabilization. These samples were then surrounded by a resin to ensure a unidirectional flow during the test. Specific permeability coefficient K_A can be calculated using the modified Darcy's equation, as follows:

$$K_A = \frac{2\mu P_0 Q L}{A(P_0^2 - P_1^2)} \quad \text{where } Q = \frac{V}{t_{avg}} \tag{7.1}$$

where μ (Pa.s), P_0 (Pa), P_1 (Pa), Q (m^3/s), L (m), A (m^2), V (m^3), and t_{avg} (s) are the dynamic viscosity of the gas, entrance and exit absolute pressure values, volumetric flow, sample thickness, surface area of the sample section, volume of the bubble flowmeter, and average passing time, respectively. It should be noted that the measured permeability coefficient is apparent permeability. Each test was performed under three different pressures of 150, 200, and 250 kPa to assess the intrinsic permeability (K_{int}). Using Klinkenberg method [38], K_{int} can be calculated as the interception of the K_A curve with respect to $1/P_m$ (where $P_m = \frac{P_0+P_1}{2}$) as:

$$K_A = K_{int}\left(\frac{\beta}{P_m}+1\right) \quad (7.2)$$

where β (Pa) is the Klinkenberg coefficient which varies with the intrinsic permeability [39].

7.2.2.4 Heat capacity

Calvet® calorimeter was used for measurement of specific heat capacity. The samples include cylinders of 7 mm in diameter and 5 cm in height. The reference cell and tested sample, in sealed cylinders, are enclosed in the calorimeter block to perform the test. In this device, samples were surrounded by 3D Calvet sensors so that all the emitted heat can be measured. A cryostat was also connected to regulate the internal temperature of the calorimeter. The test was performed in a temperature range of -10 to 40°C with a heating rate of 0.1°C/min. It is worth mentioning that since the heat loss of the 3D sensors is less than 10%, rather than those of the 2D sensors (50% to 70%), the 3D Calvet sensors are more accurate than the 2D ones.

7.2.2.5 Thermal conductivity

This inherent thermal property was measured under stationary conditions using the standard method of guarded hot plate conforming with the EN 12664 [40] and EN 12667 [41] specifications. The tested samples measured 15 × 15 cm^2 and a height of approximately 5 cm. The tests were carried out using the λ-Meter® EP500e device, as shown in Fig. 7.2. This set-up enables the heat transfer through a surface plate limited between two parallel cold and hot isotherm planes to impose a fixed temperature gradient. It is worth mentioning that transversal heat dissipation should be prevented since the longitudinal heat flow through the sample thickness should be considered. Putting guard rings surrounding the side of the samples can be favorable for this purpose. Thermal conductivity can thus be calculated through the electrical power provided by the device.

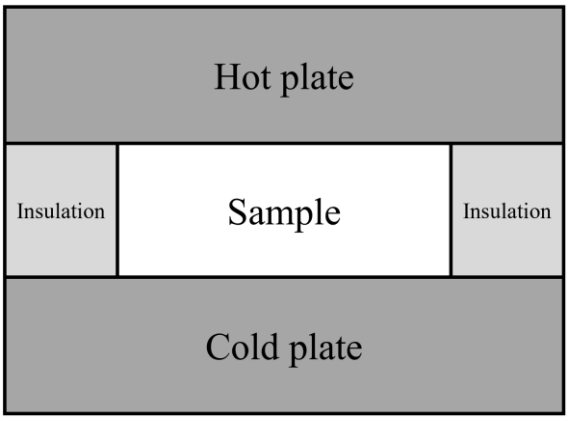

Fig. 7.2. Scheme of the Lambda-meter EP500e.

7.2.2.6 Thermogravimetric analysis (TGA)

The samples were vacuumed dried at 45°C to remove the water bound in the samples. Consequently, TGA procedure was performed on 100 mg of sample heated at a 10°C/min rate up to 1000°C.

7.2.2.7 Water porosity measurements

Three cubic samples of 5 × 5 × 5 cm^3 were used to determine the porosity of the concrete mixtures according to AFPC-AFREM [42]. Initially, the samples were water-saturated in order to obtain the saturated mass. The porosity was then calculated, as follows:

$$\varepsilon_p = \frac{M_{air} - M_{dry}}{M_{air} - M_{water}} \times 100\ (\%) \quad (7.3)$$

where M_{air}, M_{dry}, and M_{water} are the weight of saturated sample after removing from the water, dry sample weight (dried at 80 °C until mass stabilization), and hydrostatic weight of the sample saturated in water, respectively. Furthermore, surface pores and smoothness of the mixtures were also analyzed using a Keyence® VHX-7000 digital microscope.

7.2.2.8 Porosity measurements (3Flex)

The porous properties of the investigated mixtures, including surface area, pore volume, and pore size distribution, were measured using a 3Flex–high resolution surface characterization analyzer apparatus from Micromeritics®. Relative pressure (P/P_0) can be as low as 1.3×10^{-9} up to 1.0. The device allows advanced dosing method N_2 adsorption which can be measured by defining both pressure and volume increments. Hysteresis loop is associated with capillary condensation taking place in the mesopores which limits uptake at high relative pressure. It should be noted that prior to N_2 adsorption/desorption measurements, the samples (100–200 mg) were degassed in vacuum condition. The mass of each sample was measured with high precision microbalance with a resolution of ±1 µg. This testing reflects useful information for multilevel porosity, including the micropores (< 2 nm), mesopores (2–50 nm), and macropores (> 50 nm).

7.2.2.9 Mercury intrusion porosimetry (MIP)

The pore size distribution was determined using mercury intrusion. The samples were initially dried at a temperature of 45°C before the test until mass stabilization. Micromeritics Porosimeter (Autopore III 9420) with pressure range up to 400 MPa was used which can ensure the mercury to penetrate the pores ranging between 0.003 to 360 µm diameter, according to Laplace's law.

7.2.2.10 Microstructure observations

Surface microstructure observation was carried out using the CMOS-based digital microscope VHX 7000 (Keyence) with a magnification of ×6000 in the optical wavelength range. Magnifications of E20×20, E20×80, E100×150 and E500×500 were used to capture the observations. Furthermore, the morphological characteristics of the mixtures were analyzed using a scanning electron microscope (SEM) equipped with an Oxford Energy Dispersive Spectroscopy (EDS).

7.3 Results and discussion

The obtained results are discussed in terms of the hygrothermal properties of the investigated mixtures, followed by their microstructural characterization.

7.3.1 Sorption isotherm

In order to investigate the advantage of SCEC mixtures, adsorption and desorption isotherms at 23°C was assessed. The evolution of water content as a function of relative humidity is illustrated in Fig. 7.3a. As can be observed, the mixtures C_{ref} and C150-I exhibited the highest and lowest adsorption rates, respectively. The reference mixture C_{ref} showed an absorption of 3.3% compared to 1.4%, obtained with C150-I at 90% relative humidity. This can be due to the extraction of hydrophilic constituents which is responsible for low adsorption values of SCEC mixtures rather than C_{ref}. However, the obtained values for all the mixtures are lower than those of hemp concrete at different ages [43]. The reference mixture showed comparable sorption isotherm values with standard concrete, while the investigated SCEC mixtures performed similar to clay bricks [44,45]. Among the investigated SCEC mixtures, the mixture C180-I possessed the highest value which can be related to its high cement content compared to C150-I and C120-II mixtures. As can be observed in Fig. 7.3b, C_{ref} also showed the highest moisture storage capacity. A descending behavior in moisture storage capacity was observed for all the mixtures for RH less than 20% (Zone 1), while this was almost constant for RH between 20% and 60% (Zone 2), and ascending for RH values greater than 60% (Zone 3). The latter can be referred to the critical RH level above which the water content significantly increases.

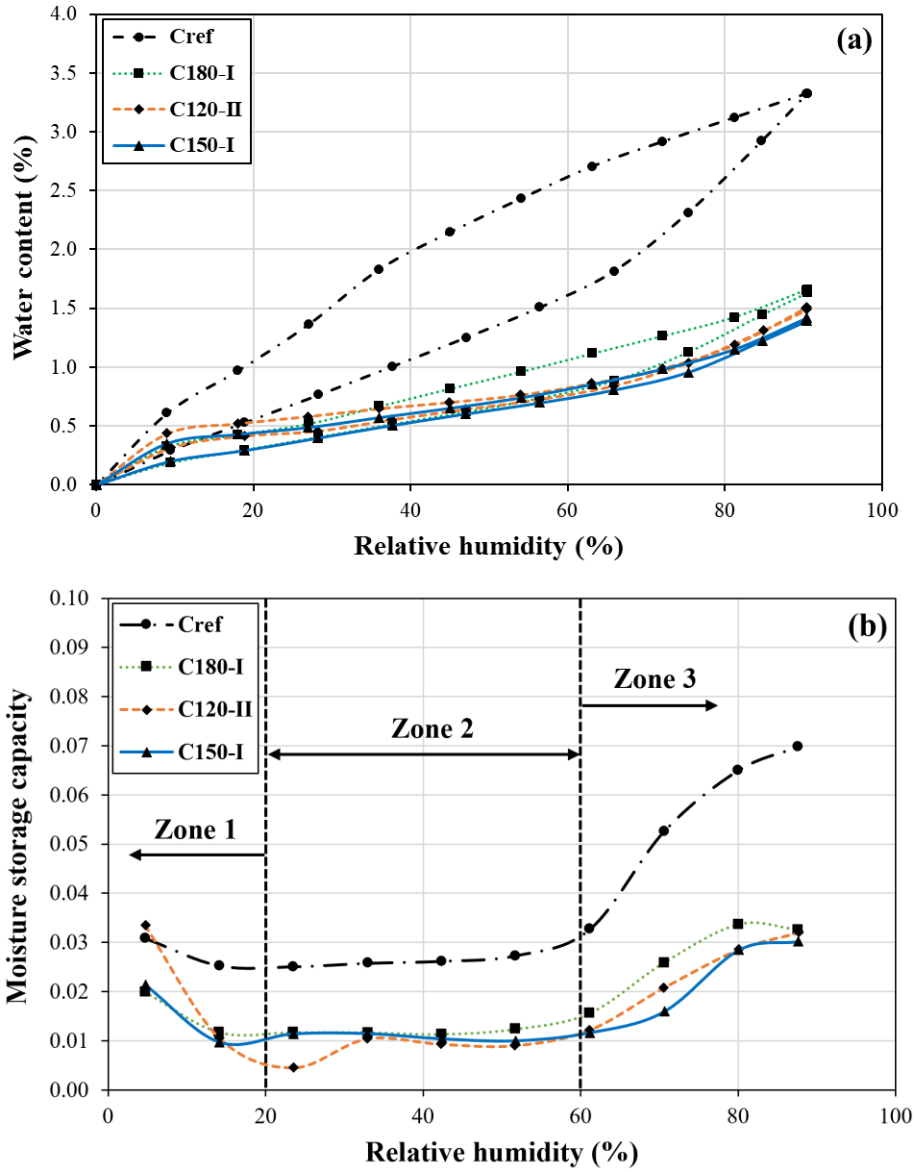

Fig. 7.3. (a) Water vapor adsorption-desorption isotherm and (b) moisture storage capacity of the investigated mixtures.

7.3.2 Water vapor permeability

Water vapor permeability and diffusion resistance factor [36] of the investigated mixtures are presented in Fig. 7.4. It should be mentioned that water vapor permeability was calculated in permanent regime after mass equilibrium of the cups. As can be observed in Fig. 7.4a, the mixtures C120-II and C_{ref} exhibited the highest and lowest water vapor permeability values, respectively. These values can be also reflected by their diffusion resistance factors (203.3 and 33.8). The results obtained with C_{ref} are in accordance with those reported in literature [45]. The obtained water vapor

permeability of the mixtures C150-I, C180-I, and C120-II are 4.1, 2.4, and 6.2 times of that of the reference mixture C_{ref}, respectively. This is due to the difference in their microstructure which affects the porosity and diffusion characteristic of the material. As can be observed in Fig. 7.4b, diffusion resistance factor is increasing with cement content. However, the obtained diffusion resistance factor results were higher than those of hemp concrete after 60 days of age (17.4) reported by Bennai et al. [43,45]. Allam et al. [46] also reported lower water vapor permeability for earth brick samples corresponding to 1.45E-10 up to 1.80E-10 $kg.m^{-1}.s^{-1}.Pa^{-1}$. This can refer to lower permeability of the investigated SCEC mixtures compared to earth bricks, yet higher than the cement concrete [45].

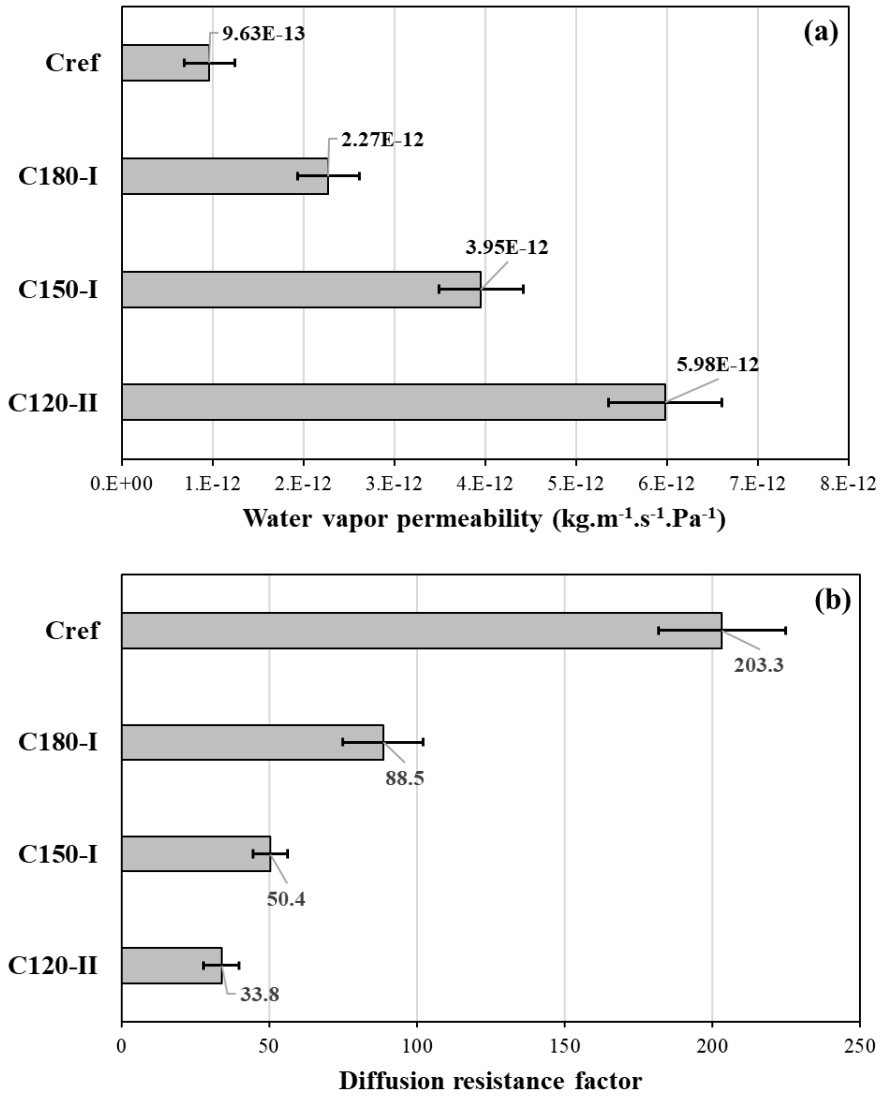

Fig. 7.4. (a) Water vapor permeability and (b) diffusion resistance factor of the investigated mixtures.

7.3.3 Gas permeability

The intrinsic gas permeability values of the investigated mixtures are summarized in Table 7.4. As can be observed, the reference mixture C_{ref} exhibited the lowest gas permeability value (1.80E-17 m^2) which is consistent with literature [47]. Among the SCEC mixtures, C180-I showed the lowest gas permeability followed by C150-I and C120-II. This can be explained by the reduction in porosity due to the higher content of cement. Indeed, permeability depends on both open porosity and connected pores based on Poiseuille's law. Garboczi [48] reported that permeability is proportional to the product of porosity and square main mode pore diameter. Similarly, several attempts were carried out to predict permeability from MIP results [49–51]. Therefore, it can confirm that C120-II should have the significant porosity and connected pores compared to the other mixtures. This will be further investigated in section 7.3.10.

Table 7.4. Intrinsic gas permeability of the investigated mixtures.

	C120-II	C150-I	C180-I	C_{ref}
K_{int} (m^2)	9.72E-16	1.25E-16	3.04E-17	1.80E-17

7.3.4 Heat capacity

Heat capacity is another important property of the heat transfer characterization of the building materials to evaluate the decrement factor and the time lag of a wall. The evolution of specific heat capacity of the investigated SCEC mixtures as a function of temperature (-10 to 40°C after drying at 40°C until mass stabilization) is presented in Fig. 7.5. The initial high increasing rate observed in Fig. 7.5 can be explained due to the strong thermal inertia inside the device, hence leading to a delay in heat transmission. Linear correlations were then fitted between the temperatures greater than 0°C and their corresponding specific capacity values for all the investigated mixtures. As can be observed, the reference mixture C_{ref} exhibited the highest specific heat value followed in a descending order by C150-I, C180-I and C120-II, respectively. For example, at temperature of 25 °C, the mixtures C_{ref}, C150-I, C180-I, and C120-II possessed specific heat capacity values of 1163, 955, 926, and 913 $J.kg^{-1}.K^{-1}$, respectively. The obtained specific heat capacity values of the investigated SCEC mixtures were comparable to those of typical raw earth materials (i.e., 800–950 $J.kg^{-1}.K^{-1}$) [52,53]. Indekeu et al. [5] reported a specific heat capacity of 939 $J.kg^{-1}.K^{-1}$ for rammed

earth. However, Porter et al. [54] reported higher values of 1321 and 1832 $J.kg^{-1}.K^{-1}$ for stabilized rammed earths with 6% cement and 20% crumb rubber in addition to 6% cement, respectively.

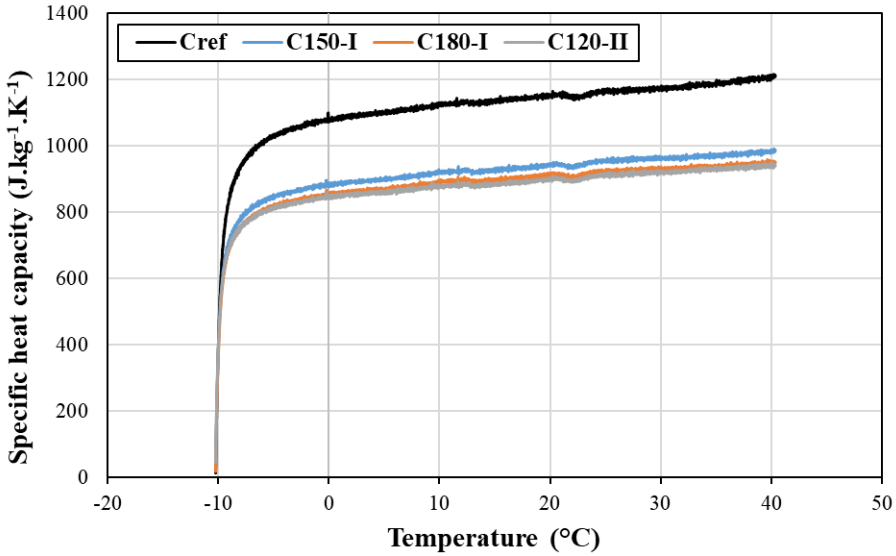

Fig. 7.5. Specific heat capacity of the investigated mixtures at different temperatures.

7.3.5 Thermal conductivity

The thermal conductivity of the investigated concrete mixtures was measured at 10, 23, and 40°C in dry state (Fig. 7.6a). It is worth mentioning that the results presented in Fig. 7.6a correspond to the mean values of three measurements in addition to their corresponding standard deviations. As expected, the reference mixture C_{ref} exhibited the highest thermal conductivity compared to the investigated SCEC mixtures. This value obtained in dry state at 10°C was 765 $mW.m^{-1}.K^{-1}$, while those of the mixtures C120-II, C150-I, and C180-I were 414, 486, and 477 $mW.m^{-1}.K^{-1}$, respectively. The incorporation of earthen materials led to almost 37%–46% lower thermal conductivity, which can be explained due to the low thermal conductivity of earthen materials and higher porosity of the earthen matrix, hence contributing to damping the heat transmission. Similar trends were also observed at 23 and 40°C. As can be observed in Fig. 7.6a, the obtained results increases linearly with temperature, which is consistent with literature [55]. Indekeu et al. [5] reported the thermal conductivity of 1.1 $W.m^{-1}.K^{-1}$ for RE which is higher than those obtained for the investigated SCEC mixtures. Moreover, the thermal conductivity values are lower than those reported for cement-stabilized rammed earth (i.e., 833–1010 $mW.m^{-1}.K^{-1}$ at dry state) [56]. Furthermore, Hall and Allison [57] reported a lower dry state thermal conductivity of 643 $mW.m^{-}$

$^{1}.K^{-1}$ for a lower dry density of 1900 kg/m^3. The obtained results for the investigated SCEC mixtures were also found lower than those reported for unfired earth (0.77–0.95 W.m^{-1}.K^{-1}) [52]. As can be observed in Fig. 7.6b, the investigated SCEC mixtures showed lower dry density values than the reference mixture C_{ref}. This lower density can explain the lower thermal conductivity values as a consequence of lower cement content and its replacement with silt and clay particles.

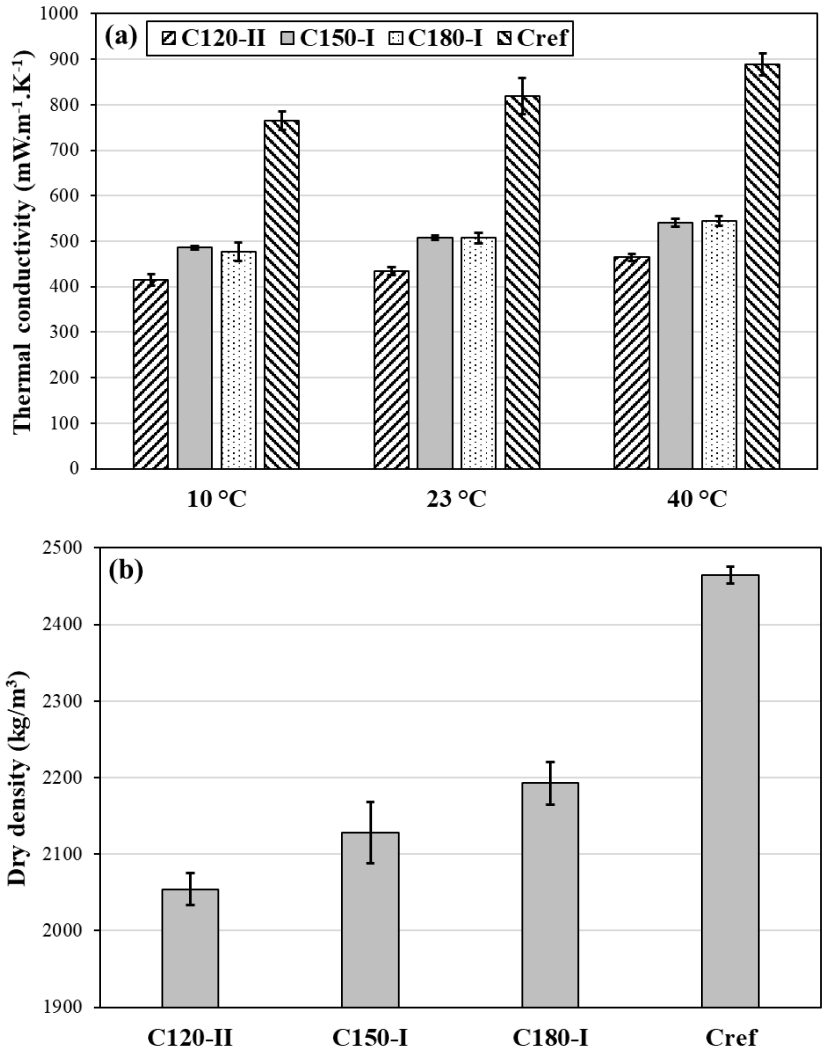

Fig. 7.6. (a) Thermal conductivity in dry state and (b) dry density of the investigated mixtures.

The thermal conductivity of wet mixtures was also determined on samples that were saturated in water to reach a constant mass. Thereafter, the saturated samples were wrapped in a stretch film to avoid any water evaporation during the measurement. The thermal conductivity of the investigated mixtures measured at temperatures of 10, 23, and 40°C in wet (saturated) state are shown in Fig.

7.7a. As can be observed, wet mixtures exhibited higher thermal conductivity than dry samples, regardless of temperature. For instance, thermal conductivity of the reference mixture C_{ref} at 10, 23, and 40°C increased by 90.4%, 93.4%, and 95.7%, respectively. The mixtures C180-I and C120-II exhibited the lowest and highest increasing rates of 51.4%, 63.0%, and 71.9% (for C180-I), and 88.5%, 102.1%, and 121.3% (for C120-II) at 10, 23, and 40°C, respectively. This behavior may be related to the presence of water in internal pores of each system, considering its significantly higher thermal conductivity than air. Similar trend was observed in the case of wet density results, as shown in Fig. 7.7b. Three SCEC mixtures showed lower thermal conductivity compared to the reference mixtures C_{ref} at all temperatures. These values were lower than those reported in literature [56] for cement-stabilized rammed earth at wet state (i.e., 1369–1820 $mW.m^{-1}.K^{-1}$). As expected, the investigated mixtures can act as insulating materials in dry state, but as conductive materials in wet state. It should be mentioned that, based on the obtained sorption isotherm results, it can be concluded that the SCEC mixtures exhibited lower water content compared to the reference mixture exposed to higher relative humidity values. The lower water content leads to lower thermal conductivity which is an advantage for the SCEC mixtures.

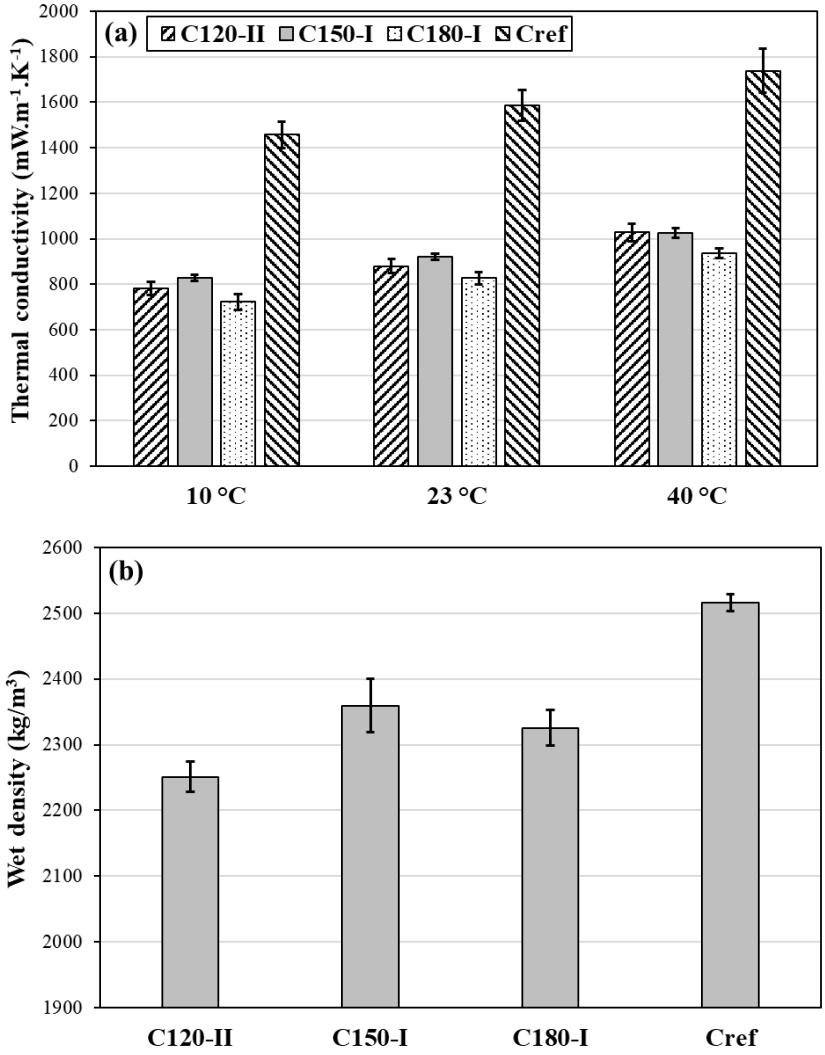

Fig. 7.7. (a) Thermal conductivity in wet state and (b) wet density of the investigated mixtures.

Thermal mass is the ability to keep the initial temperature of a material when subjected to perturbation, which is quantified by two parameters, including diffusivity (D) and effusivity (E), as follow [28]:

$$D = \frac{\lambda}{\rho C_P} \tag{7.4}$$

$$E = \sqrt{\lambda \rho C_P} \tag{7.5}$$

where λ ($W.m^{-1}.K^{-1}$), ρ ($kg.m^{-3}$) and CP ($J.kg^{-1}.K^{-1}$) are thermal conductivity, dry density, and specific heat capacity of the material, respectively. The thermal diffusivity and effusivity represent how a given material transmits temperature variation and exchanges energy with its surrounding,

respectively. The lower diffusivity reflects the higher buffering effect, while the higher effusivity means the material adsorbs heat more quickly without temperature rise at its surface. Low diffusivity and higher effusivity is the good compromise to have an appropriate thermal performance.

Fig. 7.8 presents the diffusivity and effusivity of the investigated mixtures. As can be observed, SCEC mixtures exhibited lower diffusivity compared to the reference mixture. This reveals that SCEC have an improved thermal performance in terms of heat transmission. However, reference concrete mixture showed higher effusivity, allowing to adsorb heat without much temperature rise in the surface. Soudani et al. [28] reported the lower diffusivity and effusivity of earthen materials (dry and wet earth and solid brick) in comparison with solid concrete which is in accordance with the obtained results. The authors also reported the lower diffusivity and effusivity of wood compared to earthen materials [28]. This suggest that earth can offer a good compromise of both low diffusivity and high effusivity in general. Cagnon et al. [53] reported the effusivity of 900–1100 $J.kg^{-1}.m^{-2}.s^{-1/2}$ for earth bricks which is in a comparable range of the investigated SCEC mixtures. Moreover, El Fgaier et al. [58] reported that thermal diffusivity and effusivity of unfired earth bricks lied in the range of 5.72E-7–9.23E-7 $m^2.s^{-1}$ and 936–1177 $J.kg^{-1}.m^{-2}.s^{-1/2}$, respectively. The obtained results of the investigated SCEC mixtures showed comparable effusivity, while possessing lower diffusivity values compared to those reported for unfired earth bricks [58].

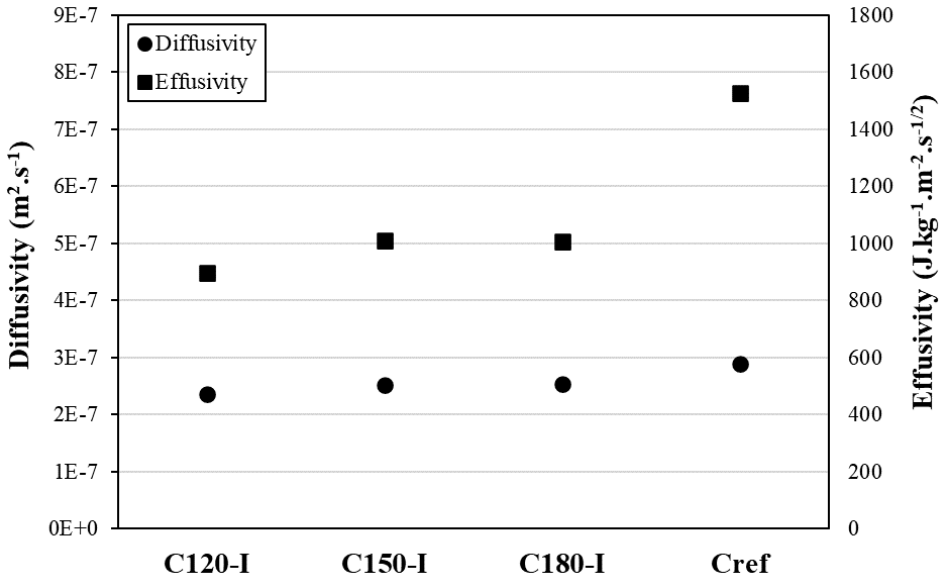

Fig. 7.8. Diffusivity and effusivity of the investigated mixtures.

7.3.6 Thermogravimetric analysis (TGA)

The water content is physically and chemically bound in the mixtures. A thermogravimetric analysis (TGA) can assess the chemically bound water to find the formation of different phases. Fig. 7.9 presents the results of the TGA analyses for all the investigated mixtures. According to the literature [59–61], Dehydration of calcium silicate hydrate (CSH), ettringite (AF_t), and hemicarboaluminate, monocarboaluminate, and monosulfoaluminate (all phases are denoted as AF_m) occurs up to 200°C, while dehydroxylation of portlandite (CH) takes place at 400–500°C. Decarbonation of calcium carbonates occurs at 700–800°C. The Af_t and AF_m phases are hard to be distinguished by TGA since their decomposition temperatures can overlay each other. As can be observed in Fig. 7.9, a large peak occurred for the reference mixture C_{ref} at approximately 150°C, compared to other SCEC mixtures. This can be attributed to the decomposition of CSH. A distinct peak at approximately 160°C was observed for SCEC mixtures which corresponds to the formation of AF_m compounds [62,63]. The mixture C120-II showed two peaks corresponding to 240 and 360°C, which can be related to the decomposition of attapulgite compounds [64,65]. The peak observed at approximately 450°C was comparable for the three SCEC mixtures and, as expected, much higher for the reference mixture due to dehydration of CH. Two mixtures with Clay Type I showed another peak at approximately 520°C which can be attributed to the dehydration of kaolinite [66,67]. Within the temperature range of 750–780°C, the decomposition of calcium carbonate was observed for all the mixtures, corresponding to the decarbonation phenomenon. In general, the reference mixture was distinguished by the highest mass losses with a more intensive rise in the CSH peak than CH and decarbonation regions.

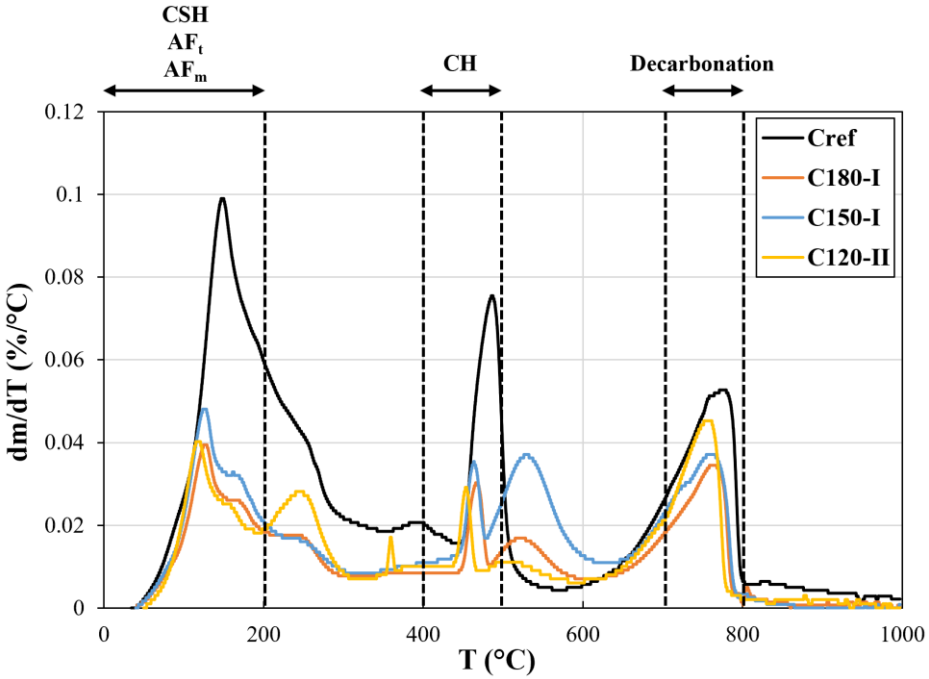

Fig. 7.9. Derivative mass changes of the investigate mixtures determined by a thermogravimetric analysis (TGA).

7.3.7 Water porosity measurements

The mean porosity values of three measurements for each of the investigated mixtures are presented in Fig. 7.10. Each mean value is calculated on three different measurements. As can be observed, the mixtures C120-II and C_{ref} showed the highest and lowest porosity values of 22.85% and 12.55%, respectively. These values are lower than to those of rammed earth reported in literature (i.e., 42.2%) [68]. The C120-II mixture incorporating Clay Type II and lower cement content showed slightly higher porosity than the SCEC mixtures containing Clay Type I and the reference mixture. It can be due to the higher surface area and heterogeneity of the Clay Type II-based mixture, hence leading to more pore development. It should be noted that this can be count as an advantage to improve the insulating capacity since thermal conductivity is inversely proportional to the porosity [69,70].

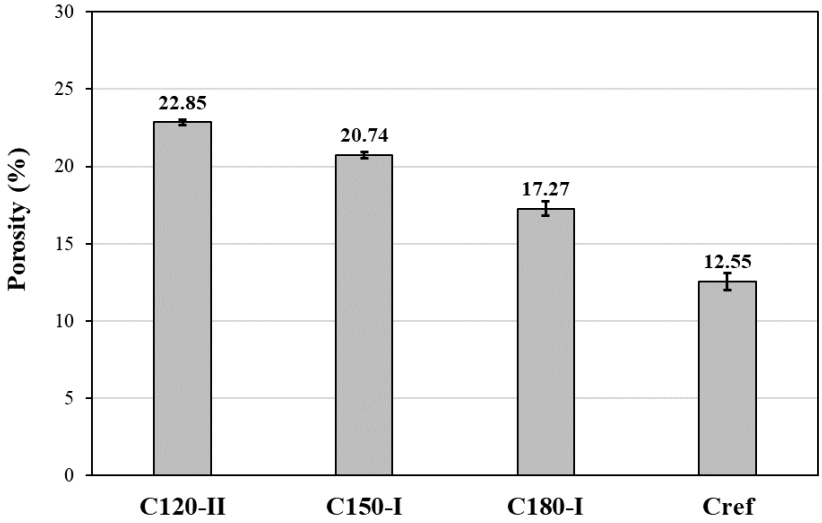

Fig. 7.10. Total porosity of the investigated mixtures.

7.3.8 Porosity measurements (3Flex)

The adsorption capacity of an adsorbent depends on the pore-size distribution and the surface area of the material. The pore-size distribution of corresponding paste matrix (P denotes paste) of the investigated mixtures determined using nitrogen adsorption-desorption isotherm is presented in Fig. 7.11a. It is important to mention that this test was performed only on paste scale since it provides useful information on very small pore diameters. As can be observed, pore size ranges between 20 to 50 nm for all the paste mixtures, hence confirming their mesoporosity. Moreover, the mixture P150-I showed the highest distribution of dominant pore diameter of 44 nm followed by P120-II with dominant pore diameter of 39 nm. As expected, Pref gained the lowest distribution of dominant pore diameter of 40 nm compared to other paste mixtures. Furthermore, the BET surface area values of the paste mixtures are presented in Fig. 7.11b. As can be observed, the mixtures P150-I and P_{ref} gained the highest and lowest BET surface area values, respectively. Due to the advantage of high specific surface area and mesoporosity of a porous material to possess higher moisture buffer [16,17], the obtained results can explain the higher permeability of C120-II and C150-I compared to C_{ref}.

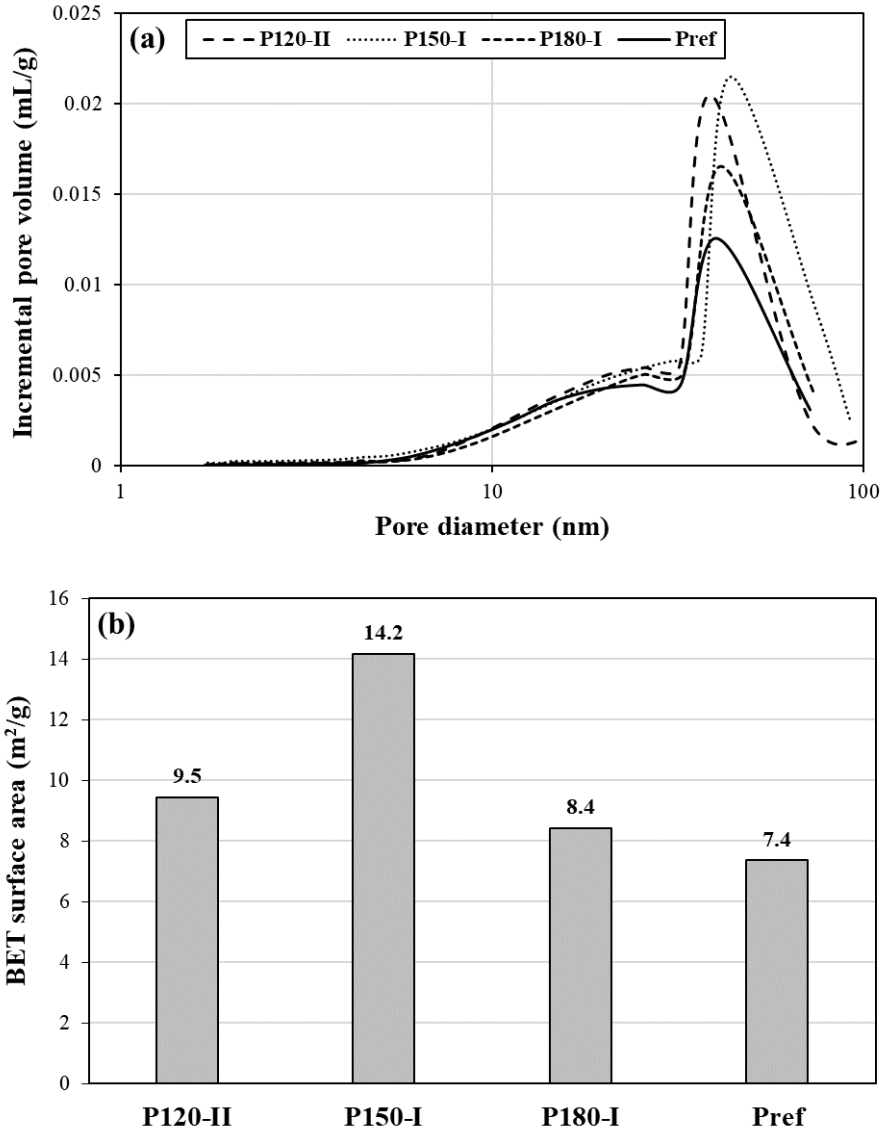

Fig. 7.11. (a) Pore size distribution and (b) BET surface area of the paste matrices of the investigated concrete mixtures.

7.3.9 Mercury intrusion porosimetry (MIP)

The mercury intrusion porosimetry results are presented in Fig. 7.12. Pore modes are commonly classified as micropores (< 2 nm), mesopores (2–50 nm), and macropores (> 50 nm), responsible for micropore filling, capillary condensation, and multilayer adsorption, respectively [71]. In order to facilitate the comparison of the mixtures, the obtained pore modes from the normal pore distributions of the investigated mixtures are summarized in Table 7.5. As can be observed, the mixtures C120-II and C150-I showed secondary pore modes which may be a consequence of an

interaction between clay particles and superplasticizer, as well as the relatively high W/P ratio compared to C180-I [47]. The smallest pore mode of the mixture C180-I can be due to its lower W/P ratio compared to other mixtures [47]. The mixtures C_{ref} and C150-I exhibited the lowest and highest distribution of pores with main pore modes of 96 and 95 nm, respectively. The mixtures containing Clay Type I showed comparable mesopore distribution and higher than that of the reference and C120-II mixtures. However, the mixture C120-II showed the highest fraction of pores greater than 100 nm among all the mixtures. As summarized in Table 7.5, the mixtures containing Clay Type I achieved the highest mesopore distribution, while the mixture made with Clay Type II exhibited the highest macropore distribution followed by C150-I and C120-I. These different pore distributions can dictate the permeability and performance of the mixtures. It is worthy to mention that the main/secondary pore modes are in the range of macropores for all the mixtures.

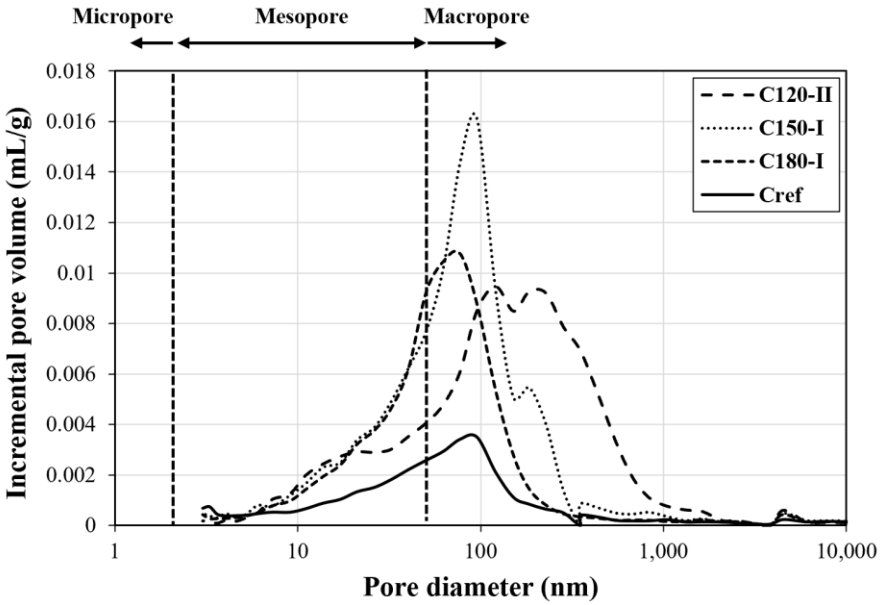

Fig. 7.12. Total porosity of the investigated mixtures.

Table 7.5. Pore modes of the investigated mixtures extracted from MIP.

Mix no.	Main pore mode D_c (nm)	Secondary pore mode (nm)	Cumulative pore volume (<50 nm) (mL/g)	Cumulative pore volume (<1000 nm) (mL/g)
C120-II	121	183	0.0276	0.1105
C150-I	95	181	0.0377	0.1070
C180-I	77	-	0.0370	0.0792
C_{ref}	96	-	0.0166	0.0331

Water vapor and gas permeability, drying shrinkage, and compressive strength results showed promising correlations with cumulative pore volume in different classes. As can be observed in Fig. 7.13a, water vapor permeability is in good agreement with cumulative pore volume of 100–200 nm. On the other hand, as shown in Fig. 7.13b, the cumulative pore volume values ranging from 100 to 300 nm can be a good indicator to predict the gas permeability. Furthermore, as presented in Fig. 7.14, higher cumulative pore volume of less than 1 μm led to higher drying shrinkage and lower compressive strength values. Thus, this can be concluded that permeability, drying shrinkage, and compressive strength parameters are highly dependent on the distribution of the pores in the mixture.

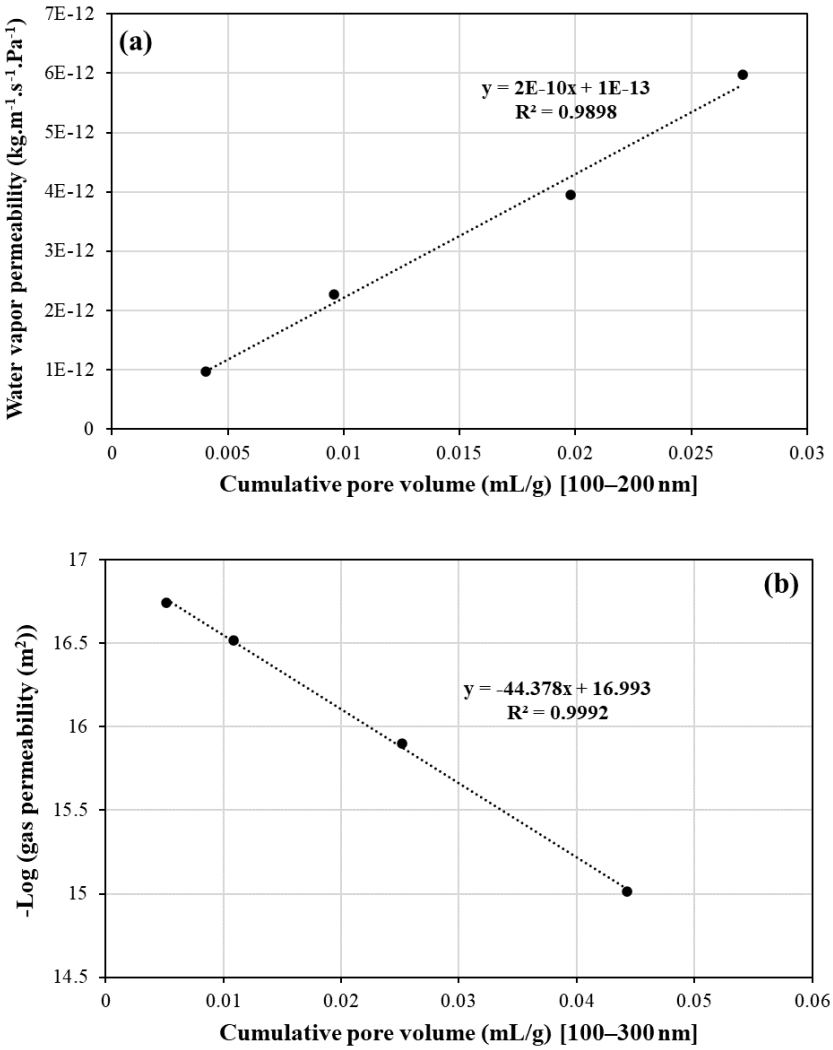

Fig. 7.13. Cumulative pore volume vs. (a) water vapor and (b) gas permeability of the investigated mixtures.

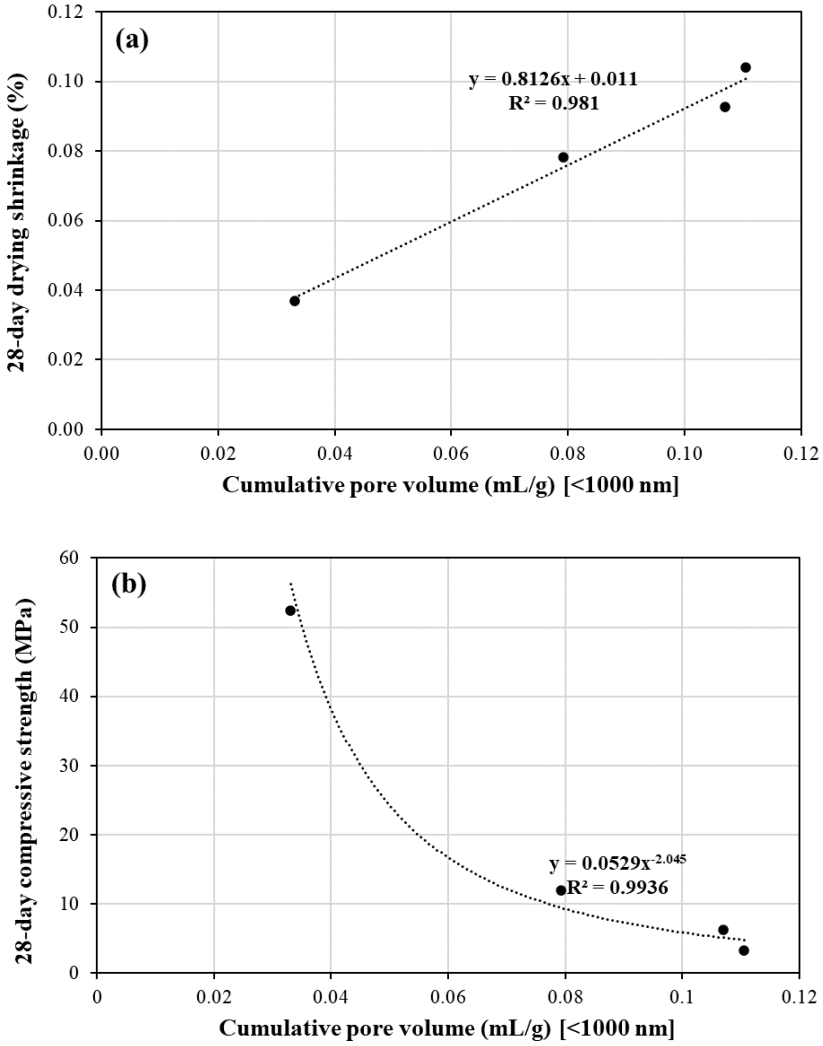

Fig. 7.14. Cumulative pore volume vs. 28-days (a) drying shrinkage and (b) compressive strength of the investigated mixtures.

7.3.10 Microstructure observations

The microscopic surface observations of the investigated mixtures are shown in Fig. 7.15. As can be observed, the reference mixture C_{ref} showed the smoothest surface with minimized pores. On the other hand, the mixtures C120-II and C150-I showed the highest number of large pores compared to C180-I and C_{ref}, hence confirming their higher porosity. The largest pore sizes of 1708 and 1169 µm were obtained on the surface of the mixtures C120-II and C150-I, respectively. This can reflect the higher distribution of macropores in these two mixtures, as concluded earlier using the MIP test. Moreover, the microscopic images showed good adhesion in the matrix with different

cement contents. The brighter color in the images corresponding to the investigated SCEC mixtures can be explained due to their different binder system (addition of clay and silt).

(a)

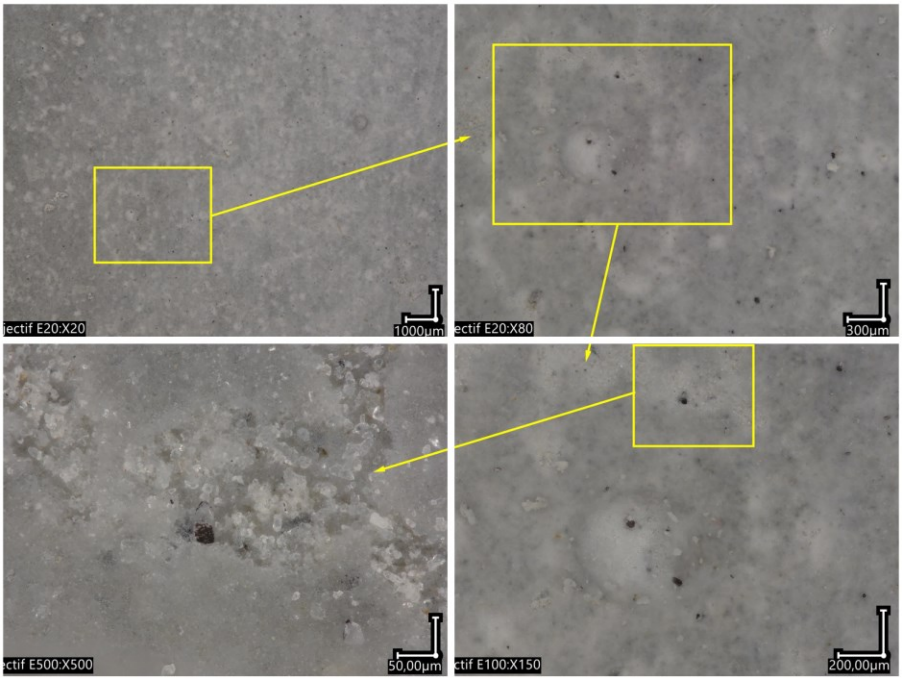

(b)

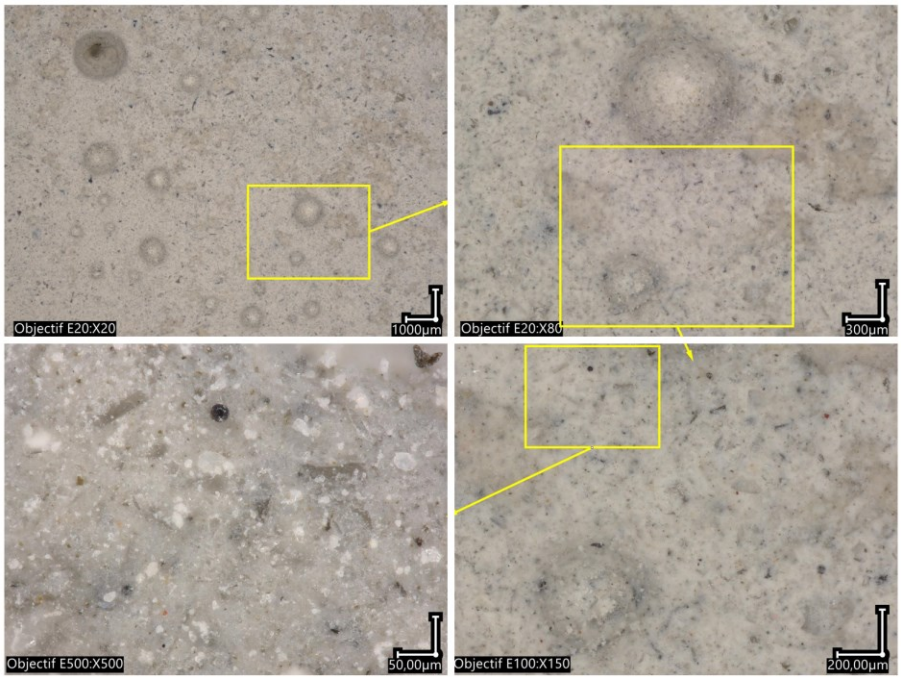

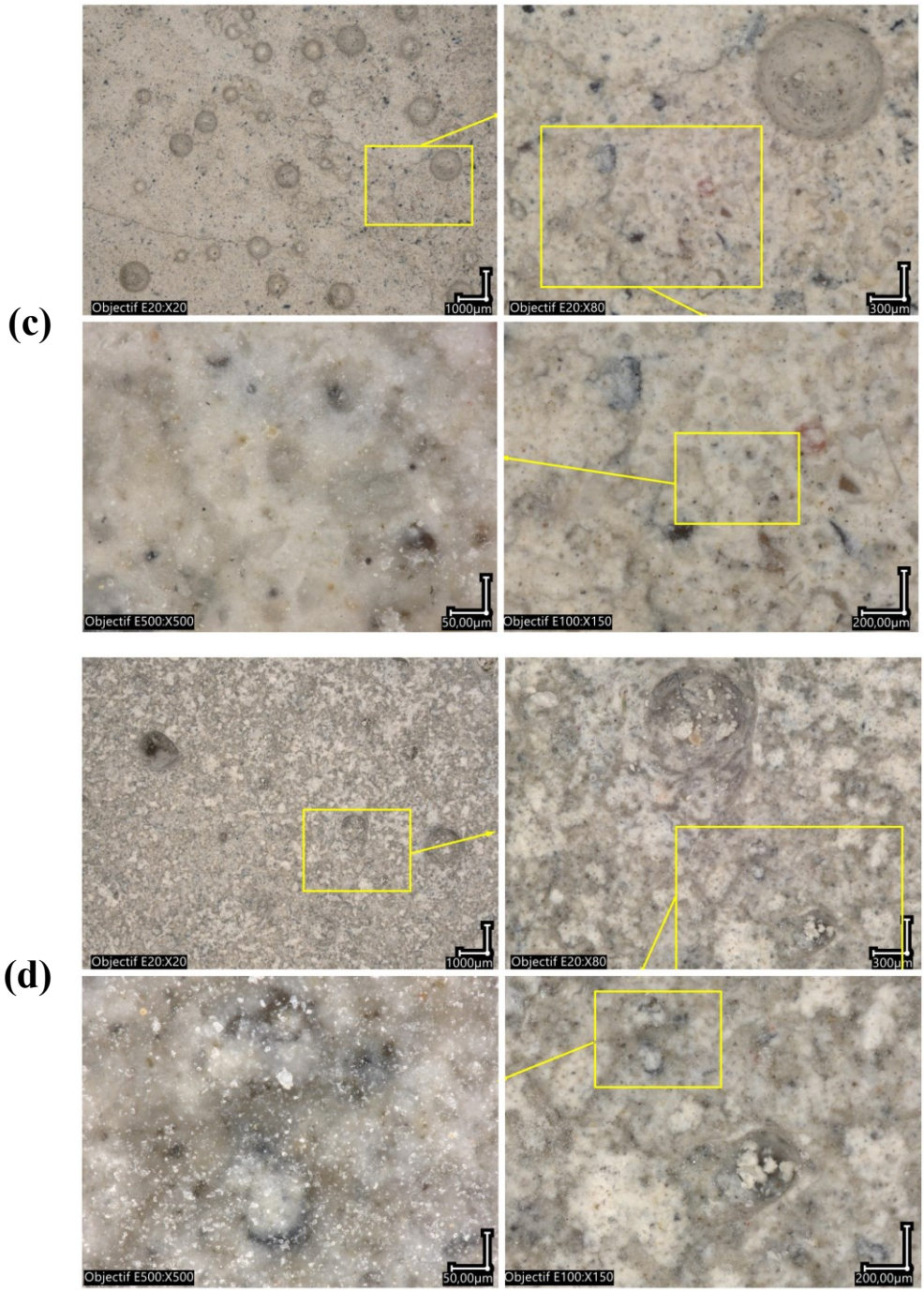

Fig. 7.15. Microscopic surface observations of (a) C_{ref}, and the SCEC ones as (b) C120-II (c) C150-I, (d) C180-I.

The scanning electronic microscope (SEM) images of corresponding paste matrices of the investigated mixtures are presented in Fig. 7.16. Typical CSH network can be observed in Fig. 7.16a–d. As expected, the main product of the reference mixture includes CSH. Furthermore,

needles of ettringite can be also obviously detected in Fig. 7.16a, 7.16c and 7.16d. Kaolin clay particles are formed in numerous micron-sized kaolinite platelets, known as kaolinite book, representing their morphological structure [72,73]. The appearance of such morphology can be observed in Fig. 7.16b, characterized by stacked pseudo-hexagonal platelets of 1–2 µm diameter with different thicknesses, depending on the kaolinite book. On the other hand, the quartz particles have regular edges with clean surface [74]. The energy dispersive spectroscopy (EDS) analysis in Fig. 7.16a confirmed presence of chemical compositions similar to that of quartz particles with regular edges which was well surrounded with main products of cement hydration. This can prove the good homogeneity in the mixture with the lowest cement content (120 kg/m^3).

(a)

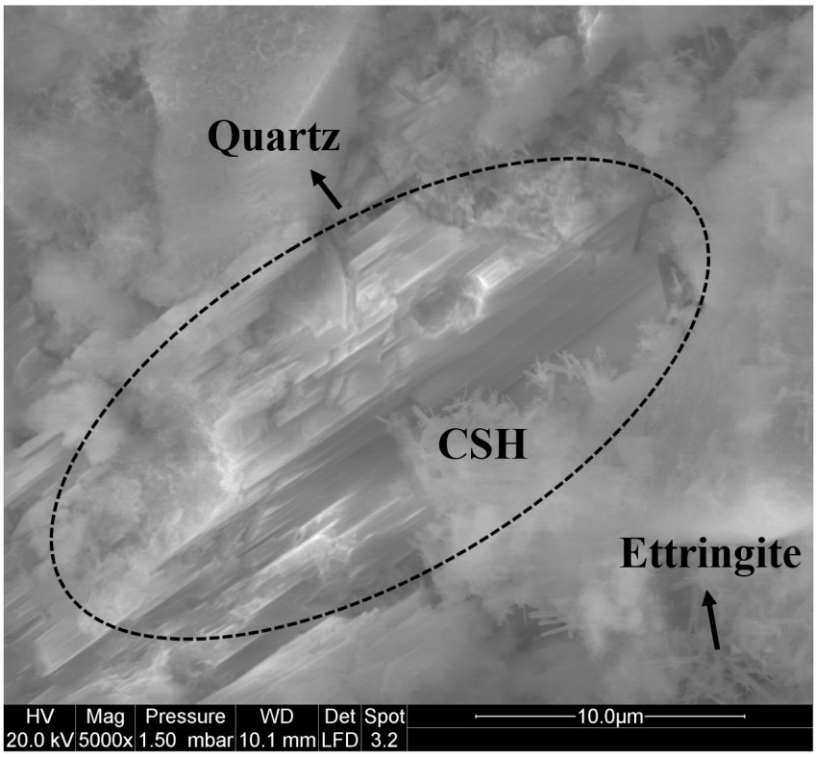

(b)

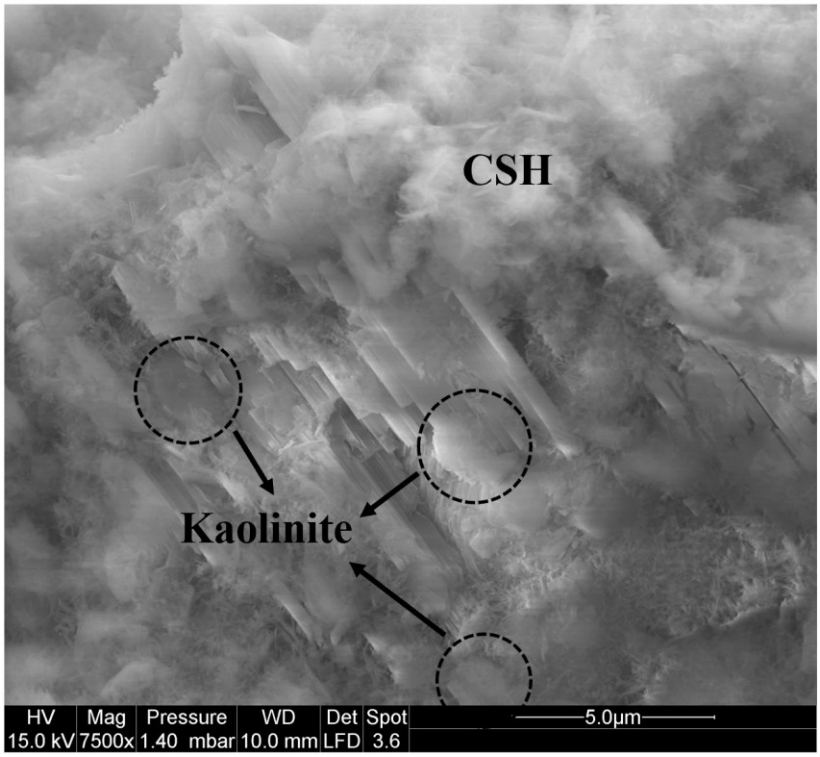
CSH
Kaolinite
HV Mag Pressure WD Det Spot
15.0 kV 7500x 1.40 mbar 10.0 mm LFD 3.6
5.0µm

(c)

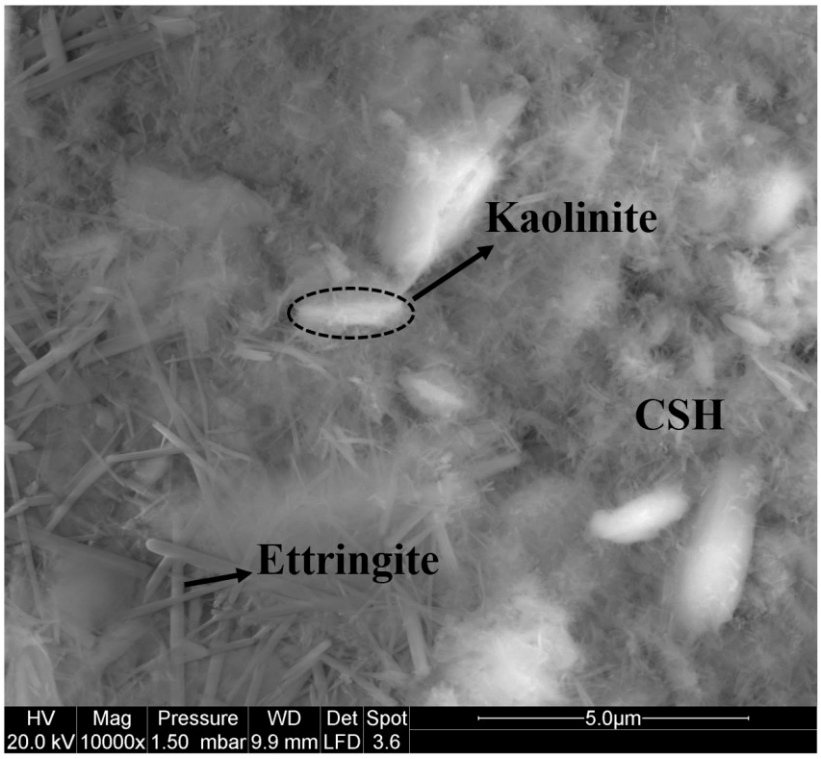
Kaolinite
CSH
Ettringite
HV Mag Pressure WD Det Spot
20.0 kV 10000x 1.50 mbar 9.9 mm LFD 3.6
5.0µm

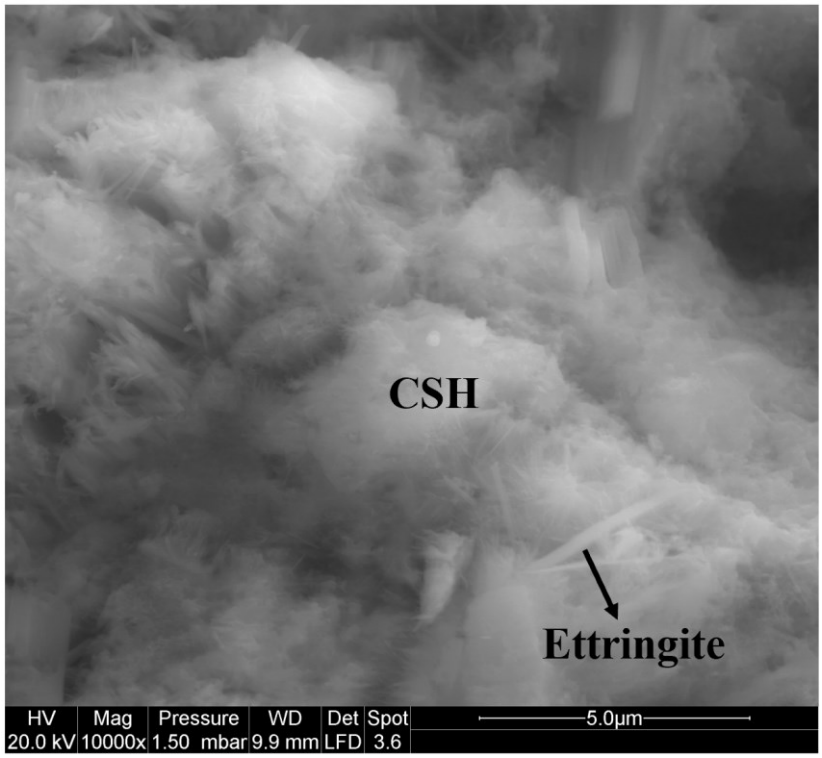

Fig. 7.16. SEM image of the investigated paste mixtures, including (a) P120-II (b) P150-I, (c) P180-I, and (d) P_{ref}.

7.4 Conclusions

In this study, hygrothermal and microstructural characteristics of three self-consolidating earth concrete (SCEC) mixtures, containing kaolinite and attapulgite clay types, and a cement-based reference mixture were investigated. These included sorption isotherm, water vapor and gas permeability, heat capacity, thermal parameters (conductivity, diffusivity and effusivity), moisture buffer value, TGA, total porosity, and pores distribution, as well as surface and SEM microstructural observations. According to the experimental results the following concluding remarks can be pointed out:

- The results of the sorption isotherm measurements revealed that the SCEC mixtures exhibited lower water content than conventional and hemp concrete when exposed to higher relative humidity values. This corresponds to clay bricks. At 90% relative humidity, the gained water content of the reference mixture C_{ref} was 3.3% compared to that of the investigated SCEC mixtures around 1.5%.

- SCEC mixtures showed higher water vapor diffusion resistance factor and gas permeability compared to clay bricks and hemp concrete, yet lower than conventional concrete. The obtained water vapor permeability result of the investigated SCEC mixtures ranged between 9.63E-13 and 3.95E-12 $kg.m^{-1}.s^{-1}.Pa^{-1}$.

- SCEC exhibited lower heat capacity and thermal conductivity values than the reference mixture in dry and wet states, regardless of temperatures. The mixture C120-II, made with Clay Type II, exhibited the lowest thermal conductivity of 414 $mW.m^{-1}.K^{-1}$ at dry state at 10 °C temperature, and 88.5% increasing rate at wet state. The investigated SCEC mixtures presented lower diffusivity and effusivity values than the reference mixture.

- TGA revealed the higher mass loss at CSH, CH, and decarbonation decompositions of the reference concrete mixture compared to the SCEC ones. The mixture C120-II showed two peaks at 240 and 360°C revealing the decomposition of attapulgite compounds. However, the mixtures containing Clay Type I (100% kaolinite) showed a distinct mass loss peak at approximately 520°C, which is attributed to the dehydration of kaolinite.

- The results showed that total porosity decreases with higher cement contents. Moreover, different pore distributions were obtained for the investigated mixtures. Furthermore, the water vapor and gas permeability were found in strong agreements with cumulative pore volume values in the ranges of 100–200 and 100–300 nm, respectively. Good correlations were also established between the cumulative pore volume of pore sizes less than 1 μm and both drying shrinkage and compressive strength values at 28 days of age.

- SCEC mixtures offer high permeability and low thermal conductivity values with satisfying effusivity and diffusivity parameters compared to other construction materials. Therefore, they can be used as building envelopes with satisfying hygrothermal performance.

7.5 Declaration of competing interest

The authors declare that they have no known competing financial interests or personal relationships that could have appeared to influence the work reported in this paper.

7.6 Acknowledgement

The authors wish to thank the financial support of the National Science and Engineering Research Council of Canada (NSERC) and the eight industrial partners participating in the NSERC Chair on Development of Flowable Concrete with Adapted Rheology and their Application in Concrete Infrastructures, held by Professor Ammar Yahia at the Université de Sherbrooke. The authors would also like to thank the staff and technicians at La Rochelle Université for helping in carrying out the tests.

REFERENCES

[1] International Energy Agency, The Reduction of Greenhouse Gas Emissions From The Cement Industry, Report PH3/7, Paris, France, 1999.

[2] F. Pacheco-Torgal, S. Jalali, Earth construction: Lessons from the past for future eco-efficient construction, Constr. Build. Mater. 29 (2012) 512–519. https://doi.org/10.1016/j.conbuildmat.2011.10.054.

[3] M. Saidi, A.S. Cherif, B. Zeghmati, E. Sediki, Stabilization effects on the thermal conductivity and sorption behavior of earth bricks, Constr. Build. Mater. 167 (2018) 566–577. https://doi.org/10.1016/J.CONBUILDMAT.2018.02.063.

[4] E. Kianfar, V. Toufigh, Reliability analysis of rammed earth structures, Constr. Build. Mater. 127 (2016) 884–895. https://doi.org/10.1016/J.CONBUILDMAT.2016.10.052.

[5] M.L. Indekeu, M. Woloszyn, A.-C. Grillet, L. Soudani, A. Fabbri, Towards hygrothermal characterization of rammed earth with small-scale dynamic methods, Energy Procedia. 132 (2017) 297–302.

[6] V. Toufigh, E. Kianfar, The effects of stabilizers on the thermal and the mechanical properties of rammed earth at various humidities and their environmental impacts, Constr. Build. Mater. 200 (2019) 616–629. https://doi.org/10.1016/J.CONBUILDMAT.2018.12.050.

[7] H. Van Damme, H. Houben, Earth concrete. Stabilization revisited, Cem. Concr. Res. 114 (2018) 90–102. https://doi.org/10.1016/J.CEMCONRES.2017.02.035.

[8] R. Bahar, M. Benazzoug, S. Kenai, Performance of compacted cement-stabilised soil, Cem. Concr. Compos. 26 (2004) 811–820. https://doi.org/10.1016/j.cemconcomp.2004.01.003.

[9] M. Hall, Y. Djerbib, Rammed earth sample production: Context, recommendations and consistency, Constr. Build. Mater. 18 (2004) 281–286. https://doi.org/10.1016/j.conbuildmat.2003.11.001.

[10] L. Miccoli, U. Müller, P. Fontana, Mechanical behaviour of earthen materials: A comparison between earth block masonry, rammed earth and cob, Constr. Build. Mater. 61 (2014) 327–339. https://doi.org/10.1016/j.conbuildmat.2014.03.009.

[11] M. Kohandelnia, M. Hosseinpoor, A. Yahia, R. Belarbi, A new approach for proportioning self-consolidating earth paste (SCEP) using the Taguchi method, Constr. Build. Mater. 347 (2022) 128579. https://doi.org/10.1016/J.CONBUILDMAT.2022.128579.

[12] C.M. Ouellet-Plamondon, G. Habert, Self-Compacted Clay based Concrete (SCCC): Proof-of-concept, J. Clean. Prod. 117 (2016) 160–168. https://doi.org/10.1016/j.jclepro.2015.12.048.

[13] G. Landrou, C. Brumaud, F. Winnefeld, R.J. Flatt, G. Habert, Lime as an anti-plasticizer for self-compacting clay concrete, Materials (Basel). 9 (2016). https://doi.org/10.3390/ma9050330.

[14] V. Costanzo, G. Evola, L. Marletta, F. Nocera, The effectiveness of phase change materials in relation to summer thermal comfort in air-conditioned office buildings, Build. Simul. 11 (2018) 1145–1161. https://doi.org/10.1007/s12273-018-0468-2.

[15] M. Salonvaara, T. Ojanen, A. Holm, H.M. Künzel, A.N. Karagiozis, Moisture buffering effects on indoor air quality-experimental and simulation results, in: Proc. Build. IX, Clearwater, Florida, 2004.

[16] M. Raimondo, M. Dondi, F. Mazzanti, P. Stefanizzi, P. Bondi, Equilibrium moisture content of clay bricks: The influence of the porous structure, Build. Environ. 42 (2007) 926–932.

[17] D.-H. Vu, K.-S. Wang, B.H. Bac, B.X. Nam, Humidity control materials prepared from diatomite and volcanic ash, Constr. Build. Mater. 38 (2013) 1066–1072.

[18] F. McGregor, A. Heath, A. Shea, M. Lawrence, The moisture buffering capacity of unfired clay masonry, Build. Environ. 82 (2014) 599–607.

[19] A. Tavil, Thermal behavior of masonry walls in Istanbul, Constr. Build. Mater. 18 (2004) 111–118. https://doi.org/10.1016/J.CONBUILDMAT.2003.08.014.

[20] V.B. LOVEC, M.Đ. JOVANOVIC–POPOVIC, B.D. ZIVKOVIC, The thermal behavior of rammed earth wall in traditional house in Vojvodina: Thermal mass as a key element for thermal comfort, Therm. Sci. (2018).

[21] H. Zhang, Heat-insulating Materials and Sound-absorbing Materials, Build. Mater. Civ. Eng. (2011) 304–423. https://doi.org/10.1533/9781845699567.304.

[22] S. Goodhew, R. Griffiths, Sustainable earth walls to meet the building regulations, Energy Build. 37 (2005) 451–459. https://doi.org/10.1016/J.ENBUILD.2004.08.005.

[23] C. MacDougall, Natural Building Materials in Mainstream Construction: Lessons from the UK, J.

Green Build. 3 (2008) 3–14.

[24] N. Desborough, S. Samant, Is straw a viable building material for housing in the United Kingdom? Sustainability 2009;2:., Sustainability. 2 (2009) 368–374.

[25] C. Williams, S. Goodhew, R. Griffiths, L. Watson, The feasibility of earth block masonry for building sustainable walling in the United Kingdom, J. Build. Apprais. 6 (2010) 99–108.

[26] J. Pinto, A. Paiva, H. Varum, A. Costa, D. Cruz, S. Pereira, L. Fernandes, P. Tavares, J. Agarwal, Corn's cob as a potential ecological thermal insulation material, Energy Build. 43 (2011) 1985–1990. https://doi.org/10.1016/J.ENBUILD.2011.04.004.

[27] V. Soebarto, ANALYSIS OF INDOOR PERFORMANCE OF HOUSES USING RAMMED EARTH WALLS, in: Elev. Int. IBPSA Conf., Glasgow, Scotland, n.d.

[28] L. Soudani, M. Woloszyn, A. Fabbri, J. Morel, A. Grillet, Energy evaluation of rammed earth walls using long term in-situ measurements, Sol. Energy. 141 (2017) 70–80. https://doi.org/10.1016/j.solener.2016.11.002.

[29] G. Giada, R. Caponetto, F. Nocera, Hygrothermal Properties of Raw Earth Materials: A Literature Review, Sustainability. 11 (2019). https://doi.org/doi:10.3390/su11195342.

[30] ASTM C39, Standard Test Method for Compressive Strength of Cylindrical Concrete Specimens, ASTM Stand. (2021).

[31] EFNARC, Specification and Guidelines for Self-Compacting Concrete, (2002).

[32] ASTM D4318 − 17, Standard Test Methods for Liquid Limit, Plastic Limit, and Plasticity Index of Soils, ASTM Stand. (2017).

[33] ASTM C157, Standard Test Method for Length Change of Hardened Hydraulic-Cement Mortar and Concrete, ASTM Stand. (2017).

[34] N. Issaadi, A. Nouviaire, R. Belarbi, A. Aït-Mokhtar, Moisture characterization of cementitious material properties: assessment of water vapor sorption isotherm and permeability variation with ages, Constr. Build. Mater. 83 (2015) 237–247. https://doi.org/10.1016/j.conbuildmat.2015.03.030.

[35] M. Maaroufi, F. Bennai, R. Belarbi, K. Abahri, Experimental and numerical highlighting of water vapor sorption hysteresis in the coupled heat and moisture transfers, J. Build. Eng. 40 (2021) 102321. https://doi.org/10.1016/J.JOBE.2021.102321.

[36] European Standard ISO 12572, Determination of water vapor transmission properties (ISO/DIS 12572:1997), PrEN ISO 12572. (1997).

[37] N.X. P18-463, Norme XP P18-463 - Essai pour béton durci - Essai de perméabilité à l'air, 1999.

[38] L.J. Klinkenberg, The Permeability Of Porous Media To Liquids And Gases, Drill. Prod. Pract. (1941) 200–213.

[39] D.R. Gardner, A.D. Jefferson, R.J. Lark, An experimental, numerical and analytical investigation of gas flow characteristics in concrete, Cem. Concr. Res. 38 (2008) 360–367. https://doi.org/10.1016/J.CEMCONRES.2007.10.001.

[40] BS EN 12664, Thermal performance of building materials and products. Determination of thermal resistance by means of guarded hot plate and heat flow meter methods. Dry and moist products of medium and low thermal resistance, (2001).

[41] BS EN 12667, Thermal performance of building materials and products. Determination of thermal resistance by means of guarded hot plate and heat flow meter methods. Products of high and medium thermal resistance, (2001).

[42] AFPC-AFREM. Durabilité des Bétons-Mode Opératoire Recommandé: Détermination de la Masse Volumique Apparente et de la Porosité Accessible à L'eau, in: Proc. Compte Rendu Des Journées Tech. AFPC-AFREM, Toulouse, France, 1997: pp. 11–12.

[43] F. Bennai, N. Issaadi, K. Abahri, R. Belarbi, A. Tahakourt, Experimental characterization of thermal and hygric properties of hemp concrete with consideration of the material age evolution, Heat Mass Transf. (2017). https://doi.org/10.1007/s00231-017-2221-2.

[44] J.F. Straube, Moisture Control and Enclosure Wall Systems, University of Waterloo, 1998.

[45] Y.E. Belarbi, M. Sawadogo, P. Poullain, N. Issaadi, A.E.A. Hamami, S. Bonnet, R. Belarbi, Experimental Characterization of Raw Earth Properties for Modeling Their Hygrothermal Behavior, Buildings. 12 (2022). https://doi.org/10.3390/buildings12050648.

[46] R. Allam, N. Issaadi, R. Belarbi, M. El-Meligy, A. Altahrany, Hygrothermal behavior for a clay brick wall, Heat Mass Transf. 54 (2018) 1579–1591. https://doi.org/10.1007/s00231-017-2271-5.

[47] A.A. Hamami, P. Turcry, A. Aït-Mokhtar, Influence of mix proportions on microstructure and gas permeability of cement pastes and mortars, Cem. Concr. Res. 42 (2012) 490–498. https://doi.org/10.1016/j.cemconres.2011.11.019.

[48] E.J. Garboczi, Mercury porosimetry and effective networks for permeability calculations in porous materials, Powder Technol. 67 (1991) 121–125. https://doi.org/10.1016/0032-5910(91)80148-C.

[49] E.J. Garboczi, Permeability, diffusivity, and microstructural parameters: A critical review, Cem. Concr. Res. 20 (1990) 591–601. https://doi.org/10.1016/0008-8846(90)90101-3.

[50] S.C. Carniglia, Construction of the tortuosity factor from porosimetry, J. Catal. 102 (1986) 401–418. https://doi.org/10.1016/0021-9517(86)90176-4.

[51] R. Kumar, B. Bhattacharjee, Assessment of permeation quality of concrete through mercury intrusion porosimetry, Cem. Concr. Res. 34 (2004) 321–328. https://doi.org/10.1016/J.CEMCONRES.2003.08.013.

[52] D. Medjelekh, L. Ulmet, F. Dubois, Characterization of hygrothermal transfers in the unfired earth, Energy Procedia. 139 (2017) 487–492. https://doi.org/10.1016/J.EGYPRO.2017.11.242.

[53] H. Cagnon, J.E. Aubert, M. Coutand, C. Magniont, Hygrothermal properties of earth bricks, Energy Build. 80 (2014) 208–217. https://doi.org/10.1016/J.ENBUILD.2014.05.024.

[54] H. Porter, J. Blake, N.K. Dhami, A. Mukherjee, Rammed earth blocks with improved multifunctional performance, Cem. Concr. Compos. 92 (2018) 36–46. https://doi.org/10.1016/j.cemconcomp.2018.04.013.

[55] E. Troppová, M. Švehlík, J. Tippner, R. Wimmer, Influence of temperature and moisture content on the thermal conductivity of wood-based fibreboards, Mater. Struct. 48 (2015) 4077–4083. https://doi.org/10.1617/s11527-014-0467-4.

[56] M. Hall, D. Allinson, Analysis of the hygrothermal functional properties of stabilised rammed earth materials, Build. Environ. 44 (2009) 1935–1942. https://doi.org/10.1016/J.BUILDENV.2009.01.007.

[57] D. Allinson, M. Hall, Hygrothermal analysis of a stabilised rammed earth test building in the UK, Energy Build. 42 (2010) 845–852. https://doi.org/10.1016/J.ENBUILD.2009.12.005.

[58] F. El Fgaier, Z. Lafhaj, E. Antczak, C. Chapiseau, Dynamic thermal performance of three types of unfired earth bricks, Appl. Therm. Eng. 93 (2016) 377–383. https://doi.org/10.1016/J.APPLTHERMALENG.2015.09.009.

[59] R. Gabrovšek, T. Vuk, V. Kaučič, Evaluation of the hydration of Portland cement containing various carbonates by means of thermal analysis, Acta Chim. Slov. 53 (2006) 159 – 165. https://www.scopus.com/inward/record.uri?eid=2-s2.0-33745946309&partnerID=40&md5=eeb5fff866c3f097eca47627a7623c2e.

[60] E.T. Stepkowska, J.M. Blanes, F. Franco, C. Real, J.L. Pérez-Rodríguez, Phase transformation on heating of an aged cement paste, Thermochim. Acta. 420 (2004) 79–87. https://doi.org/10.1016/J.TCA.2003.11.057.

[61] K. Vance, M. Aguayo, T. Oey, G. Sant, N. Neithalath, Hydration and strength development in ternary portland cement blends containing limestone and fly ash or metakaolin, Cem. Concr. Compos. 39 (2013) 93–103. https://doi.org/10.1016/J.CEMCONCOMP.2013.03.028.

[62] C. Gu, Y. Ji, Y. Zhang, Y. Yang, J. Liu, T. Ni, Recycling use of sulfate-rich sewage sludge ash (SR-SSA) in cement-based materials: Assessment on the basic properties, volume deformation and microstructure of SR-SSA blended cement pastes, J. Clean. Prod. 282 (2021) 124511. https://doi.org/10.1016/J.JCLEPRO.2020.124511.

[63] M. Mejdi, M. Saillio, T. Chaussadent, L. Divet, A. Tagnit-Hamou, Hydration mechanisms of sewage sludge ashes used as cement replacement, Cem. Concr. Res. 135 (2020) 106115. https://doi.org/10.1016/J.CEMCONRES.2020.106115.

[64] R. Giustetto, K. Seenivasan, D. Pellerej, G. Ricchiardi, S. Bordiga, Spectroscopic characterization and photo/thermal resistance of a hybrid palygorskite/methyl red Mayan pigment, Microporous Mesoporous Mater. 155 (2012) 167–176. https://doi.org/10.1016/J.MICROMESO.2012.01.024.

[65] R. Giustetto, G. Chiari, Crystal structure refinement of palygorskite from neutron powder diffraction, Eur. J. Mineral. 16 (2004) 521–532. https://doi.org/10.1127/0935-1221/2004/0016-0521.

[66] N.M. Faqir, R. Shawabkeh, M. Al-Harthi, H.A. Wahhab, Fabrication of Geopolymers from Untreated Kaolin Clay for Construction Purposes, Geotech. Geol. Eng. 37 (2019) 129–137. https://doi.org/10.1007/s10706-018-0597-5.

[67] X. Liu, X. Liu, Y. Hu, Investigation of the thermal behaviour and decomposition kinetics of kaolinite, Clay Miner. 50 (2015) 199–209. https://doi.org/10.1180/claymin.2015.050.2.04.

[68] X.D. Wang, H.Y. Zhang, G.S. Yan, Q. Pei, Durability of Ancient Earthen Architecture under Wind Erosion in the Milan Ancient City along the Silk Road of China, Adv. Mater. Res. 163–167 (2010) 3230–3236.

[69] F. Benmahiddine, R. Cherif, F. Bennai, R. Belarbi, A. Tahakourt, K. Abahri, Effect of flax shives content and size on the hygrothermal and mechanical properties of flax concrete, Constr. Build. Mater. 262 (2020) 120077. https://doi.org/10.1016/J.CONBUILDMAT.2020.120077.

[70] C. Niyigena, S. Amziane, A. Chateauneuf, Multicriteria analysis demonstrating the impact of shiv on the properties of hemp concrete, Constr. Build. Mater. 160 (2018) 211–222.

https://doi.org/10.1016/J.CONBUILDMAT.2017.11.026.

[71] B. Zdravkov, J. Čermák, M. Šefara, J. Janků, Pore classification in the characterization of porous materials: A perspective, Open Chem. 5 (2007) 385–395. https://doi.org/doi:10.2478/s11532-007-0017-9.

[72] E. Balan, G. Calas, D. L Bish, Kaolin-Group Minerals: From Hydrogen-Bonded Layers to Environmental Recorders, Elements. 10 (2014) 183–188.

[73] F. Bergaya, G. Lagaly, M. Vayer, Cation and Anion Exchange, in: Dev. Clay Sci., Elsevier, 2006: pp. 979–1001. https://doi.org/10.1016/S1572-4352(05)01036-6.

[74] R.F. Zuo, G.X. Du, W.G. Yang, L.B. Liao, Z. Li, Mineralogical and chemical characteristics of a powder and purified quartz from Yunnan Province, Open Geosci. 8 (2016) 606–611. https://doi.org/10.1515/geo-2016-0055.

CHAPTER 8. Conclusions and perspectives

8.1 Conclusions

Sustainable construction should be adopted by reducing the consumption of new industrial materials and increasing the use of recycled and locally available materials to proportion low negative environmental impacts. Earthen construction is an environment-friendly material with various advantages in terms of thermal performance, energy efficiency, economical, and environmental aspects. Since the construction process of earthen constructions can be time and energy consuming, self-consolidating earth concrete (SCEC) can solve this shortcoming to broaden the application of earthen materials. However, there are three main challenges to achieve SCEC, including: (1) dispersion of fine clay particles which can hinder the flowability, (2) setting of the material can be delayed due to low cement content, and (3) various earth types can complicate the achievement of a designing procedure.

The main objectives of this study were to (1) find the compatibility and designing the corresponding paste mixtures of self-consolidating earth concrete (SCEC) with its novel ternary binder system (i.e., clay, silt, and cement) and using Atterberg limits of the earth as their classification parameter; (2) identify the influencing parameters in designing SCEC mixtures using a new concrete-equivalent mortar (CEM) approach; (3) highlight the rheology of multiscale self-consolidating earthen materials; and (4) investigate the hygrothermal and microstructural characterization of SCEC mixtures. These main four objectives were investigated through four experimental phases of this thesis. Following the literature review on advantages and disadvantages of earthen materials and feasibility of this study, the following phases were carried out:

In the **Phase 1**, seven main influencing parameters were defined including clay type, cement content, water-to-powder ratio (W/P), cement-to-clay ratio (Ce/Cl), paste volume (V_P), sand-to-total aggregate ratio (S/A), and admixture type. The Taguchi design of experiment was used to find the optimum level of each factor for workability and compressive strength results, as responses. According to coupled effect of the investigated factors, statistical models were developed to facilitate the designing approach of self-consolidating earth paste (SCEP) mixtures.

In the **Phase 2**, a new CEM approach was proposed to facilitate the prediction of SCEC performance. The paste mixtures with satisfied properties in terms of workability and compressive strength in Phase 1 were used to carry out further testing on CEM and SCEC scales. The prediction of workability, compressive strength, and drying shrinkage of SCEC mixtures was modelled using their corresponding CEM and paste mixtures.

The thixotropy, yield stress, and plastic viscosity of of paste, CEM, and concrete mixtures were investigated to optimize the rheological parameters and facilitate the designing procedure were investigated in **Phase 3**.

The hygrothermal performance of the investigated SCEC mixtures were carried out and compared with other building materials in **Phase 4**.

Based on the results obtained in this study, the following conclusions can be pointed out:

8.1.1 Phase 1: A new approach for proportioning self-consolidating earth paste (SCEP) using the Taguchi method

- Clay type and content and W/P dictated the workability of SCEP mixtures, while their compressive strength was mainly controlled by cement content and W/P. Clay Type II, as finer clay type, with the lowest W/P ratio (0.30) led to the highest admixture demand to achieve the targeted workability.
- Using Taguchi method and signal-to-noise analysis, sodium silicate (NaSil) and sodium hexametaphosphate (NaHMP) led to the highest admixture demand, respectively, compared to the other HRWR admixtures. Regarding the minimum mini-slump flow (MSF) loss, non-esterified polycarboxylate (NE-PC) was the most efficient admixture type with the lowest demand to achieve targeted workability.
- Regarding marsh cone test (MCT) results, NE-PC and sodium polynaphtalene (PNS) resulted in the lowest values. Among other influencing parameters, Clay Type I (100% kaolinite), lower cement content, and higher W/P and Ce/Cl resulted in lower MCT values.
- Concluded from single powder paste systems, adequate clay dispersion can be achieved using NaHMP, while the use of polycarboxylate ether (PCE) was only efficient in the

presence of cement. Both clay and cement dispersions were observed with NE-PC and PNS admixtures, proving their compatibility with both of these particles. However, negligible effect of NaSil on flowability of single-powder systems was observed.

- As concluded for early compressive strength development, PNS, PCE, and NaSil admixture types showed the highest contribution. However, the later compressive strength values (7 and 28 days) were maximized by PNS, PCE and NE-PC which were almost comparable.
- Designing SCEC should be addressed based on different soil types due to existing diversity of earth. Atterberg limits, which are mainly affected by clay fraction, showed great potential to be represented as a criterion for feasibility of earth to achieve SCEC and control its workability. Liquid limit (LL) and plasticity index (PI) values lower than 40% and 25%, respectively, were recommended to achieve SCEP mixtures.
- Higher specific surface area (SSA) of the binder constituents, LL, and PI led to higher admixture demand and MCT values. These parameters were also used as a key factor to propose theoretical models to predict the workability of SCEP mixtures.
- Using the empirical models and compressive strength contours, a new proportioning approach was proposed to design SCEP mixtures with targeted workability and compressive strength was proposed.

8.1.2 Phase 2: Multiscale investigation of self-consolidating earthen materials using a novel concrete-equivalent mortar approach

- A new CEM approach was successfully used to assess workability and drying shrinkage of the corresponding concrete mixtures. W/P, excess paste thickness (e_{EP}), and S/A were the key parameters for the prediction. Regarding the relative compressive strength of concrete to CEM, e_{EP} and W/A were found to be adequate for the assessment.
- Soil characteristics (Atterberg limits), V_P, W/P, and e_{EP} were found to be reliable parameters to predict the workability of the investigated CEM mixtures from that of their corresponding paste mixtures.
- Similarly to the paste mixtures, workability of the investigated SCEC mixtures were mainly affected by the coupled effect of W/P and binder constituents. Good correlations were found for PI/(W/P) and SSA/(W/P) parameters as the most influencing parameters on the

admixture demand to achieve the targeted workability. Admixture demand increased with higher LL and PI, and lower V_P, W/P, and e_{EP} values.

- As concluded from ANOVA analysis, the MSF loss was mainly dependent on the admixture type, followed by W/P ratio. The lowest and highest MSF loss values were attributed to NE-PC and NaHMP admixtures, respectively.
- Mini V-Funnel (MVF) values mostly decreased with higher W/P ratios and V_P, independent on the binder characteristics. However, the MVF increase rate was found to be highly dependent on the admixture type. The NaHMP mixtures showed the highest MVF increase rate and shape stability over time.
- The 7- and 28-day compressive strength values were found highly dependent on the cement content and W/P, similar to the paste mixtures. However, the 1-day compressive strength ($f'_{c\text{-}1d}$) was found also dependent on LL, especially in the presence of PNS admixture.
- Early-age compressive strength showed good correlation with drying shrinkage, resulting in very high drying shrinkage values in the case of $f'_{c\text{-}1d}$ values less than 1 MPa. Furthermore, it was also revealed that the drying shrinkage values were highly dependent on V_P followed by W/P.

8.1.3 Phase 3: New insight on rheology of self-consolidating earth concrete (SCEC)

- The thixotropic and rheopectic behavior of the investigated SCEP mixtures was mainly followed by admixture type. Few paste mixtures showed thixotropic behavior, including those proportioned with PNS admixture and finer clay type, as well as the NE-PC-based systems.
- The highest thixotropy values (A_{thix}) was obtained for the finer clay type systems. However, the highest rheopectic behavior was attributed to the mixtures proportioned with PCE admixture and Clay Type II, as well as the sole mixture dispersed with NaHMP.
- Viscoplastic parameters were mainly controlled by the admixture and clay types. The mixtures proportioned with NaHMP and finer clay particles resulted in the highest yield stress and plastic viscosity values. Furthermore, the NE-PC-based paste and CEM mixtures showed relatively lower values and increasing rates of yield stress values over time, compared to PNS and PCE systems.

- The type and content of clay and W/P affected the yield stress of the investigated paste, CEM, and SCEC mixtures. Yield stress values of lower and higher than 40 Pa were obtained for the CEM mixtures proportioned with the Clay Types I and II, respectively, except the NaHMP-based CEM system. Clay Type II led to higher values and increasing rates of yield stress values over time in concrete scale. However, the plastic viscosity values were mainly affected by the W/P.
- The rheological properties of the SCEC mixtures could be controlled from their paste and CEM matrices. The V_P and e_{EP} parameters could predict the rheological properties of the CEM mixtures from those of their corresponding paste mixtures. These key parameters included e_{EP} and S/A for the relative rheological properties of SCEC mixtures to their corresponding CEM mixtures.

8.1.4 Phase 4: Hygrothermal and microstructural characterization of self-consolidating earth concrete (SCEC)

- The SCEC mixtures gained lower water content compared to conventional and hemp concrete when exposed to higher relative humidity values, in the range of clay bricks. At 90% relative humidity, the gained water content for the investigated SCEC mixtures were found lower (around 1.5%) than that of the reference mixture (3.3%).
- Regarding the water vapor diffusion resistance factor and gas permeability, SCEC mixtures showed higher values compared to clay bricks and hemp concrete, yet lower than conventional concrete. The SCEC mixtures resulted in water vapor permeability values ranged from 9.63×10^{-13} to 3.95×10^{-12} $kg.m^{-1}.s^{-1}.Pa^{-1}$.
- The reference concrete mixture resulted in higher specific heat capacity and thermal conductivity values compared to the SCEC mixtures in different temperatures at both dry and wet states. Furthermore, the investigated SCEC mixtures obtained lower diffusivity and effusivity values compared to the reference mixture, similar to those of earthen materials reported in literature.
- The reference mixture gained the highest mass loss at CSH, CH, and decarbonation decompositions compared to the SCEC ones. The Clay Type II systems showed two peaks in 240 and 360°C which were related to the decomposition of attapulgite compounds.

However, a distinct mass loss peak at approximately 520°C was observed for the mixtures containing Clay Type I which was attributed to the dehydration of kaolinite.

- Higher cement contents led to lower total porosity. As concluded from the pores distribution, the water vapor and gas permeability were found in strong agreements with cumulative pore volume values in the ranges of 100–200 and 100–300 nm, respectively. Furthermore, pore volume of pore sizes less than 1 μm showed good correlations with the drying shrinkage and compressive strength values at 28 days of age.
- SCEC mixtures can be used as building envelopes with satisfying hygrothermal performance since they offer high permeability and low thermal conductivity values with satisfying effusivity and diffusivity parameters compared to other conventional construction materials.

8.2 Future works

Sustainable construction is an emerging construction technic which should be further addressed by researchers working on construction materials. This thesis focused on achieving SCEC and investigating its rheo-thermomechanical performance. According to the achievements of this study, further investigations may be necessary for better understanding and to fill the existing research gap, as follow:

- Cement is considered as the source of strength of SCEC. Therefore, other stabilization methods, such as lime, can be introduced and compare the outcomes with the current study.
- Geopolymers can be useful to be incorporated in earthen materials and optimize the designing procedure to achieve greener self-consolidating earthen mixtures.
- A comparative study on the environmental impacts of flowable earthen materials, using different stabilization methods and admixture types, can be followed by a thorough life cycle assessment (LCA) study.
- Large-scale hygrothermal study can be informative since earthen materials are mostly used as building envelopes.
- Numerical simulation on various climatic conditions can open a new door to use these materials in different regions around the world.

- Fine clay particles facilitate the shape stability of the mixtures which can be considered as 3D printing application. Therefore, further rheological investigations are required with different clay and admixture types to assess the potential of earthen materials in 3D printing application.

CHAPTER 8. Conclusions et perspectives *(Français)*

8.3 Conclusions

La construction durable est de plus en plus en vue afin de réduire la consommation des ressources naturelles et en augmentant l'utilisation de matériaux recyclés et disponibles localement, une alternative incontournable pour réduire les impacts environnementaux de la construction. La construction en terre est un matériau respectueux de l'environnement qui présente divers avantages en termes de performance thermique, d'efficacité énergétique, d'aspects économiques et environnementaux. Comme le processus de construction des constructions en terre peut prendre du temps et de l'énergie, le béton de terre autoplaçant (BTAP) peut résoudre ce problème et élargir l'application des matériaux en terre. Cependant, il y a trois défis principaux pour pourvoir formuler le BTAP, notamment (1) la dispersion des particules d'argile qui peuvent entraver la fluidité, (2) la prise retardée du matériau en raison de la faible teneur en ciment, et (3) la grande variété des types de terre, ce qui rend difficile la sélection d'un type de terre approprié pour atteindre les performances requises.

Les principaux objectifs de cette étude étaient (1) étudier la compatibilité entre les adjuvants et poudres et concevoir les formulations de pâte correspondantes au béton de terre autoplaçant (BTAP) incorporant un nouveau système de liant ternaire (c'est-à-dire, l'argile, le silt et le ciment) et en utilisant les limites d'Atterberg de la terre comme paramètre de classification; (2) identifier les paramètres d'influence dans la conception des mélanges de BTAP en utilisant une nouvelle approche basée sur la méthode du mortier du béton équivalent (MBE) (argile, limon et ciment), et en utilisant les limites d'Atterberg de la terre comme paramètre de classification; (2) identifier les paramètres influents dans la conception des formulations de SCEC en utilisant une nouvelle approche de MBE; (3) mettre en évidence la rhéologie des matériaux à base de terre sur différentes échelles (pâte, mortier et béton); et (4) étudier la caractérisation hygrothermique et microstructurale des BTAP optimisés. Un programme expérimental adéquat est réalisé afin de répondre aux problématiques mentionnées ci-dessus et de répondre aux objectifs de cette étude. Après la revue de la littérature sur les avantages et les inconvénients des matériaux en terre et la faisabilité de cette étude, les différentes phases réalisées dans cette étude sont :

À la **Phase 1**, sept paramètres de formulation ont été identifiés et étudiés, notamment le type d'argile, la teneur en ciment, le rapport eau-poudre (E/P), le rapport ciment-argile (Ci/Ar), le volume de pâte (V_P), le rapport sable-granulat total (S/G) et le type d'adjuvant. Le plan d'expérience de Taguchi a été utilisé pour déterminer le niveau optimal de chaque facteur afin d'assurer une maniabilité et une résistance à la compression adéquate. Selon l'effet couplé des facteurs étudiés, des modèles statistiques sont proposés pour faciliter l'approche de conception des formulations de pâte de terre autoplaçante (PTAP).

À la **Phase 2**, une nouvelle approche MBE est proposée pour faciliter la prédiction de la performance BTAP. L'identification des formulations de pâtes ayant les propriétés requises en termes de maniabilité et de résistance à la compression (Phase 1) a été employée pour réaliser l'étude expérimentale sur les MBE et BTAP. La prédiction de la maniabilité, de la résistance à la compression et du retrait de séchage des formulations de BTAP a été modélisée en utilisant les propriétés des formulations de pâte et MBE correspondants.

À la **Phase 3**, la thixotropie, la contrainte d'écoulement et la viscosité plastique des mélanges de BTAP à l'échelle de la pâte, du MBE et du béton ont été étudiées pour optimiser les paramètres rhéologiques et faciliter la procédure de conception.

À la **Phase 4**, les performances hygrothermiques des formulations de BTAP optimisés ont été réalisées et comparées avec celles des matériaux de construction conventionnels.

En se basant sur les résultats obtenus et présentés dans ce manuscrit, les conclusions suivantes peuvent être soulignées :

8.3.1 Phase 1 : Une nouvelle approche pour le dosage de la pâte de terre autoplaçante (PTAP) à l'aide de la méthode Taguchi

- Le type et la teneur en argile ainsi que le rapport E/P contrôlent la maniabilité des PTAP, tandis que la résistance à la compression est principalement contrôlée par la teneur en ciment et le rapport E/P. Le type d'argile II (plus fin) combiné avec un rapport E/P de 0,30

(le plus faible) a conduit à la demande la plus élevée en adjuvants pour atteindre l'ouvrabilité ciblée.

- En utilisant la méthode Taguchi et l'analyse du signal-bruit, le silicate de sodium (NaSil) et l'hexamétaphosphate de sodium (NaHMP) ont manifesté un plus grand dosage pour assurer une maniabilité donnée par les autres adjuvants. En ce qui concerne la perte de maniabilité (mini-slump), le polycarboxylate non estérifié (NE-PC) montre une meilleure efficacité caractérisée par un faible dosage pour atteindre une fluidité donnée et un meilleur maintien de la fluidité dans le temps que les autres adjuvants.
- Dans le cas des essais d'écoulement au cône de Marsh (ECM), le NE-PC et le polynaphtalène de sodium (PNS) ont donné des temps d'écoulement plus faibles. Parmi les autres paramètres d'influence, le type d'argile I (100 % de kaolinite), une teneur en ciment plus faible et des valeurs E/P et Ci/Ar plus élevées résultent en des temps d'écoulement relativement faibles.
- Dans le cas des de systèmes de pâte proportionnés avec une poudre non mélangée, une dispersion adéquate de l'argile peut être obtenue en utilisant le NaHMP, tandis que l'utilisation de l'éther polycarboxylate (PCE) n'est efficace qu'en présence de ciment. Une bonne dispersion de l'argile et de ciment ont est achevée avec les adjuvants NE-PC et PNS, ce qui reflète leur compatibilité avec ces deux matériaux. Cependant, un effet négligeable du NaSil sur la fluidité des systèmes à poudre unique est observé.
- Les adjuvants PNS, PCE et NaSil ont montré la plus grande contribution au développement de la résistance au jeune âge. Cependant, dans le cas de la résistance à la compression à 7 et 28 jours, le PNS, le PCE et le NE-PC ont permis d'atteindre des résistances maximales, de manière presque comparable.
- Les limites d'Atterberg, qui sont principalement affectées par la fraction d'argile, montrent un effet important sur la maniabilité et constituent un critère potentiel pour la sélection des terres souhaitables pour la formulation des BTAP. Les valeurs de la limite liquide (LL) et de l'indice de plasticité (PI) inférieures, respectivement, à 40 % et 25 % sont recommandées pour réaliser des mélanges PTAP.
- Une surface spécifique (SSA) des constituants du liant, LL et PI plus élevée a conduit à une demande d'adjuvant élevée. Ces paramètres peuvent également être utilisés comme facteur

clé pour proposer des modèles théoriques permettant de prédire l'ouvrabilité des formulations de PTAP.

- En utilisant les modèles empiriques et les contours de la résistance à la compression, une nouvelle approche de formulation de PTAP avec une maniabilité et une résistance à la compression ciblées est proposée.

8.3.2 Phase 2 : Étude multi-échelle des matériaux terreux autoplaçants à l'aide d'une nouvelle approche de mortier équivalent au béton

- Une nouvelle approche de MBE est utilisée avec succès pour évaluer la maniabilité et le retrait de séchage des bétons correspondants. Les paramètres clés à considérer sont le E/P, l'épaisseur de la pâte en excès (e_{EP}) et le S/G. En ce qui concerne la résistance à la compression relative du béton par rapport à son MBE, l'e_{EP} et le S/G se sont avérés adéquats pour assurer une bonne prédiction.
- Les limites d'Atterberg du sol, le V_P, le rapport E/P et l'e_{EP} se sont avérés être des paramètres fiables pour prédire la maniabilité des formulations des mélanges MBE étudiés à partir de celle de leurs pâtes correspondantes.
- Comme pour les formulations de pâte, l'ouvrabilité des BTAP étudiés a été principalement affectée par l'effet couplé du rapport E/P et des constituants du liant. De bonnes corrélations ont été trouvées pour les paramètres PI/(E/P) et SSA/(E/P) comme étant les paramètres les plus influents sur la demande d'adjuvant pour atteindre l'ouvrabilité ciblée. La demande d'adjuvant augmente avec des valeurs plus élevées de LL et PI, et des valeurs plus faibles de V_P, E/P, et e_{EP}.
- L'analyse ANOVA montre que la perte de EMS dépend principalement du type d'adjuvant, suivi par le rapport E/P. Les pertes de EMS les plus faibles sont obtenues avec le NE-PC, alors que les valeurs plus élevées sont obtenues avec le NaHMP.
- L'utilisation des rapports E/P et VP plus élevés réduit le temps d'écoulement au Mini-cône d'écoulement (V-Funnel) (MVF) indépendamment des caractéristiques du liant. Cependant, le taux d'augmentation du MVF s'est avéré fortement dépendant du type d'adjuvant. Les mélanges contenant le NaHMP ont montré le plus haut taux d'augmentation du MVF et la plus grande stabilité de la forme dans le temps.

- Les résistances à la compression à 7 et à 28 jours sont fortement dépendantes de la teneur en ciment et du E/P, comme pour les mélanges de pâte. Cependant, la résistance à la compression à 1 jour ($f'_{c\text{-}1d}$) s'est avérée dépendante de LL, notamment en présence de l'adjuvant PNS.
- La résistance à la compression au jeune âge (c.-à-d. 1 jour) a montré une bonne corrélation avec le retrait de séchage. Des valeurs de retrait de séchage très élevées sont obtenues dans le cas des résistances à la compression $f'_{c\text{-}1d}$ inférieures à 1 MPa. En outre, il a également été observé que les valeurs du retrait de séchage dépendaient fortement de V_P, suivi de E/P.

8.3.3 Phase 3 : Nouvelles connaissances sur la rhéologie du béton de terre autoplaçant (BTAP)

- Le comportement thixotrope et rhéopectique des mélanges de PTAP étudiés a été principalement contrôlé par le type d'adjuvant. Peu de mélanges de pâte ont montré un comportement thixotrope, y compris ceux proportionnés avec l'adjuvant PNS et un type d'argile plus fin, ainsi que les systèmes à base de NE-PC.
- Les valeurs de thixotropie les plus élevées (A_{thix}) ont été obtenues dans le cas des systèmes proportionnés avec le type d'argile la plus fine. Cependant, le comportement rhéopectique le plus élevé a été observé avec les mélanges proportionnés avec l'adjuvant PCE et l'argile de type II, ainsi qu'au seul mélange dispersé avec du NaHMP.
- Les paramètres viscoplastiques sont principalement contrôlés par l'adjuvant et les types d'argile. Les mélanges proportionnés avec le NaHMP et les particules d'argile plus fines ont donné lieu à des valeurs de la contrainte d'écoulement et de la viscosité plastique les plus élevées. De plus, les mélanges de pâte à base de NE-PC et de MBE ont montré des valeurs relativement plus faibles et des taux d'augmentation des valeurs de la contrainte d'écoulement dans le temps, par rapport aux systèmes PNS et PCE.
- Le type et le contenu d'argile ainsi que le rapport E/P ont affecté la limite d'élasticité des mélanges de pâte, MBE et BTAP étudiés. Des valeurs de limite d'élasticité inférieures ou supérieures à 40 Pa ont été obtenues pour les mélanges MBE proportionnés avec respectivement les types d'argile I et II, à l'exception du système MBE à base de NaHMP. À l'échelle du béton, le type d'argile II a conduit à des valeurs plus élevées et à des taux

d'augmentation des valeurs de la limite d'élasticité dans le temps. Cependant, les valeurs de la viscosité plastique ont été principalement affectées par le rapport E/P.

- Les propriétés rhéologiques des mélanges BTAP peuvent être contrôlées par celles de leurs matrices de pâte et MBE correspondants. Les paramètres V_P et e_{EP} peuvent prédire les propriétés rhéologiques des mélanges MBE à partir de celles de leurs mélanges de pâte correspondants. Les paramètres clés pour évaluer les propriétés rhéologiques relatives des mélanges BTAP par rapport à leurs mélanges MBE correspondants sont les e_{EP} et S/G.

8.3.4 Phase 4 : Caractérisation hygrothermique et microstructurale du béton de terre autoplaçant (BTAP)

- Les mélanges BTAP ont montré une teneur en eau plus faible, dans la gamme des briques d'argile, par rapport au béton conventionnel et au béton de chanvre lorsqu'ils ont été exposés à des valeurs d'humidité relative plus élevées. À 90 % d'humidité relative, la teneur en eau des mélanges de BTAP étudiés s'est avérée inférieure (environ 1,5 %) à celle du mélange de référence (3,3 %).
- En ce qui concerne la résistance à la diffusion de la vapeur d'eau et la perméabilité aux gaz, les mélanges de BTAP ont montré des valeurs plus élevées par rapport aux briques d'argile et au béton de chanvre, mais plus faibles que le béton conventionnel. Les mélanges de BTAP ont donné des valeurs de perméabilité à la vapeur d'eau comprises entre $9{,}63\times10^{-13}$ et $3{,}95\times10^{-12}$ $kg.m^{-1}.s^{-1}.Pa^{-1}$.
- Le mélange de béton de référence a donné des valeurs de capacité thermique spécifique et de conductivité thermique plus élevées que les mélanges de BTAP à différentes températures, à l'état sec et à l'état humide. En outre, les mélanges de BTAP étudiés ont montré des valeurs de diffusivité et d'effusivité inférieures à celles du mélange de référence, similaires à celles des matériaux en terre rapportées dans la littérature.
- Le mélange de référence a subi la plus grande perte de masse due aux décompositions des CSH, du CH et de la décarbonatation par rapport aux BTAP. Les systèmes faits avec l'argile de type II ont montré deux pics à 240 et 360°C qui étaient liés à la décomposition des composés d'attapulgite. Cependant, un pic de perte de masse distinct à environ 520°C a été

observé pour les mélanges contenant l'argile de type I qui a été attribué à la déshydratation de la kaolinite.

- Des teneurs en ciment plus élevées ont conduit à une porosité totale plus faible. Comme le montre la distribution des pores, la perméabilité à la vapeur d'eau et au gaz est en forte corrélation avec les valeurs respectives cumulées du volume des pores dans les plages de 100–200 et 100–300 nm. En outre, le volume des pores de taille inférieure à 1 µm a montré de bonnes corrélations avec les valeurs de retrait de séchage et de résistance à la compression à 28 jours d'âge.
- Les mélanges de BTAP peuvent être utilisés comme enveloppes de bâtiments avec des performances hygrothermiques satisfaisantes, car ils offrent des valeurs de perméabilité élevées et de faible conductivité thermique avec des paramètres d'effusivité et de diffusivité satisfaisants par rapport aux autres matériaux de construction conventionnels.

8.4 Travaux futurs

La construction durable est une technique de construction émergente qui devrait être davantage prise en compte par les chercheurs travaillant sur les matériaux de construction. Cette thèse s'est concentrée sur la réalisation du BTAP et l'étude de ses performances rhéo-thermomécaniques. En fonction des résultats obtenus dans cette étude, des études supplémentaires sont nécessaires pour approfondir les connaissances et combler les lacunes existantes. Ainsi, les sujets peuvent être mis en avant pour des travaux futurs, comme suit :

- Le ciment est considéré comme la source de résistance du BTAP. Par conséquent, d'autres méthodes de stabilisation, comme la chaux, peuvent être introduites et les résultats comparés à ceux de l'étude actuelle.
- Il peut être utile d'incorporer des géopolymères aux matériaux de terre et aussi pour optimiser la procédure de conception afin d'obtenir des mélanges.
- Une étude comparative sur les impacts environnementaux des matériaux en terre pouvant être coulés, utilisant différentes méthodes de stabilisation et différents types d'adjuvants, peut être suivie d'une étude approfondie d'analyse du cycle de vie (ACV).

- Une étude hygrothermique à grande échelle peut être instructive puisque les matériaux en terre sont le plus souvent utilisés comme enveloppes de bâtiments.
- La simulation numérique de diverses conditions climatiques peut ouvrir une nouvelle porte pour l'utilisation de ces matériaux dans différentes régions du monde.
- Les fines particules d'argile facilitent la stabilité de la forme des mélanges qui peuvent être considérés comme une application d'impression 3D. Par conséquent, des études rhéologiques supplémentaires sont nécessaires avec différents types d'argile et d'adjuvants pour évaluer le potentiel des matériaux terreux dans l'application d'impression 3D.